Networking and Application Interface Technology for Wireless Sensor Network Surveillance and Monitoring

A Thesis submitted for the degree of Doctor of Engineering (EngD)

Darminder Singh Ghataoura

Communications and Information Systems Research Group

Department of Electronic and Electrical Engineering

University College London

Selex Galileo Ltd

Sigma House, Christopher Martin Road, Basildon, Essex

January 2012

Statement of Originality

I, Darminder Singh Ghataoura, confirm that the work presented in this thesis is my own. Where information has been derived from other sources, I confirm that this has been indicated in the thesis.

Signed: _____

Date: _____

I dedicate this thesis to my son, Master Charandeep Singh Ghataoura, who gives me inspiration and energy.

Acknowledgments

This thesis would not have been possible if it wasn't for the help that I received from others around me. To begin, I would like to thank all my past and present colleagues from room 804 for all their kind support and suggestions, during my four memorable years.

Special thanks must also be made to George Matich at Selex Galileo Ltd, for giving me the opportunity to pursue and contribute towards this project. I would like to thank him for his support and guidance, which I believe has made this project a success and a great learning experience for me.

I would also like to extend my gratitude to Dr. John Mitchell who took over the supervision of this project upon Dr. Yang Yang leaving. I would like to thank him for his many helpful suggestions, support and guidance during the project and especially, regarding the makeup of this thesis.

I am also thankful to Dr. Yang Yang for his initial thoughts, which enabled me to develop an understanding of the project requirements and subject area. I wish him all the best in his current role.

Without words of support and encouragement the completion of this thesis would have felt like a difficult prospect. For this contribution, I would especially like to thank my parents for giving me much needed encouragement, guidance and moral support.

Most importantly, I would like to pay my humble gratitude to the almighty Waheguru for giving me this opportunity and the ability and temperament to complete this thesis.

Darminder Singh Ghataoura

Abstract

Distributed unattended ground sensor (*UGS*) networks are commonly deployed to support wide area battlefield surveillance and monitoring missions. The information they generate has proven to be valuable in providing a necessary tactical information advantage for command and control, intelligence and reconnaissance field planning. Until recently, however, there has been greater emphasis within the defence research community for *UGS* networks to fulfil their mission objectives successfully, with minimal user interaction. For a distributed *UGS* scenario, this implies a network centric capability, where deployed *UGS* networks can self-manage their behaviour in response to dynamic environmental changes. In this thesis, we consider both the application interface and networking technologies required to achieve a network centric capability, within a distributed *UGS* surveillance setting. Three main areas of work are addressed towards achieving this.

The first area of work focuses on a capability to support autonomous *UGS* network management for distributed surveillance operations. The network management aspect is framed in terms of how distributed sensors can collaborate to achieve their common mission objectives and at the same time, conserve their limited network resources. A situation awareness methodology is used, in order to enable sensors which have similar understanding towards a common objective to be utilised, for collaboration and to allow sensor resources to be managed as a direct relationship according to, the dynamics of a monitored threat.

The second area of work focuses on the use of geographic routing to support distributed surveillance operations. Here we envisage the joint operation of unmanned air vehicles and *UGS* networks, working together to verify airborne threat observations. Aerial observations made in this way are typically restricted to a specific identified geographic area. Information queries sent to inquire about these observations can also be routed and restricted to using this geographic information. In this section, we present our bio-inspired geographic routing strategy, with an integrated topology control function to facilitate this.

The third area of work focuses on channel aware packet forwarding. Distributed *UGS* networks typically operate in wireless environments, which can be unreliable for packet forwarding purposes. In this section, we develop a capability for *UGS* nodes to decide which packet forwarding links are reliable, in order to reduce packet transmission failures and improve overall distributed networking performance.

Contents

List of Figures

List of Tables

List of Abbreviations

A	Total area of a deployed node network region in metres^2
$\|\|A\|\|$	Sub-set area of A in metres^2
A_{NP}	NP Detection Threshold
ACM	Association for Computing Machinery
ASE	Absolute Square Error
bps	Bits per Second
BBN	Bayesian Belief Network
BS	Belief State
BSE	Belief State Evaluation
C2ISR	Command and Control, Intelligence, Surveillance and Reconnaissance
CDF	Cumulative Distribution Function
CEP	Circular Error Probable
CH	Cluster Head
CF	Certainty Factor
CPTs	Conditional Probability Tables
CR	"Context" Ratios
CTL	Current Threat Location
$d_{Average}$	Average Forwarding Distance
d_{max}	Maximum Node Transmission Range
d_{opt}	Optimal Forwarding Distance
dB	Decibels
D_{KL}	KL discrimination
DCATT	Dynamic Clustering for Acoustic Target Tracking
DCF	Distributed Coordination Function
DPSK	Differential Phase-Shift Keying
DSDV	Destination-Sequenced Distance-Vector Routing
DSR	Dynamic Source Routing
E_{Nodes}	Expected Number of Nodes
EAX	Expected-Any-Path-Transmissions Count
EPDC	Energy Packet Delivery Consumption
ETX	Expected Transmission Count
EU	Expected Utility
FL	Fuzzy Logic
FLS	Fuzzy Logic System
GA	Genetic Algorithm
GAFLS	Genetic Adaptive Fuzzy Logic System
GDOP	Geometric Dilution of Precision
GeRAF	Geographic Random Forwarding
GI	Group Initiator
GI_{mocca}	GI Mission Objective "Context" Centric Address
GPS	Global Positioning System
H	Probability of Partner Confidence in "Context"
H_T	Maximum Set QoSI Service Provision Time
IDSQ	Information Driven Sensor Querying
IEEE	Institute of Electrical and Electronics Engineers
IET	Institution of Engineering and Technology
IQ	Information Query

k	The Number of Direct Neighbours for Node Communication
KL	Kullback-Leibler
LEACH	Low Energy Adaptive Clustering Hierarchy
LM	Location Metadata
LOS	Line of Sight
M1	Mission Objective 1 – Threat Presence Detection
M2	Mission Objective 2 – Threat Geo-location
MAC	Medium Access Control
MB	Increased Belief
MD	Disbelief
MDP	Markov Decision Process
MF	Membership Function
MFP	Most Forward Progress
MOSN	Mission Orientated Sensor Network
n	Path Loss Exponent
$N_{Forward}$	Set of Forwarding Nodes
NLOS	Non-Line of Sight
NP	Neyman-Pearson
NRZ	Non-Return-to-Zero
OAPF	Opportunistic Any-Path Forwarding
P_F	Link Reliability in Forward Direction
P_h	Upper Link Reliability Limit ($PRR > P_h$)
P_l	Lower Link Reliability Limit ($PRR < P_l$)
P_R	Link Reliability in Reverse Direction
PDF	Probability Density Function
PL	Path Loss
POE	Position Observation Estimate
POMDP	Partially Observable Markov Decision Process
PPP	Poisson Point Process
PRR	Packet Reception Rate
P_R	Probability of Threat Presence
P_{RX}	Received Power in dB
P_T	Link Existence Probability
P_{TX}	Transmitted Power in dB
QoS	Quality of Service
QoSI	Quality of Surveillance Information
R_T	Communication Transmission Radius
RDF	Restricted Directional Flooding
RMS	Root Mean Square
ROI	Region of Interest
RWP	Random Waypoint Model
SA	Situation Awareness
SI	Swarm Intelligence
Sim	Similarity Function
SNR	Signal to Noise Ratio
SPRT	Sequential Probability Ratio Test
S_{RMax}	Maximum Sensing Range
SRF	Spatial Reuse Factor
SWOB	Swarm Intelligent Odour Based Routing
TBF	Trajectory Based Forwarding
TDMA	Time Division Multiple Access
TDOA	Time Difference of Arrival

TOC	Threat Observation Certainty
TRC	Transitional Region Coefficient
UAV	Unmanned Air Vehicle
UGS	Unattended Ground Sensor
WLANS	Wireless Local Area Networks
WSNs	Wireless Sensor Networks

Glossary of Terms

Autonomic	Self-managing and self-organisation features used, in order to enhance application-orientated decision making and collaboration within UGS networks, in a distributed manner.
Content	A network transport mechanism that is used to influence the routing and discarding of packets. Content can be named attributes of interest (e.g. ROI coordinates, CF values) and be used specifically to facilitate distributed forwarding tasks and UGS collaboration through in-network processing.
"Context"	Understanding generated by deployed UGS nodes about their local surveillance environment. This is derived from sensing samples, using situation awareness level 2 operations. "Context" in this sense can then be used to characterise the current mission objective situation.
"Context-Aware"	UGS networks become "context-aware" when they can use their derived "context" to provide relevant surveillance information, where relevancy depends on the mission objective in hand and adapt their behaviour (e.g. for collaboration or transmission control) according to the awareness they have regarding their "context".
Greedy Based Forwarding	A routing technique, which selects the best forwarding neighbour that can provide the most progress of a packet towards an intended destination, according to the routing strategy employed.
In-Network Processing	The ability for UGS nodes to perform local processing of set protocol layer instructions, in order to achieve computation load balancing across the UGS network and facilitate distributed UGS collaborative behaviour.
k-connectivity	A network is said to have *k-connectivity* (k = 1, 2, 3…n) if for each node pair there exists greater than or equal to k mutually independent connectivity paths connecting them.
Mission Objective	A required objective (task) to be completed by the deployed UGS network. Mission objectives could entail threat presence detection, threat geo-location or threat classification capabilities.
Mission Objective "Context"	Through SA Level 2 operations, the level of understanding ("*context*") generated and derived by an UGS from its local surveillance environment concerning a particular mission objective in question.
Mission Orientated Sensor Network	A self-reconfigurable sensor network, capable of jointly understanding mission objectives and adapting to the dynamics of an uncertain physical environment.

Network Centric Capability	A network centric capability approach allows deployed *UGS* networks to self-manage their behaviour in response to dynamic environmental changes.
Odour Plume	The structure and dispersion of odour (pheromone) concentration levels from an odour source. Plumes are created when odour molecules released from their source are taken away by environmental forces, for example, due to a prevailing wind direction.
Olfactory Sensing	The way in which biological systems sense, detect and make decisions regarding pheromones of interest.
Opportunistic Forwarding	Exploiting the broadcast nature of wireless transmissions to create packet forwarding transmission opportunities, under an error prone wireless channel environment.
Pheromone	A biological chemical signal factor secreted by social insects that trigger social responses in members of the same species. This could be to identify paths towards a food source or to notify other members of approaching dangers.
Plume Traversing	The ability of social insects to follow plume odour concentration levels directly to its source, by way of maintaining consistent contact within an odour plume for guidance purposes.
Situation Awareness	Situation awareness is the perception of environmental elements within a dynamic and uncertain volume of time and space, the comprehension of their meaning and the projection of their status in the near future.
Stigmery	The specific social and coordination of tasks undertaken by social insects in the natural world, in response to pheromone concentrations.
Tactical	A *C2ISR* defined procedure or strategy to successfully complete an overall mission so that a threat can be nullified or restricted, in order to achieve strategic advantage.
Threat Observation Certainty	The variation in the mean separation between μ_{FAST1} and μ_{FAST0}, including μ_{SLOW1} and μ_{SLOW0} probability occurrence distributions, as shown in figure 3.2.
Unicast	Unicast transmission is the sending of messages to a single node destination identified by a unique address.

CHAPTER 1

Introduction

With the advent of intelligent electronic devices becoming cheaper and more reliable with integrated functionality (i.e. sensing, computation, actuation and communication components), this has led to them becoming more ubiquitous in daily life. Wireless sensor networks are one example of this new ubiquitous computing trend and represent a powerful new data paradigm [1]. With advancement in autonomous, battery operated sensing platforms, multi-modal sensor based systems are becoming powerful sources of information that support a wide collection of intelligent applications [2]. Examples of these intelligent applications can range from environmental and habitat study, battlefield surveillance and reconnaissance, emergency environments for search and rescue, manufacturing environments for condition based monitoring and in buildings for infrastructure health assessment [1-3]. Until recently, wireless sensor networks have also been actively studied as a means of creating smart homes, patient monitoring services and body sensor networks [4]. The rise and use of wireless sensor networks in these applications is credited to their ability to share information, which ultimately enhances an end user's awareness and perspective of a current monitored environment. In addition, user interaction can be minimised further by allowing sensor networks to perform application-specific tasks autonomously, leading to the notion of wireless "sensor-actuator" networks [5].

In military scenarios, wireless unattended ground sensor (*UGS*) networks are usually deployed to support mission objective surveillance capabilities such as threat presence detection, classification and geo-location within a security-sensitive region. The

information they generate can enhance the decision making capabilities of command control, intelligence, surveillance and reconnaissance (*C2ISR*) *tactical* mission planning. This can lead to the necessary advantages in providing a relevant, timely and concise view regarding threat monitored activities [6]. *UGS* network surveillance in military scenarios, however, present challenges for application and network protocol developers because of their dynamic operating environments. Such environments are characterised by their ad-hoc nature, unstable wireless communication links with limited bandwidth, coupled with a changing threat situation. In addition, *UGS* devices are also inherently limited by their sensing, computation and communication capabilities, which are dictated by their battery energy reserves. Deployment of *UGS* devices is usually conducted in a covert manner, making device battery replenishment difficult, due to sensors being inaccessible for long periods of time within the surveillance field [7].

Operational effectiveness for *UGS* surveillance missions, however, can be enhanced through Network Centric Capability (NCC). Within the defence research community, NCC or Network Centric Warfare (NCW) refers to the "coming-together" of multiple networks of deployed assets, so that mission-critical objectives can be completed seamlessly. The idea of NCC stems from the fact that networks should have an ability to self-adapt to a changing mission objective environment, in a similar way business organisations might adapt their processes to a changing competitive space [8]. One of the similarities to draw from this comparison is that without changes in the way an organisation does business, it is not possible to leverage the power of information to create superior advantage [9]. A deployed *UGS* network is just one part of the overall combined NCC environment, and so applying a similar self-awareness methodology to support the overall NCC goal is equally important. In this thesis, we consider both the application interface and networking technologies required to achieve an NCC mode of operation within a distributed *UGS* surveillance setting.

1.1 Motivation and Aims of the Work

The motivational aspects of this thesis can be depicted through figure 1.1, which illustrates a typical wide-area military surveillance scenario, with a number of deployed assets distributed within the surveillance field. Access to the wider NCC environment is made possible through the use of *tactical* communication links, which enables information to be shared between deployed assets in order to support surveillance activities and enhance overall mission success [10].

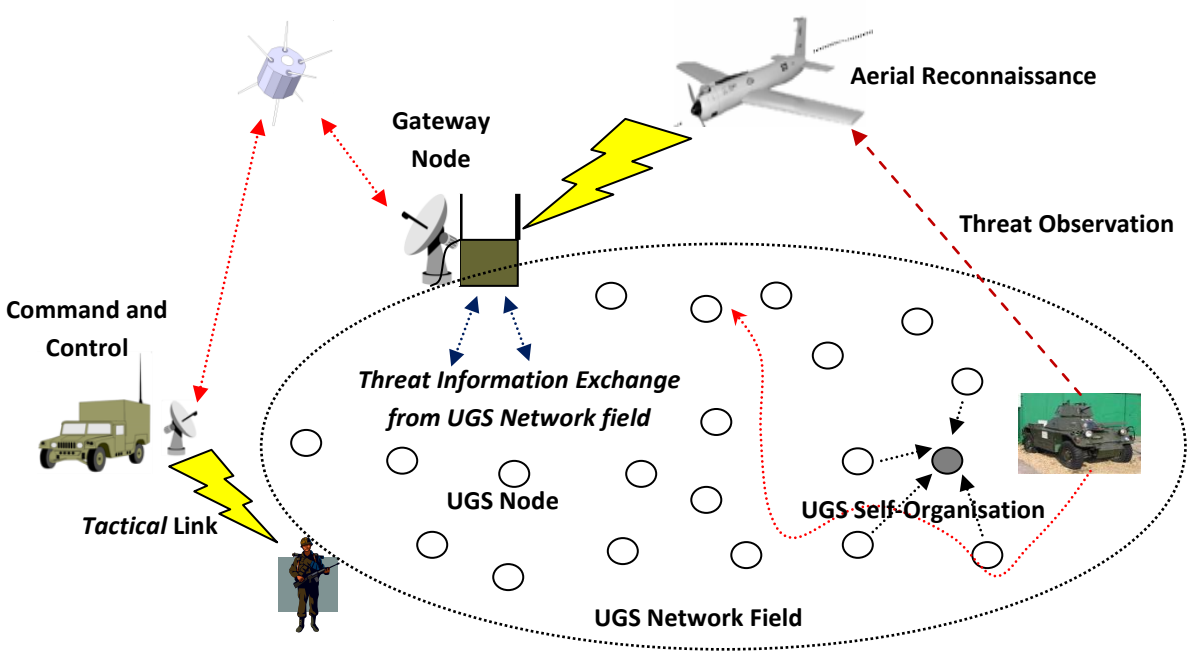

Figure 1.1: UGS surveillance scenario with links to the wider tactical networking environment

The aims of the work in this thesis, however, are mainly concerned with, and restricted to, the *UGS* network field and not the wider *tactical* networking environment, as shown in figure 1.1. From figure 1.1, *UGS* nodes are required to detect an imminent approaching mobile threat and be able to collaborate (self-organise) in order to provide timely, relevant and specific mission objective information (e.g. current threat presence detection confidence (%) and location), as the threat traverses the *UGS* network field. Information concerning the threat is typically relayed back to a gateway node located in the far-field region of the network for further evaluation purposes, and so *UGS* nodes must

also be able to support a multi-hop routing functionality. In addition, both sensor collaboration and multi-hop routing functions need to be made robust within an unstable and network resource constrained wireless environment, without reliance on any pre-existing centralised architecture. In essence, this requires deployed sensors to have an embedded and distributed mode of operation, which can enable them to make controlled self-adjustments in response to dynamic environmental changes. In this thesis, a dynamic environmental change refers to both a changing threat monitored situation and underlying wireless channel environment. With this in mind, the aims of the work presented in this thesis can be framed appropriately in terms of the communication protocol layer stack: namely at the application, network, data link and physical layers, as detailed in table 1.1 and illustrated further in figure 1.2.

Aims of the Work	**Key Features Developed**
1. Distributed Sensor Management (*Application Interface*)	• UGS's supporting a "**problem driven collection**" approach (e.g. forming dynamic groups that can best meet the objectives of a mission at a particular point in time), based on decisions derived from the shared surveillance environment. • Adaptive, application-orientated, network control in support of both timely surveillance utility provision and network resource management.
2. Geographic Routing (*Networking*)	• Employing efficient network topology control to support network resource savings, whilst ensuring that information is routed reliably within the UGS network field.
3. Robustness in surveillance information provision (*Physical*)	• Making informed choices for robust packet transmission. • Providing a channel aware decision making capability, to support reliable node selection for information forwarding.

Table 1.1: Aims of the research work in support of UGS network field operations, as shown in figure 1.1

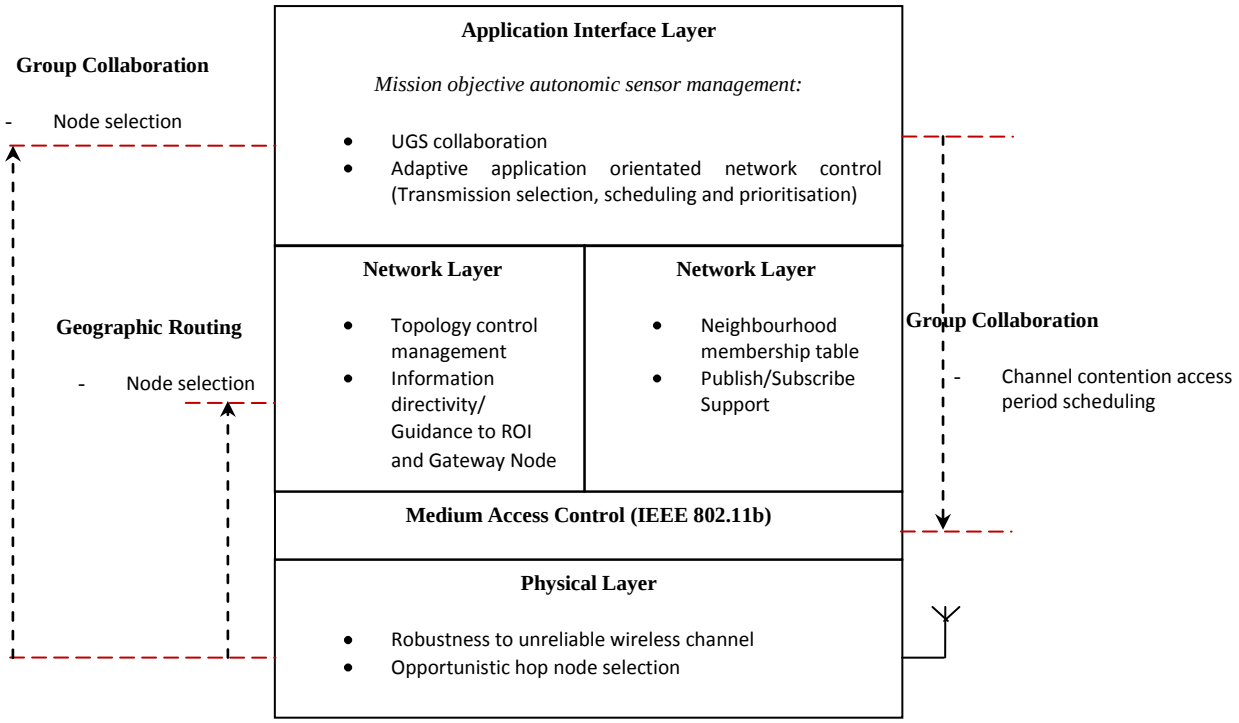

Figure 1.2: Aims of the research work in terms of the communication protocol layer stack

Table 1.1 details the key features which have been developed in this thesis to enable an *UGS* NCC perspective, within a dynamic mission-orientated environment. From table 1.1 and figure 1.2, the key focus points of this thesis can be summarised below:

- Providing distributed sensor management, according to the understanding ("*context*") derived from the shared mission objective surveillance environment.
- Ensuring the efficient management of operational network resources within both autonomous surveillance and geographic routing functionalities. In this thesis, network resources refer to both communication energy and bandwidth consumption and are considered as a means of, improving the overall network longevity goal.
- Providing a means of adapting to mitigate an unreliable wireless channel environment and integrating this within both sensor management and geographic routing functionalities, to assist their respective operations.

To enable the aims of the work presented in this thesis and as detailed in table 1.1, we have adopted the following assumptions:

- For surveillance purposes, we simulate a wide area scenario that encompasses a total area of 1×10^6 m^2 (i.e. 1km by 1km region).
- *UGS* sensing and transmission radii are equal in range. For medium access control, we use the IEEE 802.11b protocol in basic access mode.
- *UGS* nodes have GPS capability, in order to determine their position coordinates within the surveillance network field.

Our application interface development, assumes:

- A single threat presence scenario, where threat mobility is simulated using linear and random waypoint models. We focus only on threat presence detection and geo-location mission objectives and assume that threat classification algorithms are already present, for identification purposes.
- The number of *UGS* nodes used in the simulation study ranges from 5-60 and they are randomly deployed, in order to reflect a realistic scenario. In essence, the majority of the simulations conducted in this thesis are only concerned with low network density conditions and sensors that are capable of large stand-off distances (i.e. can achieve large sensing ranges).
- *UGS* devices have a fixed sensing range and we do not consider the effects of sensor modality (e.g. acoustic or seismic types) or the use of multi-modal sensors on surveillance performance.
- We assume location mechanisms are running (e.g. Time Difference of Arrival) on each *UGS* device, in order to deduce a current threat location, which can then be applied to our sensor collaboration algorithms. We do not include the effects of the additional

signalling overhead required for the location mechanism, in our performance evaluations.

Our geographic routing scheme development, assumes:

- We simulate under high network density conditions (i.e. node numbers ranging from 350-650). This is different from our main aim, which assumes low network density conditions but, in order to gauge the performance effects of integrating topology control within a geographic routing scheme, it was evident that this could only be illustrated appropriately under high network density scenarios.

Our channel aware development, assumes:

- Channel unreliability can be simulated using only large-scale and large-small-scale propagation fading models.

1.2 Organisation of the Thesis

Following this introductory chapter a common structure is employed throughout this thesis. The work presented addresses three separate aims, as detailed in table 1.1. It was found to be more appropriate that the thesis be organised into sections which address each of the aims detailed. Each section opens with an introductory part, detailing its contents and is concluded with a summary of the main contributions of the section. The exception is chapter 13, which concludes this thesis with a brief discussion of its main findings, followed by an outline of relevant areas that should be considered for further work and investigation.

In section 1, the first of our aims, namely distributed sensor management in support of autonomous surveillance is detailed. The work that has been conducted to support this section has been organised into the following five chapters:

- In chapter 2, an overview of the general system characteristics related to distributed surveillance operations is given. A review of other schemes that can support sensor

collaboration within a threat presence detection and geo-location sphere are also detailed. Chapter 2 then finishes with a general discussion on the fundamentals of our proposed *autonomic* approach to enable distributed *UGS* network management.

- Chapter 3 is concerned with the first part of our intended *autonomic* system, using the framework introduced in chapter 2. The chapter begins with an overview of the need to efficiently detect, verify and acquire information about potential threats within an uncertain (i.e. false-alarm) surveillance environment. This is then followed by a description of our developed situation assessment system, named PORTENT, based on a strategy, which combines a "fast" and "slow" threat detection approach. We then outline how we characterise threat presence detection information and finally, demonstrate PORTENT performance results.
- In chapter 4, the remaining parts of our developed *autonomic* system, named VIGILANT, are developed. VIGILANT, through integrating PORTENT operation is concerned with comprehending the uncertain surveillance environment and this is made possible through using Bayesian Belief Network (BBN) analysis. This is useful in the sense that uncertainty can be filtered through the BBN, as the decision to initiate a particular action is approached. This could entail initiating a group formation response for sensor collaboration, concerning a particular mission objective in question. The novelty in this chapter is addressed in terms of how the derived understanding ("*context*") can be further used, with additional processing functions, to manage network resource consumption and enable transmission control. Finally, VIGILANT performance results within a dynamic threat monitoring scenario are then given.
- In chapter 5, an improvement on VIGILANT is made. Here our VIGILANT^{+} system is concerned with extending our BBN network to jointly cater for threat presence detection and geo-location mission objectives and developing a means of supporting,

distributed transmission control functionality. The novelty of this chapter is the use of confidence measures, generated with our BBN, to facilitate autonomous mission objective assignment and distributed transmission control. In addition, we have modelled how understanding ("*context*") of the mission objective environment can be projected using a temporal Markov decision process (MDP). This facilitates better transmission control, as a direct relationship, in terms of the dynamics of a monitored threat situation. Performance appraisals of using a temporal Markov decision process within a simulated and test-bed environment are also given. The last part of this chapter is then concerned with managing how and when transmission control decisions should be taken within the temporal frame in order to avoid unnecessary transmission responses.

- In chapter 6, a summary with the main conclusions drawn from section 1, is then given.

In section 2, the second of our aims, namely geographic routing to support distributed surveillance operations, is detailed. The work that has been conducted to support this section has been organised into the following two chapters:

- In chapter 7, an overview of geographic routing principles is given and reviews of other applicable geographic routing schemes, which can be applied to a distributed surveillance type scenario, are further detailed. The chapter then begins to focus on our intended approach to facilitate geographic routing. Our approach has taken inspiration from how social insects (i.e. ants) may communicate to other nest members, the intended routes towards particular sources (i.e. food) of interest. This broad area of applying natural principles to routing protocols is commonly referred to as, "Swarm Intelligence". A discussion on how we intend to use "Swarm Intelligence" to a distributed surveillance scenario is given and subsequently, the remainder of the chapter concerns the development of our **SW**arm Intelligent **O**dour **B**ased Routing (*SWOB*) protocol. Specifically, the novelty of this chapter is addressed in how *SWOB*

routing uses a trajectory model to mimic the effects of odour dispersion found in nature, which can then be further used to guide (i.e. route) packets towards an intended destination (i.e. gateway node or a region of surveillance interest). The trajectory model itself can also assist as a means of, restricting direct communication to a certain number of neighbours, which are to be found within a nodes transmission radius. This can directly act as a means of, integrating network topology control within a geographic routing functionality. Finally, the chapter finishes with results concerning *SWOB* routing performance.

- In chapter 8, a summary with the main conclusions drawn from section 2, is then given.

In section 3, the third aim of this thesis, namely providing a packet forwarding mechanism, which can provide adaptability towards the unreliable channel environment, is detailed. The work that has been conducted to support this section has been organised into the following three chapters:

- In chapter 9, we begin by detailing the wireless propagation models that are used to portray channel unreliability with transmission distance. The chapter then utilises a common communication link reliability measure, namely the Transitional Region Coefficient (TRC), which can be used to describe current received channel reliability conditions. An analysis of the effects of the TRC on the optimal forwarding distance, transmission reliability and expected transmission count is then undertaken. This is conducted in order to help us to better understand the impact of the channel environment on communication link reliability. Our analysis of the TRC is then extended further to a realistic broadcast wireless channel environment. This is considered as a means of encouraging packet forwarding opportunities which might arise due to the nature of the broadcast environment.
- In chapter 10, the analysis of the TRC, made in chapter 9, is then utilised as a means of, developing an overall packet forwarding decision making mechanism. The chapter

begins by giving an overview into the fundamentals of a fuzzy logic system, which is used as the packet forwarding decision making mechanism. The novelty in this chapter is addressed in how the TRC can be integrated into an overall channel-aware fuzzy logic node selection scheme. Fuzzy logic addresses the uncertainty of the channel environment, through its membership functions. The second novelty of this chapter then addresses how the membership functions can be adapted using a genetic algorithm, according to current received channel characteristics (i.e. the TRC). It is shown that adapting membership functions, according to received channel characteristics can help to improve overall decision making performance, with regards to packet forwarding, when compared with normal fuzzy logic operation.

- In chapter 11, a summary with the main conclusions drawn from section 3, is given.

In section 4, a performance evaluation of the work from section 1 and 2 within an error prone wireless environment, is detailed. In chapter 12, an integrated performance study is conducted involving sections 1 and 3. This is then followed by a similar evaluation involving sections 2 and 3. Chapter 12 then concludes with a brief summary and the main conclusions to be drawn from this integrated system performance study.

Finally, chapter 13 concludes the thesis with a brief discussion of its main findings followed by an outline of areas where further research, may be appropriate.

1.3 Main Contributions

The contributions of this thesis can be categorised under headings of the three main sections of work addressed.

Section 1 - Distributed Sensor Management

- First experimental demonstration and application of the situation awareness (SA) framework to an *UGS* surveillance network management problem. The SA framework has the advantage of addressing the distributed sensor management problem effectively, through an integrated approach. Results show the advantage of using a SA approach for sensor management in terms of preventing "false alarm" detection and establishing relevant "*context*" of a mission objective environment for *autonomic* decision making.
- Proposed a new threat detection system, which combines the use of both a "fast" system using standard signal detection theory and a "slow" system, using the sequential probability ratio test. Results demonstrate that in combining the "fast" and "slow" threat detection approaches, we improve on event detection delay and QoSI performance, when compared with independent "fast" and "slow" operations and normal binary threat detection means.
- Proposed a new approach to enable derived mission objective *"context"* to be processed and used to establish an overall *"context-aware"* ad-hoc collaboration mechanism. The proposed certainty factor evaluation approach allows the grouping of immediate neighbours that share similar *"context-aware"* confidence levels, in a current mission objective situation. Results show that our *"context-aware"* collaboration approach reduces the impact of outliers which improves overall group surveillance performance, when compared with schemes that utilise all deployed neighbourhood sensors (or avoid the use of "*context-awareness*").
- Development of a new fully *autonomic* transmission control capability through the use of a Partially Observable Markov Decision Process (POMDP). Results show that the advantages of a POMDP approach are the reduction in reducing communication energy

consumption and surveillance update latency further, compared with centralised transmission control approaches, without compromising mission objective performance.

Section 2 - Geographic Routing to Support Distributed Surveillance

- Development of a new network topology control scheme, which adjusts to current deployed network node density conditions. We demonstrate that a desired level in topology control can be achieved and adapted through setting a desired *k-connectivity* requirement. Our experimental evaluation shows the benefits of incorporating the *k-connectivity* topology control methodology within our geographic routing scheme to achieve better throughput and energy efficiency performance, especially in conditions with increasing network node density, when compared with traditional "most forward progress" routing and restricted directional flooding schemes.

Section 3 - Channel Aware Packet Forwarding

- A new channel aware packet forwarding system, which combines the transitional regional coefficient within a genetic adaptive fuzzy logic scheme. Our experimental evaluations demonstrate that, under *opportunistic forwarding* conditions, this can enable *UGS* nodes to make relevant self-managed decisions on neighbour selection, for reliable packet forwarding. Results also show the advantages of our proposed approach in achieving dependable mission objective information collection under different channel fading conditions and an improvement in throughput and energy efficiency performance, over schemes with limited channel reliability knowledge.

1.4 List of Publications

The research work outlined in this thesis has led to a total of 10 publications and presentations being made at national and international conferences. These are listed in order of most recent publication date, as shown below:

1. Ghataoura, D.S, Mitchell, J.E. and Matich, G.E. "VIGILANT^{+}: Mission Objective Interest Groups for Wireless Sensor Network Surveillance Applications", IET Wireless Sensor Systems Journal, vol.1, no.4, pp.229-240, December 2011.

2. Ghataoura, D.S, Mitchell, J.E. and Matich, G.E. "Autonomic Control for Wireless Sensor Network Surveillance Applications", The 30th IEEE International Conference on Military Communications (MILCOM), Baltimore, Maryland, USA, 7^{h} – 10th November 2011.

3. Ghataoura, D.S, Mitchell, J.E. and Matich, G.E. "Networking and Application Interface Technology for Wireless Sensor Network Surveillance and Monitoring", IEEE Communications Magazine, vol.49, no.10, pp.90-97, October 2011.

4. Ghataoura, D. S., Mitchell, J. E. and Matich, G. E., VIGILANT: "Situation-Aware Quality of Information Interest Groups for Wireless Sensor Network Surveillance Applications", Unmanned-Unattended Sensors and Sensor Networks VII, Vol. 7833, European SPIE Defence and Security, SPIE-International, Toulouse, France, September 2010.

5. Ghataoura D.S., "An Architecture to Support Mission Orientated Wireless Sensor Network Surveillance Applications", London Communications Symposium (LCS), University College London, September 2010.

6. Ghataoura, D.S., Yang, Y., Mitchell, J.E. and Matich, G.E. "PORTENT: Predator Aware Situation Assessment for Wireless Sensor Network Surveillance Applications", Cyber Security, Situation Management, And Impact Assessment II, Vol. 7709, SPIE-Defence, Security and Sensing, SPIE-International, Orlando, Florida, USA, April 2010.

7. Ghataoura, D.S., Yang, Y. and Matich, G.E. "SWOB: Swarm Intelligent Odour Based Routing for Geographic Wireless Sensor Network Applications", The 28th IEEE International Conference on Military Communications (MILCOM), Boston, USA, 18th – 21st October 2009.

8. Ghataoura D.S., "Quality of Information and Efficient Delivery in Military Sensor Networks", London Communications Symposium (LCS), University College London, September 2009.

9. Ghataoura, D.S., Yang, Y. and Matich, G.E. "GAFO: Genetic Adaptive Fuzzy Hop Selection Scheme for Wireless Sensor Networks", The 5th International conference on Wireless Communications and Mobile Computing (IWCMC), Wireless Sensor Networks Symposium, Leipzig , Germany, 21st -24th June 2009.

10. Ghataoura, D.S., Yang, Y. and Matich, G.E. "Channel Aware Fuzzy Logic Hop Selection for Wireless Sensor Networks", The 16th International Conference on Telecommunications (ICT), Marrakech, Morocco, 25th – 27th May 2009.

SECTION 1

Distributed Sensor Management

Introduction

Unattended ground sensor (*UGS*) networks are classified as distributed systems, capable of supporting *mission objectives*, such as threat presence detection and geo-location, within a security-sensitive region. The information they provide can enhance decision making abilities for command and control, intelligence, surveillance and reconnaissance (*C2ISR*) *tactical* mission plans, primarily because of their scalability property [11]. In addition, the inherently dynamic nature of surveillance missions does not allow time for manual system configuration. Distributed systems can address this concern by minimising the burden of a centralised processing architecture and by providing the necessary savings towards network resource consumption [11-12]. As a result of distributed operation, node failures can be tolerated and the operational longevity of the deployed *UGS* network field can be increased [11-13].

Managing the distributed *UGS* network to assist threat presence detection and geo-location capabilities, however, raises some interesting questions, for example:

- How do deployed *UGS's* decide they are suitable in meeting the objectives of a mission? Monitoring threats within the surveillance field is a dynamic process, which requires sensors to have actionable and precise decision making ability, in order to minimise the propagation of false alarms, event detection delays and mission objective inaccuracies [14-15].
- When and how do deployed sensors collaborate in order to fulfil a current mission objective successfully? A single *UGS* is not adequate to provide sufficient levels of

surveillance information, whereas many sensors collaborating towards a common objective are able to provide benefits such as, increased surveillance utility and reduction of both errors and the amount of redundant information being sent [16-17].

- How do deployed sensors conserve their key network operational resources without compromising the objectives of a mission? It is shown that investing in computation efforts within the network ("*in-network processing*") can have benefits towards saving on communication costs [18-20]. This can be achieved through *UGS* collaboration, as opposed to every node transmitting their independent information to an external processing point "at the edge" of the network field.

UGS nodes, which have an ability to make their own decisions regarding a specific mission objective, are more applicable towards supporting the questions raised above. In essence, a self-managed perspective would allow *UGS* nodes to be dynamically managed and tasked, so that the overall distributed *UGS* field is better able to perform surveillance on a region. The incorporation of self-managing features within the network, however, requires use of an *autonomic* framework [21]. For network management purposes, an *autonomic* framework would entail the implementation of application-orientated features, necessary to enhance both *UGS* decision making and collaboration in a distributed manner [21-23].

The primary goal for this section is to present a potential *autonomic* system that can assist distributed *UGS* surveillance network management. We focus on providing an *autonomic* system that supports both threat presence detection (*M1*) and geo-location (*M2*) capability. Our aim is also to incorporate self-management features that can enable *UGS* nodes to dynamically adjust their transmission behaviour to current mission objectives, while also ensuring that the overall information utility provided is not compromised. Our focus on transmission behaviour (transmission control) is geared towards the efficient management of network resources, primarily communication energy and bandwidth

expenditure. This can therefore enable a potential *autonomic* system that supports the long-term operational longevity requirement.

In this section, chapter 2 begins by introducing the general system characteristics related to distributed surveillance operations. Continuing in chapter 2, we identify other applicable schemes, which can support self-managing features for surveillance operations. In section 2.4, the fundamentals of our proposed *autonomic* framework to enable distributed *UGS* network management are introduced. Based on our proposed framework, chapter 3 explains the first part of our intended *autonomic* system. In chapter 4, we then detail the first of our developed systems termed, VIGILANT, incorporating a semi-*autonomic* approach towards distributed surveillance management. In chapter 5, we improve on VIGILANT and detail our fully *autonomic* system termed, VIGILANT^{+}, to enable a distributed self-managed perspective towards *M1* and *M2 UGS* surveillance. Finally in chapter 6, we summarise and conclude the main contributions of this section.

CHAPTER 2

Distributed Surveillance Operations

Distributed surveillance operations can be strengthened through distributed processing (*"in-network processing"*) and aggregation of such surveillance information [11-13], which encourages fault-tolerant behaviour and improvements in sensing accuracy [24-25]. Support for distributed surveillance operations is possible through *UGS* collaboration, according to a common mission objective [25]. Protocols and schemas that are designed to assist ad-hoc collaboration can, as a result, provide easily accessible and high-quality information concerning the mission objective environment. Before we can begin to develop application support protocols that promote ad-hoc collaboration, it is crucial for us first to specify the necessary design requirements, as described below:

- ***Group-initiator election:*** A group initiator (GI) is dynamically elected within a group of *UGS* nodes and as such, forms a final point for aggregation in mission objective information. A GI node can also assist as an accurate reference point within the surveillance field for other deployed nodes to base their level of information accuracy.
- ***Dynamics:*** GI-led ad-hoc groups must also provide adaptability according to the dynamics of a monitored threat, allowing sensors to leave and join at any time during a mission. This can help to encourage and maintain the most timely and relevant information concerning the monitored threat.
- ***Stability:*** To establish an accurate basis in information processing, the *GI* led group structure requires a level of stability to avoid undesirable fluctuations (i.e. non-applicable nodes joining or unexpectedly priority nodes leaving) during a monitored threat situation. Ensuring stability can help to achieve reliable levels in *M1* and *M2*

surveillance provision and overall improved utility for eventual *C2ISR* decision making.

- ***Group Initiator re-election***: Dynamic re-election of new GI's during a mission is imperative in order to maintain relevant surveillance report aggregation.
- ***System Energy Efficiency***: *UGS* nodes are typically restricted in their communication energy and bandwidth resources, therefore, non-essential communication overhead should be kept to a minimum in order to prolong network lifetime and encourage bandwidth efficiency.

In sections 2.1, 2.2 and 2.3 we identify other developed and applicable schemes, namely LEACH, DCATT and IDSQ. These schemes are highlighted because they are the most common schemes to be found in the *WSN* community that can support the system requirements described above. In addition, these schemes can also provide an appropriate performance comparison against our intended solution, detailed later in section 2.4.

2.1 Low Energy Adaptive Clustering Hierarchy (LEACH)

Clustering is a form of deterministic self-organisation (collaboration) used in ad-hoc sensor networks and it can be an effective technique for achieving scalability and prolonged network lifetime [26]. A well-known clustering algorithm for continuous, data-centric application gathering sensor networks is the LEACH mechanism [27]. LEACH partitions deployed nodes in a network into clusters and in each cluster a dedicated node, the cluster-head (CH), is responsible for maintaining a time division multiple access (TDMA) schedule for localised transmission control amongst its neighbouring nodes and data aggregation, which encourages stability within the cluster group.

CH election, equivalent to GI election, as described above, is conducted randomly and independently by each node on a per-round basis of a fixed duration. This helps to

reduce further both the required signalling traffic and communication overhead. Election of CH's can be managed accordingly to task driven criteria, such as battery energy level, transmission power and network connectivity [27-28]. Subsequently, GI re-election is also based on these criteria, in order to achieve a balanced rotation of CH's within the network and promote system energy efficiency.

In essence, LEACH is a distributed single hop application protocol, which can be adjusted for specific operation towards a desired mission objective. For example, CH election and re-election can be based on both *M1* and *M2* accuracy errors and CH's can act as a point for surveillance information aggregation, using a TDMA schedule. The main disadvantage of LEACH is its deterministic self-organisation operation, which makes it difficult to adapt to the dynamics of a monitored threat situation without changing the per-round CH election and group coordination phases.

2.2 Dynamic Clustering for Acoustic Target Tracking (DCATT)

In support of *M2* operation only, self-organisation (collaboration) to perform energy efficient threat geo-localisation is equally important [29-31]. DCATT [29] proposes a simple, distributed and dynamic clustering algorithm for geo-location operation. CH nomination is conducted in terms of a physical based localisation view, based on received signal energy levels from the sensing field, as shown in (2.1).

$$r_i = a.|| x - x_i ||^{-\alpha} + n_i \tag{2.1}$$

From (2.1), r_i is the received signal strength at the i^{th} sensor, a is the unknown signal strength from the source, x is the target position, x_i is the known position of the i^{th} sensor, α is the known attenuation coefficient, n_i is white Gaussian noise with zero-mean and variance σ^2. The fundamental principle applied in energy based approaches, as shown in (2.1), is that the signal strength energy of a received signal decreases exponentially with

propagation distance [22]. In DACTT, a CH is elected when the signal strength from (2.1), is detected by a distributed node and exceeds a pre-determined system threshold. This again utilises a metric derived from task-driven management approaches. As multiple sensors may also detect the energy signal above the pre-determined threshold, DACTT ensures ad-hoc group stability is maintained by only selecting the sensor that has the best probability in reducing *M2* inaccuracies. This can help to save on channel contention access delay and as a result, increases bandwidth re-usability.

Subsequently, the elected CH broadcasts an information solicitation packet asking neighbouring sensors to join the cluster and provide their sensing information. Received information is then used to estimate the location of the threat using energy-based localisation methods [33]. This, however, has the disadvantage of being only robust in the presence of moderate noise within the received signal and small movements in trajectory concerning the monitored threat [29]. Also, due to the energy based model, random rotation of CHs will be common if the sensing environment is corrupted with high levels of noise, leading to a potential degradation in *M2* surveillance performance and utility.

2.3 Information Driven Sensor Querying (IDSQ)

Both LEACH and DACTT are schemes that can support both *M1* and *M2* operations using mostly task-driven criteria for collaboration and management of network resources. A different take towards sensor collaboration and management of network resources is to consider an *information-centric* approach [34]. Ideally, sensors should be chosen for collaboration which can contribute the most information towards answering a specific mission objective, and generally this lies in the direction of the largest amount of information gain [34-35]. IDSQ, [35] is a scheme that incorporates *information-centricity*. From [35], the authors consider the goal in providing a location estimate of an event source, as accurately as possible (low estimation error), with as little energy consumption

as possible. This is useful in support of both stability and system energy efficiency requirements. The problem of choosing which sensors collaborate at the lowest communication energy cost becomes an optimisation problem and IDSQ frames this in terms of an objective function, M_{obj}, defined as a mixture of both information utility gain and cost, as shown in (2.2).

$$M_{obj}(Belief\ State) = \beta.\varphi_{Utility}(Belief\ State) - (1-\beta)\varphi_{cost}(z_j) \tag{2.2}$$

As shown in (2.2), $\varphi_{Utility}$ is an information utility measure, φ_{Cost} is the cost of communication in terms of the Euclidean distance and β is the relative weighting given to the utility and cost functions. M_{obj}, is defined as a function of the belief state, defined as a probability distribution describing each new sensor measurement taken, z_j, combined with the current estimate using measurements taken from z_1 to z_{j-1}, as shown in (2.3), where x represents the state of the target we wish to estimate.

$$Belief\ State = p(x|z_1,...,z_{j-1},z_j) \tag{2.3}$$

It is clear from (2.3) that adding further sensor observations will improve both the estimate and information utility gain. In IDSQ, an elected GI would then seek to request z_j measurements from its immediate neighbours and combine these with its own estimate, in order to form a current belief state concerning each respective neighbour. IDSQ selects the best neighbour for collaboration based on the sensor, which can provide the highest expected information utility measure, given by $\varphi_{Utility}$ *(Belief State)*. By convention a large $\varphi_{Utility}$ *(Belief State)* would indicate less uncertainty concerning the target state. If the belief state can be approximated well by a Gaussian distribution, then covariance-based information utility gain measures are suitable such as, the *Mahalanobis* distance measure [25-26].

Using information utility measures to decide on sensor collaboration and organisation has been shown to provide a faster reduction in estimation uncertainty and

usually incurs a lower communication overhead for meeting a given estimation error requirement, compared to blind or nearest neighbour sensor selection schemes [34-35]. Since IDSQ bases its sensor collaboration on information utility measures, this supports both group dynamic and stability requirements, primarily though for *M2* operation and not *M1*. In addition, the IDSQ energy cost model is only based on a simple Euclidean distance measure and does not include metrics within the objective function, M_{obj}, which promotes conservation of bandwidth consumption.

In section 2.4, we introduce our own proposed methodology in support of the system requirements given earlier, primarily through splitting the management of *UGS* surveillance operations into a three tier system.

2.4 Distributed Autonomic Surveillance Networking

In sections 2.1 and 2.2, both LEACH and DACTT can facilitate *M1* or *M2* capabilities. Both schemes also support ad-hoc collaboration but their mechanisms to enable this are, both deterministic in nature and reliant on task driven criteria for sensor management, which cannot actively adapt to the dynamics of a surveillance mission and its supporting objectives. In 2.3, IDSQ indicates that basing sensor collaboration on information utility maximisation can achieve better accuracy and is more attuned to the dynamics of a monitored threat, however, communication energy and bandwidth efficiency considerations are not placed as a priority. From these findings, a methodology, which can support both *information-centricity* through *belief state* evaluation and allow the consumption of network resources to be managed as a direct relationship, to the dynamics of a monitored threat, is much more suitable and adaptable towards a changing surveillance situation. A framework to support this relationship is achievable in terms of "*situation awareness*" (SA) [37].

In SA, entities are required to perceive their environment within which they are situated and based upon environmental dynamics, act out (actuate) plans they have developed, either through self-learning or system defined measures. SA is an application-orientated approach, offering a different perspective to common task driven criteria used for distributed sensor management. For surveillance network management purposes, this can be depicted through expanding Endsley's SA "tripartite" model [38]. As shown in figure 2.1 and described below, Endsley's "tripartite" model describes three levels, which contribute towards the overall current SA.

- ***Level 1-Perception***-involves the correct identification of entity elements (e.g. presence of a threat) as well as, the combined detection characteristics (e.g. accuracy, certainty and timeliness), representing a measure of the detection information captured by the distributed surveillance network [39].

- ***Level 2-Comprehension***-involves derivation of the significance associated with uncertain sensor data, enabling both a relevant decision making outcome and confidence in mission objective understanding ("*context*") to be achieved.

- ***Level 3-Projection***-the ability to project future *"context"* of the mission objective environment, based on potential association of the fragmented sensor data within a temporal frame.

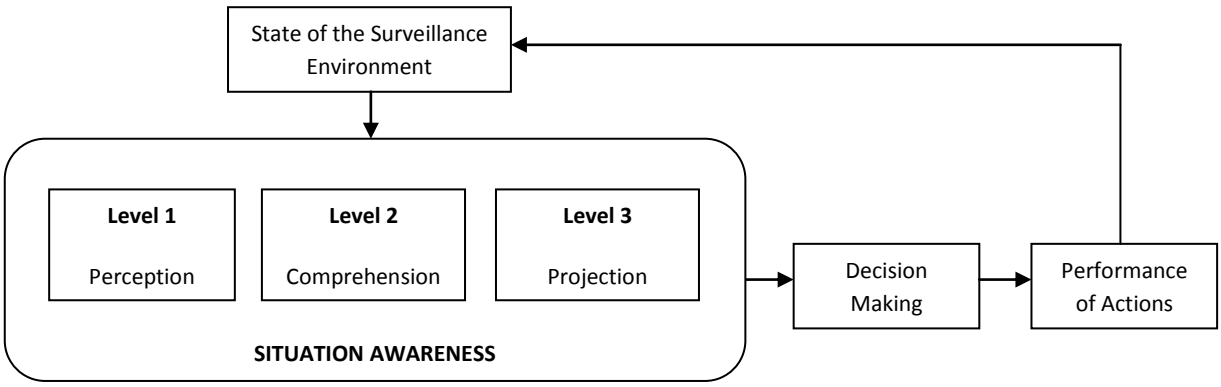

Figure 2.1: Endsley's model of situation awareness adapted for surveillance operations

As indicated in the section introduction, the primary goal for this section is the development of a potential *autonomic* system that can assist distributed *UGS* network surveillance management. This can be accomplished through using a SA framework in the following ways:

- *Level 1* and *level 2* can assist in dynamic and stable ad-hoc group collaboration, related to a current threat situation. Collaboration in this way is primarily focused on sensors perceiving correctly and establishing their localised *"context"* of the present situation (e.g. awareness to a threat), in order to allow *UGS* self-assignment to a particular mission objective.
- *Level 3* is useful in terms of enabling *UGS* nodes to self-manage their network resources according to, how the *"context"* concerning the monitored threat will change with time.

In the subsequent chapters that accompany section 1, we plan to evaluate the system performance of our developed SA framework against LEACH, DCATT and IDSQ which have been introduced earlier. To begin with, in chapter 3, the development concerning the level 1 part of our SA system, namely the perception model is described.

CHAPTER 3

Situation Assessment for Surveillance Missions

The focus of surveillance missions is to efficiently detect, verify and acquire information about potential threats within a specified region of interest. Common assessment systems used for threat detection rely on mechanisms using basic threshold values in order to define simple events that reduce detection accuracy or focus on the classification of event patterns, which reduce timeliness and do not prioritise false alarm rates [40-44].

The lack of consideration given to false alarms has an impact on level 1 perception success, as it affects positive threat detection performance. A low false alarm rate, which is needed to avoid unnecessary responses (e.g. GI election), involves a larger sample set being collected for threat verification. This implies greater sampling energy consumption and reduced timeliness [42]. Threat situation assessment systems that can incorporate a self-adjustable sensitivity towards different sensing environment uncertainties are therefore beneficial. This would also accommodate scenarios where both a higher degree of sensitivity is also desired, in order to capture all potential threats and especially where larger standoff ranges (i.e. sensing ranges) are required. In sections 3.1 to 3.6, we detail our proposed distributed situation assessment system named, PORTENT, is described which is able to model and detect potential threats within an uncertain surveillance environment.

3.1 PORTENT Situation Assessment System

Situation assessment for real-world threat detection purposes can be related to how mammals in the natural world perceive and assess potential threats towards them. Mammals have always dealt with ambiguous sensory information to determine whether predators are present or not [45]. Subsequently, through the processing of threat related

sensory observations, mammals would then initiate a suitable defensive response [45]. Mammalian species, however, have evolved at least two distinct methods in dealing with signals of threat via sensory inputs for threat detection purposes [45-46]. It has been found that almost all sensory data in mammals gets routed for a "fast" threat indication and separately to a "slow" system which offers more accurate processing function for detailed examination [46]. This provides inspiration to assume that a potential situation assessment system for *UGS* surveillance can also be comprised of decision making components that are able to process sensory data in different ways and be allowed to function at different speeds. In figure 3.1, a potential architecture, which can form the basis of emulating a "fast" and "slow" threat situation assessment system, is shown.

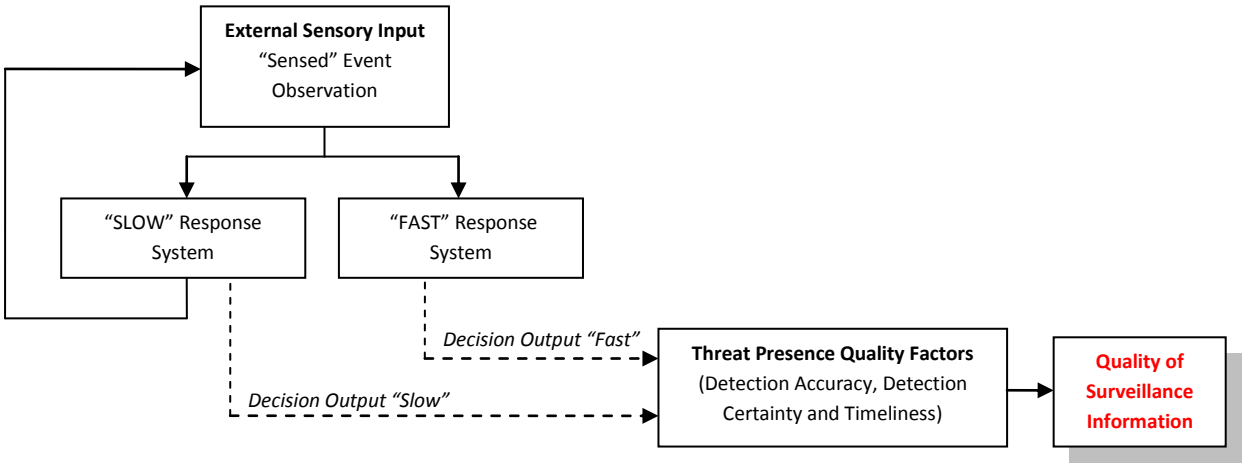

Figure 3.1: PORTENT situation assessment architecture

From figure 3.1, the "fast" system would receive a limited number of samples to base its positive detection outcome, whereas the "slow" system would continue to receive samples until a similar outcome can be achieved. In the subsequent headings, we detail the various building blocks associated with figure 3.1. In section 3.2, we begin by detailing a sensing model to realistically portray the external sensory input observations to be used by the PORTENT system.

3.2 Sensing Model

Performance of situation assessment systems can be affected by factors such as sensor type (e.g. acoustic, seismic or infra-red), sensing environment and threat related factors, such as: threat-to-sensor distance, propagation characteristics and the motion pattern of the threat [42-43]. A common approach in simplifying these factors is to assume a simple binary sensing detection model [44]. Here the sensor detects a threat with probability of one only if the threat-to-sensor distance, $\boldsymbol{d}$, is below a threshold distance, $\boldsymbol{d_t}$, as shown in (3.1) and zero otherwise.

$$S(p,q) = \begin{cases} 1 \ : \ ||p-q||_2 \leq d_t \\ 0 \ : \ Otherwise \end{cases} \tag{3.1}$$

Accordingly in (3.1), the relationship for threat detection, *S (p, q)*, is defined in terms of the sensor node position at position $\boldsymbol{p}$, observing an event at position $\boldsymbol{q}$, where $||.||_2$ is the Euclidean distance between them. Such a simplification where $\boldsymbol{d}$ alone determines threat detection is acceptable for indoor deployments and where a line of sight can be guaranteed [43]. However, in outdoor settings, such as *UGS* networks, signal quality is dependent on the propagation environment and for this reason a better sensing model is required for realistic situation assessment design. This can be achieved if we assume that the sensing signal characteristic is an exponentially decaying function of $\boldsymbol{d}$ [42] [47]. For our proposed PORTENT system, a function to depict a realistic sensing input observation model is shown in (3.2). From (3.2), it is shown that the need for both $\boldsymbol{d}$ and $\boldsymbol{d_t}$ is minimised and the sensing model itself becomes a direct relationship with the maximum sensing range, S_{RMAX}, employed and $||.||_2$.

$$S(p,q) = \begin{cases} \left(1 + e^{b_1\left(\frac{\frac{S_{RMAX}}{2} - ||p-q||_2}{\frac{S_{RMAX}}{2}}\right)}\right) \times \frac{1}{1+e^{b1}} & if\ (0 \geq ||p-q||_2 \leq \frac{S_{RMAX}}{2}),\ b_1 = \ln 3 \\ \left(e^{-b_2\left(\left(\frac{2*||p-q||_2}{S_{RMAX}}\right) - 1\right)}\right) \times 0.5 & if\ (\frac{S_{RMAX}}{2} \geq ||p-q||_2 \leq S_{RMAX}),\ b_2 = 3.91 \end{cases} \quad (3.2)$$

For the purposes of our situation assessment model, we assume only one possible threat is present and therefore, the probability of there being no threat present is (1- *S (p, q)*), where *S (p, q)* is given, as shown in (3.1) or (3.2). In headings 3.3 and 3.4, we detail how the *S (p, q)* relationship can be integrated to form part of the overall "fast" and "slow" threat response system models, in accordance with figure 3.1.

3.3 Fast Response System Model

We represent the initial received set of sampled signals, *x*, by the "fast" response system as normally distributed according to $N\ (\mu_{FAST1},\ \sigma^2_{FAST})$ or $N\ (\mu_{FAST0},\ \sigma^2_{FAST})$ depending upon whether, a threat is present or not respectively, as shown in figure 3.2. The PORTENT "fast" response system model can then be formulated in terms of, standard signal detection theory [48]. The basis for standard signal detection theory relies upon a general detection pay-off matrix, a critical detection threshold, $L(x_0)$, for the initial signal *x* and an observation criterion, $L(x)$. The decision at any stage for "fast" detection depends upon the pay-off values for correct detection ($V_{SN,Y}$), incorrect rejection ($V_{SN,N}$), false alarm ($V_{N,Y}$) and correct rejection ($V_{N,N}$), as shown in table 3.1, in the form of a general pay-off matrix where P_R is the probability of a threat being present, given by *S(p, q)*, in (3.1) or (3.2). Using the pay-off matrix of table 3.1, the critical threshold for initial signal level *x*, $L(x_0)$, as shown in figure 3.2, is given in (3.3).

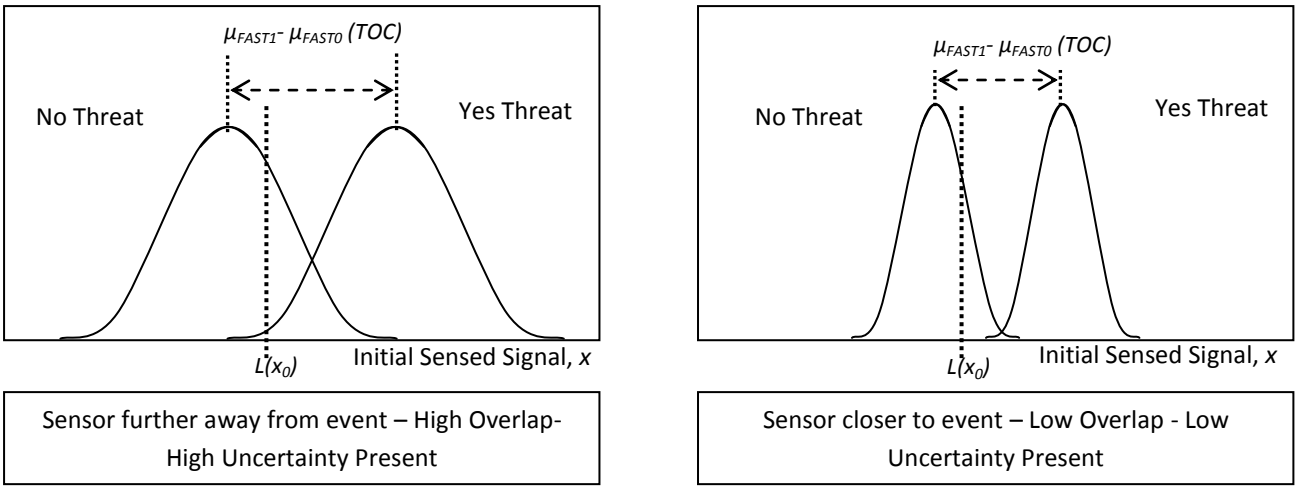

Figure 3.2: Probability of occurrence curves presented to the "fast" response system

EVENT	**RESPONSE**: Positive Detection	**RESPONSE**: No Detection
THREAT (P_R)	*"CORRECT DETECTION"* ($V_{SN,Y}$)	*"INCORRECT REJECTION"* ($V_{SN,N}$)
NO THREAT (1-P_R)	"*FALSE ALARM*" ($V_{N,Y}$)	"*CORRECT REJECTION*" ($V_{N,N}$)

Table 3.1: Pay-off matrix for PORTENT "fast" system response detection

$$L(x_0) = \frac{(1-P_R)}{P_R} \times \left[\frac{V_{N,N} - V_{N,Y}}{V_{SN,Y} - V_{SN,N}} \right] \tag{3.3}$$

The decision rule for taking a positive detection response action, depends on the observation criterion, *L(x)*, formulated in terms of a probability ratio concerning the present observed event, as shown in (3.4).

$$L(x) = \frac{p(Positive\ Detection \mid Threat\ Event)}{p(No\ \ Detection \mid No\ Threat\ Event)} = \frac{1 - E\left(\frac{L(x_0) - \mu_{FAST1}}{\sigma_{FAST}} \right)}{1 - E\left(\frac{L(x_0) - \mu_{FAST0}}{\sigma_{FAST}} \right)} \tag{3.4}$$

In (3.4), $E(.)$ denotes the cumulative distribution function for the standard normal distribution. The decision on whether to invoke a positive detection action can be based on the likelihood-ratio criterion, $L(x)$ and $L(x_0)$, as shown in (3.5).

$$IF \quad L(x) > L(x_0) \quad THEN \quad "Yes: Take Positive Detection Action" \tag{3.5}$$

3.4 Slow Response System Model

The PORTENT "slow" response mechanism, forming an extensive situation assessment system, is best framed using the sequential probability ratio test (SPRT), in terms of the Neyman-Pearson (NP) detection threshold [49-50]. The SPRT approach utilises two alternative hypotheses representing the presence and absence of a threat, while updating the relative likelihood ratio of each as new sensory samples arrive. The PORTENT "slow" system design is based on using the following alternative hypotheses:

H_0: Likelihood of threat presence is low gather additional sensory data (Null Hypothesis)

H_1: Likelihood of threat presence is high that "positive detection" action should be taken

Assuming that an *UGS* receives a sequence of sampled values from the surveillance environment, if no threat is present, each sampled value, $x_{i\ (No\ Threat)}$, is an independent, identically distributed random variable from a normal distribution, $N(\mu_{SLOW0}, \sigma^2_{SLOW})$. If a threat is present each sampled value, $x_{i\ (Threat)}$, is an independent, identically distributed random variable from a normal distribution, $N(\mu_{SLOW1}, \sigma^2_{SLOW})$. We always assume $\mu_{SLOW0} < \mu_{SLOW1}$. After a series of ***n*** sensory samples have been taken within a time period, *t*, the relevant information captured by the sensor, can be expressed as a cumulative sum of log-likelihood ratios, $Z(n)$, as shown in (3.6).

$$Z(n) = \sum_{i=1}^{n} q_i \quad where \quad q_i = ln\left[\frac{f_1(x_{i(Threat)})}{f_0(x_{i(No\ Threat)})}\right] \tag{3.6}$$

In (3.6), $f_1\ (x_{i\ (Threat)})$ denotes the probability density of signal, $x_{i\ (Threat)}$, when a threat is present and likewise $f_0\ (x_{i\ (No\ Threat)})$ denotes the probability density of signal, $x_{i\ (No\ Threat)}$, when no threat is present. A decision in favour of either H_0 or H_1 is made by comparing the updated ratio, $Z\ (n)$, against the NP detection threshold (sensitivity), which is designed to self-adjust in order to maximise the detection probability, subject to the current probability of false alarm, $\boldsymbol{\alpha}$.

The NP-SPRT is a statistical method, which endeavours to use the minimum number of samples, in order to reach a decision regarding H_1 [50]. The number of samples required to assess the current situation is governed, however, by the corresponding probability of false alarm, $\boldsymbol{\alpha}$. The NP detection threshold, $\boldsymbol{A_{NP}}$, takes this factor into account and governs both the decision time (i.e. number of samples taken) when a threat is present and the likelihood of false alarm when there is no threat. The NP-Threshold, $\boldsymbol{A_{NP}}$, can be obtained by representing, hypothetically, the probability of time taken for a decision when a threat is present, as a function of the probability of false alarm, $R\ (\alpha)$, as shown in table 3.2, representing the "slow" system payoff matrix. The probability of incorrect rejection is denoted by β_{IR}.

EVENT	**RESPONSE**: (H_1)	**RESPONSE**: (H_0)
THREAT (P_R)	*"CORRECT DETECTION"* $R(\alpha)(V_{SN,Y})$	*"INCORRECT REJECTION"* $\beta_{IR}(V_{SN,N})$
NO THREAT (1- P_R)	"*FALSE ALARM*" $\alpha(V_{N,Y})$	"*CORRECT REJECTION*" $(1-\alpha)(V_{N,N})$

Table 3.2: "Slow" response system pay-off matrix for PORTENT threat detection

Using table 3.2 the expected pay-off, $E\ (payoff)$, for taking H_1 action is shown in (3.7).

$$E(payoff) = (1-P_R)(\alpha V_{N,Y} + (1-\alpha)V_{N,N}) + P_R\ (R(\alpha)\ V_{SN,Y} + \beta_{IR}\ V_{SN,N}) \tag{3.7}$$

To calculate the current optimum probability of false alarm, $\boldsymbol{\alpha_{opt}}$, matched to the current sensing environment, it is noted that *E (payoff)* is a maximum when $dE\ (payoff) / d\alpha_{opt} = 0$, as shown in (3.8).

$$\frac{dE(\ payoff)}{d\alpha_{opt}} = P_R\ \frac{dR}{d\alpha_{opt}}\ V_{SN,Y} - (1 - P_R)\ (V_{N,Y}\ - V_{N,N}\ ) = 0 \tag{3.8}$$

Z (n), given in (3.6) represents a summary of the accumulated sensory threat related information up to *t*, which is a multiple of $1/\boldsymbol{n}$. At each small time step, δt, the movement of *Z (n)* can be assumed to be normally distributed according to, $N\ (\mu\delta t,\ \eta^2\delta t)$, where both μ and η are given in (3.9) and (3.10), respectively.

$$\mu = \frac{(\mu_{SLOW1} - \mu_{SLOW0}\ )^2}{2\sigma_{SLOW}{}^2} \tag{3.9}$$

$$\eta^2 = \frac{(\mu_{SLOW1} - \mu_{SLOW0}\ )^2}{\sigma_{SLOW}{}^2} \tag{3.10}$$

Since, the time step, δt, is known, the amount of accumulated information gain through *Z(n)* in that time, is a random variable with normal distribution parameters given in (3.9) and (3.10). For a total of $\boldsymbol{n}$ sensory observations per unit time, *t*, the total uncertainty in information gain from incoming sensory samples, *k1*, can be quantified, as shown in (3.11).

$$k1 = \frac{-n\mu + \sqrt{n(\mu^2\ + 2\eta^{\ 2}\ )}}{n\eta^2} \tag{3.11}$$

From (3.11), it is apparent that both $\boldsymbol{\alpha_{opt}}$ and $\boldsymbol{A_{NP}}$ are linked to *k1*, since this reflects the current degree in H_1 uncertainty, as a result of the observations being made from the surveillance environment. Setting $R\ (\alpha) = \boldsymbol{\alpha_{opt}}^{k1}$ and substituting $dR/d\boldsymbol{\alpha_{opt}} = k1\boldsymbol{\alpha_{opt}}^{k1-1}$ into (3.8), $\boldsymbol{\alpha_{opt}}$ can be rearranged to be solved, as shown in (3.12).

$$log_{10}(\alpha_{opt}) = \left(\frac{1}{k1-1}\right) log_{10}\left(\frac{(1-P_R)(V_{N,Y}-V_{N,N})}{P_R\ k1\ V_{SN,Y}}\right) \quad (3.12)$$

The NP detection threshold, $\boldsymbol{A_{NP}}$, can subsequently be set to the calculated, $\boldsymbol{\alpha_{opt}}$, value obtained from (3.12). The corresponding decision for the "slow" system to take a positive detection action and accept H_1 is shown in (3.13).

$$if\ (Z(n) \geq ln(A_{NP}))\quad THEN\ "Accept\ H_1" \quad (3.13)$$

As shown in (3.12) and (3.13), $\boldsymbol{A_{NP}}$ is an optimisation between decision-speed, this being the number of samples taken and the detection certainty, representing the confirmation level of the identified event within an uncertain sensing environment, as shown in figure 3.3.

For the purposes of illustration, figure 3.3 represents an arbitrary threat detection scenario using 10 sensors randomly deployed in a 1km by 1km region, with S_{RMAX} set to 500m, monitoring a mobile target at a constant velocity of 5m/s, using a full sampling rate of 100 samples/sec. Detection certainty performance is an aggregated score per sensor and is measured against level-1 threat observation certainty (*TOC*), which represents the variation in the mean separation between μ_{FAST1} and μ_{FAST0}, including μ_{SLOW1} and μ_{SLOW0} probability occurrence distributions, as shown in figure 3.2. A number of simulations (> 50) with random topologies are run for a duration of 100 detectable events.

As shown in figure 3.3 (b), as the probability of false alarm, $\boldsymbol{\alpha}$, reduces, the need for extensive sampling reduces as well. This is because $\boldsymbol{A_{NP}}$, which is matched to the current uncertainty in observation of the surveillance environment (i.e. low false alarm, high *TOC*) falls accordingly to the expression given in (3.12). This results in a faster positive-detection outcome time (i.e. lower event detection delay) as a result of the threshold expression in (3.13). However, as shown in figure 3.3(a), performance in obtaining a better certainty in event score is reduced slightly, due to less samples being taken, as a result of a

lower defined A_{NP} and in accordance with the threshold condition given in (3.13). In 3.5, we show that the certainty in event score can be improved by combining both the "fast" and "slow" systems, in order to create greater heightened detection awareness and further improve on event detection delay performance.

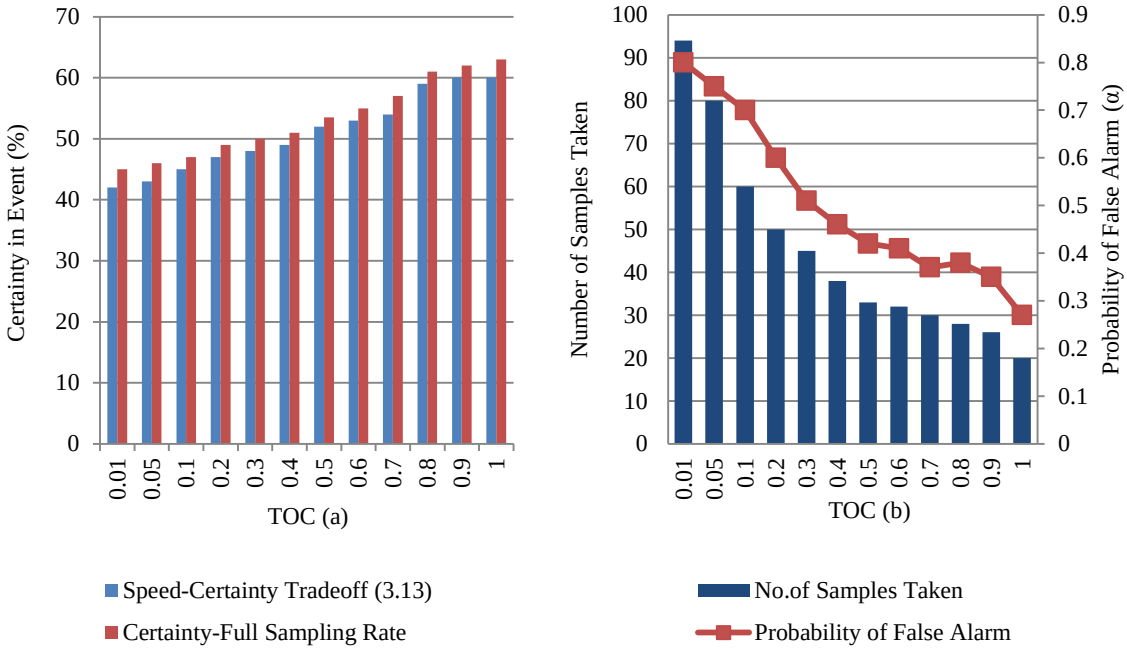

Figure 3.3: Independent "slow" response system speed-certainty trade off performance

3.5 PORTENT Combination Strategies

As shown in figure 3.1, both "fast" and "slow" systems may perform as independent operations for threat situation assessment or also have the potential to operate, as a combined system. A combination of both systems can bring advantages for mitigating missed detection and minimising the need for extensive sampling, as shown in figure 3.3(b) and subsequently, conserve sampling energy consumption. In section 3.5, we present two options that allow both system operations to be combined and we investigate whether this has any impact on situation assessment performance, through improved event detection delay performance.

3.5.1 PORTENT Combination-Option 1

If the "fast" response system fails to make a decision concerning "positive detection", therefore, resulting in a potential missed detection, the "slow" response system can begin to receive sensory data. The likelihood, therefore, of a threat being present if the "fast" response system fails to act becomes less than P_R. A new probability of a threat being present, conditional upon the "fast" system failing to act, P'_R, is then required and can be formulated, as shown in (3.14).

$$P'_R = \frac{P_R \times p(IncorrectRe\,jection)}{P_R \times p(IncorrectRe\,jection) + (1 - P_R) \times p(FalseAlarm)} \tag{3.14}$$

$$P'_R = \frac{P_R \times E\left(\frac{L(x_0) - \mu_{FAST1}}{\sigma_{FAST}}\right)}{P_R \times E\left(\frac{L(x_0) - \mu_{FAST1}}{\sigma_{FAST}}\right) + (1 - P_R) \times E\left(\frac{L(x_0) - \mu_{FAST0}}{\sigma_{FAST}}\right)}$$

The probability P'_R from (3.14) can be substituted for P_R and used to calculate $\boldsymbol{\alpha_{opt}}$, required for the NP-threshold, $\boldsymbol{A_{NP}}$, calculation described in (3.12). This then allows the overall "slow" system to function and take over "positive detection" decision making, given by the condition in (3.13).

3.5.2 PORTENT Combination-Option 2

Again if the "fast" response system fails to make a "positive detection" outcome, it is feasible to consider the "slow" response system having access to the signal level criterion, $L(x)$, used by the "fast" response system, given in (3.4). The signal level criterion, $L(x)$, could have the potential to provide a more accurate estimate of the probability of a threat being present, P''_R, as shown in (3.15).

$$P''_R = \frac{P_R \times f_{Fast1}(L(x))}{P_R \times f_{Fast1}(L(x)) + (1 - P_R) \times f_{Fast0}(L(x))} \tag{3.15}$$

From (3.15), $f_{FAST1}(x)$ denotes the probability density when a threat is present and $f_{FAST0}(x)$ denotes, the probability density when no threat is present. The probability, $P''_{R,}$ from (3.15) can then be substituted for P_R and used to calculate, $\boldsymbol{\alpha_{opt,}}$ which is required for the threshold $\boldsymbol{A_{NP}}$ calculation described in (3.12). This then allows the overall "slow" system to function and take over "positive detection" action decision making, according to (3.13).

3.5.3 PORTENT Event Detection Delay Performance

For the purposes of illustration, figure 3.4, represents the same threat detection scenario used for figure 3.3. As shown in figure 3.4, PORTENT combination strategies, given as option 1 and 2 can increase the awareness of a threat presence, since the potential event becomes more critical to the overall threat detection operation success.

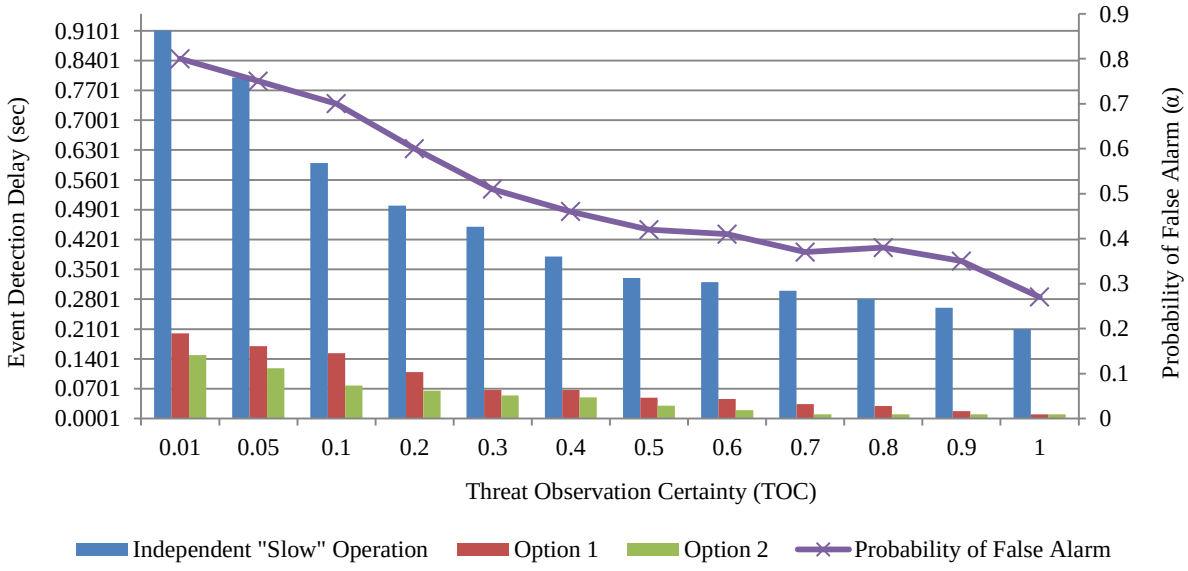

Figure 3.4: PORTENT option 1 and 2 event detection delay performance

As shown in figure 3.4, for the defined threat detection scenario the overall event detection delay reduces considerably when the above options are incorporated into PORTENT situation assessment, when compared with independent "slow" sub-system operation, which uses a full sampling rate and just P_R. Both option 1 and option 2 can achieve lower event detection delay by increasing the sensitivity of the "slow" response system further, by reducing the NP-threshold, $\boldsymbol{A_{NP}}$, given in (3.12) as β_{IR} tends to zero

and $\boldsymbol{\alpha}$ reduces. Figure 3.4 also indicates that option 2 has the potential to improve the situation assessment in conditions where the "fast" response system fails to act by achieving an overall lower, event detection delay performance. The flow chart describing the overall combined PORTENT situation assessment system, in relation to the two options described above is detailed in **Appendix A, part 1**.

3.6 Characterising Threat Detection Information

Event detection delay is just one way of measuring situation assessment performance. In 3.6, we incorporate other, relevant, threat detection measures and aggregate them into an overall figure of merit to describe situation assessment performance. Aggregation of captured threat detection information in this manner, is commonly referred to as, quality of surveillance information (QoSI) [51-52]. QoSI is therefore a characterisation of the salient features (quality factors) associated with situations of interest, detected by and flowing through the *UGS* network (e.g. detection accuracy). For PORTENT threat detection performance purposes, detection accuracy (q_1), detection certainty (q_2) and detection timeliness (q_3) quality factors, are specifically used.

3.6.1 Detection Accuracy

In the surveillance domain, accuracy of threat detection refers to the total number of correctly detected events to the total number of events that occurred in the environment, as shown in (3.16). From (3.16), $E_{C,j}$ is the number of correctly detected instances of the j^{th} event by the system over a period of time and $E_{T,j}$ the total number of instances of the j^{th} event.

$$q_1 = E_{C,j} \Big/ E_{T,j} \tag{3.16}$$

3.6.2 Detection Certainty

Detection certainty represents the confirmation level of the identified event, in the form of a probability score. The score represents the confirmation that an identified event exists, within an uncertain environment, as shown in (3.17).

$$q_2 = Avg(\, p(I_j \mid L^n \,)) \tag{3.17}$$

From (3.17), $p\ (I_j \mid L^n\ )$ represents the probability of existence of the information item I_j (e.g. the occurrence of the j^{th} event) based on the set of L^n samples. *Avg* is a function to average the certainty level of an individual information item over a period of time.

3.6.3 Detection Timeliness

Detection timeliness is a measure of the timeliness of information being available at the desired time and the ability to link related events that occur at different times (i.e. building a coherent picture over time). PORTENT is expected to detect the j^{th} information item (event) at time T of its occurrence, however if the system takes an additional time, $T + \Delta$, where Δ is the event detection delay, the timeliness is then given, as shown in (3.18).

$$q_3 = T \big/ T + \Delta \tag{3.18}$$

3.6.4 Quality of Surveillance Information

After evaluating each respective quality factor, a linear weighted fusion strategy can be applied to each quality factor through the assignment of normalized weights (W_b), where the sum of all the W_b values used is equal to 1 [51-52]. Localised captured *QoSI*, can then be expressed as an aggregation of these weighted quality factors, as shown in (3.19), where *V*, represents the total number of quality factors used.

$$QoSI = \sum_{b=1}^{V} W_b \times q_b \tag{3.19}$$

3.7 PORTENT Performance

PORTENT situation assessment performance is conducted using the OMNeT++ simulation platform [63], using the parameters described in **Appendix A, part 1**, and is measured in terms of QoSI. From a surveillance perspective, QoSI is a valuable figure of merit, which can signify increased confidence and trust in the threat detection performance of the deployed *UGS* system. For an initial indication regarding PORTENT performance, an illustrative example of a surveillance scenario, where *UGS* sensors are deployed at their various fixed positions in metres within a 1km by 1km region of interest, is depicted in figure 3.5.

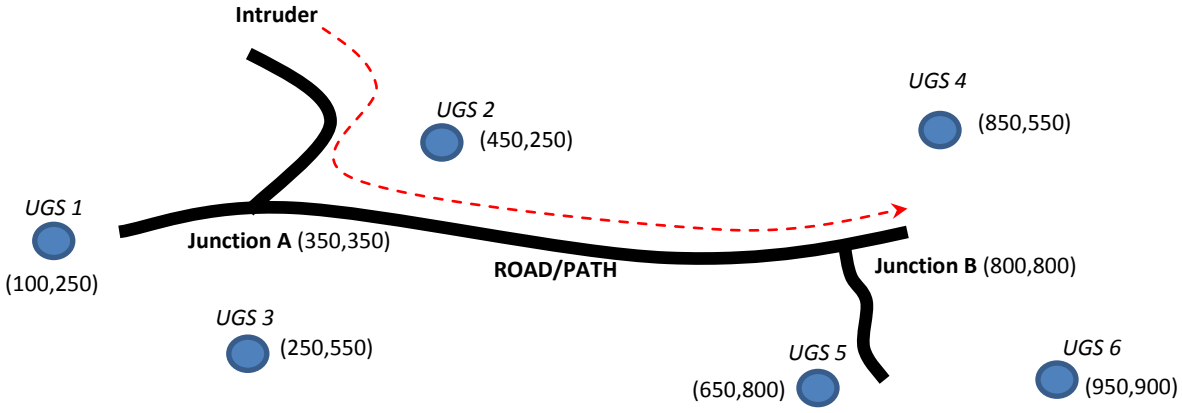

Figure 3.5: PORTENT surveillance scenario

UGS node positions are chosen arbitrarily and in our illustrative scenario, we do not consider, nor analyse, what the level of sensing coverage is required to detect a threat at each junction. Our evaluation is primarily concerned with PORTENT QoSI performance under different TOC conditions (i.e. false alarm conditions) in relation to a dynamic threat.

In our evaluation, maximum sensing ranges (S_{RMAX}) are set to 500 meters and we model the intruder crossing the region of interest with a constant velocity of 5 m/s , in a linear diagonal direction, at an initial starting grid position of (50, 50). A full sampling rate of 100 samples/sec is used and the values for the pay-off matrix given in table 3.1 and 3.2 are set respectively to ($V_{SN,Y}$ = 1), ($V_{SN,N}$ = -1), ($V_{N,Y}$ = -1) and ($V_{N,N}$ = 1). We also assume that higher level application algorithms are present on each *UGS* for intruder classification and that a current threat geo-location position is readily available. QoSI at junction A involves a combined score from *UGS's* 1, 2, 3, while junction B involves *UGS's* 4, 5 and 6. Figure 3.6 shows PORTENT QoSI performance using its various situation assessment options, under two different TOC conditions.

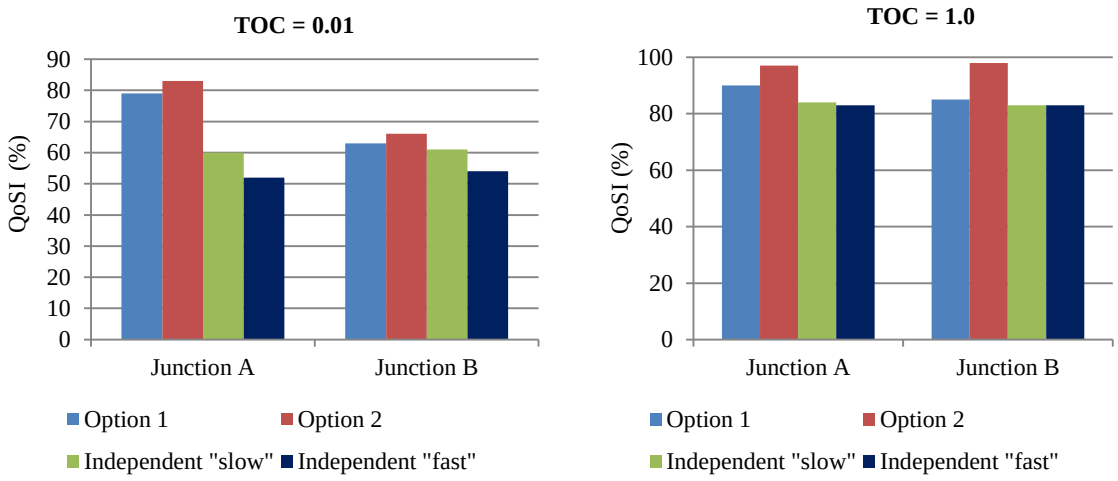

Figure 3.6: PORTENT QoSI performance for intruder position ± 10m from each respective junction

As shown in figure 3.6, under high threat observation uncertainty conditions (TOC =0.01) the independent "fast" system has the lowest QoSI performance, mainly due to it having a less intensive sampling operation and also because both its critical threshold, $L(x_0)$, given in (3.3) and observation criterion, $L(x)$, given in (3.4) do not incorporate a measure evaluating the probability of false alarm. This ultimately reduces both the detection timeliness and certainty quality factors. This observation is confirmed, as

indicated in figure 3.7, which shows that the "fast" response has a lower combined detection certainty and timeliness performance at both monitored junctions, when compared with options 1 and 2.

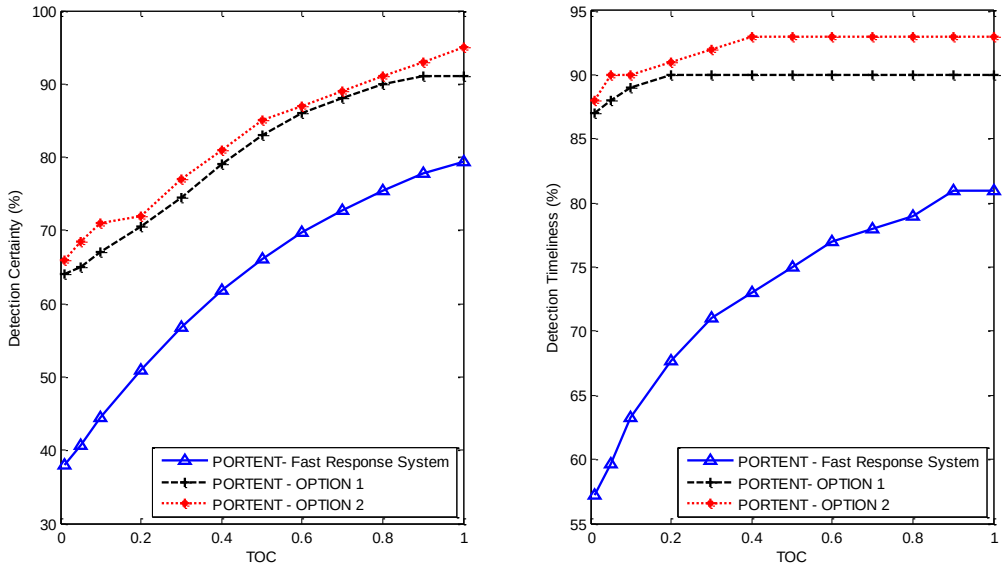

Figure 3.7: PORTENT combined detection certainty and timeliness performance at both junctions

Incorporating a NP-detection threshold, which is a function of the present observed probability of false alarm, results in a better performance for QoSI, as is the case for options 1, 2 and "independent "slow" response systems, as shown in figure 3.6. From figure 3.6, under higher uncertainty, it is suggested that option 2 can provide the better QoSI performance out of all the possible options. This is primarily because option 2 can achieve a lower event detection delay performance through it being able to provide a better self-adjustment towards the false alarm detection environment, as indicated in figure 3.4. This helps to increase option 2 detection timeliness performance over both options 1 and independent "fast" systems by 6% and 20% respectively, as shown in figure 3.7. Under lower observation uncertainty conditions (TOC = 1.0), both independent "fast" and "slow" systems have comparable QoSI performance, mainly because the probability of false alarm

is now reduced, which allows potential events to be easily detected using only a smaller set of samples. In option 2, because of its ability to achieve a better evaluation of threat presence, given in (3.15), this can help to increase detection certainty performance over option 1, as shown in figure 3.7 and as a result an improved QoSI score under both TOC conditions is obtained, as shown in figure 3.6.

To give an indication as to PORTENT performance under different possible surveillance scenarios, we again measure the QoSI for various random node deployments according to a uniform distribution. QoSI performance is evaluated against an incremental increase in the number of deployed nodes used for each random deployment. Again, the same intruder characteristics and network region size are used from figure 3.5. Simulations are run a number of times for each node deployment used and for a total of 100 possible detectable events. In terms of comparison, PORTENT QoSI is measured against the QoSI achieved using the binary detection model, as described earlier in section 3.2 and given in (3.1). Figure 3.8, shows QoSI performance for the various random deployments against node density.

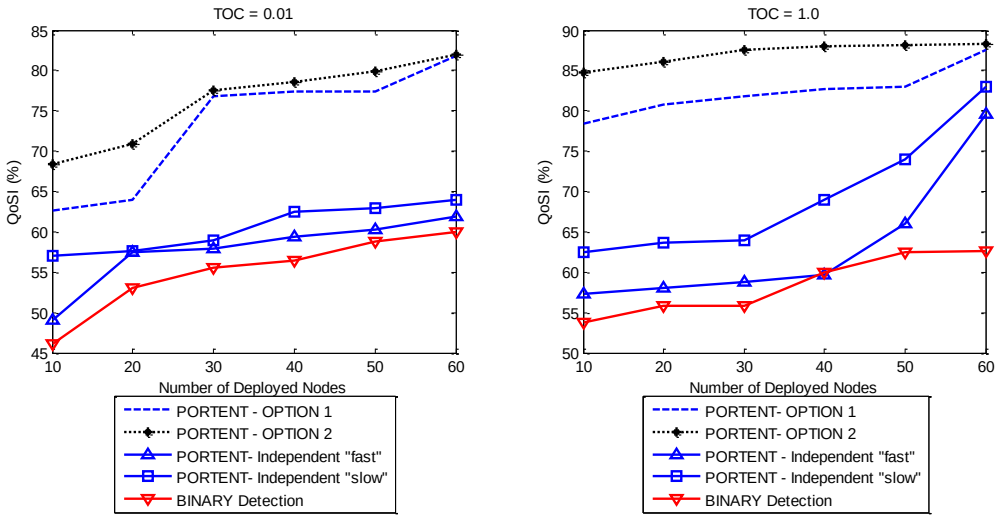

Figure 3.8: QoSI performance against network node density

From figure 3.8, it is clear that as the number of deployed nodes increases the QoSI increases also. This is because of the increased sensing coverage available for threat detection, as more nodes are deployed within the network. As shown in figure 3.8, PORTENT achieves a higher QoSI performance, when compared with binary detection means because it uses all possible options for threat detection purposes.

For binary detection, events are detected when they occur at a distance of less than S_{RMAX}. This implies that if an event occurs in the far sensing field region and within a high observation uncertainty environment (TOC = 0.01), the probability of false alarm is likely also to be high, which reduces detection certainty performance. A simple binary detection threshold, therefore, achieves a lower resultant QoSI performance since the false alarm constraint is not incorporated. Through PORTENT options 1, 2 and independent "slow" systems a consideration of the false alarm constraint is given, thus improving on overall QoSI performance. The PORTENT "fast" system does not incorporate a false alarm constraint but instead evaluates the observed probability ratio concerning, positive to negative detection through the *L(x)* criteria calculation, thus providing a lower QoSI performance.

From figure 3.8 shows that with increasing node density and for the number of random node deployments simulated, PORTENT option 2 again achieves better QoSI performance over all other PORTENT options. Again this increase is primarily due to an improved detection timeliness and certainty performance, as described earlier.

In the next chapter and in line with figure 2.1 shown earlier in chapter 2, we detail how PORTENT-Option 2 can be integrated with levels 2 and 3, in order to enable a complete SA system for distributed *UGS* surveillance management.

CHAPTER 4

VIGILANT Situation Awareness System

VIGILANT is primarily focused on the detection of a threat using PORTENT, with the added benefit of exploiting the *"context"* of the threat situation environment (level 2) and as a result, utilising the awareness generated to invoke network control decisions matched to the dynamics of the threat situation (level 3), as shown in figure 4.1. From figure 4.1, utilising an integrated approach through levels 1, 2 and 3 has potential to facilitate a better and more informed perspective regarding the presence of a threat, in terms of the QoSI metric. Based on level 2, sensors are able to establish their own localised view of the threat situation and whether to invoke their decision for group formation. Upon the decision for group formation, by a group initiator (GI), level 3 requested *"context"* information from neighbouring sensors can then be evaluated and used to determine the degree of confidence associated with the *"context"*.

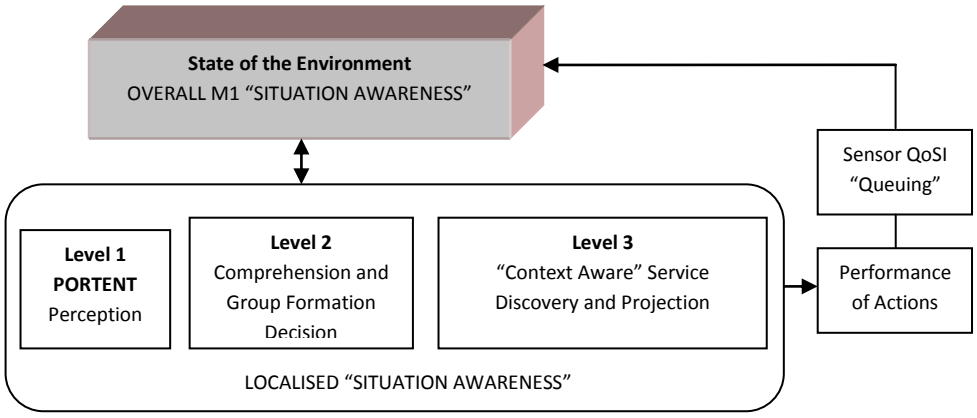

Figure 4.1: Overall combined VIGILANT "situation awareness" system, derived from figure 2.1

The evaluation of confidence in *"context"* enables the GI to select, which sensors are more suitable for collaboration at a particular point in time. Subsequently, by informing the most suitable sensors for collaboration, *M1* "situation aware" groups can be created and

their respective QoSI values aggregated. In section 4.1, we detail the level 2 process involved for deriving relevant *"context"* concerning the *M1* surveillance situation.

4.1 VIGILANT – Comprehension and Group Formation Decision

VIGILANT level 2, involves comprehending the significance associated with raw sensor data captured within an uncertain environment. Comprehending the environment in which potential threats exist, can be argued as the most critical part of the mission requirement since this reduces the chance of relevant events remaining undetected. Comprehension of situations occurring in an uncertain environment requires a level of cognitive capability, in order to derive the relevant "*context"* of those situations [53]. In general, there exist two approaches to the modelling of situations within uncertain environments of interest [53-54]. These are:

- *State orientated* approaches look on situations as aggregated state entities of the world.
- *Action orientated* approaches consider situations as sequences of actions and viewpoints originating from some declared initial world state [55].

Both these approaches facilitate the view of the current perceived situation and this promotes a concise structure.

For VIGILANT level 2, we utilise an action orientated design approach in the form of a Bayesian Belief Network (BBN). When compared with other action orientated techniques, such as Dempster-Schafer theory, designs that involve BBN's have always proved very useful and effective in a variety of decision aiding domains, especially in dealing with issues concerning inference within an uncertain environment [56-57]. A BBN is a directed acyclic graph, using a collection of nodes denoting the random variables, which represent hat situation domain [58]. Corresponding links between the nodes define

the casual relationships between them, with conditional probability tables (CPTs) encoding the quantitative influence. Where no link exists between nodes, the quantitative influence can be given as marginal probabilities. The BBN network used to describe VIGILANT level 2 is shown in figure 4.2. From figure 4.2, the topology describing the situation "domain" for threat detection purposes consists of six binary variables, which together encodes the qualitative knowledge of the "domain" in the following ways:

1. Sensed observation influences *"yes" threat present*.
2. Sensed observation influences *"no" threat present*.
3. Both *"yes and no" threat presence* jointly have a direct effect on the understanding concerning the "*current threat*".
4. The *"current threat"* influences the decision to *form situation awareness group*.
5. The *"current threat"* influences the decision to *wait for next observation*.

Table 4.1, summarises the probability expressions derived from our VIGILANT level 2 BBN. Based on table 4.1, derivation of the *"context"* concerning the current situation, in order to aid final decision making for initiating group formation, *"context-aware"* collaboration and network management functions, is achieved and is described further in 4.2 and 4.3.

4.2 VIGILANT Level 2 – "Context-Aware" Collaboration

VIGILANT collaboration is driven by the *UGS*, which perceives the highest current threat established in level 2, named the Group Initiator (GI), as shown in figure 4.2. The ability to infer situations (i.e. current threat level), is a critical function for *"context-aware"* systems, acting as driver for adaptive behaviour at the application level and can be initiated using *"context-aware"* service discovery mechanisms [59].

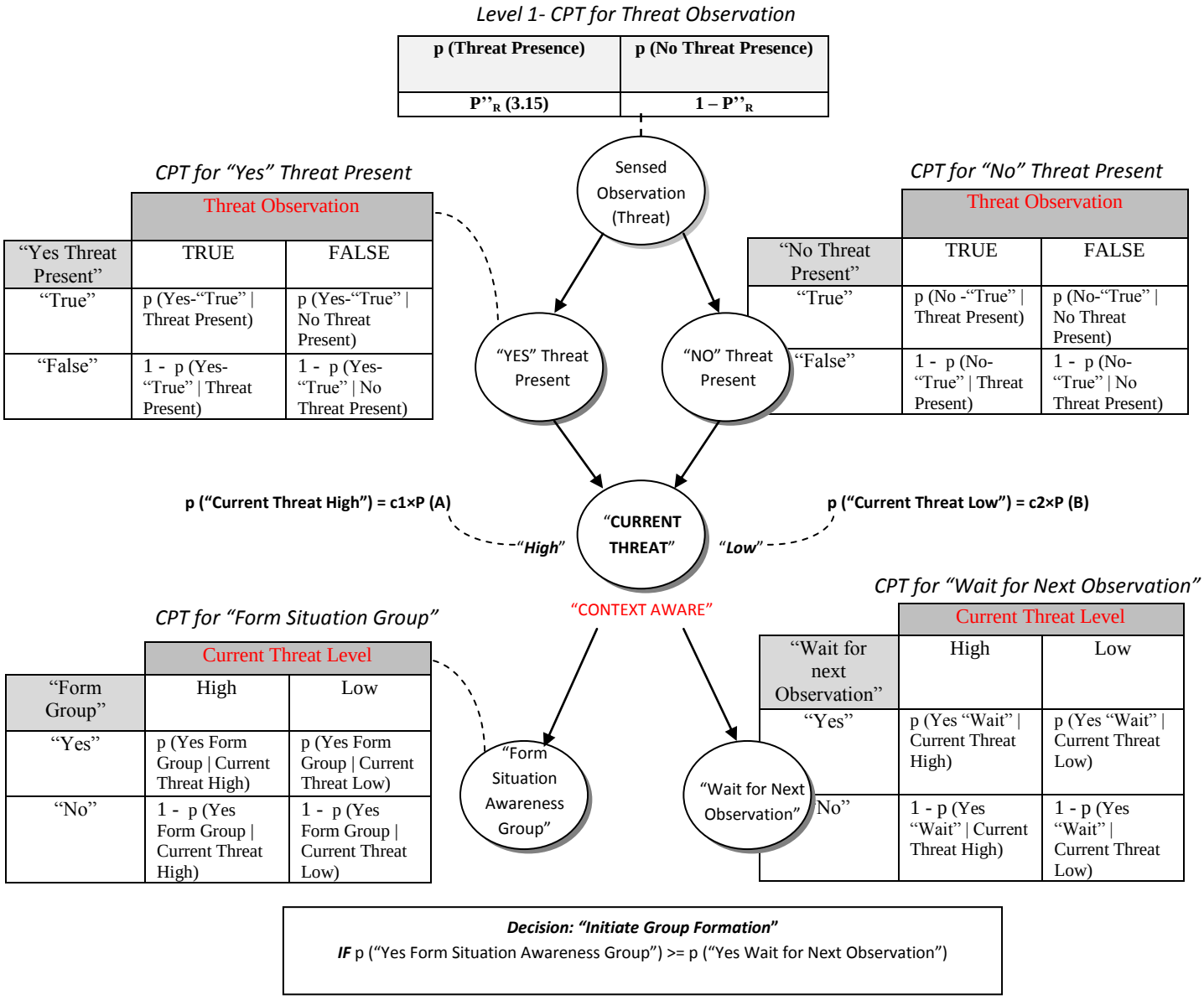

Figure 4.2: VIGILANT level 2 UGS localised BBN and decision for initiating group formation

Probability Expression	Probability Derivation from figure 4.2 using CPT Analysis
1. p(Yes Threat Present)	P(A) = p (True – Yes Threat Present | Threat Presence True) × P''_R + p(True – Yes Threat Present | Threat Presence False)× (1 – P''_R)
2. p(No Threat Present)	P(B) = p (True – No Threat Present | Threat Presence True) × P''_R + p(True – No Threat Present | Threat Presence False)×(1 – P''(r))
3. p(Current Threat – High)	C1 × P(A) (C1 = 1 – ($\|\|p\text{-}q\|\|_2 / S_{RMAX}$))
4. p(Current Threat – Low)	C2 × P(B) (C2 = 1 – C1)
5. p(Form Situation Awareness Group)	p (Yes-"Form"| Current Threat High)× p (Current Threat High) + p (Yes-"Form"| Current Threat Low)×p (Current Threat Low)
6. p(Wait for Next Observation)	p (Yes-"Wait"| Current Threat High)× p (Current Threat High) + p (Yes-"Wait"| Current Threat Low)×p (Current Threat Low)

Table 4.1: Probability derivations from figure 4.2 for the purposes of "context-aware" decision making

For *M1* operation, sensors collaborate to facilitate collection of additional information concerning the present, in order to satisfy the requirement in achieving a high QoSI aggregation score and thus, confidence in threat presence notification. A *"context-aware"* service discovery thus utilises the deployed distributed *UGS* network, in order to assist the grouping of single hop *UGS* nodes that exhibit common *"context"* about the current threat situation. In 4.2.1 we detail how VIGILANT achieves this.

4.2.1 "Context-Aware" Service Discovery

"Context-aware" service discovery can be achieved through establishing the level of confidence in *"context"*, concerning the threat presence situation. The certainty factor (CF) model is one approach towards evaluating and measuring this confidence (e.g. *"context"* in threat presence) between two random entities (e.g. GI and its immediate neighbour) [60].

The CF model operates according to proportional measures of increased belief (MB) and disbelief (MD) about a certain hypothesis. For VIGILANT, the hypothesis stems from the degree of certainty in MB and MD that an individual *UGS* should form a partnership with their GI according to, its current threat presence *"context"*, as shown in (4.1), where MB and MD supporting (4.1) are derived from table 4.1 and are given in (4.2) and (4.3) respectively.

$$CF\,"Sensor" = (MB - MD) \Big/ 1 - min(MB, MD) \tag{4.1}$$

$$MB = \frac{p(Form\ SA\ Group \mid Current\ threat\ level\ high) - p(Current\ threat\ level\ high)}{1 - p(Current\ threat\ level\ high)} \tag{4.2}$$

$$MB = \frac{p(Current\ threat\ level\ high) - p(Form\ SA\ Group \mid Current\ threat\ level\ high)}{p(Current\ threat\ level\ high)} \tag{4.3}$$

To facilitate an on-going dynamic *"context-aware"* discovery mechanism, sensors would compute their *CF "sensor"* values throughout a *M1* surveillance mission and only report

their values, upon receiving a GI "REQUEST" broadcast notification. GI's would then seek to evaluate the current level of common confidence in *"context"* by combining their own *CF "Group Initiator"*, calculated in the same way as (4.1), with *CF "Sensor"*, received on a per sensor basis by utilising the "**confidence evaluation in context**" rule shown in (4.4). The resulting common confidence in *"context"*, *CF Situation "Context"*, is given in (4.5).

$$IF\ CF\ "Group\ Initiator", Current\ Threat\ Level\ \ AND\ \ CF\ "Sensor", Current\ Threat\ Level$$
$$THEN\ \ Confidence\ in\ Current\ Threat\ Level, CF\ Situation\ "Context" \tag{4.4}$$

$$CF\ Situation\ "Context" = \begin{cases} if\ CF\ "GI"\ and\ CF\ "Sensor" \geq 0 : CF\ "GI" + CF\ "Sensor" (1 - CF\ "GI"\ ) \\ if\ CF\ "GI"\ and\ CF\ "Sensor" < 0 : CF\ "GI" + CF\ "Sensor" (1 + CF\ "GI"\ ) \\ Otherwise \qquad\qquad : \dfrac{(CF\ "GI" + CF\ "Sensor"\ )}{1 - min(|\ CF\ "GI"\ |, |\ CF\ "Sensor"\ |\ )} \end{cases} \tag{4.5}$$

The final combined CF evaluation, given in (4.5) provides an overall measure concerning the degree of confidence that both a GI and its immediate neighbours should form a partnership, due to their respective current perceived *"context"*. For completeness, the *"context-aware"* service discovery protocol described in this chapter section is illustrated in figure 4.3. This figure shows that a immediate neighbour is only accepted for collaboration purposes if the *CF Situation "Context"* is greater than a system-defined probability of confidence in *"context"*, *H*. As a result, the number of collaborators being used at a given point in time depends on the value of *H* used.

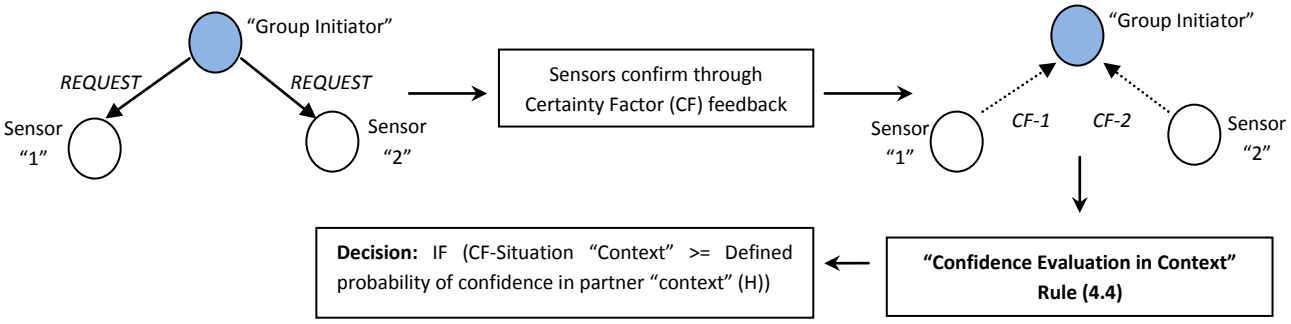

Figure 4.3: GI led "context aware" service discovery with partnership decision for UGS self-organisation

4.3 VIGILANT Level 3 – "Context-Aware" Network Management

Upon the GI deciding which immediate neighbours are applicable to form collaboration with, it also, subsequently, determines a QoSI service provision time bound. The service provision time itself is solely based on the level of common *"context-awareness"* there is concerning a threat presence. A bound on the QoSI service provision time evaluated in this manner has the potential to facilitate the management of the collaborating group in the following ways:

- Aggregated QoSI processing at the GI. This requires a level of stability within the collaborating group and can be supported if group members are encouraged to communicate their QoSI scores at defined time slot periods, which is matched to the level of common *M1 "context-awareness"* they have with the GI.

- Communicating at defined periods has potential in reducing both packet collisions and latency (e.g. increase bandwidth efficiency) for QoSI reporting, especially when a contention based medium access control scheme is being utilised.

4.3.1 Evaluating Common Threat "Context-Awareness" for Group Stability

Providing an accurate basis for QoSI aggregation, implies that the group structure has to provide a level of stability for cases where there are no *"contextual"* changes. This entails that group stability is actively encouraged in conditions where the level of common *M1 "context-awareness"* is high. Group stability can be evaluated by modelling the joint probability in common low threat presence *"context"* between the GI and its corresponding neighbour, as a random variable, *U*, with probability density function (PDF_1) and cumulative distribution function (CDF_1), $U\sim N(\mu_{common\ low\ threat"context"},\sigma^2_{common\ low\ threat\ "context"})$. Additionally the joint probability of common high threat presence *"context"* is a random variable, *T*, with a PDF_2 and CDF_2 , $T\sim N(\mu_{common\ high}$

threat"context",σ^2*common high threat "context"*). A GI would determine the probability of partnership stability by evaluating the level of common threat presence *"context"*, based on a threshold ***S***, which is chosen as the intersection point of the two respective PDF's. The intersection point, ***S***, is chosen in this way so as to minimise the sum of probabilities of an incorrect determination of common threat presence *"context"* being made [61]. We denote P_1, as the probability of a correct detection of non-common high threat presence *"context"* and Q_1, as the probability of a correct detection of common low threat presence *"context"*, as shown in (4.6) and (4.7). The probability of partnership stability in the form of a P_1, Q_1 ratio, is an indication as to the current level of common threat presence *"context-awareness"*, as shown in (4.8).

$$P_1 = p(\text{correct detection of non-common high "context"} \mid T) = CDF_2(S) \tag{4.6}$$

$$Q_1 = p(\text{correct detection of common low "context"} \mid U) = CDF_1(S) \tag{4.7}$$

$$\text{Partnership Stability} = P_1 / Q_1 \tag{4.8}$$

Clearly probabilities P_1 and Q_1 should be as low as possible, in order to represent the view that a GI-sensor partnership does indeed have a high level of *"context-awareness"* to the current threat situation. From (4.8), the degree of partnership stability will of course vary according to the characteristics of the underlying joint probability distributions, PDF_1 and PDF_2, which are dictated by the dynamic threat situation and the level of observation uncertainty (e.g. TOC) present within the sensing environment.

4.3.2 QoSI Service Provision Time Bound - Projection

A QoSI service provision time, ensures that the delivery of QoSI updates from collaborating sensors to their GI can be reliably achieved, primarily through reducing the chances of packet collision. Evaluation of a service provision time bound depends on the partnership stability, given in (4.8) and how this might change when projected in terms of

time. An evaluation in this manner requires a way of mapping the current level of partnership stability into a discrete time representation, which can be achieved using a binomial distribution [61-62]. The bound on the QoSI service provision time, (*M*), can be formulated in terms that a GI-sensor partnership, achieves a common stability for a minimum time history, H_{min}, out of a total possible, H_T, time steps in seconds. This is given as the CDF of a binomial distribution as shown in (4.9).

$$M \approx Binomial(H_T, Partnership\ Stability) \tag{4.9}$$

$$p(Partnership\ Stability \leq H_{min}) = \sum_{k=H_{min}}^{H_T} \binom{H_T}{k} Partnership\ Stability^{k} (1 - Partnership\ Stability)^{H_T - k}$$

The expected QoSI service provision time, *E (M)* can also be determined from (4.9), as shown in (4.10).

$$E(M) = Partnership\ Stability \times H_T \tag{4.10}$$

In figure 4.4, an illustration of the overall GI led QoSI service provision time evaluation and notification mechanism, is shown.

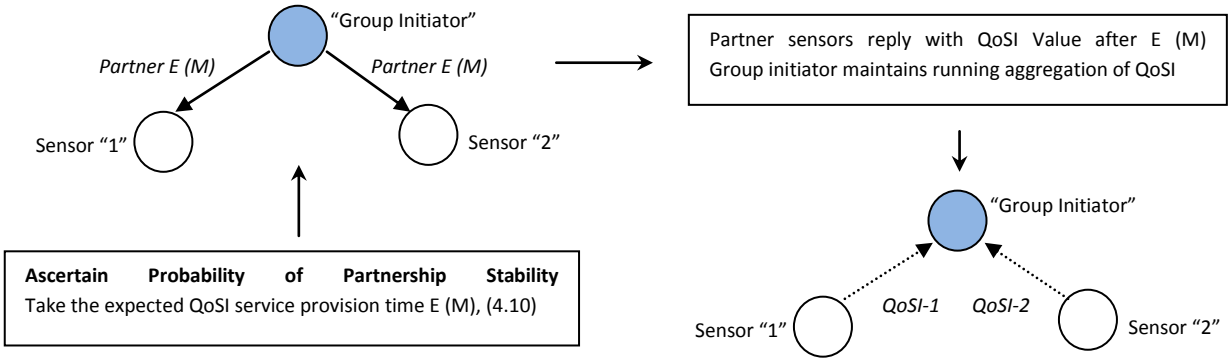

Figure 4.4: "Context-aware" partnership stability for QoSI service provision

4.3.3 Group Initiator Re-Election

To facilitate maintaining both relevant QoSI aggregations while minimising communication overhead, which is commonly required in group re-setup phases, GI re-election is conducted dynamically in the process of a mission. Received QoSI updates from

collaborating sensors, can be used by the GI to re-evaluate their current GI status, using a relative QoSI ratio metric, as shown in (4.11).

$$QoSI_{Relative\ Ratio} = \frac{QoSI_{GI}}{QoSI_{Partner\ Sensor}} \tag{4.11}$$

Group initiators would invoke the process of passing on their lead status to a collaborating sensor if, the $QoSI_{Relative\ Ratio}$ is less than or equal to 1. Notification of the new GI status is then broadcast to the identified partner sensor, as shown in figure 4.5, which then re-initialises the collaborating group, as detailed earlier in figures 4.3 and 4.4. Operations describing the overall combined VIGILANT situation awareness system are described further in **Appendix A, part 2**.

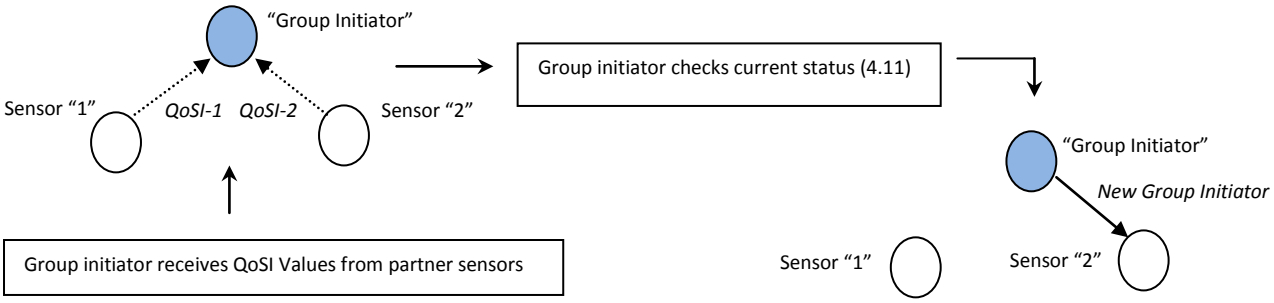

Figure 4.5: VIGILANT group initiator re-election operation

As shown in, **Appendix A, part 2,** the VIGILANT concept is concerned with the collaboration of sensor nodes into groups that share common *"context"*, where this *"context"* is expressed in terms of the presence of a threat situation. This helps to support the primary *M1* concern for higher maintained QoSI (aggregated detection certainty, accuracy and timeliness) provision levels, concerning the presence of a threat.

4.4 VIGILANT System Performance

VIGILANT performance is simulated through the OMNeT++ network simulation platform [63]. We utilise a fixed, 20 node and static *UGS* network, deployed randomly in a grid coordinate system within a 1km by 1km region of interest. Maximum sensing ranges (S_{RMAX}) are set to 500 meters and we assume that higher level application algorithms are present on each sensor for threat intruder classification purposes. Simulations are run using a number of random deployments (>50), each with duration of 100 detectable events, using a full sampling rate of 100samples/second and under loss free channel conditions. *UGS* transmission ranges are also set to 500 metres and the IEEE802.11b protocol, in distributed coordination function (DCF) basic access mode, is utilised for medium access control (MAC). Surveillance is based on a mobile threat, moving at a constant velocity of 5m/s within the region of interest in a diagonal direction.

As part of our system evaluation we do not consider the effects of sampling rate, number of deployed nodes, velocity of threat and sensing coverage range on VIGILANT performance. Our evaluation is more concerned about the effects of collaborating and managing network resource consumption according to the *"context-awareness"* of a threat presence within the surveillance environment. In 4.4.1, we begin by evaluating the QoSI performance against the various VIGILANT system defined parameters.

4.4.1 Quality of Surveillance Information Performance

Since QoSI is a figure of merit characterising the presence of a threat, it is important from a VIGILANT *M1* perspective that accurate levels in QoSI are maintained. For VIGILANT comparison purposes we use LEACH, as described earlier in chapter 2, under heading 2.1. Using LEACH for comparison purposes is suitable since, it also supports ad-hoc collaboration, utilising all immediate neighbours, but does not consider a *"context-aware"*

approach towards sensor collaboration and network resource management. Comparing VIGILANT against LEACH in this way can hopefully bring out the benefits of managing sensor collaboration and network resource consumption according to, the *"context"* about the threat presence surveillance environment. We measure QoSI performance against TOC, which effectively portrays the level of observation uncertainty, found within the threat presence surveillance environment. Figure 4.6, shows QoSI performances for both VIGILANT and LEACH.

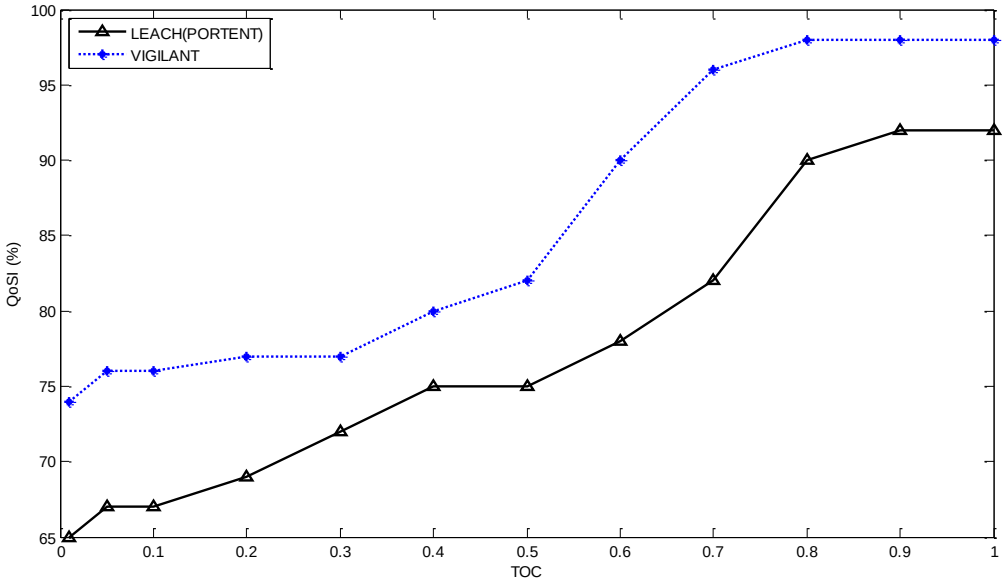

Figure 4.6: QoSI performance for H = 0.9, H_T = 5sec against threat observation certainty (TOC)

From figure 4.6, it can be seen that the QoSI improves for both VIGILANT and LEACH as the TOC increases, mainly because the observation uncertainty reduces, thus making threat detection easier (i.e. lower false alarm). The QoSI performance for VIGILANT, however, is better than LEACH, which suggests that collaborating according to common *"context",* is far better than utilising all available immediate neighbours. The primary reason for this is that VIGILANT inherently reduces the influence of QoSI contributed by outliers in the network. Outlier nodes represent GI neighbouring sensors, which are more distant in terms of the *"context"* concerning the presence of the threat, when compared with the rest of the contributing group. The degree of outlier

contribution, in terms of VIGILANT operation, is determined by the system defined value, used for the probability of confidence in partner *"context"*, *H*, in the *"context-aware"* discovery mechanism described earlier, in 4.2.1 and illustrated in figure 4.3. The effect of *H*, on the resultant VIGILANT QoSI performance is shown in figure 4.7 for two different TOC conditions.

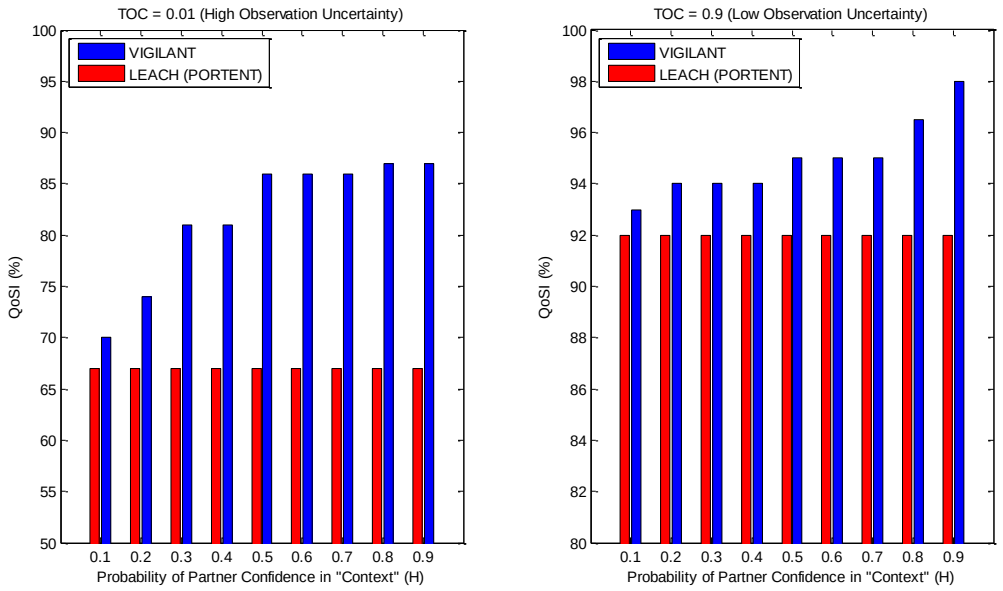

Figure 4.7: The effect of, H, on QoSI performance under two different TOC conditions

As shown in figure 4.7, since the LEACH operation is independent of *H*, the QoSI performance is consistent across the different *H* values and only changes according to the TOC setting used. From figure 4.7, by reducing *H*, VIGILANT is encouraged to use the majority of all one-hop neighbours for collaboration and the aggregation of their QoSI. This forces VIGILANT to behave in a similar way to LEACH operation and hence, explains why VIGILANT has a QoSI value approximately equal to LEACH, when *H*= 0.1 under both TOC = 0.01 and TOC = 0.9 conditions. As we begin to increase *H*, the number of collaborating neighbours reduces but they tend to be neighbours restricted to representing a better *"context-awareness"* concerning the threat presence. This helps to minimise on outlier contribution and improve QoSI performance in both high and low TOC conditions, as shown in figure 4.7. Utilising a higher *H*, can therefore lead to better

collaboration between the GI and its immediate neighbours by ensuring that only sensors with a high level of confidence in common *"context"* about the presence of a threat, as determined using the *CF* model given in (4.5), are utilised. This provides an advantage for ensuring that the relevant sensing coverage is extended over outlier nodes, in order to maintain accurate levels of threat QoSI, a necessity for *M1* surveillance operations.

4.4.2 "Context-Aware" Partner Service Provision Time Adaption

VIGILANT can improve on its own QoSI performance and continually over LEACH because of the use of feedback from the sensing environment, as detailed in **Appendix A, part 2**. The feedback is used to re-evaluate the current partnership stability given in (4.8), on every QoSI update received from immediate GI collaborating neighbours. As a result, QoSI service provision times, *E (M),* given in (4.10), can adapt according to changes in common threat presence *"context"*. The effect of ensuring QoSI service provision times are refreshed to guard against changes to common threat presence *"context"*, is shown in figure 4.8. From figure 4.8, VIGILANT–No Adaption entails collaborating sensors that continue to send their QoSI updates at every H_T seconds and not at a re-evaluated time, *E (M)* given in (4.10), according to figure 4.4 and **Appendix A, part 2**.

As shown in figure 4.8, non-adaption of the QoSI service provision times as H_T increases (VIGILANT-No adaption), can lead to a degradation in QoSI performance when compared with VIGILANT. QoSI updates, which are sent on every H_T second, ignore the dynamics of the monitored threat. VIGILANT ensures that QoSI provision levels are maintained according to the *"context"* of a dynamic threat presence, through re-evaluating the current partnership stability given in (4.8), on every received QoSI update. This can help to both improve and maintain a more consistent QoSI performance, as the TOC environment increases.

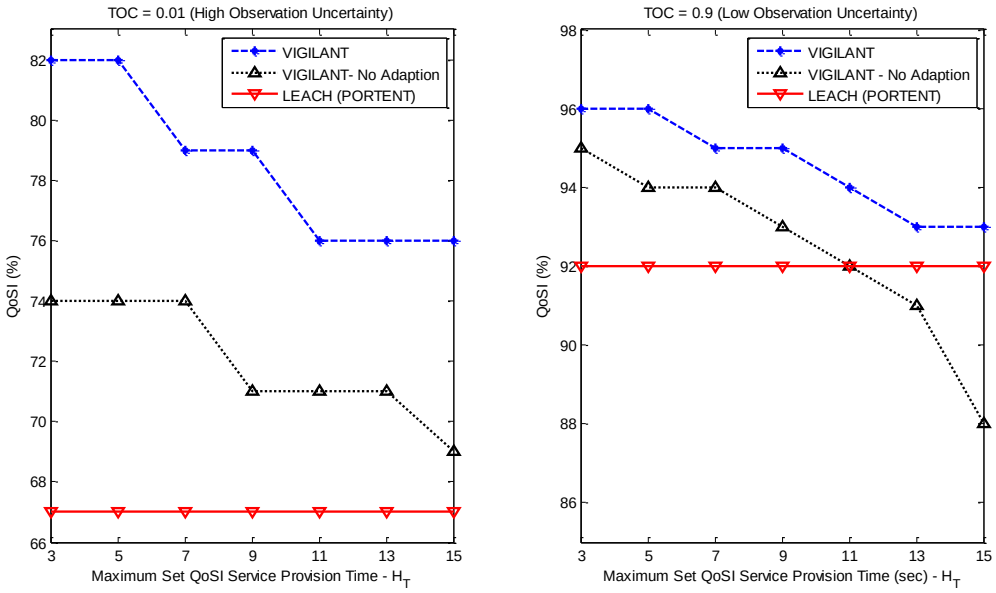

Figure 4.8: VIGILANT QoSI Service Provision Time Adaption, H = 0.9

Following on from figures 4.7 and 4.8, group formation according to a high level of confidence in common *"context"* concerning a threat presence and with *"context aware"* adaption (VIGILANT), can propagate increased QoSI provision, allowing *M1* surveillance missions to perform their tasks effectively within an uncertain sensing environment.

4.4.3 Latency and Communication Energy Consumption Performance

VIGILANT, evaluates the level of common threat presence *"context"*, to allow unique defined service provision times for QoSI updating to become possible within the GI-led collaborating group. This is illustrated in figure 4.4 and is provided, in order to prevent packet collisions from occurring within the collaborating group. Potentially, this can help to improve on message latency (bandwidth efficiency) and to manage the frequency of transmissions made by collaborating sensors, according to the dynamics in threat presence *"context"*. Latency can be measured as the time between the generation of a QoSI packet at a collaborating sensor and the delivery of that packet to the GI. For communication

energy consumption, we utilise the same model provided in LEACH, detailed as shown in (4.12) [27].

$$E_{TX}(k,d) = E_{elec} \times k \; + \; E_{amp} \times k \times d^{n} \qquad (4.12)$$
$$E_{RX}(k,d) = E_{elec} \times k$$

The model in (4.12) provides an indication as to the energy required for transmitting a *k*-bit message to a distance *d*, $E_{TX}(k, d)$ and the energy consumed in receiving a *k*-bit message, $E_{RX}(k, d)$, from a distance *d*, where *n* is the path loss exponent. From (4.12) the electronics energy, E_{elec}, depends on factors such as coding, modulation, pulse shaping and matched filtering. The amplifier energy, E_{amp}, depends on the distance to the receiver and the acceptable bit error rate [27]. Total communication energy consumption is then given as $E_{TX}(k, d) + E_{RX}(k, d)$. In terms of VIGILANT operation, both latency and communication energy consumption performance can be managed according to the system defined value, H_T, given in (4.9). The effect of H_T, on QoSI message latency and communication energy consumption with, k = 500 bits, under two different TOC conditions, are shown in figures 4.9 and 4.10.

From figure 4.9, the QoSI update latency for LEACH with PORTENT operation is independent of H_T and as a result, is constant across all H_T values used. LEACH, as described in chapter 2, 2.1, utilises TDMA for medium access control and as a result, nodes will only be able to transmit their QoSI updates within a certain time slot, according to the neighbourhood TDMA schedule. This explains why the latency performance of LEACH is consistent, since QoSI updates are always guaranteed to arrive at the GI within a designated slot time.

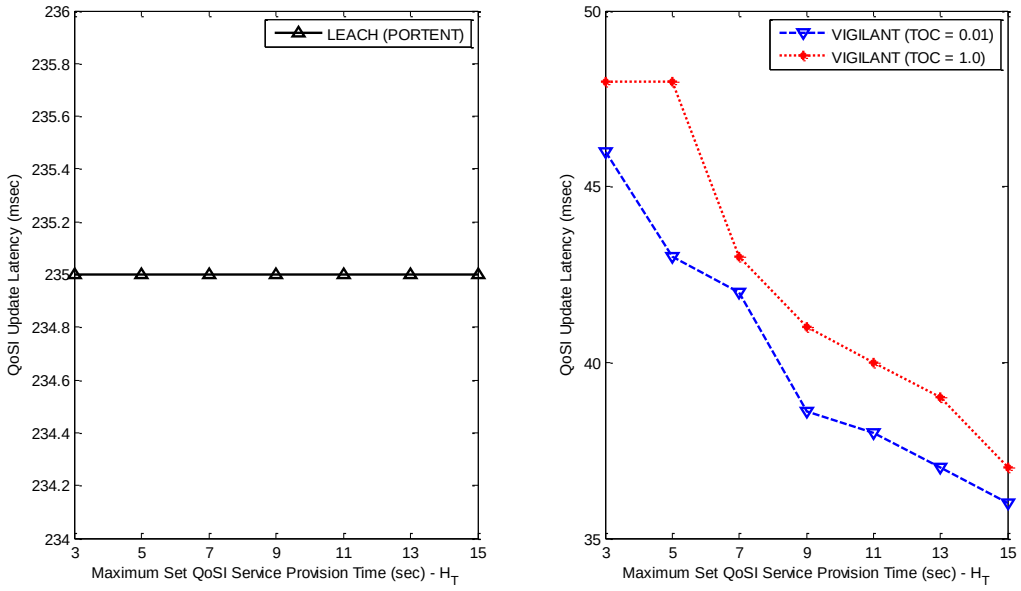

Figure 4.9: H_T on latency performance, with H = 0.9

QoSI message latency for LEACH is dependent only on the delay, due to a node being allocated a time-slot by the Cluster Head. Since LEACH operation utilises a non-*"context-aware"* approach to managing its QoSI transmission updating, latency performance is found to be independent of TOC conditions and as expected, dependent only on the fixed TDMA schedule adopted that determines the period of time slots.

As shown in figure 4.9, VIGILANT QoSI update latency is slightly higher for TOC =1.0 than compared with when, the TOC = 0.01. The reason for this is that under higher observation uncertainty conditions (TOC = 0.01), with *H* = 0.9, the number of potential collaborating sensors decreases, due to a lower resulting level in common confidence regarding the *"context"* of a threat presence. Less collaboration implies that less neighbours will be competing for channel access within a collaborating group and explains therefore, why QoSI message latency is slightly reduced under TOC = 0.01 conditions. Under lower observation uncertainty (TOC =1.0) the *"context"* regarding the presence of threat increases within the collaborating group, therefore enabling both a higher

partnership stability, given by (4.9) and more neighbours contributing their QoSI, which is the main factor that can increase the channel access delay.

From figure 4.9, by increasing H_T, this also has the effect of reducing QoSI message latency for VIGILANT under both high and low TOC conditions, increasing the potential to improve bandwidth efficiency. This is primarily because the maximum time allowed before neighbours within the collaborating group can access the medium increases, which has the effect of reducing the current traffic load. While it is noted that this can help to improve bandwidth efficiency performance, it does, however, produce a lower VIGILANT QoSI performance, as indicated in figure 4.11. A lower QoSI performance is produced, since increasing H_T, results in the frequency of QoSI updating within the collaborating group to be reduced and therefore effects the level in the reported QoSI being made available at the GI.

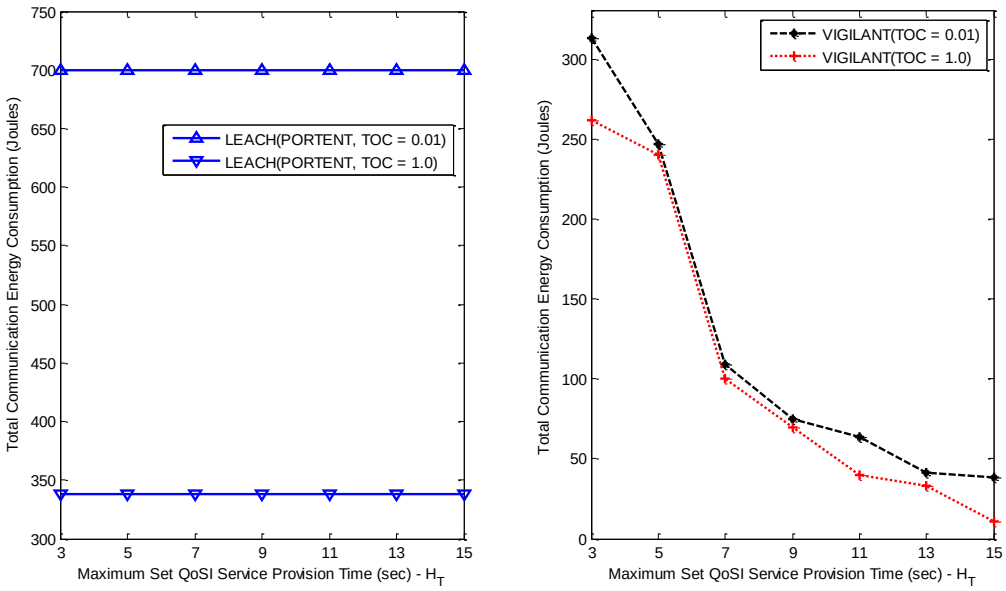

Figure 4.10: H_T on communication energy performance, with H = 0.9, n=2, E_{amp}=2nJ/m^{2}and E_{elec}= 50nJ/bit

Figure 4.10, shows the effect of H_T on communication energy consumption performance for LEACH and VIGILANT. For the case of LEACH where all one-hop neighbours that also include outlier nodes, are used, greater communication energy

is consumed and a lower resulting QoSI performance occurs when compared with VIGILANT, as indicated in figures 4.6 and 4.10.

An observation from figure 4.10, also shows that the communication energy consumption for LEACH is independent of H_T but can be reduced by using a lower observation uncertainty (TOC = 1.0). LEACH for the purposes of comparison has been integrated with PORTENT-Option 2 operation, in order to assist the CH re-election and rotation phases, as described earlier in chapter 2, under section 2.1. This has been enabled according to, which sensors can achieve the greatest threat detecton certainty. Under a higher threat observation uncertainty (TOC = 0.01), when the probability of false alarm is deemed to be at its greatest, this can lead to a greater fluctuation in threat detection certainty being captured within the cluster group. This can result in a greater number of CH's being re-elected during the CH rotation phase. A greater number of CH's being used is a possiblity as to why higher communication energy is consumed for LEACH under TOC = 0.01 conditions, than compared with TOC = 1.0 since, the probabilty of false alarm is reduced and the detection certainty becomes much more stable within the cluster group, leading to a lower number of CH's being rotated.

VIGILANT, however through its integrated level 1 and 2 operation can avoid the unneccessary rotations in GI's and ensures GI's are only elected according to QoSI, which is a combined threat charcterisation measure, rather than just threat detection certainty, as used in LEACH. This can lead to VIGILANT having a much more stable operation and as a result, a lower communication energy consumption profile. In addition, managing the number of colloborating neighbours according to the level of confidence in common threat presence *"context"*, can subsequently, manage the number of active communicating neighbours at a given point in time. This explains why VIGILANT helps to improve on communication energy consumption, while also maintaining a higher QoSI output level,

by utilising only those neighbours that can achieve a higher confidence in common threat presence *"context"*, as indicated in figures 4.6 and 4.10.

An additional observation from figure 4.10 also shows, VIGILANT communication energy consumption is lower under TOC = 1.0 conditions than when TOC = 0.01. Again, a lower observation uncertainty (TOC = 1.0), implies greater confidence and awareness in common *"context"* about the presence of a threat within the collaborating group. Greater awareness increases the partnership stability, given by (4.9) and as a result, increases the expected QoSI service provision time, *E (M)*, given by (4.10). This assists in further reducing the frequency of QoSI updating, which invokes less communication energy expenditure and as shown in figure 4.10, reduces further, as H_T is increased under both TOC conditions. As in the case with VIGILANT latency performance, increasing H_T can lower latency and encourage less communication energy expenditure but as shown in figure 4.11, this does have an effect in reducing the overall QoSI performance possible.

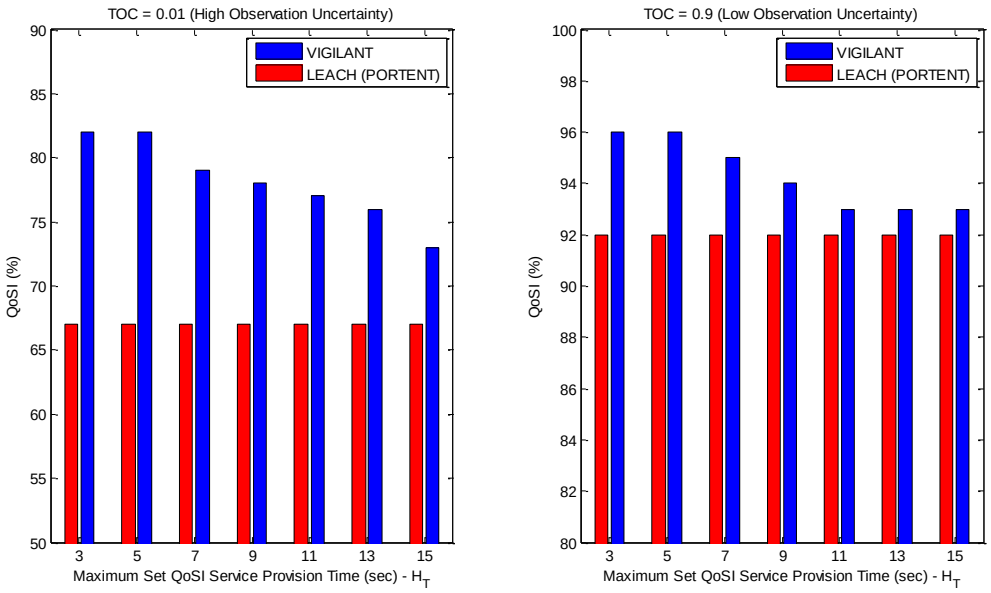

Figure 4.11: The effect of H_T on QoSI performance, with H = 0.9

From figure 4.11, it is evident that a trade-off analysis might be necessary to further examine the relationship between QoSI update latency and communication energy

expenditure through variations in H_T and the level of QoSI performance required, under different TOC conditions. Alternatively, developing an improved VIGILANT system that can decide itself the correct confidence measure in *M1 "context"* to use for collaboration purposes (replacing *H*) and when to transmit their surveillance update packets (replacing H_T), is an interesting option. In chapter 5, we describe how an improved VIGILANT system can be developed in order to cater for these concerns.

CHAPTER 5

VIGILANT+: Distributed Autonomic Sensor Management

In chapter 4, VIGILANT has shown the potential of using an SA enabled approach to encourage sensors to form groups according to, the level of common *"context"*, where this *"context"* is expressed in terms of a threat presence situation. The *"context"* itself is derived using level 2 operations, which can then be further applied and processed to assist in a *"context-aware"* service discovery mechanism. "*Context-awareness*" improves the process of identifying suitable sensors for collaboration and provides the capability to assist in the management of network resource consumption.

One of the main drawbacks associated with the current VIGILANT operation is that all *"context"* enabled features are conducted by the current GI. This GI led responsibility again encourages centralised control, which can lead to increased communication overhead in the form of greater communication energy and bandwidth consumption. In addition to current VIGILANT operation, the *"context"* enabled features are also predominantly associated with facilitating a *M1* capability and no attempt has been made, as yet, to supporting a *M2* capability. In this chapter, we cater for these concerns by improving VIGILANT operation in the following ways:

- We redefine the SA level 2 BBN to incorporate a joint *M1* and *M2* perspective towards the surveillance environment, as shown in 5.1.
- By redefining SA level 2 operations we can extract the relevant *"context"* confidence measures, concerning the current *M1* and *M2* environment, in order to provide

deployed *UGS* sensors with an ability to assign themselves to a particular mission objective autonomously, as shown in section 5.1.1, rather than using the current VIGILANT *"context-aware"* service discovery mechanism.

- Improving on SA level 3 operations to enable collaborating sensors to adjust their network resource consumption, through distributed self-managed transmission control according to the level in common mission objective *"context"*, as shown in section 5.2.

Figure 5.1, illustrates the proposed improvements to be made over current VIGILANT operation, primarily to improve further the operational resource efficiencies. This can be achieved through adaptive networking according to the SA of the surveillance environment. As indicated in figure 5.1, being efficient in the consumption of network resources, requires an incorporation of the awareness concerning the *"context"* to a current specific mission objective.

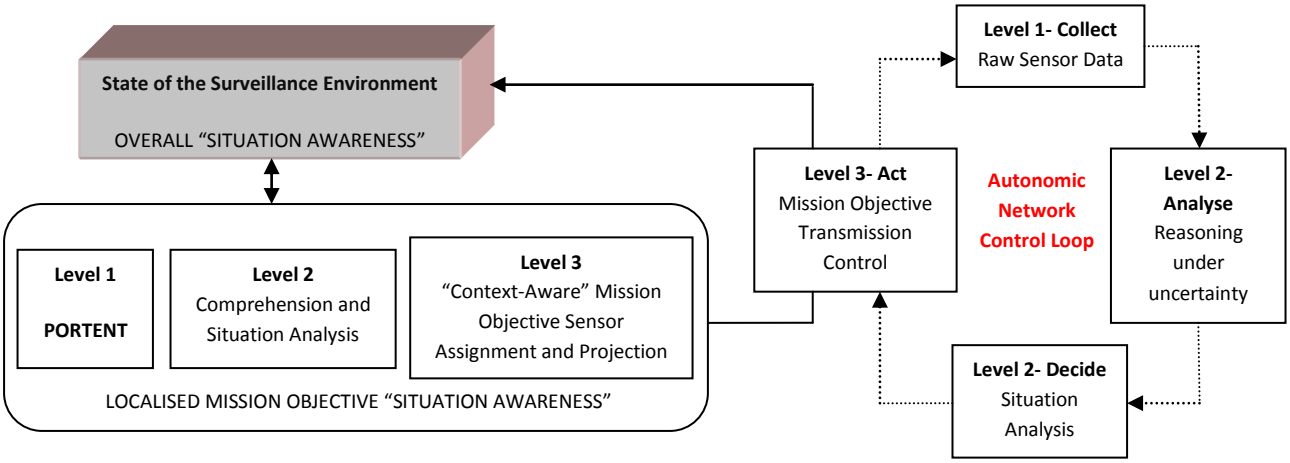

Figure 5.1: VIGILANT+ approach to SA informed autonomic networking, derived from figure 4.1

In section 5.1, we highlight a potential mechanism to enable a fully distributed GI-sensor mission objective collaboration capability, through level 2 and level 3 operations, as indicated in figure 5.1. The new system is called VIGILANT Plus, denoted VIGILANT+.

5.1 VIGILANT+ Collaboration

VIGILANT+ collaboration is focused on sensors that can establish their own localised level 2 *"context"* of the present *M1* or *M2* situation (e.g. awareness to, and geo-location of, a current threat), in order to allow sensor self-assignment to a particular mission objective. We still utilise PORTENT- option 2 for the purposes of SA level 1 perception and this is integrated into the re-defined BBN describing a joint *M1* and *M2* surveillance perspective, as shown in figure 5.2. Table 5.1, summarises the relevant probability derivations made from figure 5.2 for initiating *"context"* based decisions at local *UGS* level, concerning the current threat situation for each respective mission objective. In 5.1.1, we detail how the derivations made from figure 5.2 can assist the ad-hoc collaboration process.

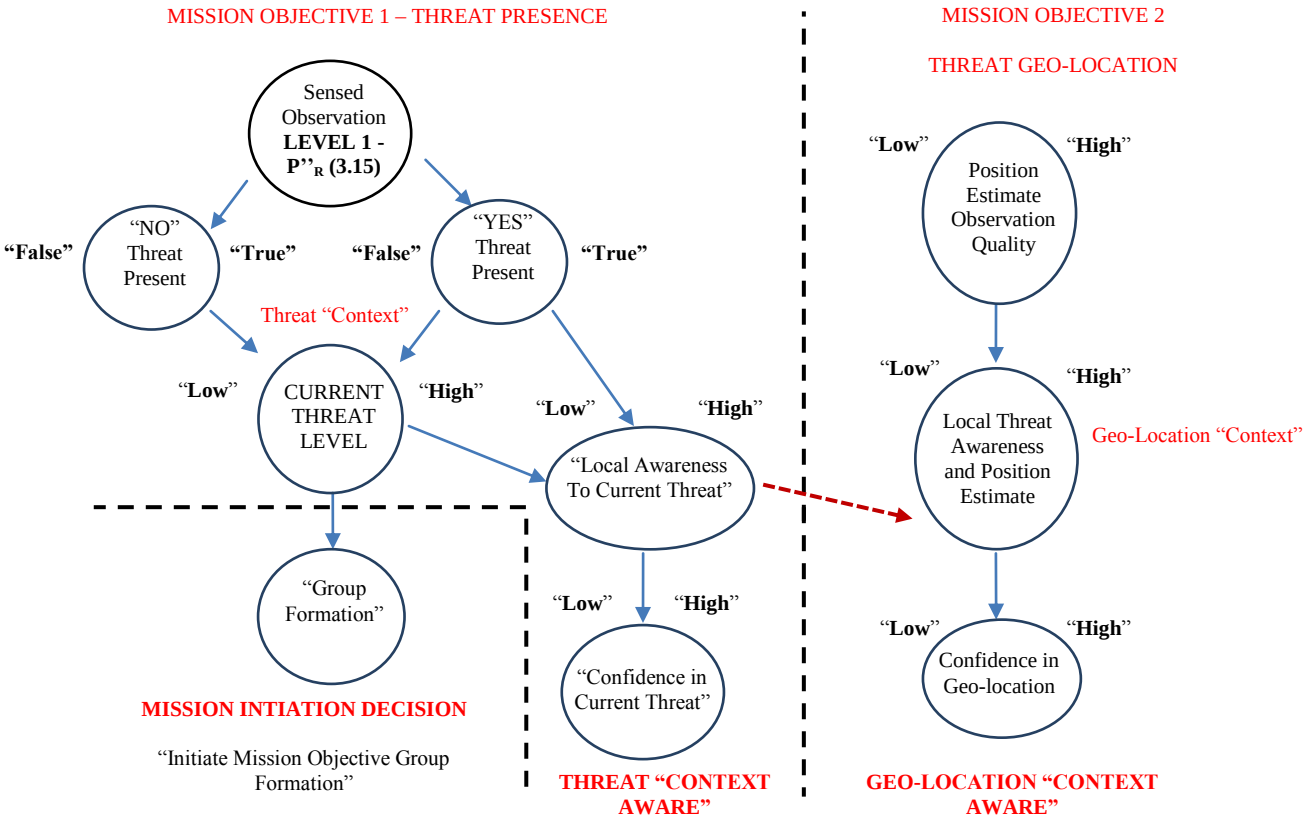

Figure 5.2: VIGILANT+ BBN for localised mission objective situation analysis

Probability Expression	Probability Derivation from figure 5.2 using CPT Analysis
1. p(Yes Threat Present – "True" (C))	p(C | Threat Presence True) × P''_R + p(C| Threat Presence False)× $(1 - P''_R)$
2. p(No Threat Present – "True" (D))	p(D | Threat Presence True) × P''_R + p(D | Threat Presence False)× $(1 - P''_R)$
3. p(Current Threat Level – "High" (F))	[p(F| C,D) × p(C) × p(D)] + [p(F | ~C,D) × p(~C) × p(D)] + [p(F|C,~D) × p(C) × p(~D)] + [p(F | ~C,~D) × p(~C) × p(~D)]
4. p(Threat-High) ***Group Formation**: if p(Threat-"High") > 1 – p(Threat- "High")*	p(Yes-"Form"| F)× p(F) + p(Yes-"Form"| ~F)×p(~F)
5.p(Local Awareness to Current Threat)– "High" (L)	[p(L | C,F) × p(C) × p(F)] + [p(L | ~C,F) × p(~C) × p(F)] + [p(L | C,~F) × p(C) × p(~F)] + [p(L | ~C,~D) × p(~C) × p(~F)]
6. ***Mission Objective 1*** *p(Confidence in Current Threat – "High" (Q))*	p(Q | L) × p(L) + p(Q| ~L)× p(~L)
7. p(L and Position Observation Estimate (POE) – "High" (E))	[p(E | L,POE) × p(L) × p(POE)] + [p(E | ~L,POE) × p(~L) × p(POE)] + [p(E | L,~POE) × p(L) × p(~POE)] + [p(E | ~L,~POE) × p(~L) × p(~POE)]
8. ***Mission Objective 2*** *p(Confidence in Geo-Location – "High" (S))*	p(S | E) × p(E) + p(S | ~E)× p(~E)

Table 5.1: Probability derivations from figure 5.2 for initiating group formation and facilitating "context-aware" decisions regarding a specific mission objective

5.1.1 Querying for Sensor Mission Objective Self-Assignment

The development of VIGILANT has already shown that ad-hoc collaboration of single hop sensors can be enhanced by assigning sensors to a group that have similar confidence in common *"context"* concerning a threat presence, using the CF model. The evaluation of confidence in common threat presence *"context"*, however, in VIGILANT, is conducted by the GI using CF feedback from immediate neighbours, as shown in chapter 4, figure 4.3. The CF model, however, is a procedure which can also be performed locally by the immediate neighbourhood. This is made possible if neighbours are notified by the GI of its own CF value, named as *CF "GI"*, which is only sent as *content* within a publish "request" packet during the group formation phase, after the condition in entry 4, table 5.1, is met.

Evaluation of distributed mission objective *"context"* assisted through, *CF "GI"*, in this way, enforces uncoupled coordination, where distributed sensors are modelled as a set of components interacting with each other through, analysing and reacting to their

"context" independently [64-65]. This supports flexibility within dynamic *UGS* surveillance network scenarios where *UGS's* are free to leave and join the collaborative group independently, during a surveillance mission. Figure 5.3, illustrates the overall publish-subscribe *"context-centric"* operation used for GI led sensor self-assignment and subsequent collaboration, concerning the mission objective in question.

From figure 5.3, a combined *CF "Mission Objective"* evaluation is conducted by the local distributed *UGS* in the same way, as shown earlier in chapter 4, (4.4) and (4.5) and quantifies, in the same manner, that a GI and its immediate neighbour should collaborate, due to their respective current mission objective *"context"*. Table 5.2, shows the relevant MB and MD expressions for local *UGS* mission objective CF evaluation derived using table 5.1, which can then be substituted into the expression given in chapter 4, equation (4.5).

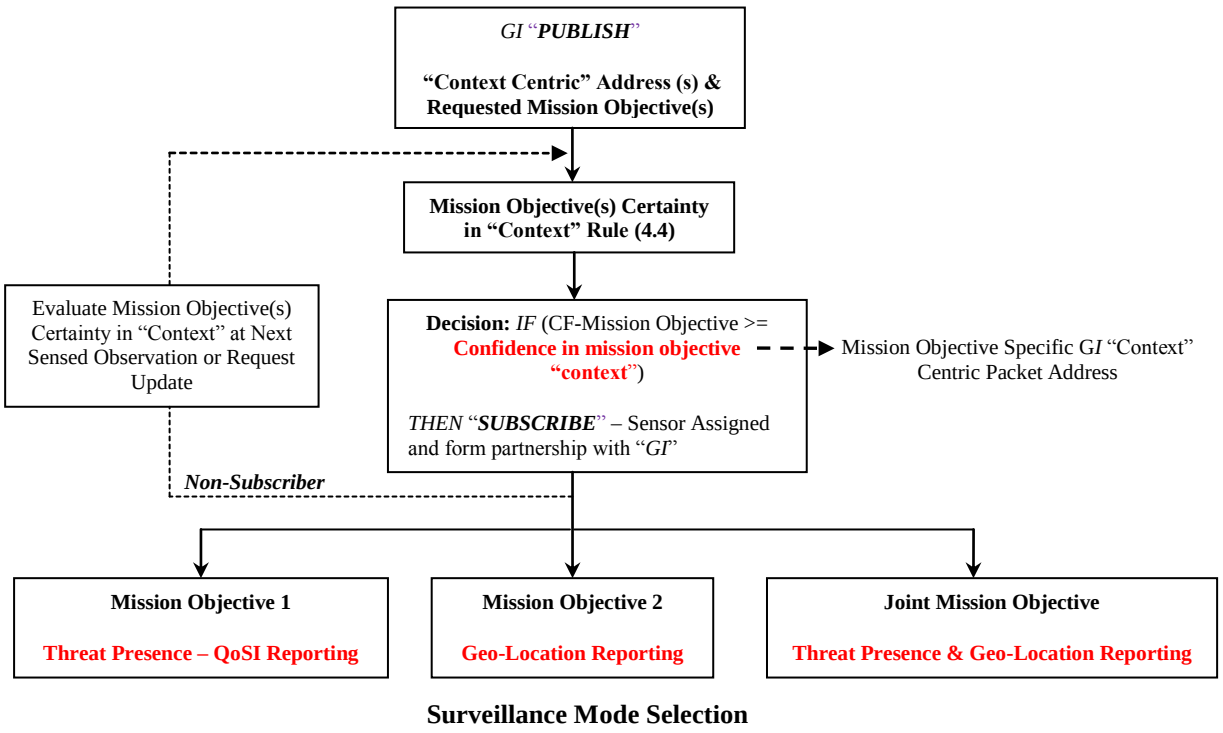

Figure 5.3: "Context" centric publish-subscribe querying for local UGS mission objective self-assignment

	Mission Objective 1 – Threat Presence	Mission Objective 2 – Threat Geo-Location
Increased Belief (MB) Expression	$\frac{p(\text{AwarenesstoThreat}\mid L)-p(L)}{1-p(L)}$	$\frac{p(\text{Geo}-\text{LocationAwareness}\mid E)-p(E)}{1-p(E)}$
Increased Disbelief (MD) Expression	$\frac{p(L)-p(\text{AwarenesstoThreat}\mid L)}{p(L)}$	$\frac{p(E)-p(\text{Geo}-\text{LocationAwareness}\mid E)}{p(E)}$

Table 5.2: MB, MD expressions for local UGS CF-Mission Objective evaluation, using table 5.1

As indicated in figure 5.3, the GI itself specifies which mission objective is required within the received publish "request" packet. The querying for mission objective self-assignment is then conducted against the GI *"context-centric"* address, which is derived using entries 6 and 8, from table 5.1 and sent within the *content* of the received GI publish "request" packet. In figure 5.3, feedback is also used by non-subscribers to re-evaluate their position if local *"contextual"* changes do occur. This can help to improve the GI led collaborating group performance by maintaining a relevant and up-to date group perspective towards, the *M1* or *M2* surveillance environment during a mission.

Querying against the GI *"context-centric"* address can also help to minimise the communication overhead incurred during the collaboration phase, compared with VIGILANT, since both CF evaluation and mission objective assignment are conducted locally by the *UGS* and not at the GI. In addition, the need for a fixed, system defined value for sensor confidence in *"context"* for CF evaluation comparison, as in the case with VIGILANT (given by *H*) is not required. Instead, sensor confidence becomes a dynamic value, which varies according to *"contextual"* changes during a dynamic surveillance mission, given by entries 6 and 8, in table 5.1.

5.1.2 Group Initiator Re-Election

GI re-election is dynamically conducted in the process of a mission. Assigned sensors rely on the current *GI* mission objective *"context"* centric address (GI_{mocca}) sent in the initial publish "request" packet, to re-evaluate whether a "new" *GI* status needs to be initiated, as shown in (5.1).

$$if(Confidence\,in\,current\,mission\,objective"\,context"\,) \geq (GI_{mocca}) \tag{5.1}$$

$$Then, Publish"\,New"\,GI\,Mission\,Objective\,Re\,quest\,Status$$

Upon the condition in (5.1) being satisfied, locally, distributed sensors re-evaluate their mission objective *"context"* certainty, as shown in figure 5.3. The resulting new ad-hoc collaborating group can further facilitate in maintaining, a relevant and on-going aggregation of mission objective information utility.

5.2 VIGILANT+ Autonomic Transmission Control

UGS's that decide to assign themselves to a specific or joint mission objective follow by initiating *autonomic* transmission control, which is orientated towards the management of network resources at infrastructure level, through applying direct feedback and acting upon temporal environmental dynamics. Being efficient to network resource consumption implies an approach, which provides projection capabilities (level 3) concerning the *"context"* to a current specific mission objective. This indicates the need to employ a temporal framework that can establish and evaluate future *"context-awareness"* of the progressive mission objective surveillance environment, in order to assist the transmission control decision making process. Transmission control can be formalised using a random discrete time state representation, commonly referred to as either a, Markov Decision Process (*MDP*) or Partially Observable *MDP* (*POMDP*) and is detailed further in 5.2.1 and 5.2.2.

5.2.1 MDP Formulation for Transmission Control

A MDP is a model that allows us to take inputs regarding the state of the environment and generate actionable outputs, which themselves affect the state of the environment. In the MDP framework it is never assumed that there is any uncertainty concerning the current state of the environment. A MDP representation therefore stipulates that a belief probability towards the current state environment is conditionally independent of all previous states and actions taken, due to the Markov property exhibit memory-less operation [66-67]. This property implies that current actions regarding transmission control decision making are dependent only on the current state, as shown in figures 5.4 and 5.5. From figures 5.4 and 5.5, evaluating a current belief state (BS_{k+i}), to facilitate transition to the next state ($STATE_{k+i}$), where i=0 at initialisation, is based only on the conditional joint probability of the current observation, z_{k+i} (A_1) and current transmission action taken, a_{k+i} (A_3), as shown in (5.2).

$$BS_{k+i} = p(\, STATE_{k+i} \,|\, A_1, A_3 \,) \tag{5.2}$$

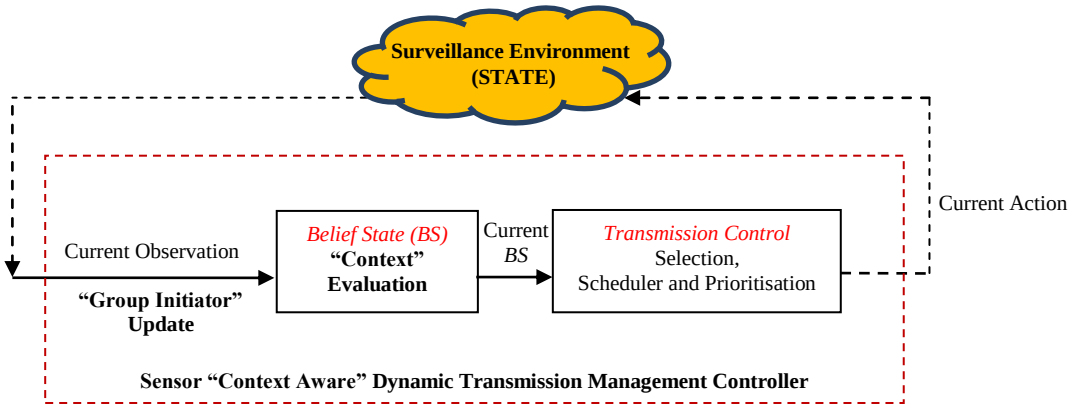

Figure 5.4: MDP representation of the underlying shared state environment

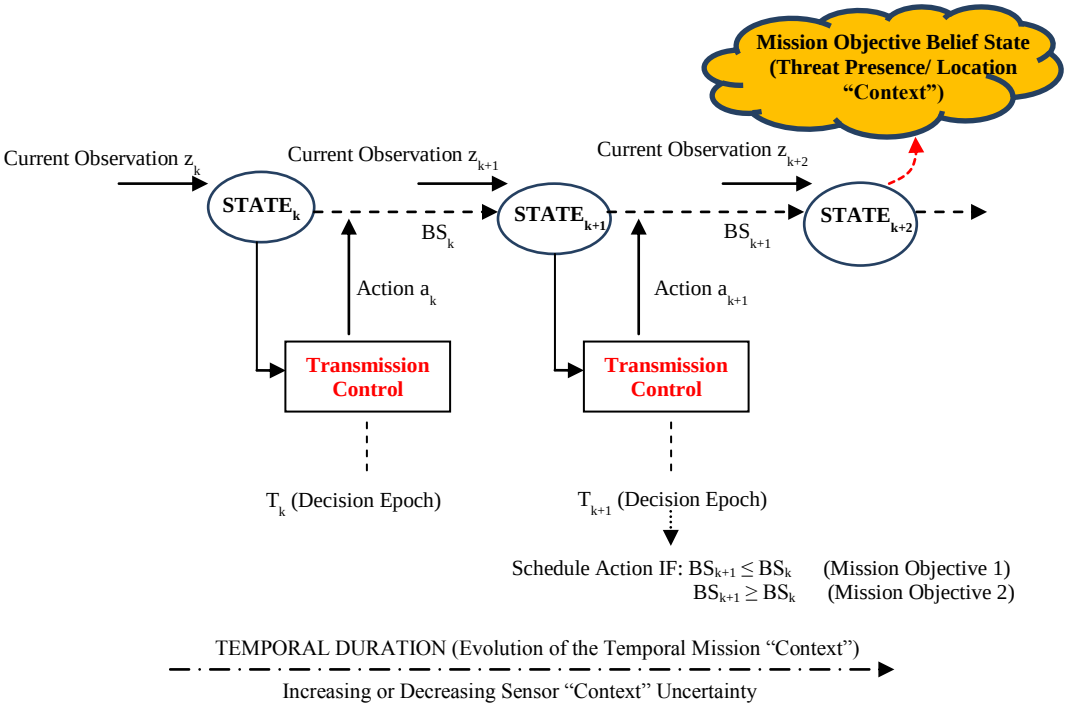

Figure 5.5: MDP projection of the decision chain to future states is driven by BS_{k+i}

From figure 5.4, further GI updates are utilised to deduce the current observable common state environment and also to fulfil the memory-less MDP operation condition, as indicated in figure 5.5. This implies that an evaluation of the *"context"* of the mission objective surveillance environment at each decision epoch can, only be undertaken after a GI update concerning its *"context"* is received. A higher GI update rate would therefore suggest a better evaluation of the *"context"* of the *M1* or *M2* surveillance environment. A consequence of using further GI updates would be to increase network communication energy and bandwidth. We seek to explore this possibility when evaluating VIGILANT$^+$ MDP system performance, with a view to considering the increase in *M1* or *M2* information utility if any, due to an informed perspective about the current common state environment, at the expense of greater network resource consumption.

5.2.2 POMDP Formulation for Transmission Control

A *POMDP* implementation is similar to an *MDP* implementation, but the decision maker (*UGS*) has an incomplete perspective regarding the common state environment (partially observable). In order to behave effectively in a partially observable state environment, it is necessary to remember previous actions and state observations to aid in the disambiguation associated with the evaluation of common *"context"* regarding the surveillance environment. This implies that operating within a partial observable state environment requires feedback control of previous actions and observations, as shown in figures 5.6 and 5.7 [68-69]. The essential task for a *POMDP* transmission feedback-control implementation is the belief state estimation (*BSE*), as shown in figures 5.6 and 5.7. *BSE* represents the most probable view regarding the current common state environment, given past experiences. From figures 5.6 and 5.7, evaluating a current *BSE* (BSE_{k+i}) , to facilitate transition to the next state ($STATE_{k+i}$), where i=1 at initialisation, is based on the conditional joint probability of the current observation z_{k+i} (A_1), previous transmission action a_{k-i} (A_3) and previous BSE_{k-i} (A_4), given in (5.3).

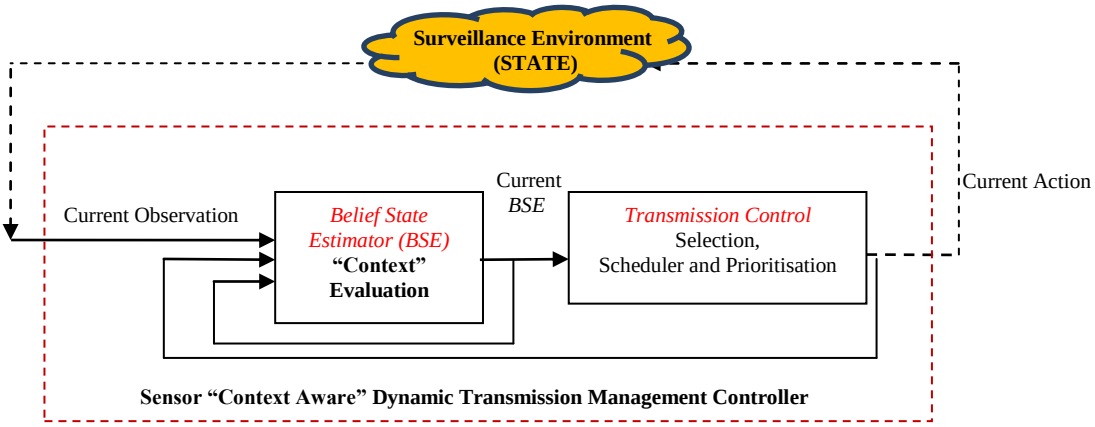

Figure 5.6: POMDP representation of the underlying common state environment

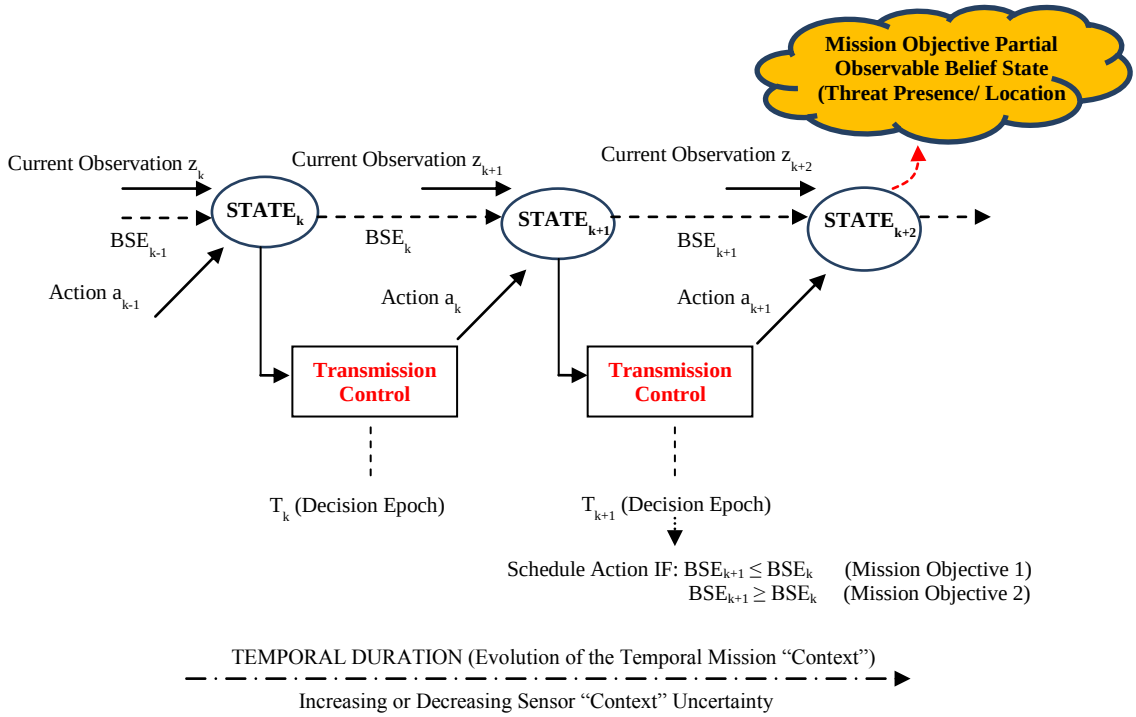

Figure 5.7: POMDP projection of the decision chain to future states is driven by BSE_{k+i}

$$BSE_{k+i} = p(STATE_{k+i} \mid A_1, A_3, A_4) \tag{5.3}$$

Transmission control decisions are made at each decision epoch with the frequency interval only dependent on the rate at, which local *UGS* observations are made. A POMDP model is considered as a means of allowing a fully distributed, self-managed transmission control system since, further use of GI updating, as with the MDP case, is not utilised and all *"context"* evaluation is undertaken locally. Not relying on further GI updating regarding the mission objective *"context"* would substantiate whether any improvements in communication energy and bandwidth consumption can be made, at the expense of any degradation in reported *M1* or *M2* information utility.

As detailed so far in 5.2.1 and 5.2.2, being in a particular state signifies an evaluation of the current common *"context"* to a specific mission objective at that point in time. For *M1* operation this has already been detailed earlier in chapter 4, under 4.3.1, for the

VIGILANT system and the probability of correct detection in common threat awareness *"context"*, T_1, is equal to (1- P_1), where P_1, given in (4.6) forms the basis for the eventual evaluation of BS_{k+i} or BSE_{k+i}, as shown in (5.4).

$$BS_{k+i} = p(STATE_{k+i} | T_1, A_3) \tag{5.4}$$

$$BSE_{k+i} = p(STATE_{k+i} | T_1, A_3, A_4)$$

In 5.2.3, we detail how the evaluation of current common *M2 "context"* can be made to facilitate MDP and POMDP transmission control. Evaluating *"context"* for each respective mission objective according to either the MDP or POMDP framework, as shown in figures 5.5 and 5.7, can then enable us to make the necessary transmission control decisions (selection, scheduling and prioritisation), detailed further in 5.2.4 to 5.2.6.

5.2.3 Determination of Common Threat Geo-location "Context"

For *M2* operation, we assume that the sensors have the ability to obtain current threat position (x_{Threat}, y_{Threat}) using techniques such as time difference of arrival (TDOA). Obtaining a current threat position can subsequently be used to calculate the current geometric dilution of precision ($GDOP_k$), with respect to the *GI*. $GDOP_k$ measures the accuracy in common geo-location *"context"*, quantifying the mapping of measurement errors into position errors, magnified by the geometric relation of *UGS* to threat geometry [70-71]. The geometry matrix $\mathbf{H}^{\mathbf{T}}\ \mathbf{H}$, at each decision epoch, for *N* active sensors, is expressed in (5.5). In all cases we assume, *GI* (x_{GI}, y_{GI}) and active sensor (x_i, y_i) positions are known.

$$H^T H = \begin{bmatrix} \sum_{i=1}^{N-1} (a_{xi} - a_{xr})^2 & \sum_{i=1}^{N-1} (a_{xi} - a_{xr})^2 (a_{yi} - a_{yr}) \\ \sum_{i=1}^{N-1} (a_{xi} - a_{xr})^2 (a_{yi} - a_{yr}) & \sum_{i=1}^{N-1} (a_{yi} - a_{yr})^2 \end{bmatrix} \tag{5.5}$$

Where, $a_{xi} = (x_{Threat} - x_i) \Big/ \sqrt{(x_{Threat} - x_i)^2 + (y_{Threat} - y_i)^2}$, $a_{xr} = (x_{Threat} - x_{GI}) \Big/ \sqrt{(x_{Threat} - x_{GI})^2 + (y_{Threat} - y_{GI})^2}$

$a_{yi} = (y_{Threat} - y_i) \Big/ \sqrt{(x_{Threat} - x_i)^2 + (y_{Threat} - y_i)^2}$ and $a_{xi} = (x_{Threat} - x_i) \Big/ \sqrt{(x_{Threat} - x_i)^2 + (y_{Threat} - y_i)^2}$.

Since the matrix **($\mathbf{H^T H}$)** is symmetric and positive definite, all eigenvalues λ_1, λ_2 are real and positive [71]. The eigenvalues λ_1, λ_2 gives an indication as to the current amount of error present, in relation to the GI and sensor to-threat geometry and therefore smaller values of λ_1, λ_2 correspond to a lower dilution of error and better geo-location accuracy [72]. The trace of the matrix **($\mathbf{H^T H}$)**, then quantifies the total error present and is equal to the sum of the eigenvalues λ_1, λ_2, given in (5.6).

$$trace(H^T H) = \lambda_1 + \lambda_2 = \sum_{i=1}^{N-1} [\,(a_{xi} - a_{xr})^2 + (a_{yi} - a_{yr})^2\,] \tag{5.6}$$

A final current precision measure in GI-sensor-to-threat geometry error, $GDOP_k$, is therefore given as shown in (5.7).

$$GDOP_k = \sqrt{trace(H^T H)^{-1}} \tag{5.7}$$

Utilising the $GDOP_k$ measure to serve as an approximation of the current threat location (*CTL*) in terms of circular error probable (CEP) [73-74], we can obtain a likelihood measure for common *"context"* (Q_1), forming the basis for eventual BS_{k+i} or BSE_{k+i} evaluation, given in (5.8).

$$BS_{k+i} = p(STATE_{k+i} \,|\, Q_1, A_3) \tag{5.8}$$

$$BSE_{k+i} = p(STATE_{k+i} \,|\, Q_1, A_3, A_4)$$

$$Q_1 = p(CTL \,|\, GDOP) = exp\left(-\frac{(GDOP_{MAX} - GDOP_k)^2}{2\sigma^2_{RangeError}}\right) \Big/ \sqrt{2\pi}\sigma_{RangeError}$$

The CEP is a measure of the uncertainty in the *CTL* estimate relative to its mean value. If the *CTL* estimate is unbiased, the CEP forms a direct measure of the *CTL* uncertainty relative to its true position [74]. From (5.8), $GDOP_{MAX}$, represents the maximum

permissible *GDOP* error and $\sigma_{Range\text{-}Error}$, is the standard deviation in passive range measurement errors taken between an *UGS* and the monitored *CTL*.

5.2.4 Mission Objective Transmission Control: Selection

Selection for transmission at each decision epoch can be formulated in terms of state information gain, using information discrimination techniques such as, *Rényi* divergence, also known as α-divergence [13][75]. Utilising a state information gain approach can form a direct measure on the quality for sensor transmission selection; this being either to select transmission or not, with an expected utility calculated for each. The calculation of information gain between two probability densities p_1 and p_0 using *Rényi* divergence denoted by, $(p_1 \,||\, p_0)$, is given in (5.9), where α, is used to adjust how heavily one emphasises the tail of the two distributions p_1 and p_0.

$$D_\alpha(p_1 \,||\, p_0) = \frac{1}{1-\alpha} \ln \int p_1^\alpha(x) p_0^{1-\alpha}(x)\, dx \tag{5.9}$$

In the limiting case of $\alpha \rightarrow 1$ the Rényi divergence becomes the commonly used Kullback-Leibler (KL) discrimination and is an appropriate information gain measure for sensing applications, as shown in (5.10) [76-77].

$$\lim_{\alpha \rightarrow 1} D_\alpha(p_1 \,||\, p_0) = \int p_0(x) \ln \frac{p_0(x)}{p_1(x)} \tag{5.10}$$

If probability state representations are taken from a normal distribution, $p_1 \sim N(\mu_1, \sigma_1^2)$ and $p_0 \sim N(\mu_0, \sigma_0^2)$ the KL discrimination (D_{KL}) is shown in (5.11).

$$D_{KL} = \lim_{\alpha \rightarrow 1} D_\alpha(p_1 \,||\, p_0) = \frac{(\mu_1 - \mu_0)^2}{2\sigma_0^2} + \frac{1}{2}\left(\frac{\sigma_1^2}{\sigma_0^2} - 1 - \ln\left(\frac{\sigma_1^2}{\sigma_0^2}\right)\right) \tag{5.11}$$

For *M1* operation, the requirement is to have as much divergence between p_1 (non-common threat awareness) and p_0 (common threat awareness), in order to represent an increase in information gain. The expected utility (*EU*) in (5.12) illustrates how risk attitudes are managed according to the current uncertainty towards high threat presence awareness.

$$EU_{M1-Yes-TX} = \frac{1}{1+e^{(\beta - D_{KL})}} \times (BS_{k+i} \; or \; BSE_{k+i}) \qquad (\beta = 2/D_{KL-MAX}) \tag{5.12}$$

For *M2* operation, the requirement is to have as much convergence between p_1 ($GDOP_{MAX}$) and p_0 ($GDOP_k$), in order to represent an increase in information gain. Transmission selection risk attitudes are modelled by (5.13), on $GDOP_k$, this being a direct approximation of the current CEP, a measure for geo-location accuracy.

$$EU_{M2-Yes-TX} = \frac{1}{1+e^{(D_{KL} - \beta)}} \times (BS_{k+i} \; or \; BSE_{k+i}) \qquad (\beta = D_{KL-MAX}/2) \tag{5.13}$$

Transmission is selected by ensuring that the current expected utility for "yes" transmission is greater than or equal to the expected utility of selecting "no" transmission, as given in (5.12) and (5.13) but with complementary weighting.

5.2.5 Mission Objective Transmission Control: Scheduling

M1 or *M2* surveillance update scheduling can be activated according to BS_{k+i} or BSE_{k+i}, which represents a belief transition probability from the current to future state environments. Figures 5.5 and 5.7, illustrate the decision for selecting *M1* and *M2* transmission scheduling under either a MDP or POMDP framework with both conditions derived to provide group stability, for situations where no state *"contextual"* discrepancy occurs. For *M1* operation, this means a non-scheduling action, as long as, the evaluated BS_{k+i} or BSE_{k+i} continues to increase the level of common threat presence *"context"*, according to (5.4). For *M2* operation a positive scheduling action is only undertaken, as long as, the BS_{k+i} or BSE_{k+i} increases the level in common geo-location *"context"*. This

represents an improved evaluation of $GDOP_k$ from the previous state, which is a direct approximation of the current improvement in *CTL* accuracy in terms of the CEP, as shown in (5.8).

5.2.6 Mission Objective Transmission Control: Prioritisation

In a similar fashion to QoSI provisioning for VIGILANT, we utilise the same method in order to ensure reliable *M1* or *M2* surveillance report delivery. As discussed earlier, provisioning according to common *"context"* within a collaborating group can promote improved communication energy consumption and bandwidth efficiency. Collaborating sensors, which invoke a positive transmission scheduling action, determine a service priority time based on the current BS_{k+i} or BSE_{k+i}. A surveillance service priority time (M), is then evaluated in terms of how the common state environment, will achieve a common stability out of a progressive total of H time steps in seconds, given as the CDF of a binomial distribution, as shown in (5.14). Figure 5.8 details the surveillance service priority time algorithm, according to (5.14).

$$M \sim Binomial(\ H, MissionObjectiveSpecific BS_{k+i}\ or\ BSE_{k+i}\ ) \tag{5.14}$$

$$p(M = H) \sim (\ MissionObjectiveSpecific BS_{k+i}\ or\ BSE_{k+i}\ )^H$$

From figure 5.8, the value of derived M is dependent on the present degree of common *"context"* regarding the state of the mission objective environment, with respect to the current GI. A higher belief state transition probability therefore implies a higher M (lower urgency), since the present uncertainty within the shared state environment is low. Surveillance service provision according to the belief state transition probability, therefore allows a unique and dynamic sensor channel access mechanism by adapting individual schedule channel access periods according to mission objective *"context"*, with aim of promoting minimal congestion within the collaborating group for reliable *M1* or *M2* surveillance updating.

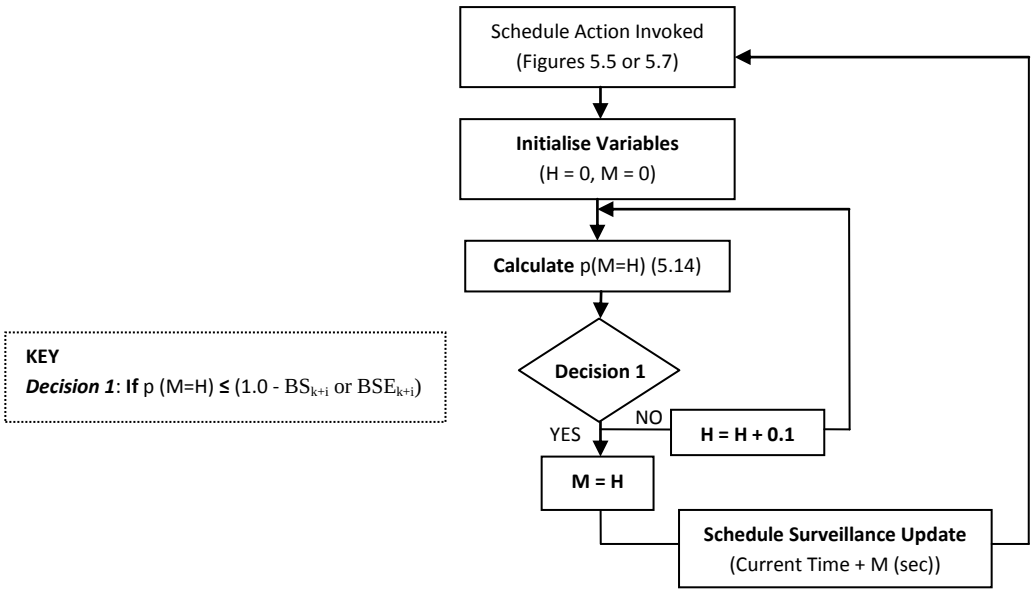

Figure 5.8: M1 and M2 surveillance service priority time algorithm

Figure 5.9 illustrates the complete integrated process for VIGILANT$^+$ distributed sensor management, for the purposes of mission objective self-assignment and self-managed transmission control. As indicated in figure 5.9, VIGILANT$^+$ shows how a *"context"* centric approach can actuate distributed *UGS* surveillance management, in terms of GI-sensor collaboration and subsequent management of network resource consumption. Autonomic transmission control is only initiated when a *UGS* decides to collaborate. If self-assignment is not activated then *UGS's* would continue only to re-evaluate their *"context"* for collaboration independently and not invoke transmission control. As indicated in figure 5.9, the *"context"* centric surveillance management procedure is re-initialised upon receiving a "New GI" publish request packet.

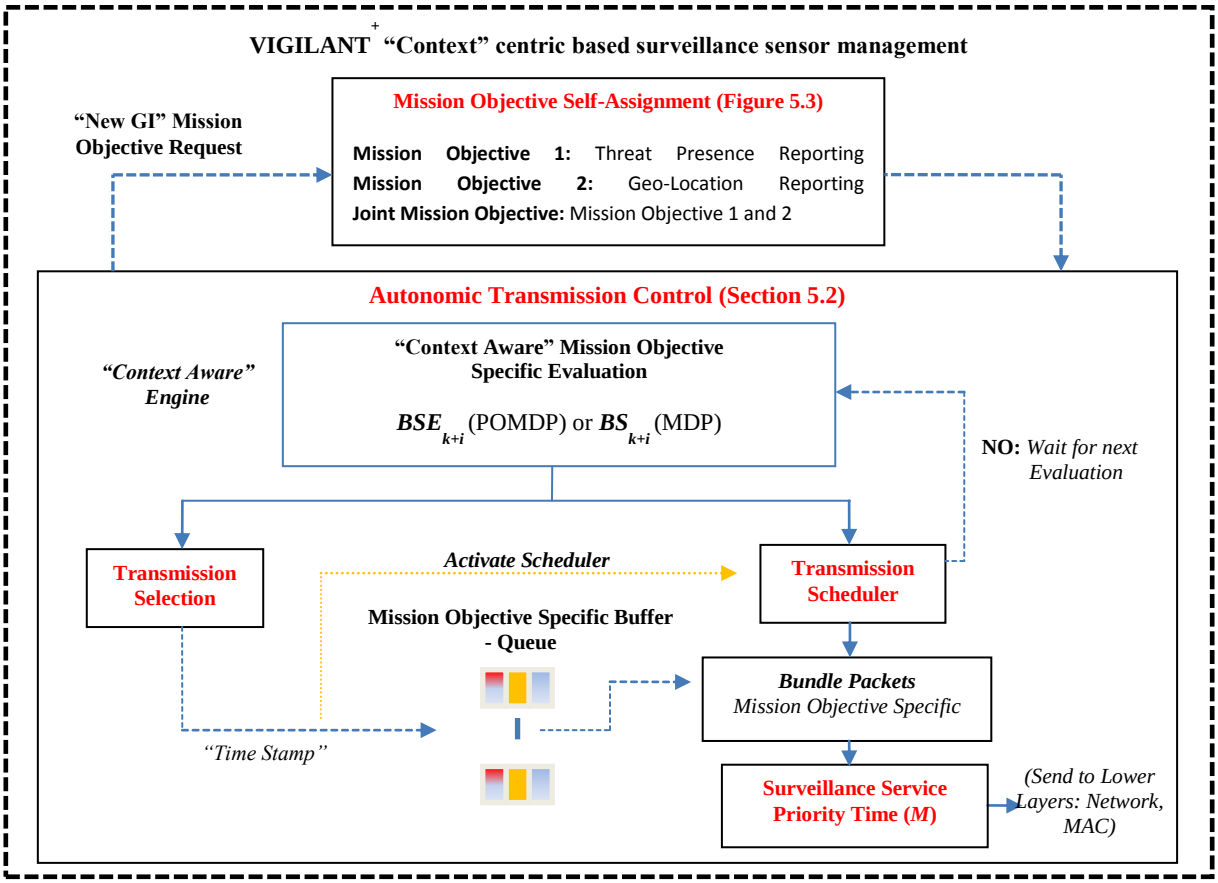

Figure 5.9: VIGILANT+ distributed autonomic sensor management

5.3 VIGILANT+ System Performance

System performance is evaluated using the OMNeT++ network simulation platform [63]. We utilise the same network deployment and threat monitoring characteristics, as already described for VIGILANT performance, in chapter 4, section 4.4. Surveillance performance is measured either against level-1 threat observation certainty (*TOC*), through varying the mean separation in yes threat (μ_{Fast1} , $\mu_{Slow1)}$, no threat (μ_{Fast0} , μ_{Slow0}) probability occurrence distributions, required in PORTENT "fast" and "slow" operation or velocity of the mobile threat, *v* m/s. In figures 5.4 and 5.5, it was noted that further GI updates are required, to fulfil the memory-less MDP operation condition. The GI update rate itself affects the evaluation accuracy made, with regards to the *"context"* concerning the *M1* or *M2* surveillance environment. Rather than specify the GI update rate ourselves and in order

to operate under fully *autonomic* conditions, we employ the following threat dependent strategies:

- *MDP-Option 1* implies a GI update is sent every time a positive PORTENT-Option 2 detection is made, as shown in figure 3.1, in chapter 3.
- *MDP-Option 2* implies a GI will only initiate the sending of updates once the condition for confidence in current threat, given in table 5.1, entry 6, is less than the previous evaluated confidence. Once this condition is satisfied, then an update is sent every time a positive PORTENT-Option 2 detection is made.

As part of our system evaluation, we again do not consider the effects of sampling rate, number of deployed nodes and sensing coverage range on VIGILANT$^+$ performance. Our evaluation is again concerned with the effects of collaborating and managing network resource consumption according to, the joint *"context-awareness"* of the *M1* and *M2* surveillance environment.

5.3.1 Surveillance Utility Performance

Performance for threat presence detection is again measured using QoSI, as the level-1 *TOC* is varied. Figure 5.10, shows VIGILANT$^+$ QoSI performance compared against VIGILANT and LEACH. As indicated in figure 5.10, LEACH operation with continuous updating, employing all one-hop neighbours and without giving consideration of the common threat presence *"context"*, decreases *M1* utility in terms of QoSI. This is especially true within a low TOC environment (TOC = 0.1 to 0.3), when compared with VIGILANT and VIGILANT$^+$. Both VIGILANT and VIGILANT$^+$ integrate threat presence *"context"* evaluation features during the collaboration set-up phase. A GI within VIGILANT operation would reduce the contribution from outlier nodes through requested sensor CF feedback and in the case of VIGILANT$^+$, distributed *UGS* nodes would query their threat presence *"context"* against the GI publish *"context"* centric address packet, to

ensure they are appropriate *M1* collaborators. In essence, both collaboration mechanisms are able to ensure only those sensors, which have a high *"context awareness"* concerning the presence of a threat are selected. This ensures both VIGILANT and VIGILANT+ can maintain consistent QoSI performance across a range of *TOC* conditions.

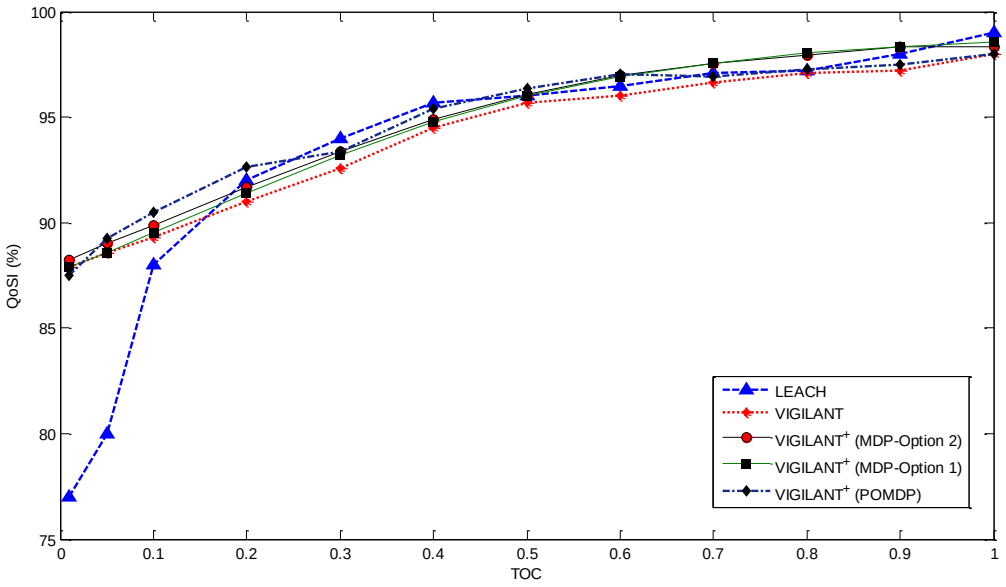

Figure 5.10: M1 performance, QoSI with level-1 TOC, v= 5m/s

An additional observation from figure 5.10, suggests that for the considered network deployment characteristics, VIGILANT+ POMDP, MDP-Options 1 and 2 have comparable QoSI performance. It appears that using further GI updating through a MDP framework (memory-less operation) does not increase QoSI performance over POMDP operation. This suggests that employing a partially observable mode of operation, through an initial GI update and applying feedback on past observation experiences, can maintain consistent levels of QoSI and does not degrade overall *M1* performance. This indication provides potential to suggest that a fully distributed *M1* surveillance capability is possible.

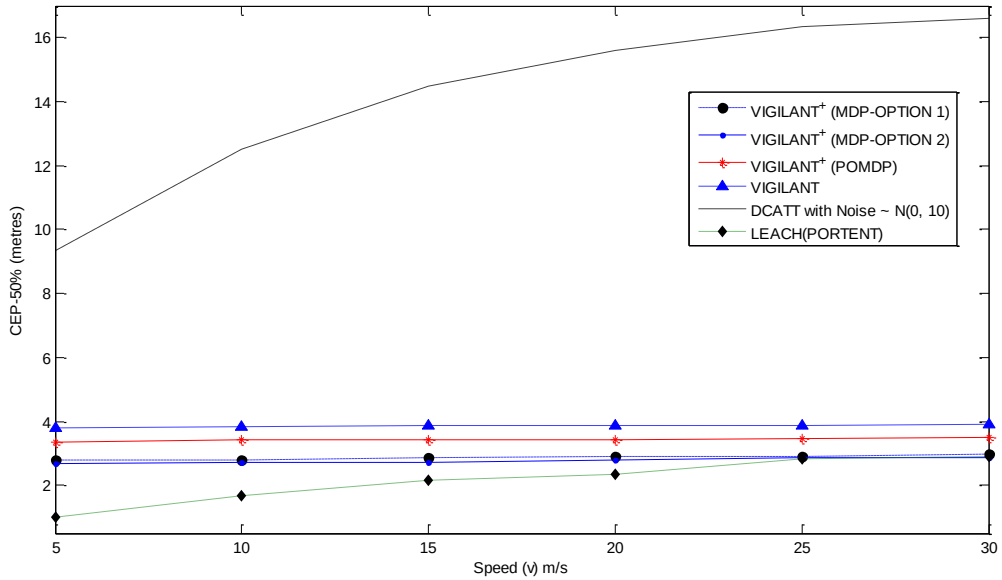

Figure 5.11: M2 performance CEP-50% with threat velocity, v m/s, TOC = 0.01

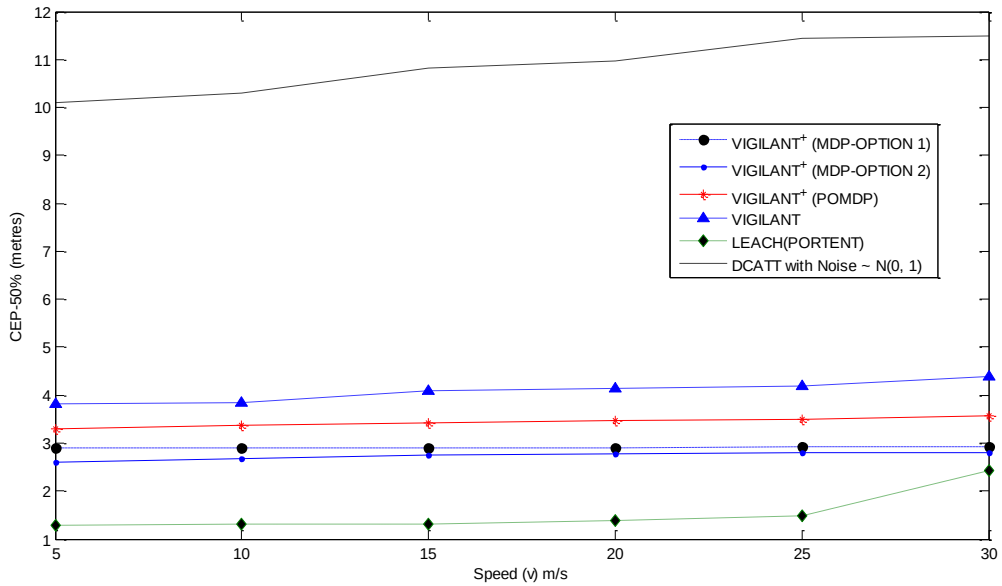

Figure 5.12: M2 performance CEP-50% with threat velocity, v m/s, TOC = 0.9

Figures 5.11 and 5.12 show VIGILANT+ geo-location performance compared against VIGILANT, LEACH and DCATT under low and high *TOC* conditions. Performance for threat geo-location is measured using CEP, as the threat velocity is varied. The CEP itself is a common geo-location accuracy metric [74] and is defined as the radius of a circle that has its centre at the true position, containing half the realisation

uncertainties of the random vector. A lower CEP value would provide a basis for distinguishing a better geo-location performance. As shown in figures 5.11 and 5.12, LEACH threat geo-location performance degrades with increasing threat velocity and this is more prevalent under TOC = 0.01 conditions. This is because utilising just PORTENT-Option 2 detection certainty, as a means of selecting and rotating the GI, can lead to far greater fluctuations under a low *TOC* setting (higher observation uncertainty) since, the probability of false alarm is at its greatest. SA level 2 operations can minimise on false alarm effects propagating down to GI selection and "New GI" rotation decision making, as in the case with VIGILANT^{+}, leading to a greater group stability and consistent geo-location performance across a range of threat velocities.

Both figures 5.11 and 5.12 also illustrate the fact that by not integrating a geo-location *"context"* capability, in terms of GDOP (i.e. VIGILANT) or relying on received signal energy corrupted with noise from the sensing environment (i.e. DCATT) can result in geo-location performance shortfalls, when compared with VIGILANT^{+}. Under conditions with a high level of noise corruption, figure 5.11 shows how DCATT geo-location performance degrades with increasing threat velocity. Increasing the noise in the environment leads to greater group instability since DCATT relies on the CH which receives the greatest signal energy in the neighbourhood and as a result, CH rotation becomes more unstable. Random CH election and rotation can lead to greater inaccuracies, as a point of reference, in order to conduct geo-location from, leading to CEP performance shortfalls. Under low noise corruption this can lead to a better geo-location performance for DCATT, primarily because the rotation of CHs is less, increasing group stability slightly.

For VIGILANT its operation is mainly focused on threat presence detection and not geo-location. Both figures 5.11 and 5.12 confirm that geo-location based on just using

threat presence *"context"* can lead to CEP performance shortfalls when compared with VIGILANT+. VIGILANT+ incorporates both an ability to evaluate threat presence and geo-location *"context"* and this can help to maintain both a consistent and improved geo-location performance across the range of threat velocities, when compared with VIGILANT, as shown in figures 5.11 and 5.12.

In terms of VIGILANT+ CEP performance figures 5.11 and 5.12 suggest that utilising a MDP framework, which relies on further GI updates to maintain the memory-less Markov condition, improves geo-location performance over using just the POMDP framework. In addition MDP-Option 2, which ensures greater GI confidence in threat presence is established before initiating GI updating, has the greatest improvement in geo-location performance out of all VIGILANT+ modes of operation.

Utilising further GI updates clearly encourages a better evaluation of geo-location *"context"* in terms of GDOP and figures 5.11 and 5.12 proposes to us to consider that geo-location is an exercise best preserved to some degree as a centralised operation, rather than a fully distributed operation. Evidence to support this notion is also shown through LEACH operation, which provides the most improvement (lower CEP) in geo-location performance, as shown in figures 5.11 and 5.12. From (5.5), the GDOP error itself is magnified through the geometry matrix, $\mathbf{H}^{\mathbf{T}}\mathbf{H}$ and can be reduced if the number of active sensors utilised, N, increases. LEACH in itself is centralised and utilises all one-hop neighbours to gauge a level of geo-location accuracy. Utilising all one-hop neighbours incorporates the use of a greater N and so improves on LEACH geo-location performance, confirmed through figures 5.11 and 5.12, when compared with VIGILANT and VIGILANT+.

With the POMDP framework a fully distributed mode of operation is encouraged and as a result, threat position updates at each decision epoch interval can only be conducted

using local measurements. This can potentially lead to a greater *CTL* uncertainty and therefore a higher GDOP error. In addition, a higher GDOP error is encouraged since, *N* used in (5.5), is also reduced under a POMDP framework, which contributes towards a loss in geo-location performance when compared with LEACH.

5.3.2 Communication Energy Consumption Performance

The same communication energy model is used, as described in chapter 4, in heading 4.4.3 and given in (4.12). Figures 5.13 and 5.14 show VIGILANT$^+$ communication energy consumption performance compared against VIGILANT and LEACH. Both figures 5.13 and 5.14 show how VIGILANT$^+$ and VIGILANT, through adopting transmission control, which is evaluated according to mission objective *"context"* can help to minimise on non-essential and continuous updating, when compared with LEACH. This can ultimately provide a means of improving network longevity, while preventing the degradation in surveillance utility performance, as shown in figure 5.10 and figures 5.11 and 5.12. Network communication energy consumption under VIGILANT$^+$ is improved through distributed self-managed transmission control, as highlighted in section 5.2 by making self-adaptive transmission control decisions according to, common *"context"* in a specific mission objective.

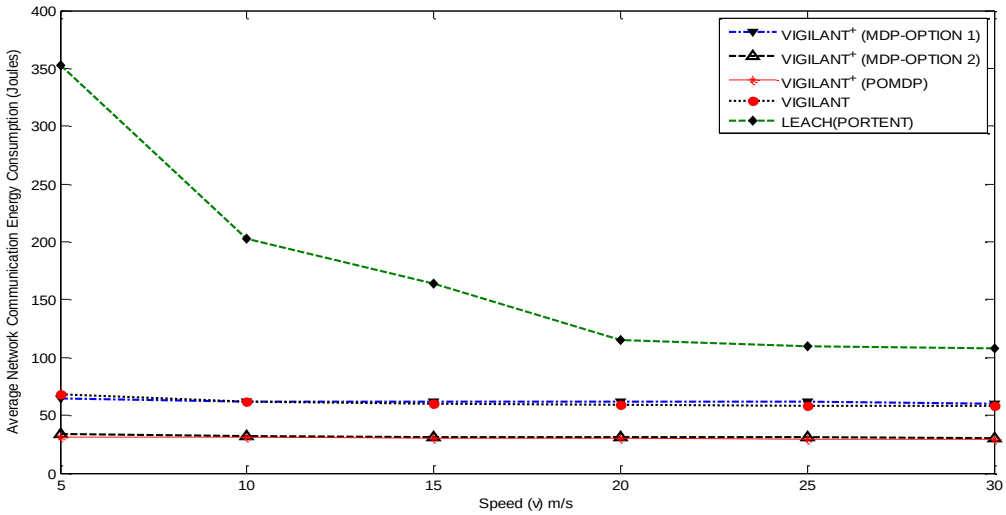

Figure 5.13: Communication energy consumption performance, with threat velocity, v m/s, TOC = 0.01

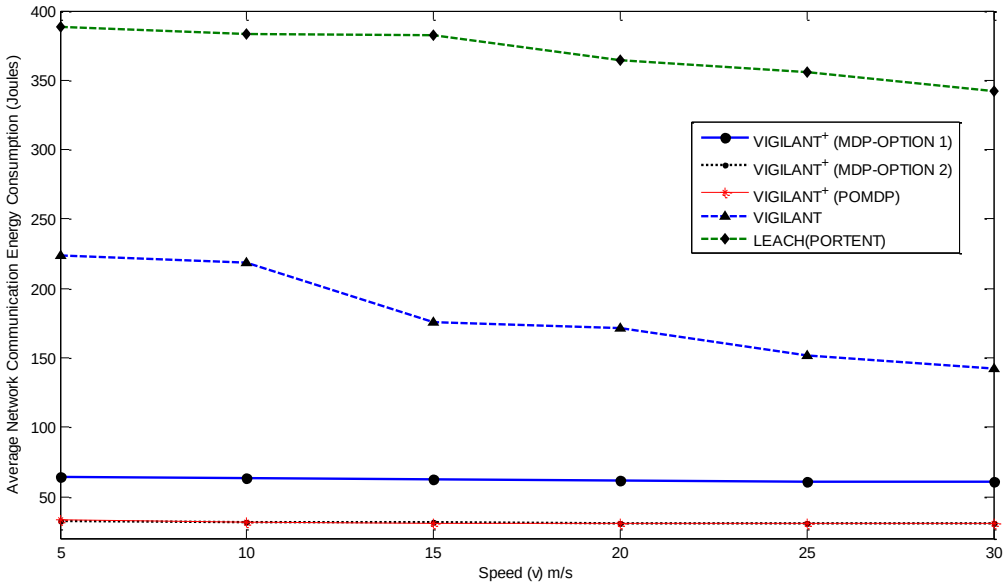

Figure 5.14: Communication energy consumption performance, with threat velocity, v m/s, TOC = 0.9

Being able to make self-adaptive transmission control decisions, as shown with VIGILANT^{+} is imperative since *UGS* nodes are typically restricted in their energy resources, therefore non –essential communication and overhead should be kept to a minimum in order to prolong network lifetime, which VIGILANT^{+} operation can support. Adopting a centralised transmission control approach for surveillance updating, as in the case with VIGILANT and LEACH, does not promote this and as a result increases energy consumption on average by some 40%, over VIGILANT^{+}. VIGILANT communication energy consumption is increased primarily through, GI-sensor CF feedback and further notifications for both GI-sensor collaboration and adapted QoSI service provision times. VIGILANT^{+} reduces this burden through *"context"* centric operation for both collaboration and transmission control phases, as shown in figure 5.9. This enables a fully distributed *UGS* surveillance management operation by promoting greater dependency on "*in-network processing*".

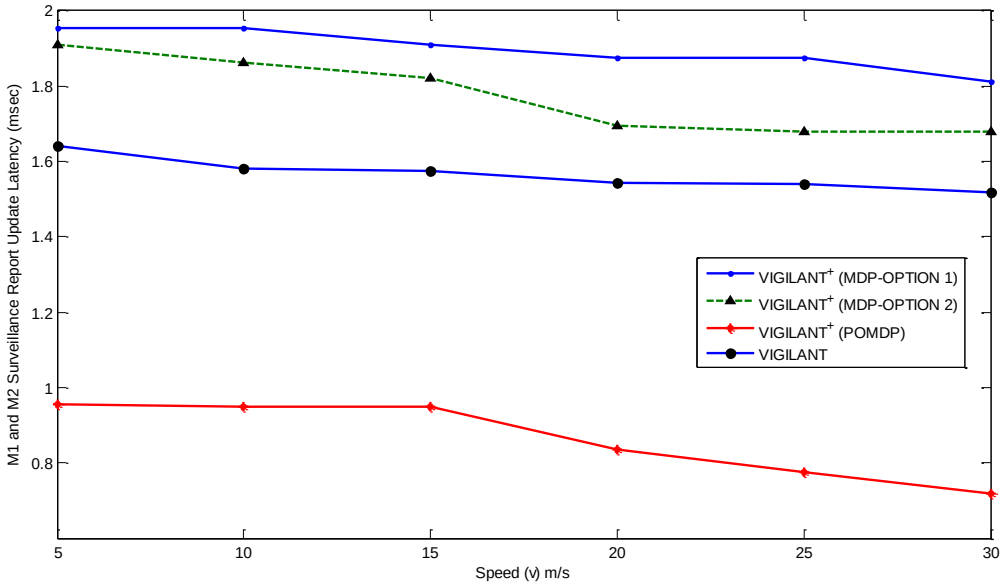

Figure 5.15: M1 and M2 surveillance report update latency, with threat velocity, v m/s, TOC = 0.01

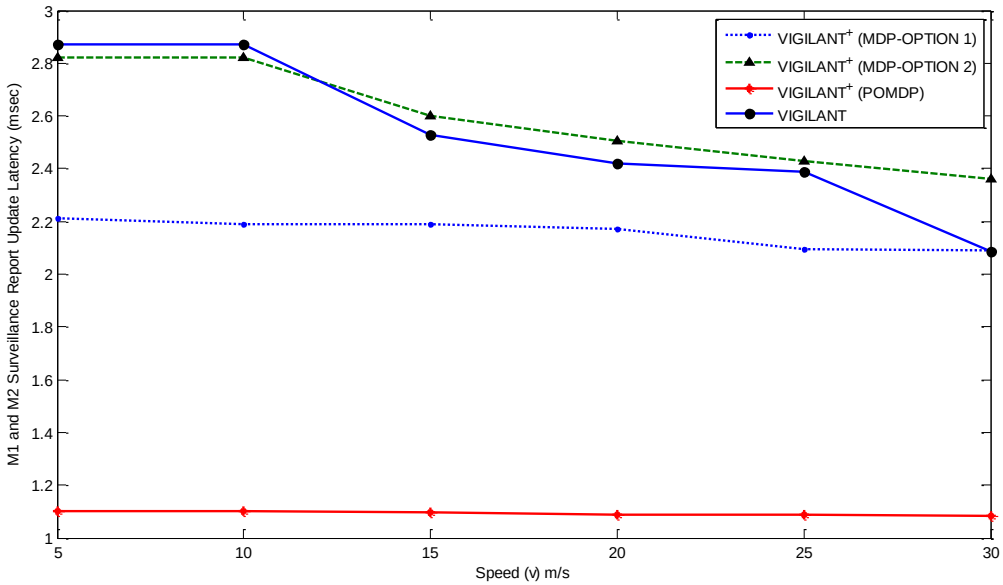

Figure 5.16: M1 and M2 surveillance report update latency, with threat velocity, v m/s, TOC = 0.9

5.3.3 Message Latency Performance

Latency is measured in terms of the time between the generation of a *M1* or *M2* surveillance packet at a collaborating sensor and the delivery of that packet to the GI, as shown in figures 5.15 and 5.16. A higher latency value would also imply that the channel

is busy and therefore, more bandwidth is being utilised. The results of figures 5.15 and 5.16 indicate that utilising a *MDP* or *POMDP* methodology coupled with a surveillance service priority scheduling algorithm detailed in figure 5.8, improves on bandwidth efficiency over LEACH, which was found to follow the same latency characteristics, as already indicated earlier in chapter 4, figure 4.9.

Bandwidth efficiency is increased by allowing individual sensors to schedule and contend for channel access using a duty cycle approach. VIGILANT^{+} adopts a contention-schedule medium access control, where schedule access periods vary according to common mission objective *"context"* (priority), which offers better efficiency compared to purely schedule based (LEACH) operation through TDMA control. In addition, VIGILANT^{+} bandwidth efficiency is increased, without degradation in mission objective surveillance utility, as shown in figure 5.10 and figures 5.11 and 5.12.

As indicated in figures 5.15 and 5.16, utilising a MDP framework, which invokes the use of further GI updates can decrease bandwidth efficiency when compared with VIGILANT and VIGILANT^{+} (POMDP). VIGILANT latency is generally increased through the use of GI-sensor CF feedback and further notifications in adapted QoSI service provision times. A POMDP framework on the other hand can increase bandwidth efficiency levels by not relying on further GI updates or the need for adapted surveillance provision times. This is possible since POMDP *"context"* evaluation requires only local current state observations and the knowledge of previous state observations for transmission control decision making, facilitating a fully distributed capability. Plus, all self-adjustments concerning *"context-aware"* surveillance provisioning are conducted locally, allowing the channel medium to be accessed only for surveillance updating purposes. This is important in scenarios where operational bandwidth can be limited, such as *tactical UGS* networks.

5.3.4 VIGILANT+ Test Bed Evaluation

Results from sections 5.3.2 and 5.3.3 suggest utilising a POMDP framework can provide better means and capability for saving on network resource consumption. To verify this within a real-world scenario with VIGILANT+ (POMDP) running on a hardware test-bed platform, would also add to the credentials of utilising a POMDP type framework. A series of test bed trials were conducted, as part of a student Master of Science (MSc) project, in order to evaluate VIGILANT+ system performance. The details concerning our test bed experimental setup and the nature of tests conducted are described further in **Appendix A, part 3**. Figures 5.17 to 5.19 show the key test bed trial results for VIGILANT+ system performance, in terms of QoSI, communication overhead and hardware processing time. Again evaluations were primarily conducted to establish the effects of collaborating and managing network resource consumption according to, *"context"* of a threat presence within a real world distributed setting.

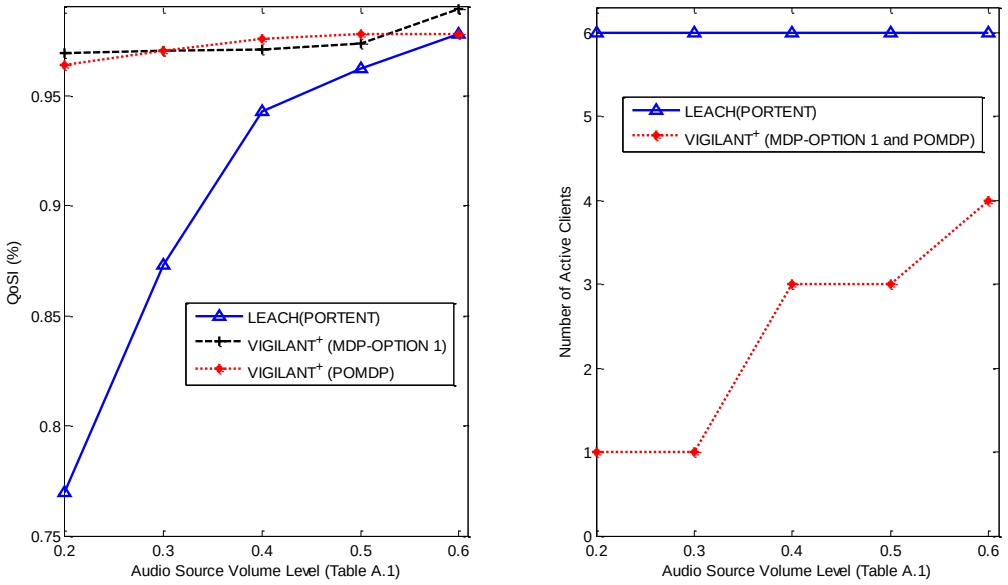

Figure 5.17: M1 QoSI performance and number of active clients involved

From figure 5.17, the effect of introducing outlier nodes for QoSI aggregation (LEACH) again degrades *M1* QoSI performance when compared with VIGILANT+. The use of evaluating common *"context"* as to the presence of an audio source (threat), as shown with VIGILANT+, can improve QoSI performance under higher observation uncertainty conditions (audio source volume range from 0.2 to 0.4). In addition, a more consistent QoSI performance across the range of audio volumes used is also provided with VIGILANT+. The use of evaluating common *"context"* to manage the network is also clearly shown in the number of active clients participating in QoSI updating, as the audio source volume is increased. LEACH operation utilises all clients, in this case six, while VIGILANT+ through *"context"* centric publish-subscribe querying, as described in figure 5.3, allows distributed clients to decide themselves whether they should collaborate or not and to re-evaluate their *"context"* position accordingly. This explains why the number of clients increases with audio source volume for VIGILANT+, since the observation uncertainty reduces, which improves the confidence levels in threat presence (audio source) *"context"* but at the same time still ensures the influence of the outlier nodes is minimised, which are clients 5 and 6.

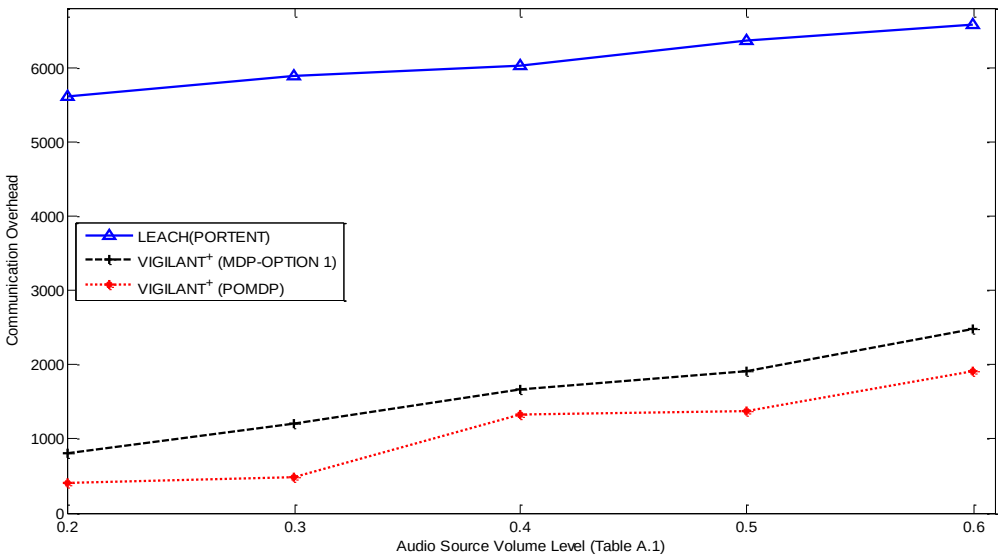

Figure 5.18: Communication overhead, total messages sent between server and clients

Figure 5.18 shows the total number of messages sent between the server and clients (communication overhead) and gives us an indication as to the level in network resources consumed. With LEACH, as expected, utilising all nodes to participate in QoSI increases the communication overhead and would imply greater communication energy and bandwidth consumption. Utilising all nodes degrades *M1* QoSI performance and inflicts greater network resource consumption, making this inefficient from an *UGS* surveillance management perspective.

VIGILANT+ again shows the benefit of introducing self-managed transmission control according to common *"context"* concerning the presence of an audio source (threat). As observation uncertainty reduces (higher audio source volume level), naturally this increases the number of messages sent since there is greater confidence in *"context"* but a higher level of control over LEACH is still achieved. From a VIGILANT+ performance point of view the benefits of not utilising further GI updates, as occurs with MDP operation, is clearly shown with the POMDP framework. The lower communication overhead incurred with VIGILANT+ POMDP operation over MDP operation would imply potential to save on network resource consumption. This is also an added benefit given that the POMDP framework does not subject degradation in *M1* QoSI performance, as indicated in figure 5.17.

Figure 5.19 gives an indication as to the average level of processing time required to execute VIGILANT+ commands according to, the described SA levels 1, 2 and 3 at each client, across the full range of audio source volumes used. Test-bed trial results indicate that processing times associated with SA levels 1 and 2 are similar for both VIGILANT+ MDP and POMDP operations and this is expected since, the functionality for these two levels is common. The difference in processing time performance is really felt within SA level 3, which is the associated self-managed transmission control methodology.

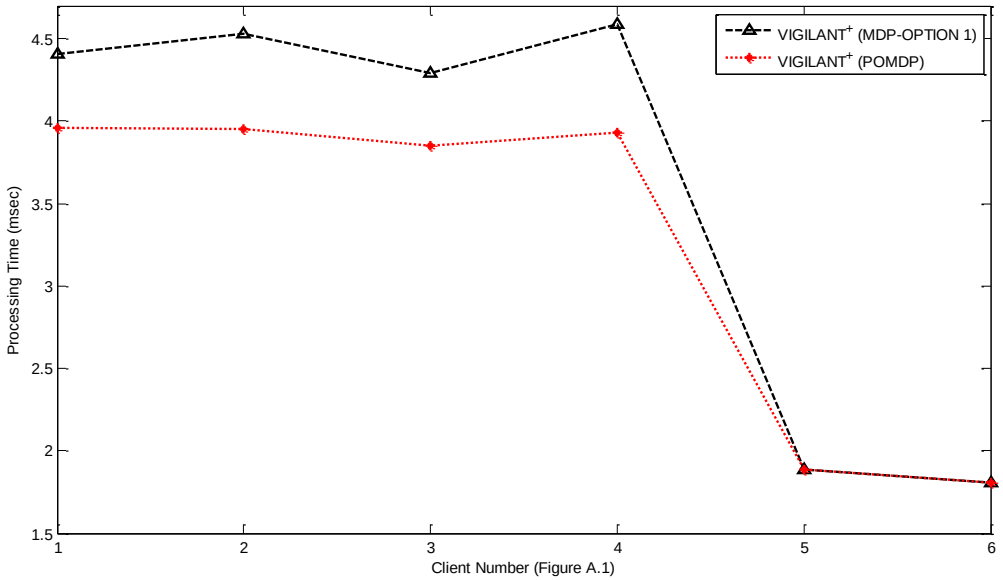

Figure 5.19: Average processor time consumption executing VIGILANT+ SA levels 1, 2 and 3

As shown in figure 5.19, the VIGILANT+ POMDP operation achieves a much lower processing time when compared with MDP operation. The primary reason for this is, minimising again on the need for further GI updates being sent. In addition, from an implementation perspective the POMDP client software is "lighter" in terms of programming consisting of fewer lines, when compared with MDP functionality and also in general performs fewer functions than the MDP framework, in terms of the *"context"* evaluation features for transmission control. Both system processing time performances converge to similar values at clients 5 and 6, since these are outlier nodes and as a result from figure 5.9 did not invoke their self-managed transmission control functionality. Processing time performance here is therefore only associated with SA levels 1 and 2, which have the same operating functionality.

5.4 VIGILANT+ POMDP Epoch Control Strategies

VIGILANT+ performance evaluations have revealed that for the simulated network deployment scenario and from additional test bed evaluation trials, that utilising a POMDP framework, can increase the savings to be made on network resource consumption. This is achieved primarily through minimising the need for further GI updates. Evaluations have also indicated that, while not using further GI updates has little impact on *M1* surveillance utility performance it can affect the level of *M2* surveillance performance possible. There are two main reasons for this, firstly, a POMDP framework for *M2* operation requires *CTL* observations to be made locally and secondly, *M2 "context"* evaluations are conducted using a fixed decision epoch interval, which ignores the dynamic characteristics of the monitored threat.

A MDP framework for *M2* surveillance performance has the advantage of considering the dynamics of the monitored threat and this is reflected in the frequency in GI updating, according to MDP options 1 or 2. Subsequently, GI updating would either increase or decrease as the dynamics of the threat (i.e. TOC) change, giving a better evaluation of current *M2 "context"*. A POMDP framework being fully distributed cannot achieve this without implementing some form of self-adaption to its own decision epoch interval selection. Utilising a fixed decision epoch interval at a pre-determined observation frequency may also encourage unnecessary transmission control actions to occur, leading to an unnecessary increase in network resource consumption. In order to maintain the POMDP advantage of providing savings in network resource consumption and maintaining a fully distributed capability over the MDP framework, in this section, we seek to develop strategies to allow self-adaptable POMDP decision epoch interval selection.

5.4.1 POMDP Epoch Control Strategy Formulation

Providing control strategies for when POMDP decision epochs should occur is mostly aimed at further improving network resource consumption efficiency. Extending the POMDP operation to adapt decision epoch frequencies according to the characteristics of a monitored threat situation, is one possible way of achieving improved efficiency savings. We portray and define the characteristics associated with a monitored threat in two ways:

- Physical characteristics (i.e. position observations in order to derive changes in threat velocity dynamics).
- Mission objective specific *"context"* characteristics (i.e. probabilistic confidence measures derived in SA level 2 with respect to *M1* or *M2*).

To formulate the decision epoch control process we employ a time frame window in which characteristics concerning the monitored threat are observed. This is detailed as follows with further illustration, given in figure 5.20:

- A total of l threat characteristic observations are made within a designated time frame window (T_j) in seconds, where j denotes the identification of the monitored threat.
- Threat characteristics are observed at each time interval $(\hat{T}_j)^n$, equal to $1 / l$ seconds, where $n = 0$, at the start of an observation time frame, with condition, $n < l$.
- A current decision epoch interval (ΔDE_j) is evaluated and scheduled at the end of each (T_j).
- $(\Delta DE_j)_{Previous}$ denotes the decision epoch interval calculated in the previous designated time frame window (T_j).

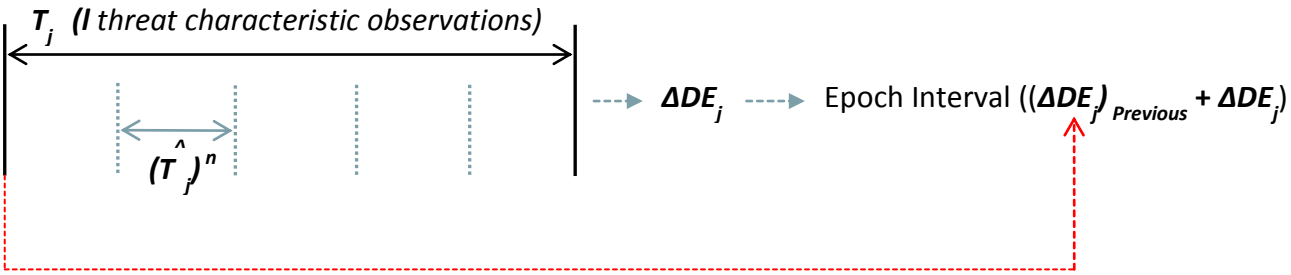

Figure 5.20: Decision epoch control formulation

Figure 5.20 shows how the decision epoch interval is controlled according to ΔDE_j determined by the monitored threat characteristics. For example, if a threat were to move at a constant velocity or remain static, this would imply setting a larger decision epoch interval through ΔDE_j, with strategies used to define ΔDE_j being specified in a suitable way to reflect this, as detailed in headings 5.4.2 to 5.4.4.

5.4.2 Strategy 1: Threat Position

Threat position observation estimates (*POE*), ($x_{Threat\text{-}j}$, $y_{Threat\text{-}j}$), are conducted by local *UGSs* within an x-y plane, representing the surveillance field. Location Metadata (*LM*) of the last *l* observations taken within T_j, concerning the monitored threat is modeled, as shown in (5.15).

$$LM(T_j) = d_j / d_{tj} \tag{5.15}$$

Where d_j denotes the net distance travelled by the monitored threat, during the last *l* observations, as shown in (5.16).

$$d_j = \sqrt{x_{Threat-j}^{n=0} - x_{Threat-j}^{n=l-1})^2 + (y_{Threat-j}^{n=0} - y_{Threat-j}^{n=l-1})^2} \tag{5.16}$$

The total distance travelled by the threat during the last *l* observations, d_{tj}, forming the threat position observation history within T_j, is given in (5.17).

$$d_{tj} = \sum_{n=0}^{n<l} \sqrt{(x^{n}_{Threat-j} - x^{n+1}_{Threat-j})^2 + (y^{n}_{Threat-j} - y^{n+1}_{Threat-j})^2} \quad (5.17)$$

In (5.17), ($x_{Threat\text{-}j}{}^{n+1}$, $y_{Threat\text{-}j}{}^{n+1}$) are the updated threat positions observed at $(T^{\wedge}_{j})^{n+1}$. As shown in (5.15), *LM*, dictated by d_{tj}, is equal to unity if the threat moves in a completely uniform manner and is < 1, if threat dynamics change in a non-uniform manner. Therefore, *LM* is bounded by the interval ($0 < LM <= 1$), within (T_j). For strategy 1, ΔDE_j, is assumed to be a linear function of *LM*, $\Delta DE_j = f(LM(T_j))$, and can be calculated, as shown in (5.18).

$$\Delta DE_j = (\Delta DE_j)_{Previous} + LM(T_j) \quad (5.18)$$

5.4.3 Strategy 2: Mission Objective "Context"

Mission objective "context" characteristics can be derived using SA- level 2 and follows the probability derivations made from figure 5.2, which are summarised in table 5.1. Using table 5.1, strategy 2 provides probabilistic confidence measures for presence (P_{1j}) and geo-location (P_{2j}) of threat, given as entries six and eight respectively. Utilising P_{1j} and P_{2j} derivations, specific mission objective "context" ratios (*CR*) can be established, as shown in (5.19) and (5.20).

$$CR_{M1j}(T_j) = min(P^{n=0}_{1j}, \ldots P^{n=l-1}_{1j}) \big/ max(P^{n=0}_{1j}, \ldots P^{n=l-1}_{1j}) \quad (5.19)$$

$$CR_{M2j}(T_j) = min(P^{n=0}_{2j}, \ldots P^{n=l-1}_{2j}) \big/ max(P^{n=0}_{2j}, \ldots P^{n=l-1}_{2j}) \quad (5.20)$$

From (5.19) and (5.20), *min* and *max* are functions calculating the final minimum and maximum confidence measures obtained, within T_j. Using *min* and *max* functions in this instance, helps to determine the degree of *"contextual"* variation, present within T_j. If there is low variation present, this would imply a higher *CR* being set. The value of *CR*, is therefore bounded by the interval ($0 < CR <= 1$), within T_j. For strategy 2, ΔDE_j, is assumed to be a linear function of *CR*, $\Delta DE_j = f(CR(T_j))$, and can be calculated, for each specific mission objective, as shown in (5.21) and (5.22).

$$\Delta DE_j = (\Delta DE_j)_{Previous-M1} + CR_{M1j}(T_j) \quad (5.21)$$

$$\Delta DE_j = (\Delta DE_j)_{Previous-M2} + CR_{M2j}(T_j) \quad (5.22)$$

5.4.4 Strategy 3: Similarity in Mission Objective "Context"

Confidence measures P_{1j} and P_{2j}, can assist in portraying the level of similarity that exists about the current mission objective surveillance environment. We define dimensional (l -1) confidence measure vectors, B and X, where $B = (P_{1j}{}^{n=0}, \ldots, P_{1j}{}^{n=l-1})$ and $X = (P_{2j}{}^{n=0}, \ldots, P_{2j}{}^{n=l-1})$, observed within T_j. Utilising a similarity function we can capture the extent to which B and X, convey similar *"context"* towards the mission objective surveillance environment, within T_j. A similarity function (*Sim*) can be defined as a logical distance measure of *"context"* between B and X. This implies that if B and X have high similarity, they exhibit a small *"context"* distance between them. *"Context"* distance, measuring a similarity towards the current mission objective surveillance environment at two time intervals, can be illustrated as shown in figure 5.21.

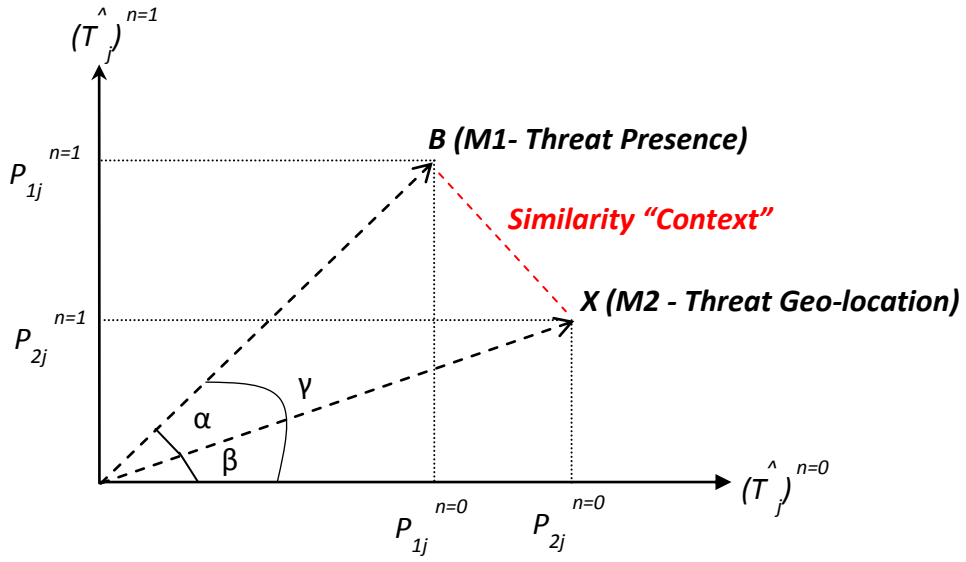

Figure 5.21: Similarity "context" within the M1 and M2 surveillance environment at two time intervals

As shown in figure 5.21 the degree in similarity in *M1* and *M2 "context"* is reflected through the included angle, α and can be formulated using figure 5.21, as shown in (5.23).

$$cos(\alpha)=cos(\gamma-\beta)=cos\gamma\, cos\beta+sin\gamma\, sin\beta \tag{5.23}$$

$$cos(\alpha)=\frac{P_{1j}^{n=0}P_{2j}^{n=0}+P_{1j}^{n=1}P_{2j}^{n=1}}{\sqrt{(P_{1j}^{n=0})^2+(P_{1j}^{n=1})^2}\sqrt{(P_{2j}^{n=0})^2+(P_{2j}^{n=1})^2}}$$

Taking into consideration the full, (*l-1*) dimensional vectors *B* and *X*, within an allocated T_j and by expanding (5.23), the complete summary of the similarity in *B* and *X* in T_j, is shown in (5.24).

$$cos(\alpha)=\frac{\sum_{n=0}^{n=l-1}P_{1j}^{n}P_{2j}^{n}}{\sqrt{\sum_{n=0}^{n=l-1}(P_{1j}^{n})^2}\sqrt{\sum_{n=0}^{n=l-1}(P_{2j}^{n})^2}} \tag{5.24}$$

As shown in (5.24), the cosine of the included angle of *B* and *X*, α, is in fact an accuracy description of correlations (similarity) between two types of *"context"* measures, in view of the current mission objective surveillance environment. Defined in this way, *cos (α)* will vary between *0* when *B* and *X* are orthogonal (low similarity *"context"*) and *1* when *B* and *X* are identical or proportional (high similarity *"context"*). For strategy 3, we define $Sim\ (T_j) = cos\ (\alpha)$, reflecting the distance measurement between *B* and *X*, which increases if *B* and *X* have more common similarity *"context"*. ΔDE_j is assumed to be a linear function of $Sim\ (T_j)$, $\Delta DE_j = f\ (Sim\ (T_j))$, as shown in (5.25).

$$\Delta DE_j=(\Delta DE_j)_{Previous}+Sim(T_j) \tag{5.25}$$

5.4.5 VIGILANT+ POMDP Epoch Control Strategy Performance

System performance is evaluated using the OMNeT++ network simulation platform [63]. We utilise the same network deployment characteristics already described for VIGILANT and VIGILANT+ performance evaluations, in 4.4 and 5.3. Threat mobility characteristics are however different and simulated using the random waypoint (RWP) model, with a dynamic velocity (m/s) set from a uniform distribution, *uniform* (0, v_{max}). A RWP simulation model is considered because of its extensive use within surveillance type

evaluations, in order to mimic the random movement characteristics of a realistic monitored threat [78-79].

As part of our system evaluation, we again do not consider the effects of sampling rate, number of deployed nodes and sensing coverage range on VIGILANT+ performance. Our evaluation is concerned with the effects of collaborating and managing network resource consumption, according to the POMDP *"context"* of the *M1* or *M2* surveillance environment and how the decision epoch interval selection strategies can influence POMDP performance. For a comparison basis we use the IDSQ strategy, as already described in 2.3. IDSQ selects a sensor at each observation time step according to maximising the measured information utility (lower threat position uncertainty) and minimising the communication cost. IDSQ has a similar limitation to normal POMDP operation in using a uniform fixed time interval for decision making, without taking into account threat dynamic characteristics. Figures 5.22 to 5.25 present the network resource consumption, *M1* and *M2* surveillance utility performances with respect to v_{max}, under two different *TOC* conditions, when using a fixed *l* equal to 5 threat observations per second.

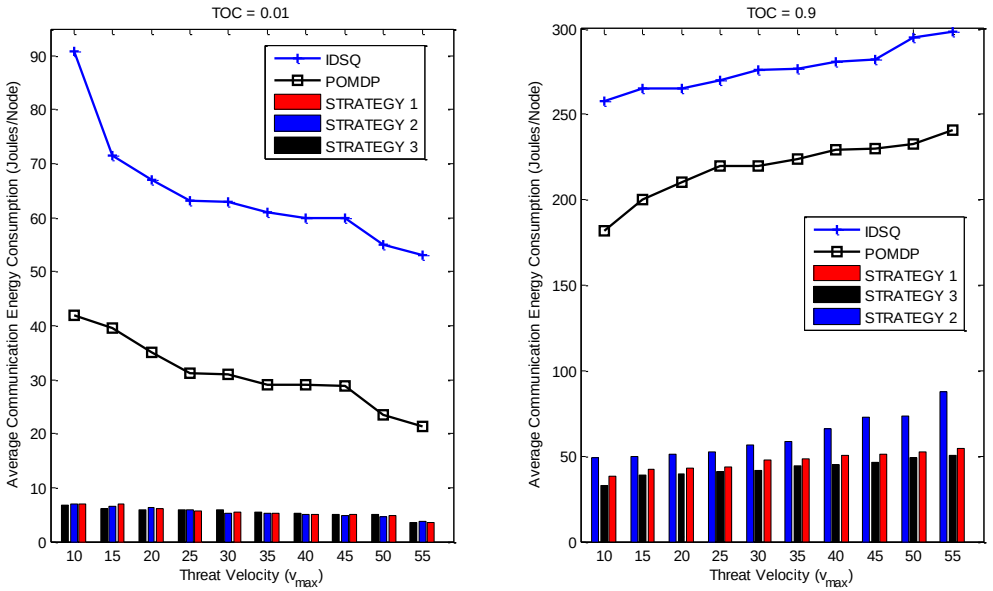

Figure 5.22: VIGILANT+ average communication energy consumption with v_{max} for TOC = 0.01 and 0.9

As indicated from figure 5.22, employing decision epoch interval control strategies can improve on communication energy consumption from a total deployed network perspective (i.e. joules consumed/node), when compared with non-adaption (IDSQ and POMDP). Both the normal POMDP framework and IDSQ in our simulation would invoke a transmission control decision on every observation made per second. Managing decision epoch intervals according to threat characteristics (strategies 1, 2, 3) can adapt the interval selection, in order to reflect on the dynamics of the threat (i.e. changes in threat velocity) and therefore, as a result, achieve improved energy consumption performance.

From figure 5.22, it suggests that strategy 3 achieves the most improved communication energy consumption performance in both TOC conditions. Strategy 3 itself measures the similarity *"context"* within the *M1* and *M2* surveillance environment through *cos (α)*, given in (5.24). This suggests the *cos (α)* metric can offer a better *"context"* derivation as to the dynamics associated with the combined *M1* and *M2* environment, which can influence better control on POMDP epoch interval selection for transmission control decision making. Strategy 2 achieves a lower communication energy consumption performance under both TOC conditions, which suggests that finding the degree in individual *M1* or *M2 "context"* variation present within the environment is not an appropriate method to use.

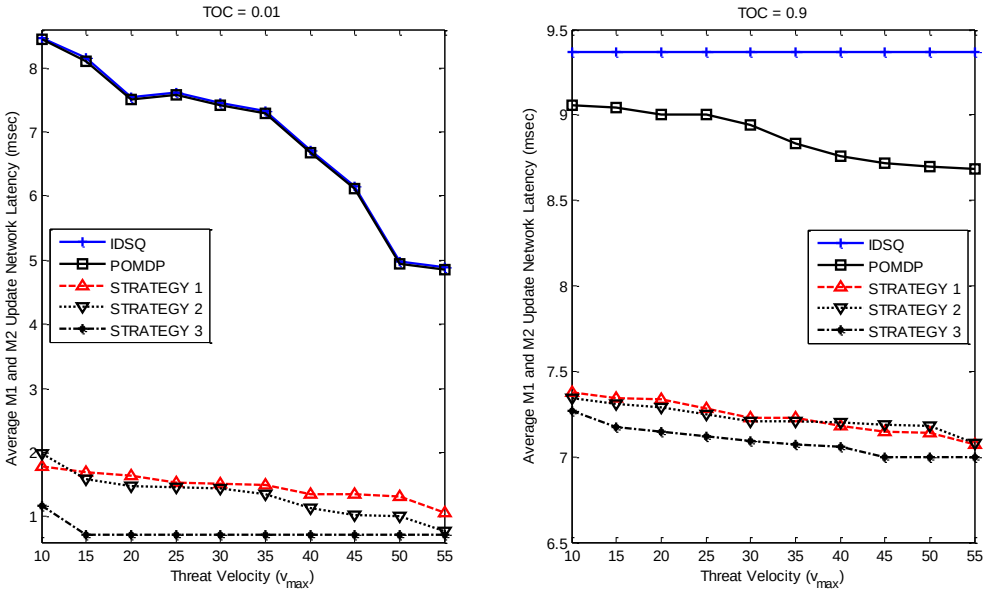

Figure 5.23: VIGILANT+ average network latency with v_{max} for TOC = 0.01 and 0.9

The effect of adapting decision epoch interval selection (strategies 1, 2 and 3) on network latency, a measure of bandwidth efficiency, is also clearly shown in figure 5.23. Again, using a fixed interval selection scheme (POMDP and IDSQ) can degrade both communication energy and latency efficiency performance making them expensive options if we were to consider the overall operational longevity goal. The results from figure 5.23 again shows that strategy 3 can achieve better bandwidth efficiency performance, for the same reasons described above.

Both figures 5.22 and 5.23 also illustrate how a *"context-aware"* strategy achieved using integrated SA level 1, 2 and 3 approaches, as shown with VIGILANT+ POMDP and its strategies can achieve better performance, over just belief state evaluation using updated sensor values from immediate neighbours, as shown with IDSQ. With IDSQ, updated sensor values concerning the uncertainty associated with a threat position would be sent on each observation event. This again incorporates centralised control within a distributed

mode of operation, which increases network resource consumption in a similar fashion to VIGILANT+ MDP, as shown before. In addition, VIGILANT+ POMDP through SA level 1 (PORTENT) would firstly ensure a threat is present (mitigating false alarm effects) and secondly with SA level 2 (BBN) derive the associated confidence associated with the current *M1* or *M2* environment. Ensuring these two levels are fulfilled can then allow transmission updating to be invoked rather than IDSQ, which does not consider the false alarm environment and assumes a threat is already present, leading to unnecessary consumption of network resources.

In addition, both normal VIGILANT+ POMDP and the decision epoch control strategies integrate figure 5.9, which manages *M1* and *M2* updating according to the level in common mission objective *"context"*. Subsequently, update selection intervals are reflected accordingly to the degree in common *"context"* and not updated on every observation event as currently with IDSQ operation, which encourages bandwidth inefficiency. This also explains why communication energy consumption and latency increases for VIGILANT+ from TOC = 0.01 to TOC = 0.9 since, the confidence in *"context"* concerning the *M1* and *M2* environment improves and thus, more nodes become available for *M1/M2* updating.

The effect of being *"context-aware"* is again reflected through VIGILANT+ *M1* (QoSI) and *M2* (CEP) performances, as shown in figures 5.24 and 5.25. IDSQ, being predominantly a tracking algorithm, selects sensors for collaboration based only on threat position uncertainty and so naturally performs less well within a *M1* surveillance setting, when compared with VIGILANT+.

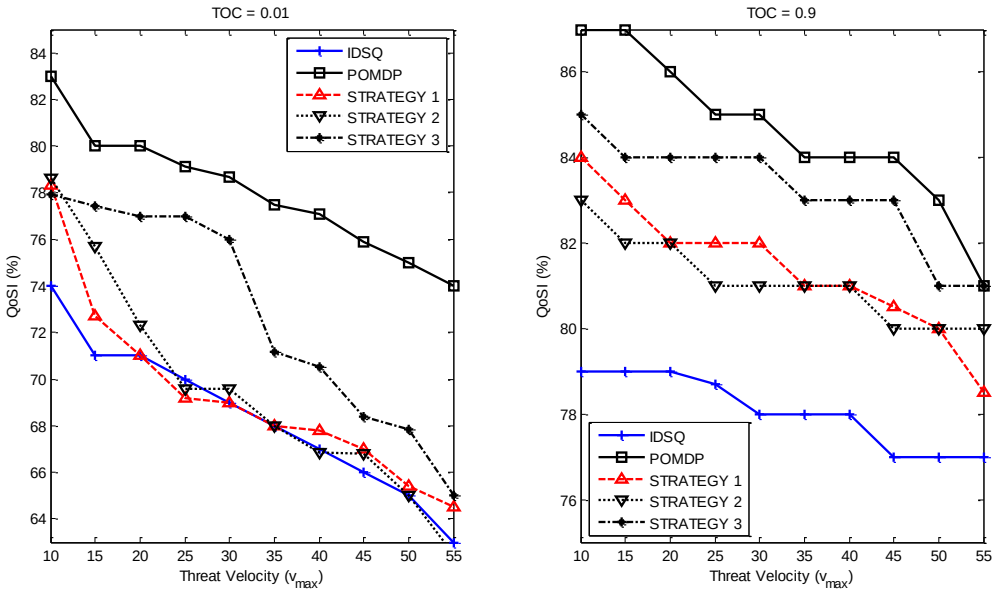

Figure 5.24: VIGILANT+ M1 performance with v_{max}, for TOC = 0.01 and 0.9

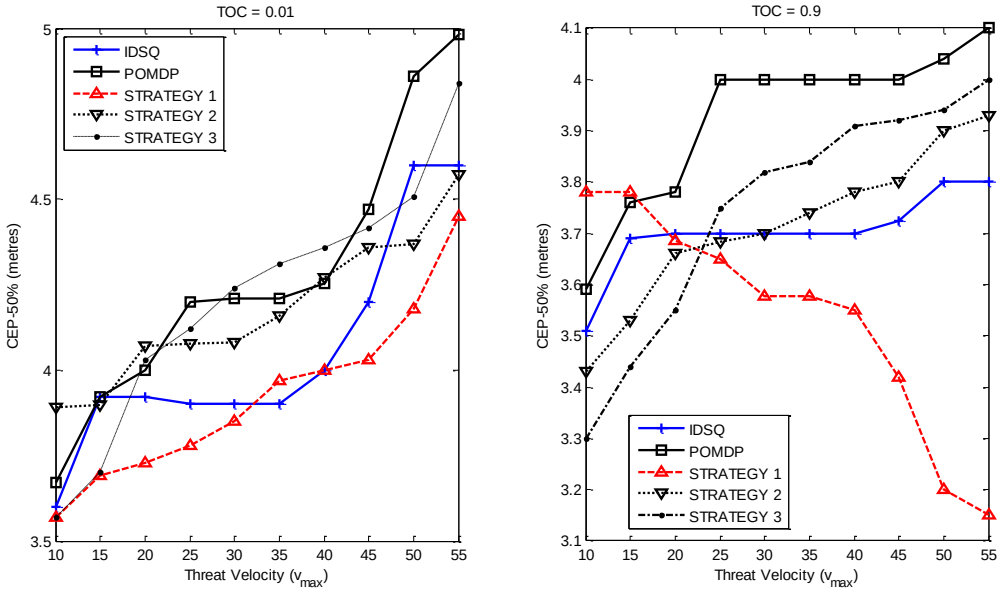

Figure 5.25: VIGILANT+ M2 performance with v_{max}, for TOC = 0.01 and 0.9

Again with VIGILANT+ a joint perspective concerning the *"context"* towards the combined *M1* and *M2* environment is enabled, which induces a better overall combined information utility performance concerning the monitored threat. This is possible since

VIGILANT+ incorporates both threat presence *"context"* and GDOP to achieve a better QoSI and geo-location estimate (CEP) when compared with IDSQ, which just relies on threat position uncertainty and ignores the associated uncertainty concerning the presence of threat (non-consideration of false alarm effects).

For *M2* performance shown in figure 5.25, results indicate that incorporating a decision epoch interval strategy using updated physical threat position observations (strategy 1) can achieve better performance over IDSQ, POMDP and strategy 2 and 3. Threat geo-location performance is, in itself, dependent on the velocity of the threat since this naturally influences current threat position at each observation time, when a GDOP evaluation is made. Incorporating the changes associated with the velocity of the threat is therefore crucial, which explains why strategy 1 performs well as v_{max} increases, as shown in figure 5.25. Strategies ignoring the physical effects of threat position (i.e. velocity) do not perform as well and thus CEP performance degrades with threat velocity, v_{max}. Due to threat observation certainty being poor under a TOC = 0.01 setting, CEP performance degrades as v_{max} increases, but with strategy 1 incorporating physical threat velocity effects it is still able to provide a better performance over the other options tested.

The disadvantage of using a decision epoch interval selection strategy however is portrayed through *M1* QoSI performance, as shown in figure 5.24. When compared with POMDP, strategies 1, 2 and 3 all induce a loss in performance. This would imply strategies 1, 2 and 3 through decision epoch interval adaption encourages a loss in threat presence *"context"* evaluation, which increases with threat velocity, v_{max}. Results from figures 5.24 and 5.25 would therefore suggest employing a decision epoch interval strategy has benefits only for *M2* CEP performance and not *M1* QoSI performance.

Utilising a normal POMDP decision epoch interval framework where *M1 "context"* evaluations are matched to the number of observations to be made per second (l), is more suitable for maintaining consistent QoSI performance against v_{max}. Overall though, one should not discredit the benefits of using strategy 3 to promote improved network resource consumption performance, as discussed earlier and also as a means of providing the most improved QoSI performance out of strategies 1 and 2.

CHAPTER 6

Section 1: Summary and Conclusions

Deploying distributed unattended ground sensor (UGS) networks are primarily used to support mission objective surveillance capabilities such as, threat presence detection and geo-location, within a security-sensitive region. Distributed operation can provide the following advantages for *tactical* mission plans through:

- Promoting scalability, which increases the *tactical* reach that *C2ISR* planners can operate at.
- Minimising the burden for centralised processing architecture and manual system configuration.
- Catering against *UGS* node failures and improving the operational longevity of the deployed *UGS* network.

Managing the distributed *UGS* network to support these mission objectives, however, present challenges because of their inherently dynamic network operating environments. Such environments are characterised by limited bandwidth, coupled with a changing threat situation. *UGS* devices are also limited by their sensing, computation and communication capabilities, which are dictated by their battery energy reserves. The management of network resources therefore becomes crucial in extending the operational longevity of the overall deployed *UGS* network field. The primary goal of section 1, therefore, concerns the *autonomic* management of distributed *UGS* networks deployed to support specific mission objectives (*M1 or M2*) and the conservation of their network resources.

Incorporating a methodology, which allows the consumption of network resources to be managed as a direct causal relationship to the dynamics of the monitored threat, is much more suitable and adaptable towards a changing surveillance situation. Utilising the

situation awareness (SA) framework can achieve this and ensures that sensed elements from a current changing threat scenario are integrated (levels 1, 2 and 3) effectively, to create new SA meaning and establish relevant *autonomic* decision making outcomes for critical operations such as, distributed surveillance.

In chapter 3, our level 1 perception system named PORTENT is highlighted with its primary aim of ensuring that false alarm effects are minimised within an uncertain threat observation environment. False alarm rates have a distinct impact on surveillance performance and especially on intruder detection. Enforcing a low false alarm rate to avoid unnecessary response costs implies a larger data set (samples taken) and hence greater sampling energy consumption. In critical scenarios, a high degree of sensitivity is also desired to capture all potential threats. PORTENT alleviates these concerns through a system that has self-adjustable sensitivity towards capturing relevant QoSI, while also accommodating to the varying uncertainties present within the sensing environment.

PORTENT consolidates both a "fast" sensing system allowing a broad assessment and quick overview of the current situation and a "slow" extensive threshold assessment system. The "slow" system can be used either independently or to verify current situations, in cases where the "fast" system fails potential threat detection. The "slow" system uses a threshold designed to self-adapt to the current uncertainty (false alarm) present in the sensed observation environment, thus minimising on both false alarm detection and the need for full extensive sampling. PORTENT in addition, incorporates options involving the efficient combination of both the "fast" and "slow" sensing system.

Extensive simulation evaluations show that PORTENT does indeed provide increased QoSI threat situation assessment performance over just simple binary detection means. In high uncertainty environments (TOC = 0.01) involving operation under higher probabilities of false alarm, PORTENT through options 1 and 2 provides improved QoSI

performance gains, when compared with the baseline independent "fast" and binary threat detection sensing systems. Findings from simulations conducted under a realistic surveillance scenario suggests that PORTENT option 2, under a low threat observation certainty environment improves overall QoSI performance, predominantly by reducing threat detection delay when compared with option 1. The advantage provided with option 2 when compared with option 1, lies in increasing further the level of sensitivity, due to an increased level of a perceived threat being present, through reducing the detection threshold, incorporated within the "slow" PORTENT system. As a result, heightened threat awareness is achieved within the sensing environment, in conditions where potential missed threat detection can result, providing suitability for surveillance missions. This allows increased QoSI relevancy to be captured with reduced threat detection delay, while also ensuring threat detection sensitivity remains matched to the current uncertainty (false alarm) levels of the sensed observation environment.

In chapter 4, the first of our SA enabled *autonomic* system named, VIGILANT is described, which allows the consumption of network resources to be managed as a direct causal relationship to the dynamics of the monitored threat, through the complete integration of SA levels 1, 2 and 3. VIGILANT itself is primarily aimed at supporting *M1* (threat presence detection) operations.

VIGILANT as a system, through SA level 2 operations promotes effective comprehension of the uncertain surveillance environment. VIGILANT level 2 employs Bayesian Belief Network (BBN) analysis to ascertain and derive relevant understanding (*"context"*) of the pervading uncertain surveillance situation, for localised active decision making. Derived *"context"* is used to gauge the level of confidence a *UGS* node might have, in order to fulfil the required threat presence detection capability. Utilising derived *M1"context"*, primarily through level 2 Bayesian Belief Network operations can also assist

in filtering the uncertainty associated with a current threat situation, in order to improve on surveillance utility performance (QoSI). The *"context"* itself can also assist the efficient management of the deployed network, through SA level 3 operations. The use of a *"context-aware"* ad-hoc collaboration mechanism, as described in 4.2.1, allows the grouping of immediate neighbours, which share the same level of confidence concerning the *"context"* of a current threat detection situation. Simulation results indicate that collaborating according to a high level of confidence in *M1 "context"* maintains accurate levels in QoSI by:

- **Minimising on outlier contribution**. Outliers represent neighbouring sensors, which are distant in terms of *"context"* when compared with the rest of the contributing group. Facilitating collaboration according to a high confidence in sensor *"context"* can propagate increased QoSI surveillance provision and robustness. A higher QoSI surveillance value indicates better urgency and utility for effective *C2ISR* decision making.

The level in *M1 "context-awareness"* can also facilitate the requirement for stability within the collaborating group. This is essential for ensuring an accurate basis in aggregated QoSI processing can be supported. In 4.3 and also indicated from simulation results in 4.4, QoSI updating from collaborating sensors using a service provision time bound, which is evaluated according to the level of common *"context-awareness"* concerning a threat presence, promotes better network management performance in the following ways:

- Maintaining accurate levels in QoSI provision through *"context-aware"* adaption as indicated **Appendix A, part 2**. Re-evaluating QoSI service provision times to cater for changes in *M1 "context"* propagates increased QoSI provision, allowing surveillance applications to perform their tasks effectively.

- Improving on bandwidth efficiency, when compared with a continuous updating approach, which utilises a schedule based MAC scheme (e.g. LEACH-TDMA). Results indicate that setting a high confidence measure on sensor *"context"* and utilising a contention-schedule MAC scheme, where access schedule periods are adapted according to the level of common *M1 "context-awareness"*, promotes reception of QoSI update packets in a timely manner.
- By limiting transmissions according to the evaluated QoSI service provision time bound, improved communication energy consumption performance is promoted. Managing transmissions according to *M1 "context-awareness"* can minimise on non-essential communication, which ultimately improves network longevity and prevents QoSI performance degradation.

The main drawback with VIGILANT operation is that all *"context"* enabled features are conducted by the current group initiator (GI). This again encourages more centralised network management control functionality, which can increase unnecessary communication overhead and as a result, greater communication energy and bandwidth consumption. In addition, no consideration has also been made to providing a *M2* capability.

In chapter 5, an improvement on VIGILANT is made through VIGILANT^{+}, which essentially places more of the management control functionality onto the distributed network, through greater "*in-network processing*", in the following ways:

- A consideration of the *M1* and *M2* surveillance environment is made by VIGILANT^{+} through redefining the SA level 2 BBN, to incorporate a joint *M1* and *M2* perspective towards the surveillance environment.

- Communication overhead is minimised by VIGILANT^{+}, through incorporating a partial and fully observable Markov Decision Process within SA level 3 operations enabling a fully autonomic transmission control capability.

VIGILANT^{+} adopts a distributed SA design approach for sensor network self-management, in order to provide an improvement in operational effectiveness. Such an approach firstly allows for *autonomic* collaboration of sensors to meet the needs of a specific mission objective, through *"context"* querying, as described in 5.1.1, within sensing environmental constraints. Secondly, utilising a MDP or POMDP methodology for *autonomic* transmission control can enable efficient management of network resource consumption, without compromising on mission objective surveillance utility. VIGILANT^{+} simulation results indicate that by incorporating the above system improvements, a better combined *M1* and *M2* surveillance utility and network resource consumption performance, can be achieved by:

- Integration of a geo-location *"context"* capability through GDOP evaluation leads to an improved *M2* performance than when compared with VIGILANT, which performs geo-location based only on threat presence *"context"*, through QoSI updating.
- Minimising on the need for further notifications required for sensor collaboration and adapted QoSI service provision times to be sent, as the case with VIGILANT.

In addition, simulation results for VIGILANT^{+} performance reveal the following observations:

- Utilising a POMDP framework encourages the best use of communication energy and bandwidth consumption. MDP operation through using further GI updates increases bandwidth consumption even when compared with VIGILANT.

- Results indicate that utilising a MDP or POMDP framework induces comparable QoSI performance, which leads us to suggest that a fully *M1* distributed surveillance capability is achievable through a POMDP operation.
- Utilising further GI updates to maintain the memory-less MDP condition, improves geo-location performance over just using the POMDP framework.
- LEACH provides the best overall geo-location performance, which implies geo-location should be kept as a centralised mode of operation with the utilisation of all immediate neighbours, to evaluate current geo-location accuracy.

Test bed evaluation trials, as described in 5.3.4, also indicate that a POMDP mode of operation encourages better communication overhead and processing time performance. POMDP has advantages in promoting a fully distributed surveillance management capability and only relies on local and previous *"context"* evaluations (memory), to perform self-managed transmission control. However, as shown with *M2* performance results, a POMDP framework can induce a lower geo-location performance. This is because a POMDP framework ignores the dynamic characteristics of the monitored threat, in order to adapt its decision epoch interval selection when *M2 "context"* evaluations are made accordingly.

In 5.4, a consideration towards adapting the POMDP decision epoch interval selection is made. This is undertaken in order to, maintain a fully distributed surveillance management capability through a POMDP framework, to encourage better *M2* performance using the POMDP and to increase further, the savings made on network resource consumption. Simulation results from the strategies employed to facilitate POMDP decision epoch interval adaption reveal the following observations:

- Adapting POMDP decision epoch interval selection according to the *"context"* and physical threat position observations of a dynamic monitored threat, can improve on

both consumption of communication energy and bandwidth, when compared with normal POMDP and IDSQ, which employ a fixed non-adaptable interval selection strategy.

- Strategy 3, which adapts decision epoch interval selection by measuring the similarity *"context"* within the combined *M1* and *M2* surveillance environment, induces the most improved network resource consumption performance.
- Strategy 1, which adapts decision epoch interval selection according to, physical threat position observations, achieves the most improved geo-location performance against threat velocity.
- The disadvantage of using decision epoch interval selection strategies is felt through *M1* QoSI performance, which shows normal POMDP operation can achieve better and more consistent performance against threat velocity.

In summary, both VIGILANT and VIGILANT+ systems have shown how the management of the distributed *UGS* network, from both a mission objective collaboration and transmission control perspective can be enhanced through being, "*context-aware*" towards the *M1* or *M2* surveillance environment. *Autonomic* behaviour can be achieved through sensors evaluating their common "*context*" associated within the *M1* and *M2* surveillance environment. Overall this can assist in reducing the network resource burden, promoting a more distributed capability and help to achieve a more consistent surveillance utility performance according to, dynamic threat characteristics. It should be noted that no consideration has yet been made, as to the effects of operating within an error prone wireless environment. This ultimately influences the overall and possible *M1* and *M2* utility performance that can be achieved. In section 3, a consideration of the error prone wireless environment is given and afterwards in section 4, an evaluation to gauge VIGILANT^{+} *M1* and *M2* surveillance performance within an unreliable wireless channel environment, is undertaken.

SECTION 2

Geographic Routing to Support Distributed Surveillance

Introduction

As highlighted in section 1, supporting battlefield surveillance and monitoring missions requires *UGS's* that are distributed across the surveillance field, so that they can provide both a *tactical* reach and advantage for *C2ISR* mission planning. In addition, unmanned air vehicles (UAV's) are becoming increasingly common in military operations, in order to provide support for distributed *UGS* surveillance operations [80-83]. This is illustrated in figure 7.1, where UAV's have the potential to perform airborne surveillance and to notify through a gateway node, sensors within a relevant geographic, region of interest (ROI), to initiate sensing operations. A benefit of using this approach is that only those sensors relevant to a ROI are utilised, in order to enable the correct sensing coverage to verify airborne threat observations and fulfil current surveillance mission objectives.

As shown in figure 7.1, potential threats, which are identified using airborne reconnaissance, are usually restricted to a specific geographic region. Generation of information queries (IQs) regarding a potential threat can also be constrained, to the identified geographic region. Such a method, which effectively utilises geographic partitioning to achieve surveillance goals, can offer better *UGS* network management since:

- This focuses *C2ISR* efforts for surveillance provision needs concerning a current threat (e.g. classification, current location and future track of threat) towards a specific identified geographic ROI, therefore increasing the utility in information received for *tactical C2ISR* mission planning purposes.

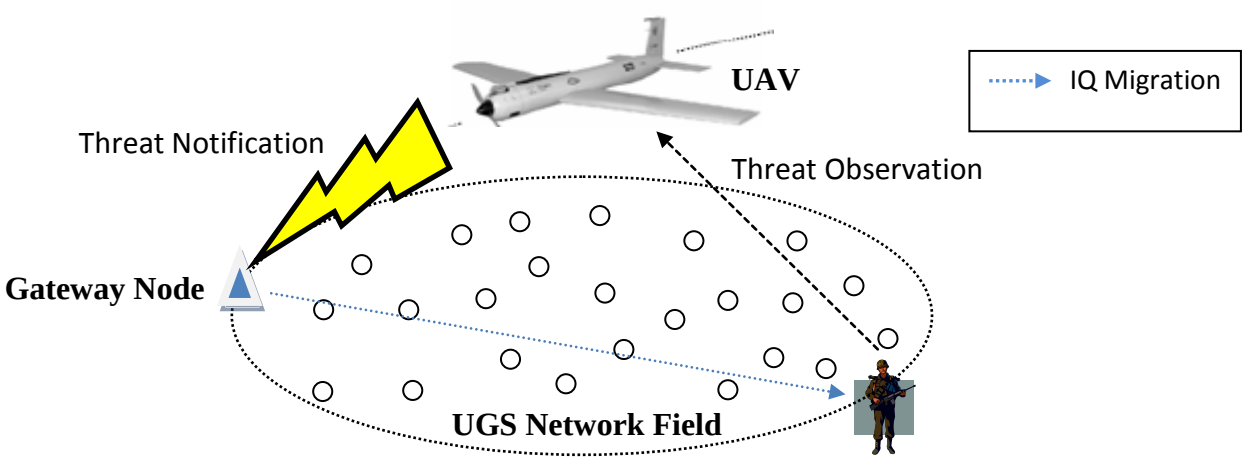

Figure 7.1: UGS network and UAV collaboration for supporting surveillance missions

- Deployed *UGS* nodes, which are distant in terms of geography to the current potential threat, can, therefore, conserve sampling energy consumption, since they are more likely to decrease the overall required information relevancy.

Migration of geographic constrained IQs from a gateway node, to a specified ROI can be assisted if, *UGS* nodes are aware of their geographic position within the surveillance field, in order to facilitate routing of a specific IQ. This entails forwarding of IQs towards the current coordinates of where a threat might be approaching within the *UGS* network field. Protocols, which can facilitate this functionality, are generally classified as geographic routing protocols. Their primary goal is to keep communication overhead small, by exploiting the underlying geometry of node positions. The goals of section 2 are therefore to firstly, highlight geographic routing as an ideal candidate to support surveillance operations and secondly, to develop and present our own geographic routing strategy in support of distributed IQ migration for surveillance missions, within network resource constraints.

In this section, chapter 7 begins by summarising both the nature of geographic routing and the common packet forwarding strategies that can be used to support geographic routing schemes. In 7.1.4, an initial discussion on using biological strategies from the social insect's domain and the advantages found, in terms of how they locate and route to particular distant sources of interest, is given. Based on this initial discussion, in 7.1.5, a strategy is then outlined as to how some of these basic natural principles can be transferred and implemented, to support a geographic routing surveillance scenario. In 7.2, based on the discussion made in 7.1.4 and 7.1.5, a presentation of our own bio-inspired geographic routing protocol to support IQ migration to an identified ROI, as shown in figure 7.1, is highlighted. Performance results are provided for our bio-inspired geographic routing protocol, in 7.3, with comparisons made against the techniques described in 7.1.1 to 7.1.3 and a well-known geographic routing protocol. Finally in chapter 8, we then summarise and conclude our main contributions of this section.

CHAPTER 7

Swarm Intelligence for Geographic Routing

7.1 Geographic Routing

When the position of a source and destination pair is known including the positions of intermediate *UGS* nodes, their location information can be used to assist the routing process [84]. To do so, the destination has to be specified using either physical geographic coordinates or some form of geographic mapping technique, for example location based services [85]. In location based services, positions of *UGS* nodes can be estimated on the basis of incoming signal strengths or time delays in direct communications. Physical geographic coordinates may be obtained using the Global Positioning System (GPS) if *UGS* nodes are equipped with small, low power GPS receivers [80]. Upon obtaining positional information, this can then be exchanged with neighbouring *UGS* nodes across the network field, in order to assist the overall distributed geographic routing process. Geographic routing therefore, has the advantage of being both a distributed and localised process, where the forwarding of IQs to a required ROI is primarily based on the position coordinates of a packets destination (e.g. ROI (x , y) coordinates) and the position of the forwarding *UGS* nodes immediate one-hop neighbours. The position of the destination is usually sent within the IQ packet itself.

Taking advantage of position location information in this sense is very valuable for distributed *UGS* surveillance networks since:

- This can assist and support the need for scalable surveillance operations, increasing the reach required for *tactical C2ISR* mission planning.

- The routing states required to be setup and maintained is a minimum (stateless), reducing the communication routing overhead further.
- Most importantly, IQ migration to a specified ROI can be made responsive to the dynamics of a monitored threat [85]. This implies, if various ROIs need to be specified in scenarios where multiple threats have been identified or to maintain continuous monitoring of a threat as it traverses the *UGS* network field, this can be easily supported, without the need for further exchange and maintenance of new routing state information.

Routing tables are typically constructed as a list of direct forwarding neighbours associated with a local *UGS* node, each with their respective 2-Dimensional (i.e. *x, y*) position coordinates. These respective coordinates can then be used to make routing decisions as to node selection for IQ forwarding in accordance with the geographic forwarding strategy in operation. Operations to support geographic routing schemes are mainly segregated in terms of how the next-hop is selected for packet forwarding. Typically, this can be distinguished and classified as being greedy based, restricted directional flooding and trajectory based forwarding, as described further in 7.1.1, 7.1.2 and 7.1.3.

7.1.1 Greedy Based Forwarding for Geographic Routing Schemes

In greedy based packet forwarding an *UGS* node may forward a packet to a one-hop neighbour in a unicast manner, which is located closer to the destination than the forwarding node itself. This implies that intermediate *UGS* nodes upon receiving a packet (e.g. IQ) tend to forward to a neighbour lying in the general direction of the destination. Ideally this process is repeated until the destination has been reached, as shown in figure 7.2. Greedy forwarding may entail the following possible strategies, for a source (S) and destination (D) pair, within the sources maximum communication range *r*, as shown in figure 7.2:

- The first intuitive strategy is to forward the packet to the node that makes most progress towards D. As indicated in figure 7.2, this would be node C. This greedy based strategy tries to minimise the number of hops a packet has to traverse, in order to reach D, making it ideal for time-sensitive applications, such as surveillance missions.
- The second strategy would be still to make forward progress towards D but also minimise on the probability of packet collisions occurring within the neighbourhood of S. This greedy based strategy therefore tries to increase the likelihood of successful transmission and therefore the average progress a packet makes towards D. As indicated in figure 7.2, this would be node A.
- The third strategy is to select neighbours closest to the straight line between source and destination, making selection closer in direction rather than closer in distance to D. This greedy based strategy is classified as **directional** and tries to minimise on the spatial distance a packet travels [86]. As indicated in figure 7.2, this would be node B, since it has the minimum deviation, in terms of directional line angle α, from D.

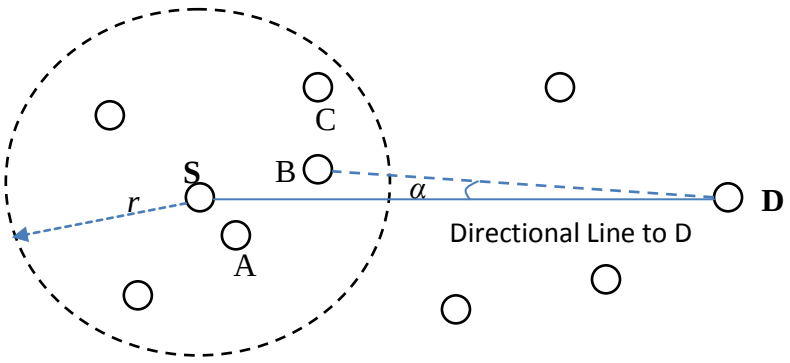

Figure 7.2: Greedy based geographic forwarding strategies

Greedy based forwarding is very efficient in dense uniform networks, where it is possible to make progress at each step [84]. Greedy forwarding, however, fails in the presence of voids or dead-ends, which can occur in scenarios when less dense networks are in operation. In this case, a dead-end node cannot find a one-hop neighbour closer to the

destination and therefore a forwarding path to the intended destination, even though alternative routing paths may exist. A possible remedy is to use limited flooding at the dead-end node as a recovery strategy. Only nodes that are closer to the destination then reply back, with the closest node to the destination among those nodes, being chosen to forward the packet [87]. Alternatively a probabilistic approach, which picks a random intermediate node and routes the packet through it to the destination, is suggested [88]. The random intermediate node is picked randomly from an area between the source and destination and is increased, each time the routing recovery strategy decision fails.

7.1.2 Restricted Directional Flooding for Geographic Routing Schemes

Alternatively, forwarding of data packets to a destination can be achieved by using a subset of nodes that are located in an indicated region. Forwarding in this sense is referred to as geo-casting [89-90]. A simple way to implement geo-casting is to base it on flooding but also somehow restrict the area where packets are forwarded, in order to avoid flooding the whole network. Positional information of deployed *UGS* nodes can assist this by placing a geographical "forwarding zone". Only nodes within the forwarding zone are allowed to forward a received data packet, while nodes outside the forwarding zone discard the packet. The forwarding zone can be defined in various ways as indicated in [89] and [91]:

- *Static Zone*. This represents the smallest rectangle that contains both the source and the entire destination region, with its sides parallel to the axes of the 2-dimensional coordinate system, (x, y), as shown in figure 7.3 (a).
- *Adaptive Zone*. Each forwarding node recalculates the forwarding zone definition, using its own position as the source. This way, nodes that would be included in the static zone but would represent a detour from the intended destination are excluded from packet forwarding. This implies the adaptive zone is calculated in terms of

ensuring packet progression, by including forwarding nodes that are progressive in hop distance towards the destination, from the source node.

- *Adaptive Distance*. While the two above schemes contained the forwarding zone explicitly in each packet, the adaptive distance scheme computes the forwarding zone at each step, on the basis of information about the destination region and coordinates of the previous hop. A node only forwards a packet to its one hop neighbours if its distance to the centre of the destination region is smaller than the distance of the previous hop to the centre, as shown in figure 7.3 (b). In this sense, the packet has made progress, in a similar way to greedy based strategy 3, but without unicast forwarding.

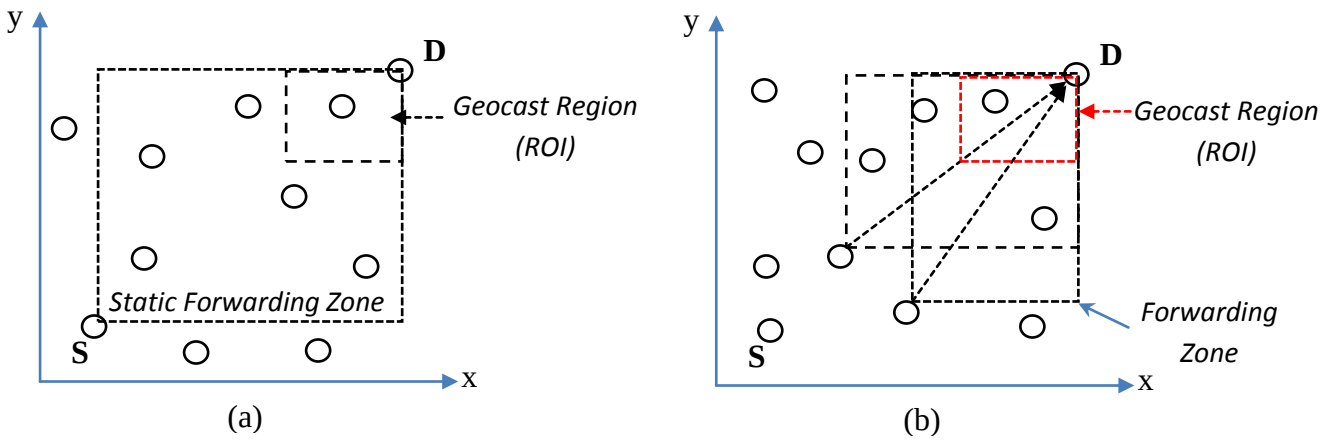

Figure 7.3: Restricted directional flooding (a) Static zone scheme (b) Adaptive distance scheme

The performance of restricted directional flooding relies heavily on the need to accurately define the forwarding zone, since this ultimately affects the probability of packet reception at all destination nodes. Though restricted directional flooding has been found to increase both accuracy and packet delivery to a geo-cast region (e.g. ROI) [91], it still incurs considerable communication overhead. This can have a bearing on overall network communication energy and bandwidth expenditure, reducing the longevity and performance of time-sensitive mission objective surveillance missions.

7.1.3 Trajectory Based Forwarding for Geographic Routing Schemes

Trajectory based forwarding (TBF) is a hybrid technique combining source based routing [91] and greedy based forwarding, but uses a continuous representation of the route. Similar to source based routing, in TBF, the path is indicated by the source, but without actually specifying all the intermediate nodes. Decisions taken at each node are greedy, as highlighted in 7.1.1, but are not based on distance to the destination rather the measure is based on the distance along a desired trajectory. Packets follow a trajectory established at the source with each forwarding node making a decision to select a neighbour that is geographically closest to the trajectory, which is indicated by the source. The trajectory between a source-destination pair, can be specified in the packet header being forwarded and can either be specified simply as a straight line, which reduces the packet forwarding to strategy 3, as described in 7.1.1 or in terms of a function, in the form $Y = f(X)$ describing a curved trajectory line, as shown in (7.1) [92].

$$Y = f(X) = r_{max} \sin(s) \tag{7.1}$$

As shown in 7.1, the parameter s indicates, the direct incremental distance travelled from the source towards the destination, while r_{max} being the set maximum *UGS* transmission range, as shown in figure 7.4. The amplitude of the function $Y = \sin(s)$, can therefore be varied, according to the maximum set *UGS* transmission range. Since, choosing a next hop for packet forwarding should be towards the advancement on the curved trajectory line towards the destination, only the portion of the curve with s being greater than the x-coordinate of the forwarding node, should be considered. Several policies of choosing a next hop are possible based on the trajectory in operation [92]. The most common policy would be to consider nodes closest to the curve, with the minimum residual (Δy_r), since this would tend to produce a lower deviation from the ideal trajectory, as shown in figure 7.4.

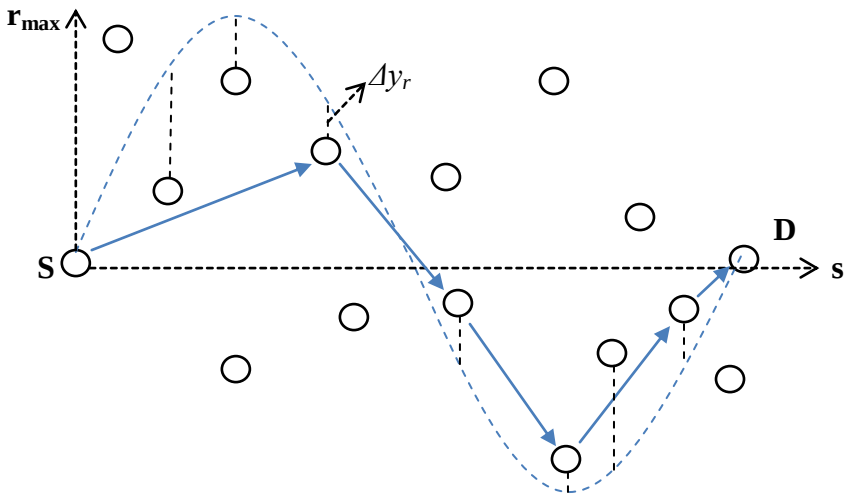

Figure 7.4: Trajectory based forwarding on a sinusoidal curve

Following a path as close to the intended trajectory also reduces the likelihood for a packet to diverge away from the destination, due to errors that might occur in position localisation [92]. Using TBF based on a sinusoidal curve can therefore provide advantages in providing cheap path diversity, when compared with traditional methods of finding alternative paths, such as in pro-active routing [84]. In addition, specifying a pre-defined trajectory trades off communication for computation (in-network processing), by declaring paths instead of searching for them, this can provide necessary savings in both bandwidth consumption and communication energy expenditure [94].

Since, surveillance applications are predominantly time-sensitive, geographic routing protocols and their underlying forwarding strategies, which can support a low latency packet delivery requirement to a ROI, should be developed. This implies, a greedy based forwarding strategy should be applied wherever possible, in order to make as much progress towards a destination, on a per hop basis. Routes that can be initially pre-defined by a source, with trajectory descriptions sent as *content* within the forwarding packet header, similar to TBF, can also assist to reduce the communication burden through *in-*

network processing, thus allowing decisions as to forwarding node selection, to be made easier [95]. The use of source based routing in this sense is very effective in reducing per packet processing requirements and to avoid unnecessary forwarding loop conditions from occurring, through topology control [95]. In addition, pre-defined routes established at a source (e.g. gateway node) can aid directionality and offer better control of forwarding packets towards a destination (ROI) under distributed conditions, when compared with just basic or restricted directional flooding [96].

In 7.2, the greedy and source based qualities described above are further developed, in order to assist our proposed geographic routing strategy, which utilises a pre-defined bio-inspired trajectory model to support directionality (guidance) and control of forwarding tasks, towards the intended ROI. Before going into details of our proposed design, 7.1.4 and 7.1.5, introduce some of the common biological techniques used in nature, which can be transferred to support our proposed geographic routing strategy. This has mainly been achieved through utilising techniques, which social insects have developed for locating and identifying forwarding paths towards particular odour sources of interest.

7.1.4 The Principles of Swarm Intelligence

Development of new routing protocols to support *UGS* network surveillance missions, as illustrated in figure 7.1, is most challenging when we consider that these networks are large-scale in nature, dynamic in operation, resource constraint and are always left unattended. The design of routing schemes to support the requirements mentioned above, can be made effective and efficient when the complexity associated with the forwarding task becomes less. This entails reducing the mechanisms adopted for route discovery and implementing more self-managing and self-organising features within the network layer operations [97].

Until recently, existing investigations into developing self-managing features for routing protocols in *WSNs* have begun to take inspiration from biological systems, as a source of innovative network design [98]. The use of biological principles in network design begins by observing the dynamics of natural systems, which have used established laws, as a result of millions of years of evolution to govern them. Typically these laws that govern particular biological functions or tasks are found to be surprisingly small in number and generic. It is only through applying these simple generic rules that biological systems or societies have been found to yield collaborative and effective patterns of complex behaviour, for task coordination and resource management purposes. In addition, application of these simple rules to network scenarios, can facilitate the necessary scalable features required in surveillance missions, including efficient task allocation and inherent resiliency to node failures, without the need for any external controlling entity [99].

Swarm Intelligence (*SI*) is a novel field that was originally defined as *"Any attempt to design algorithms or distributed problem-solving devices inspired by the collective behaviour of social insect colonies and other animal societies"* [100]. More recently, *SI* generally refers to the study of collective behaviour of multi-component distributed systems that coordinate their tasks, according to defined, de-centralised controls. The basic rationale of *SI* for routing purposes lies in the observation that insect societies, as a collective unit, do actually solve routing problems. Insects themselves need to discover and establish paths that can be used by single insects, to effectively move back and forth from the nest of the colony, to sources of food. Routing paths then emerge through *synergistic* interactions among a large number of simple individual insects that concurrently sample paths and inform others about their characteristics, using a variety of communication schemes (e.g. *pheromone*-mediate communication in ants) [101]. In 7.1.5, the principles of *Swarm Intelligence* are transferred to a geographic routing scenario to potentially support surveillance operations, as shown in figure 7.1.

7.1.5 Applying Swarm Intelligence to a Geographic Routing Scenario

It has been observed that ants tend to converge on the shortest among different paths connecting their nest (source) and their food (destination) [99-100]. Ants tend to exhibit shortest path behaviour, by following *pheromone* (volatile chemical) signals released in the environment by their fellow colony members to invoke specific social responses and coordination of tasks, known as *stigmergy* [100]. The general rule applied here, is that ants tend to preferentially move towards areas of higher pheromone intensity, through *olfactory sensing* [100], since this represents a higher order of relevance in finding a required, designated food source [102]. These paths will then attract more ants, which in return will increase the pheromone intensity, until there is a convergence of the majority of ants on to the shortest path. Applying this *SI* principle to a geographic routing process inspired by ant foraging behaviours as described above, seems to suggest ants use both an exploration phase, where routes are discovered towards the destination and a set-up phase, to communicate potential routes accordingly, between the source-destination pair.

In our intended scenario, the exploration phase however, can be avoided, since the intended ROI destination coordinates are known to the gateway node, as shown in figure 7.1. In this sense, all that remains is a way to model and mimic *UGS* nodes, as potential deposits of *pheromone* concentration made within the network field, in order to guide the forwarding of IQs to the intended ROI, as shown in figure 7.5. Avoiding the exploration phase also helps to minimise the transmission and use of control packets, which would have been required to set-up *pheromone* concentration levels between the intended gate-way node-destination pair. This can therefore provide benefits towards reducing both network communication energy and bandwidth expenditure further. With the exploration phase avoided, the scenario as illustrated in figure 7.5 then becomes simplified to one of locating an odour source, through *plume traversing* techniques, based on *pheromone*

concentration levels [103]. *Plume traversing* in the natural world, is the prescribed technique used by insects, in order to follow a plume odour (pheromone) concentration trail directly to its source, by way of maintaining consistent contact with an odour plume for guidance purposes. This can be mainly achieved by means of closely following the maximum *pheromone* concentration trajectory gradient, towards the intended odour source [104].

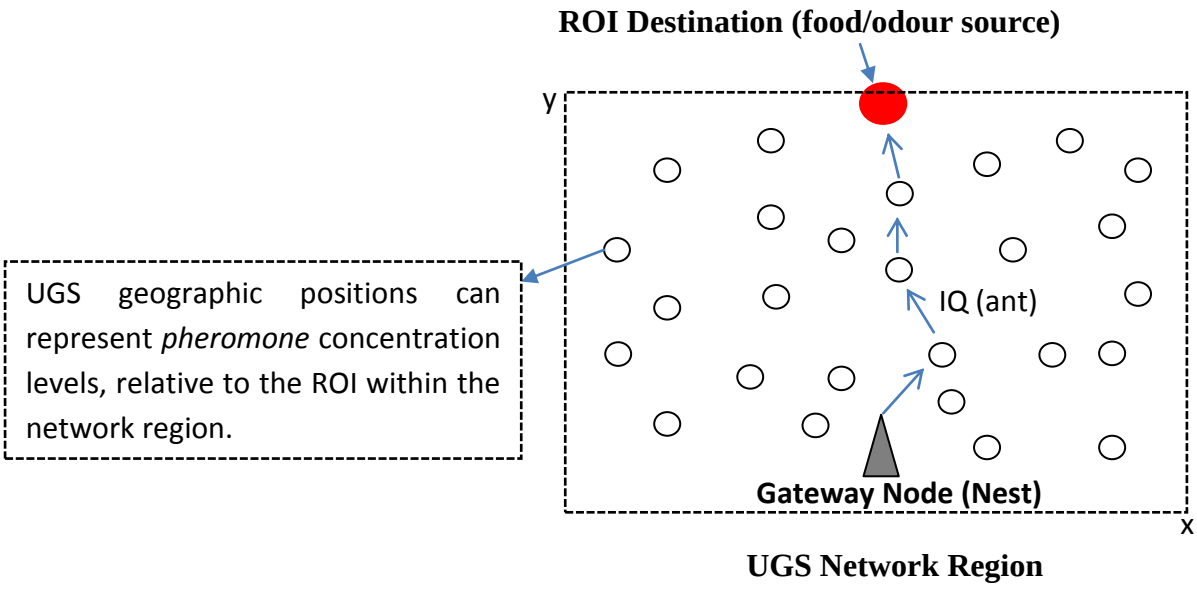

Figure 7.5: Relating UGS geographic node positions to pheromone concentration levels to guide IQ migration

As shown in figure 7.5, the maximum concentration trajectory gradient of a forwarding IQ (ant) can be influenced and controlled by the amount of artificial *pheromone* deposited at different points in the network field. In this sense, regions of higher *pheromone* (i.e. higher concentration levels) within an *UGS* neighbourhood can therefore be used to influence forwarding node selection. Ideally, as the case in the natural world, higher concentration levels would represent a higher order of relevance in finding a required designated food source, which when applied to a surveillance geographic routing scenario, can lead IQ forwarding behaviour towards the intended ROI destination. In a geographic surveillance routing scenario, creating artificial *pheromone* deposits at different

points in the network field can be accordingly governed by considering, the relative positions of deployed *UGS* nodes, to the designated destination (ROI/food source). To achieve this aim, requires firstly a way of modelling the concentration dispersion effects from an odour source (ROI), as found in nature, so that artificial *pheromone* concentration levels can be mapped and established onto the *UGS* network region, to facilitate IQ forwarding.

In 7.2 an odour plume model is introduced, in order to allow *UGS* node positions to be geographically mapped with artificial *pheromone* concentrations. Subsequently, each distributed *UGS* node can then become aware of their local concentration levels, relative to the intended ROI. The ability to achieve this forms the basis towards formulating our own proposed geographic routing strategy, utilising both greedy and source based techniques, which were highlighted previously in 7.1.1 and 7.1.3.

7.2 Swarm Intelligent Odour Based Routing

In 7.2, our bio-inspired routing protocol namely, **SW**arm Intelligent **O**dour **B**ased Routing (*SWOB*), is described further. *SWOB* itself takes its inspiration from the basic principles and examples provided by social insects in odour localisation and the methods they use for route finding towards an intended odour source, through *plume traversing*. Locating odours of interest is a twofold strategy. Firstly odours need to discovered and then followed as to make positive progress towards the direction of the source. In 7.2.1, a model is highlighted to mimic the odour dispersion effects of a discovered source, as a way of establishing *plume traversing* and subsequently a shortest-path route towards an odour source. A discovered odour source in our scenario, relates to the given coordinates of a ROI, which can be identified through using airborne reconnaissance methods, as shown in figure 7.1.

7.2.1 Virtual Gaussian Odour Plume Model

In natural circumstances, the structures of odour concentration plumes are established by the physics of atmospheric dispersion. Odour plumes are created when odour molecules released from their source are taken away by environmental forces, for example, due to a prevailing wind direction. In nature and the real world, the strength and length of a plume is commonly dictated by the size of the odour source and general wind speed conditions [104]. A common observation however to draw from this fact is that, odour plume structures tend to naturally exhibit high levels of odour concentration at the source, but with the average odour concentration levels falling away, if travelling further down-wind from the origin of the source [104].

A common way to sufficiently portray this real-world odour diffusion characteristic can be achieved through using a Gaussian function model. A Gaussian model of diffusion is a widely used and accepted model to accurately portray the natural odour dispersion phenomenon, for a wide range of atmospheric conditions [105]. Using a Gaussian model assumes conservation of mass and a continuous odour emission effects from a source, within steady state conditions [105]. In 7.2.1, a 2-Dimensional Gaussian function plume model with ground level odour point source, is used to artificially construct odour and *pheromone* concentration levels, given by $C(x , y)$, within the *UGS* network region, as shown in (7.2) [105].

$$C(x,y) = A_g \times e^{-\left[\frac{(x-x_0)^2}{2\sigma_x^2} + \frac{(y-y_0)^2}{2\sigma_y^2}\right]} \tag{7.2}$$

From (7.2), x and y denote the 2-Dimensional geographic position coordinates of a deployed *UGS* node within the network region, x_0 and y_0 denote the designated centre coordinates of the specified ROI, which behaves as the odour source, A_g represents the

amplitude of the Gaussian plume model and both σ_x and σ_y, denote the standard deviations of the Gaussian function to describe the breadth of the plume in the horizontal and vertical directions respectively, from the odour source. The use of A_g can be avoided, by considering normalised odour concentration levels, ranging between 0 and 1. This implies, a value of 1 is registered when at coordinates (x_0, y_0) and then falling away towards 0, as we move further away vertically from the odour source, with geographic distance (i.e. distances that satisfy the condition $y < y_0$), as shown in figure 7.6. Using the Gaussian function given in (7.2), provides us with the ability to virtually map *pheromone* concentration levels at specific geographic *UGS* node positions (x, y), within the designated network region. In this sense, IQs can then be forwarded in a *unicast* fashion to nodes that represent higher levels of odour concentration, dictated by the guidance of the constructed virtual odour plume.

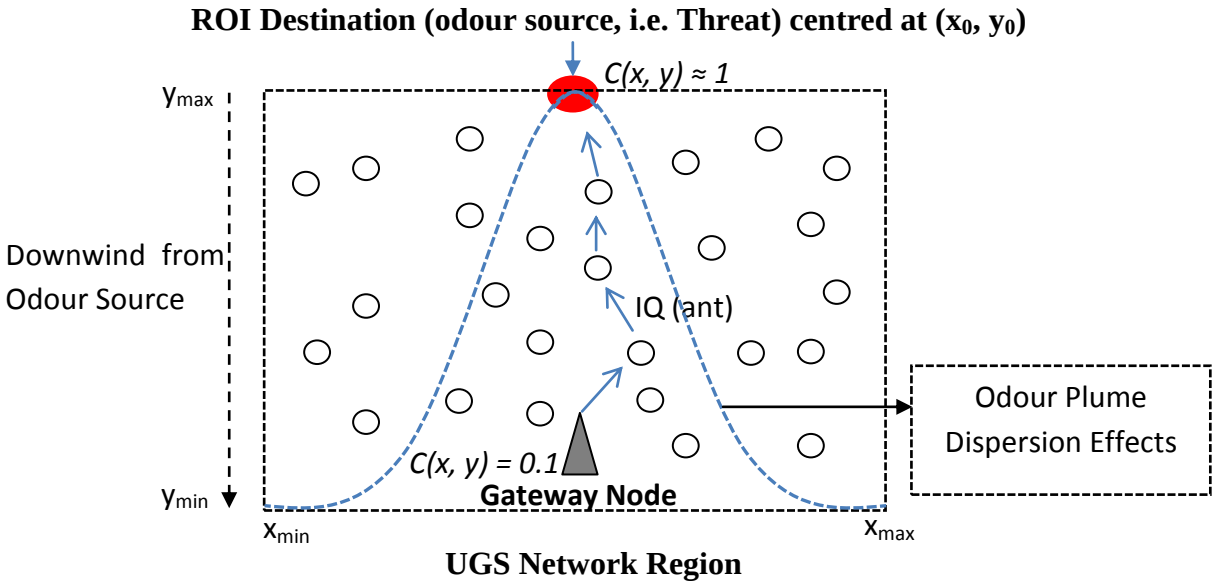

Figure 7.6: Network "birds-eye" view representation of our proposed virtual Gaussian plume model to facilitate IQ forwarding to the ROI

The characteristics of the plume model, in terms of the breadth that an odour plume may have and its subsequent $C(x, y)$ values are predominantly determined by σ_x and σ_y.

Calculating the required standard deviations, from (x_0, y_0) can be conducted in terms of user defined, **unit less concentration levels**, given as **α** at the gateway node with coordinates (x_{sink} , y_{sink}) and **β** at a communication transmission radius, R_T, away from the odour source, with condition **β > α**. The derived simultaneous equations relating **α** and **β** to σ_x and σ_y are shown in (7.3) and (7.4).

$$\alpha = e^{-\left[\frac{(R_T)^2}{2\sigma_x^2}+\frac{(X_1)^2}{2\sigma_y^2}\right]} \tag{7.3}$$

$$\beta = e^{-\left[\frac{(R_T)^2}{2\sigma_x^2}+\frac{(R_T)^2}{2\sigma_y^2}\right]} \tag{7.4}$$

From (7.3), $X_1 = \sqrt{[(x_0 - x_{sink})^2 + (y_0 - y_{sink})^2]} - R_T$, denoting the Euclidean distance up to R_T, from the odour source. As shown in (7.3), **α** is a derived expression, which relates *C(x, y)* values to be found at a distance R_T in the *x* direction and X_1 in the *y* direction from the gateway node. Dividing (7.3) by (7.4) provides us with a method of comparing the ratio of artificial concentration values, at the gateway node and at a distance of R_T from the odour source, as shown in (7.5).

$$\frac{\alpha}{\beta} = \frac{e^{-\frac{(X_1)^2}{2\sigma_y^2}}}{e^{-\frac{(R_T)^2}{2\sigma_y^2}}} \tag{7.5}$$

Setting user defined values **α** and **β** accordingly, for example $\alpha = 0.1$ and $\beta = 0.9$, σ_y can be solved for a known R_T, with designated ROI centre coordinates (x_0, y_0) and gateway node coordinates (x_{sink} , y_{sink}). The solved σ_y value can then be substituted back into (7.3), in order to obtain the required network value for σ_x.

Figure 7.7, shows the relationship for **α / β** ratio concentration values and subsequent σ_x and σ_y values obtained through solving (7.5), for a 1km by 1km network region, with odour source coordinates (x_0, y_0), reflecting the centre coordinates of an intended ROI, being (500, 900) respectively, with **α** fixed at 0.1, (x_{sink} , y_{sink}) = (500, 100), and R_T =

100m. As shown in figure 7.7, if the value set for **β** continually increases (i.e. a low (α / β) concentration ratio) σ_x increases in value, while σ_y decreases linearly. Similarly, figure 7.8 illustrates the transfer of the 2-Dimensional Odour plume model, given in (7.2), with calculated σ_x = 182.9986 m and σ_y = 337.3128 m, through solving (7.5), into our intended geographic routing scenario and how the resulting virtual odour concentration levels can be used to guide IQ migration towards the surveillance ROI.

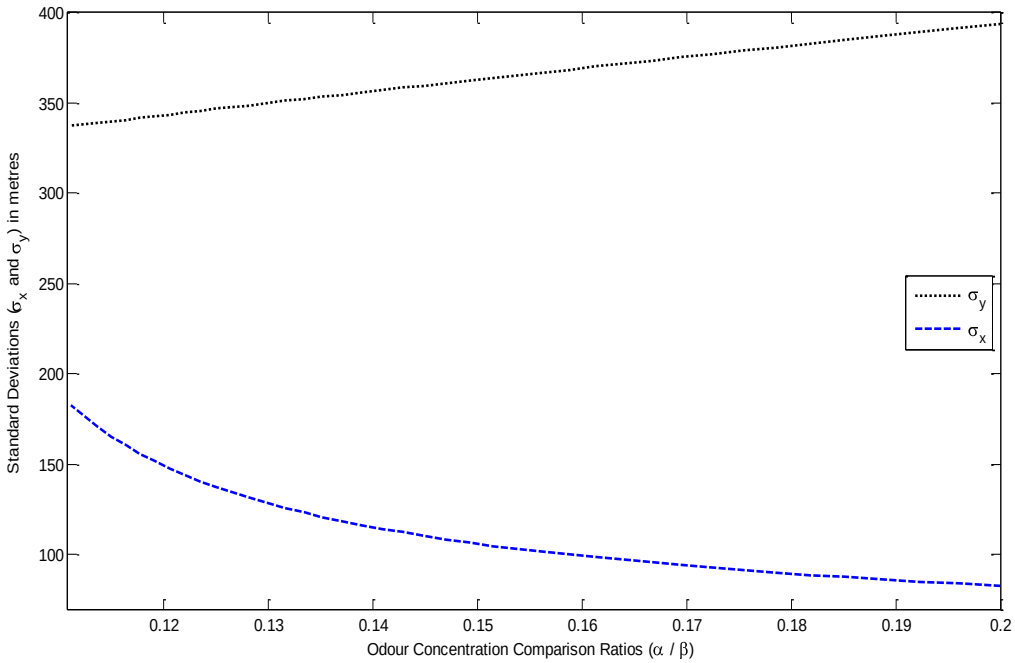

Figure 7.7: Relationship of odour plume σ_x and σ_y values with (α / β)

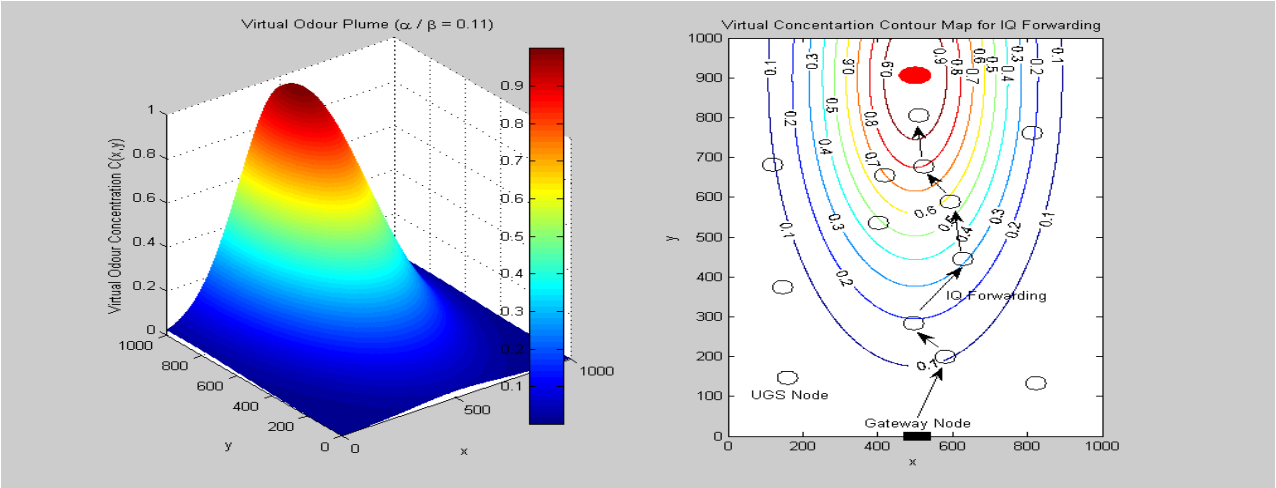

Figure 7.8: Virtual odour plume model and concentration contour map for IQ forwarding purposes

Figure 7.8, illustrates and reveals some potential benefits inherently achieved through using a Gaussian type model, which can be used to provide support for *UGS* network management. These potential advantages are as follows:

- The virtual Gaussian plume model and resulting contour map reveals that not all deployed *UGS* nodes will have designated *C(x,y)* values, relative to the ROI that can be used for IQ forwading purposes. These nodes are typically found geographically outside of the Gaussian plume shape and resulting contour map. This is a useful observation to make since, realistically, these nodes will not take part in IQ forwarding, which can assit in balancing overall network load and also additionally support the notion of making bandwidth and communication energy consumption savings, wherever possible.
- Using a virtual Gaussian plume model allows forwarding and eventual IQ migration to be controlled within the bounds of the plume, with the eventual aim of providing guidance (*plume traversing*) to the designated region of interest, as shown by the contour map.

These inherent characteristics, as detailed above, can be used to develop a mechanism, which can restrict routing and subsequent IQ forwarding to particular areas only, but without loosing the necessary guidance required towards the designated ROI. Such a mechanism can provide an advantage as a means of integrating network topology control functionality, within normal geographic routing. Utilising a topology control implementation can also provide a far better way of defining the necessary σ_x or σ_y values required for the Gaussian plume shape, since this can be directly related to the characteristics of a current deployed network, rather than, them being based on user defined values, as described earlier.

Topology control in our proposed scheme, is essentially governed by the breadth a Gaussian plume may have, through σ_x or σ_y and to vary these variables accordingly, in order to reflect on the degree of control (restriction) required. A reliable way of achieving and establishing a required plume breadth shape, is to formulate σ_x or σ_y , in terms of ensuring that any deployed node, found within the Gaussian plume, will still have a certain number of direct neighbours to communicate with. Formulating a topology control mechanism in this manner is important since, it ensures nodes will not be prevented from carrying out their normal IQ forwarding tasks, even in the presence of topology restriction. To define such a topology control relationship, firstly requires a way of modelling probabilistically the location of *UGS* nodes within the network region and secondly relating this to a desired network connectivity, in order to ensure direct, restricted communication, while also avoiding the condition for *UGS* node isolation, as explained further in 7.2.2.

7.2.2 Swarm Intelligent Odour Based Network Topology Control

In densley deployed *UGS* networks (> 100 nodes), a single *UGS* node may have many neighbouring nodes with which direct communication is possible depending on the communication transmission radius, R_T, being used. While dense networks can create the necessary connectivity opportunities for *UGS* node communication it can, however, also aggrevate node intereference. This primarily places a burden on the medium access control, resulting in an increased number of retransmissions required to successfully deliver a packet and limiting the ability of the deployed network to reuse wireless bandwidth.

A potential way of overcoming some of the problems mentioned above, is to apply some form of topology control. The idea here is to deliberatley restrict the set of *UGS* nodes that are considered neighbours of a given node, therefore controlling a set of active

links a node may have and subsequently it's connectivity. Common ways of achieving connectivity control would be to directly control transmission power, by turning off nodes for certain periods of time (sleep-wakeup scheduling) or to implement hierarchy, in the form of clustering, within the network [106]. An alternative way is to force the fact that deployed nodes, to only communicate with *k* direct neighbours (connectivity) within a certain geographic distance [107]. A network is set to be connected if for every pair of nodes, a path exists between them. All nodes of a connected network can therefore communicate with each other over one or multiple hops (links). Equivalently a network is said to be *k-connected* ($k = 1, 2, 3 \ldots n$), if for each node pair there exists greater than *k* mutually independent paths connecting them [28]. Applying this to our *SWOB* routing scenario therefore requires a way of calculating the σ_x value, according to, the relationship of being *k-connected*.

The relationship of being *k-connected* is best defined in terms of the probabilty of being *k-connected*. Obtaining a probabilty expression, which defines a certain *k-connectivity* firstly requires an ability to evaluate the average number of nodes to be found within an *UGS* node's R_T. This implies a network toplogy representation and a random node location model is essential as described further in headings 7.2.2.1 and 7.2.2.2 . In 7.2.2.3, an expression is then formulated and described , in order to calculate the required standard deviation value in the x-direction, σ_{xr}, to ensure a desired *k-connectivity* for toplogy control purposes, under different network node densities. In 7.2.2.4, a confirmation as to the validity of our *SWOB* topology control mechanism is then given, in terms of saturated throughput performance, using the IEEE 802.11b MAC protocol.

7.2.2.1 UGS Network Topology Representation

The topology of the underlying deployed *UGS* network can be represented as an *undirected geometric random graph* [108-109], denoted by $G(\mathbf{N}, R_T)$ at each time instant,

in which a total of ***N*** nodes are independently, uniformly and randomly distributed in metric space, with transmission range R_T. A "graph" in this setting refers to a collection of vertices or "nodes" and a collection of *edges* that connect pairs of vertices. The random graph used is modelled as *undirected*, meaning that there is no distinction between the two vertices associated with each *edge* and also to denote the fact that the *edges* of the graph do not have any orientation, meaning all link connectivity relations on node pairs, are symmetric in nature. An assumption is to also consider that the transmission range of a random *UGS* node can be modelled as "Disk Graph" of radius R_T [110]. In other words, the topology can be represented as a random graph in which the link existence probability (P_T) between two nodes ***u*** and ***v*** is determined by their geometric distance, in a way that $P_T = 1$ for $\| u - v \| \leq R_T$ and $P_T = 0$ otherwise. Here $\| u - v \|$ represents the Euclidian distance between u and v.

7.2.2.2 UGS Node Location Model

The modelling of the random geographic *UGS* node locations within a vast 2-Dimensional region can be assisted if it is assumed, the locations are uniformly and independently distributed within the region. Such an assumption is clearly viable in scenarios where *a priori* knowledge of the network region is not available, due to the mode of deployment in operation, for example, *UGS's* being air-dropped into unfriendly environments [111]. Under this direct assumption, the location of *UGS* nodes can be modelled by utilising a stationary 2-Dimensional Poisson Point Process (*PPP*) [112-113]. Denoting the node density of the underlying *PPP* as λ, which represents the expected number of *UGS's* to be found per unit area and is calculated as (***N*** */ Total Network Area*). The exact number of *UGS's* located in a network region with total area *A* m^2, *M (A),* follows a Poisson distribution of parameter $\boldsymbol{\lambda \times A}$, with $i = 1, 2 \ldots, \boldsymbol{N}$, as shown in (7.6).

$$P(M(A)=i) = \frac{e^{-\lambda A}(\lambda A)^i}{i!} \tag{7.6}$$

We denote the subset of the network region, with total area, A m^2 , by ||A|| m^2. The expected number of nodes (E_{Nodes}) therefore to be found in a region ||A|| is given, as shown in (7.7).

$$E_{Nodes} = \lambda \times ||A|| \tag{7.7}$$

7.2.2.3 The Required Standard Deviation to Ensure k-Connectivity

In any topology control scheme, such as *SWOB* the existence of isolated nodes is an undesirable characteristic, since in static scenarios isolated nodes cannot communicate any information. If communication connectivity of *UGS* nodes is to be restricted through a virtual Gaussian odour plume, by variation of the standard deviation, $\sigma_{xr,}$ in the horizontal x-direction from x_0, we require finding the probability that each node has greater than k neighbours, within $x_0 \pm \sigma_{xr}$. This requires us to formulate the following conditions, as detailed below:

- We denote t_i (i =1, 2…, m) as the two dimensional (x, y) coordinates of $\boldsymbol{N}$ Poisson Point distributed nodes, where m represents the number of deployed nodes.
- For j = 2, 3…, m we denote $t_j - t_{j-1}$ by Δi, which represents the Euclidian distance between two random nodes of the network.
- Δi is a measure of the nearest neighbour distance, which represents the distance of a random node to its closest neighbouring node.

Taking into account the above conditions for a homogenous *PPP* in two dimensions, the probability density function of Δi is given, as shown in (7.8).

$$f(\Delta i) = 2\pi\lambda\Delta i e^{-\lambda\pi(\Delta i)^2} \tag{7.8}$$

For a random node to be connected it must have a Δi that is $\leq R_T$, as described earlier in 7.2.2.1 and therefore the probability that a random node has at least one neighbour and is connected is given, as shown in (7.9).

$$P(\Delta i \leq R_T) = \int_{\Delta i=0}^{R_T} f(\Delta i)\, d\Delta i = 1 - e^{-\lambda \pi R_T^2} \tag{7.9}$$

Since we require a network in which none of the $\boldsymbol{N}$ deployed nodes are isolated and using the statistical property that Δi is mutually exclusive for each deployed node, the probability that $\boldsymbol{N}$ nodes have Δi lengths $\leq R_T$ and therefore remain connected, denoted by $P_{Connected(N)}$, is given as shown in (7.10).

$$P_{Connected(N)} = (1 - e^{-\lambda \pi R_T^2})^N \tag{7.10}$$

As shown in (7.10), the expression relates to the connectivity for $\boldsymbol{N}$ nodes within a network region of total area, $A\ m^2$, as function of R_T. The equation in (7.10) however, represents a lower bound on what is required to achieve a connected network. To achieve robustness for node or link outages we need to ensure that a random node is *k-connected*. This implies that a random node should have greater than or equal to k neighbours. The probability that a random node, assuming statistical independence, with transmission range R_T, has greater than or equal to k neighbours and therefore is *k –connected* within a network region with total area $A\ m^2$ is given, as shown in (7.11).

$$P(\text{Random Node in } A \text{ is } k-\text{connected}) \approx P(\text{Random Node in } A \geq k \text{ Neighbours}) \tag{7.11}$$

$$= \left[1 - \sum_{n=0}^{k-1} \frac{(\lambda \pi R_T^2)^n}{n!} \times e^{-\lambda \pi R_T^2} \right]$$

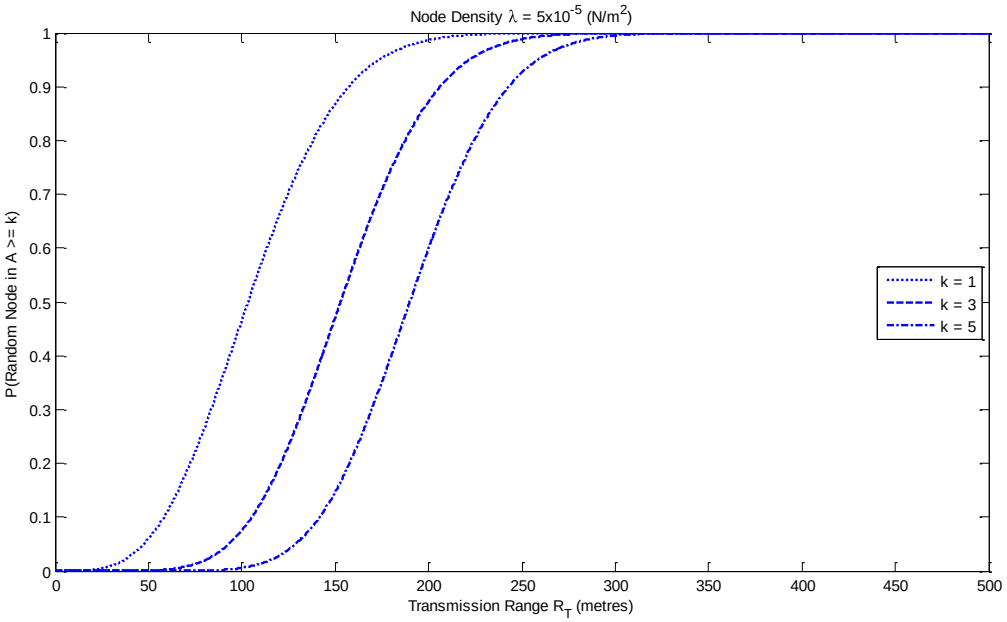

Figure 7.9: Probability of being k-connected with transmission range R_T, for 50 node network

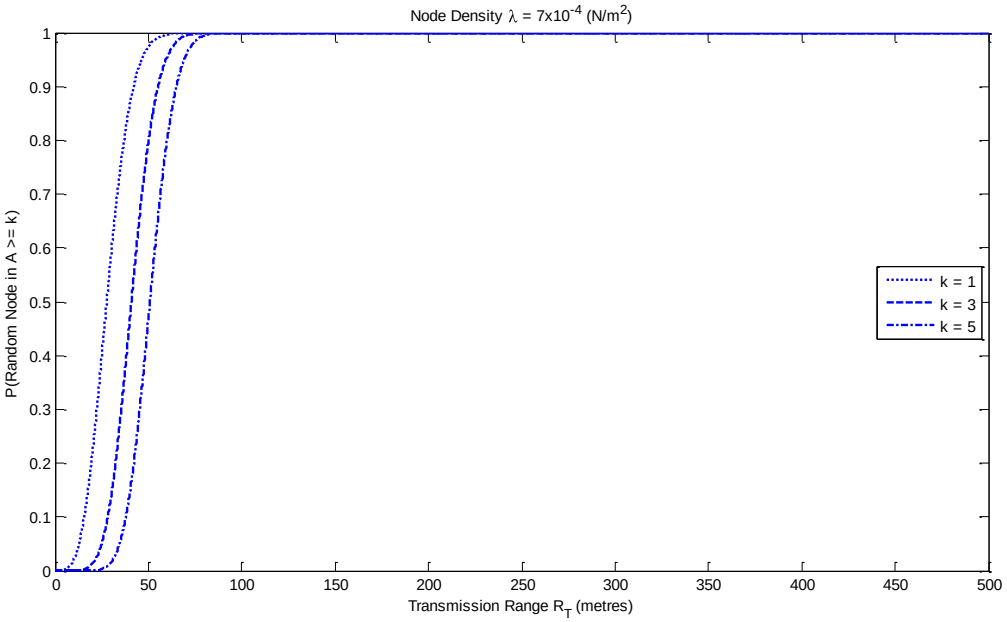

Figure 7.10: Probability of being k-connected with transmission range R_T, for 700 node network

Figures 7.9 and 7.10 show the relationship of being *k-connected* with transmission range R_T, for a total network area, A, of $1x10^6$ m^2, under two different network node density conditions. Under low density conditions (50 nodes), increasing the number of neighbours a random node might have, for *k- connectivity*, while also ensuring a high

reliability, requires a node to have a large R_T , approximatley 300m, as shown in figure 7.9. Under high density conditions (700 nodes) as expected, the condition to increase *k-connectivity* is reversed for R_T. In all cases, increasing the condition for *k-connectivity*, increases the required R_T. This observation is common and in accordance with the "*phase-transition*" phenomenon (i.e *k-connectivity*) in random geometric graph theory, which states most standard properties of random graphs arise rather suddenly [108]. In figure 7.9 and 7.10, this "*phase-transition*" phenomenon is primarily due to an increasing R_T.

If we are concerned with implementing *k-connectivity*, within a subset region, ||A||, of total network area A m^2, in order to ensure topology control, we need to satisfy that each node found within ||A||, has greater than or equal to *k* neighbours and that any node found in ||A|| continues to remain un-isolated, for the *k* neighbour requirement. The probability expression that has potential to satisfy this need, is expressed and can be formulated, as shown in (7.12).

$$Maximum\ Bound\ \sigma_{xr}\ \ calculation\ \ for\ k\text{-}connectivity\ within,\ ||A||: \tag{7.12}$$

$$P(Finding > E_{Nodes}\ in\ ||A||) \times P(RandomNode in\ ||A|| \geq k) \geq P(A\ Node in\ ||A|| > k)$$

$$\approx \left[1 - \sum_{i=0}^{E_{Nodes}} \frac{(\lambda A)^i}{i!} \times e^{-\lambda A}\right] \times \left[1 - \sum_{n=0}^{k-1} \frac{(\lambda \pi R_T^2)^n}{n!} \times e^{-\lambda \pi R_T^2}\right] \leq \left[1 - \sum_{i=0}^{k} \frac{(\lambda \pi R_T^2)^i}{i!} \times e^{-\lambda \pi R_T^2}\right]$$

From (7.12), the probability expression to the left of the in-equality relates to remaining *k-connected* for > E_{Nodes} and to the right, relating to a random node found in ||A|| is not *k*-isolated. The expression in (7.12), determines the approximate number of nodes (E_{Nodes}) needed to cover a certain Gaussian plume area ||A||, in the *x*-direction, in order to maintain a desired *k-connectivity*. This expression ultimately reflects and determines the flexibility possible for network topology control, which is ascertained firstly by, the expected number of neighbours (*k*) to be found in a node's transmission neighbourhood and secondly the probability of a random node in ||A|| as not being *k*-isolated. The

probability expression in (7.12), is only true, when the probability of having *k-connectivity* in ||A|| is less than or equal to a random node in ||A|| being *k*-isolated, which as a result determines the required σ_{xr} maximum bound value, through E_{Nodes}, required to achieve this.

From (7.12), E_{Nodes} can be expressed as the expected number of nodes to be found in ||A||, as given in (7.7). Solving (7.12) therefore requires finding the sub-set area of the network region, ||A||, in terms of the virtual Gaussian odour plume model. Since, topology control is expressed through node *k-connectivity*, which is to be restricted within $x_0 \pm \sigma_{xr,}$ this can be formulated, according to a Gaussian function along the horizontal *x*-axis, as shown in (7.13).

$$||A|| = \int_{-\infty}^{\infty} A_g \times e^{-\left[\frac{(x-x_0)^2}{2\sigma_{xr}^2}\right]} dx = A_g \times \sigma_{xr} \times \sqrt{2\pi} \tag{7.13}$$

The expression for calculating ||A|| given in (7.13) uses integral limits, which define the network region as being infinite in length along the x-axis, for conditions that satisfy $x_0 - 4\sigma_{xr} > x_{min}$ and $x_0 + 4\sigma_{xr} < x_{max}$, therefore ensuring the total Gaussian plume in the x-direction is contained within the start, x_{min} and the end of the network region, x_{max}. The definition of the condition described above for use in (7.13), is a measure concerning the number of standard deviations, σ_{xr}, from the mean x_0. As shown in (7.13), these conditions have been derived as being plus or minus $4\sigma_{xr}$, because this is a direct approximation, of being 99.9% certain under normalised conditions that the complete Gaussian plume function will be found within x_{min} and x_{max}.

In a realistic scenario however, the Gaussian plume function can be expected to operate within a restricted network region, which does not usually satisfy the condition, $x_{min} > x_0 \pm 4\sigma_{xr} < x_{max}$. If this is true, it cannot be guaranteed, therefore, to find an accurate evaluation of all possible E_{Nodes} to be found within the Gaussian plume in the x-direction, making the equation given in (7.13) invalid. In this case, it is required to find the difference

in plume area restricted using $\sigma_{xr,}$ to the total plume area, which is < x_{min} or > x_{max}, according to the following given bounded network region conditions, as shown in (7.14) and (7.15). The conditions used in (7.14) and (7.15) have been derived to reflect and approximate the situation of not finding the total Gaussian odour plume contained within a specific network region, dictated by the condition $x_0 \pm 4\sigma_{xr}$. As shown in (7.14) and (7.15) the fraction of the total Gaussian plume area outside the network region is approximated using the error function, denoted as *erf (.)*.

$$if(x_0 + 4\sigma_{xr}) > x_{max} \tag{7.14}$$

$$||A|| = \left[\left[\int_{-\infty}^{\infty} A_g \times e^{-\left[\frac{(x-x_0)^2}{2\sigma_{xr}^2}\right]} dx\right] - \left[\int_{x_{max}}^{\infty} e^{-\left[\frac{(x-x_0)^2}{2\sigma_{xr}^2}\right]} dx\right]\right]$$

$$||A|| \approx \left[\left[\int_{-\infty}^{\infty} A_g \times e^{-\left[\frac{(x-x_0)^2}{2\sigma_{xr}^2}\right]} dx\right] \times \left[\int_{x=0}^{x=4\sigma_{xr}-x_{max}} e^{-\left[\frac{(x-x_0)^2}{2\sigma_{xr}^2}\right]} dx\right]\right]$$

$$||A|| \approx (A_g \times \sigma_{xr} \times \sqrt{2\pi}) \times \left[erf\left(\left(4 - \left(\frac{4\sigma_{xr} + x_0 - x_{max}}{4\sigma_{xr}}\right)\right)/\sqrt{2}\right)\right]$$

$$if(x_0 - 4\sigma_{xr}) < x_{min} \tag{7.15}$$

$$||A|| = A_g \times \left[\left[\int_{-\infty}^{\infty} e^{-\left[\frac{(x-x_0)^2}{2\sigma_{xr}^2}\right]} dx\right] - \left[\int_{-\infty}^{x_{min}} e^{-\left[\frac{(x-x_0)^2}{2\sigma_{xr}^2}\right]} dx\right]\right]$$

$$||A|| \approx \left[\left[\int_{-\infty}^{\infty} A_g \times e^{-\left[\frac{(x-x_0)^2}{2\sigma_{xr}^2}\right]} dx\right] \times \left[\int_{x=x_{min}-4\sigma_{xr}}^{x_{min}} e^{-\left[\frac{(x-x_0)^2}{2\sigma_{xr}^2}\right]} dx\right]\right]$$

$$||A|| \approx (A_g \times \sigma_{xr} \times \sqrt{2\pi}) \times \left[erf\left(\left(4 - \left(\frac{4\sigma_{xr} - x_0 - x_{min}}{4\sigma_{xr}}\right)\right)/\sqrt{2}\right)\right]$$

In conditions, where the Gaussian odour plume can be found outside both x_{min} and x_{max}, it is therefore required to find the combined fraction of the total area, which is < x_{min} and > x_{max} and subtract this from the total plume area, as shown in (7.16).

$$if(x_0 - 4\sigma_{xr}) < x_{min} \;\&\; (x_0 + 4\sigma_{xr}) > x_{max} \tag{7.16}$$

$$||A|| = A_g \times \left[\left[\int_{-\infty}^{\infty} e^{-\left[\frac{(x-x_0)^2}{2\sigma_{xr}^2}\right]} dx \right] - \left[\int_{-\infty}^{x_{min}} e^{-\left[\frac{(x-x_0)^2}{2\sigma_{xr}^2}\right]} dx + \int_{x_{max}}^{\infty} e^{-\left[\frac{(x-x_0)^2}{2\sigma_{xr}^2}\right]} dx \right] \right]$$

$$||A|| \approx \left[\left[\int_{-\infty}^{\infty} A_g \times e^{-\left[\frac{(x-x_0)^2}{2\sigma_{xr}^2}\right]} dx \right] \times \left[\int_{x=x_{min}-4\sigma_{xr}}^{x_{min}} e^{-\left[\frac{(x-x_0)^2}{2\sigma_{xr}^2}\right]} dx + \int_{x_{max}}^{x=4\sigma_{xr}-x_{max}} e^{-\left[\frac{(x-x_0)^2}{2\sigma_{xr}^2}\right]} dx \right] \right]$$

$$||A|| \approx (A_g \times \sigma_{xr} \times \sqrt{2\pi}) \times \left[erf\left(\left(4 - \left(\left(\frac{4\sigma_{xr} - x_0 - x_{min}}{4\sigma_{xr}} \right) + \left(\frac{4\sigma_{xr} + x_0 - x_{max}}{4\sigma_{xr}} \right) \right) \right) / \sqrt{2} \right) \right]$$

If the above conditions do not hold, then ||A|| can continued to be calculated in the same manner, as detailed in (7.13). Evaluating the correct ||A|| expression to use, according to the bounded network region conditions, allows the approximated E_{Nodes} value to be calculated and substituted back into (7.12).

The inequality expression given in (7.12) can also be rearranged to show how the Gaussian plume area, ||A||, can be increased or decreased by σ_{xr} ,through E_{Nodes}, in order to reflect the ratio of being *k*-isolated and having *k-connectivity*, for a current underlying deployed node density, as shown in (7.17).

$$\left[1 - \sum_{i=0}^{E_{Nodes}} \frac{(\lambda A)^i}{i!} \times e^{-\lambda A} \right] \leq \frac{\left[1 - \sum_{i=0}^{k} \frac{(\lambda \pi R_T^2)^i}{i!} \times e^{-\lambda \pi R_T^2} \right]}{\left[1 - \sum_{n=0}^{k-1} \frac{(\lambda \pi R_T^2)^n}{n!} \times e^{-\lambda \pi R_T^2} \right]} \tag{7.17}$$

Following on from (7.17), the complete algorithm developed to solve this inequality, which determines the required σ_{xr} value, to ensure nodes have a desired *k-connectivity* within ||A||, is outlined further in **Appendix B, part 1**. For the network scenario shown in

figure 7.8, described earlier in section 7.2.1, figure 7.11 shows how the relationship for topology control through the required maximum bound σ_{xr} values, varies against network node density, for various *k-connectivity* requirements.

As shown in figure 7.11, increasing the node density has the effect of decreasing the required σ_{xr} value, for various *k-connectivity* requirements. Figure 7.11 also shows, however, that by increasing the *k-connectivity* requirement it has the effect of increasing σ_{xr}. This is expected since increasing the number of *k*-neighbours a node should have, requires a larger plume search area to achieve this, but this is also dependent on node density. For example, a 100 node network σ_{xr} increases by 13.5% for $k \geq 1$ to $k \geq 5$, while for a 750 node network σ_{xr} increases by 6.2% for $k \geq 1$ to $k \geq 5$.

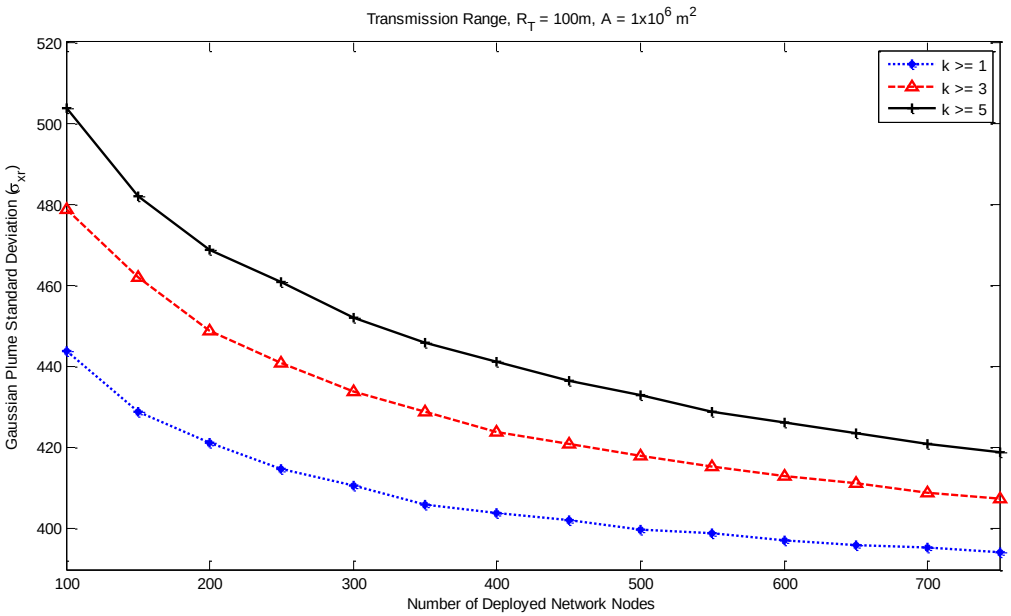

Figure 7.11: Relationship for topology control against network density, for various k-connectivity

The difference in percentage increases for these two node deployments is primarily due to the fact that under higher node densities, the requirement for node *k-connectivity* (topology control), primarily through the *P (A Node in A is not k-isolated)* $\rightarrow$ *1*. As this limit is approached and reached, a smaller plume coverage area can then be guaranteed for a certain *k-connectivity* requirement, while also ensuring the condition for the inequality in

(7.17) is still met. The *P (A Node in A is not k-isolated)* → *1* plays an important contribution towards topology control implementation since, this then implies the *P (Random Node in ||A|| ≥ k Neighbours)* can also be guaranteed to be the case, for all *N* deployed nodes. In addition if the *P (A Node in A is not k-isolated)* is shown to be approximately equal to *P (Random Node in A ≥ k Neighbours)* for all *N*, the proposed inequality expression in (7.17), catering for a required maximum σ_{xr} bound, to ensure a certain *k-connectivity*, is not needed.

The condition described above is valid and can be considered as a means of deciding when to refrain from calculating a maximum σ_{xr} bound since, this directly reflects on there being little chance, for *N* deployed random nodes, to ever being *k*-isolated, as shown in figure 7.12. If we set the condition for $P\ (A\ Node\ in\ A\ is\ not\ k\text{-}isolated)^N \approx P\ (Random\ Node\ in\ ||A|| \geq k\ Neighbours)^N \geq 0.99$, figure 7.12 illustrates this can, however, only be true for certain deployed node densities when using a defined set R_T.

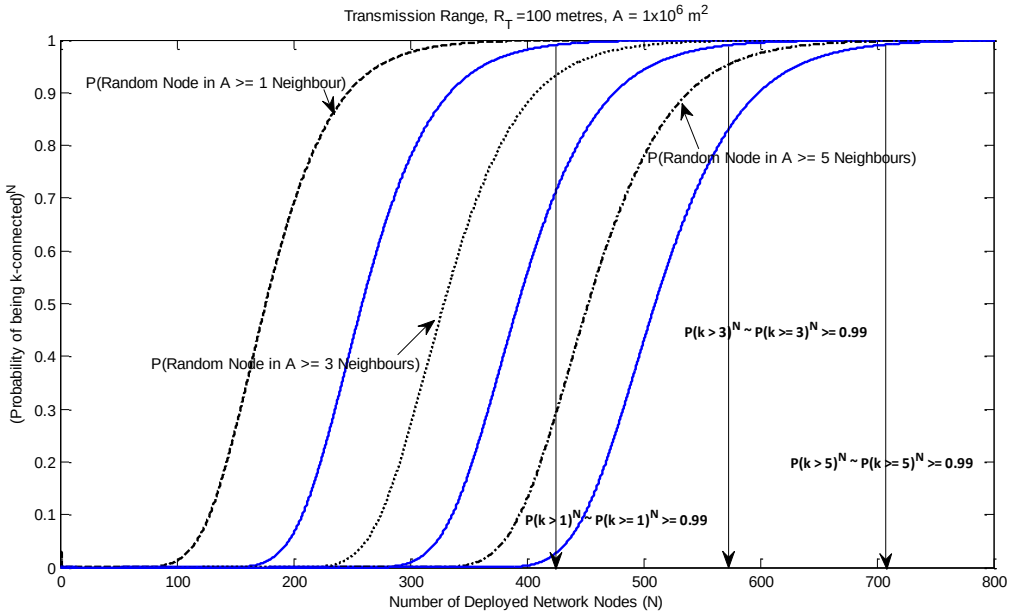

Figure 7.12: Relationship for P (A Node in A is not k-isolated)^N ≈ P (Random Node in A ≥ k Neighbours)^N, with Node Density, for different k-connectivity

From figure 7.12, this condition can then be further extended and expressed for topology control operation within a Gaussian plume area, ||A||. By guaranteeing the *P (A*

Node in ||A|| is not k-isolated)^{ENodes} ≈ *P (Random Node in A ≥ k Neighbours)*^{N} is true to within a 99% reliability for a certain *k-connectivity* requirement, enables a minimum σ_{xr} bound requirement to be placed, for maintaining a known reliable *k-connectivity in* ||A||, as shown in (7.18). The expression in (7.18), which assumes statistical independence, therefore reflects the minimum number of E_{Nodes} required, to ensure a node is not *k*-isolated, before losing the condition for a certain *k-connectivity* requirement, when all *N* deployed network nodes are considered.

Minimum Bound σ_{xr} *calculation for k - connectivity within,* $||A||$*:* (7.18)

$$[1 - P(\text{A Node in } ||A|| > k)]^{E_{Nodes}} \leq [1 - P(\text{Random Node in } ||A|| \geq k)]^{N}$$

$$\approx \left[\sum_{n=0}^{k} \frac{(\lambda\pi R_T^2)^n}{n!} \times e^{-\lambda\pi R_T^2} \right]^{E_{Nodes}} \leq \left[\sum_{i=0}^{k-1} \frac{(\lambda\pi R_T^2)^i}{i!} \times e^{-\lambda\pi R_T^2} \right]^{N}$$

$$\approx E_{Nodes} \times log_{10} \left[\sum_{n=0}^{k} \frac{(\lambda\pi R_T^2)^n}{n!} \times e^{-\lambda\pi R_T^2} \right] \leq N \times log_{10} \left[\sum_{i=0}^{k-1} \frac{(\lambda\pi R_T^2)^i}{i!} \times e^{-\lambda\pi R_T^2} \right]$$

$$\approx E_{Nodes} \geq N \times \frac{\left[\sum_{i=0}^{k-1} \frac{(\lambda\pi R_T^2)^i}{i!} \times e^{-\lambda\pi R_T^2} \right]}{\left[\sum_{n=0}^{k} \frac{(\lambda\pi R_T^2)^n}{n!} \times e^{-\lambda\pi R_T^2} \right]}$$

The inequality expressions in (7.17) and (7.18) therefore grant us an ability to calculate a maximum or minimum σ_{xr} bound required for *k-connectivity*, which is only dependent in terms of the current deployed network node density. The complete operation for evaluating the maximum or minimum σ_{xr} bound value, according to a maximum-minimum σ_{xr} bound threshold, is outlined further in **Appendix B, part 2**. As shown in **Appendix B, part 2**, which inequality expression to use ultimately depends on the condition being met for, *if P (A Node in ||A|| is not k-isolated)*^{N} ≈ *P (Random Node in ||A|| ≥ k Neighbours)*^{N} ≥ *0.99.* For the network scenario described earlier in 7.2.1, figure 7.13 shows the relationship for topology control, through the required σ_{xr} values, in

accordance to the algorithm detailed in **Appendix B, part 2**, against network node density, for various *k-connectivity* requirements.

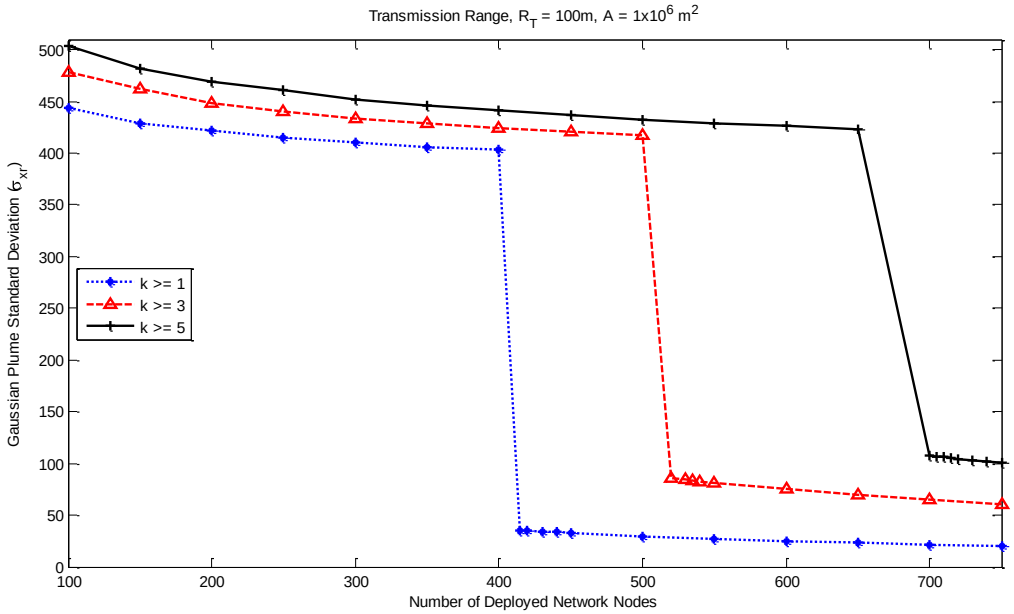

Figure 7.13: Max-Min relationship for topology control against network density, for various k-connectivity

As shown in figure 7.13, the maximum or minimum σ_{xr} bound values are appropriately calculated for various *k-connectivity*, as the limit condition for the *P (A Node in A is not k-isolated)* $\rightarrow$ *1* is approached, for different network densities. Figure 7.13, also clearly indicates at which particular network densities, for a certain *A*, the minimum bound inequality expression in (7.18) can be used, according to the condition *if P (A Node in* $||A||$ *is not k-isolated)*$^N \approx$ *P (Random Node in* $||A|| \geq$ *k Neighbours)*$^N \geq 0.99$, as detailed in **Appendix B, part 2**. In 7.2.2.4, a validation of the analysis made in this section is given, in terms of the saturated throughput performance, using the IEEE 802.11b protocol based on the distributed coordination function (DCF), in basic access mode.

7.2.2.4 Relationship to Throughput Performance using IEEE 802.11b

Implementing a topology control mechanism within a deployed multi-hop network requires a way to validate the topology control model. For the purposes of our validation an analytical model is developed, in order to measure the multi-hop "*saturation throughput*"

of the network, as the desired *k-connectivity* is increased for various network densities. The author in [114] was the first to analyse and define the "*saturation throughput*", *S*, as the throughput limit reached by the system, as the offered load increases, thus representing the maximum load that the system can carry in stable conditions. The correct *S* in our case depends on using the correct expressions given in (7.13), (7.14), (7.15) or (7.16) and as detailed in **Appendix B, part 2**. If this were not the case, then incorrect *S* values and loss of accuracy in *S* will be apparent, when a direct comparison of the analytical and simulation results is made.

From [114] a single-hop throughput model is developed for the IEEE 802.11b DCF MAC protocol, assuming ideal channel conditions (i.e. no hidden terminals or capture [115]) and that a node within a fixed deployed network, will always have a packet available for transmission. The single-hop model from [114] is shown in (7.19), with P_{TR} being, the probability for a least one node transmission occurring and P_S being, the probability of a successful transmission given that one of the channel contending nodes transmits. Table 7.1, details the various parameters used in (7.19) and in general for the throughput, topology control validation exercise.

$$S(N_{1-Hop}) = \frac{E[P]P_S P_{TR}}{(P_S P_{TR} T_S) + (1-P_{TR})\,\sigma + P_{TR}(1-P_S)T_C} \tag{7.19}$$

$$With\ , P_{TR} = 1-(1-\tau)^{N_{Cont}} \quad and \quad P_S = \frac{N_{Cont}\,\tau\,(1-\tau)^{N_{Cont}-1}}{P_{TR}}$$

Within a multi-hop network setting, a node only contends with a fraction of the total nodes in the network, namely N_{Cont}, which can then be substituted into (7.19). As shown in table 7.1, N_{Cont} is directly related to the number of E_{Nodes} found within the approximated Gaussian plume area, ||A||, according to the conditions, as detailed in **Appendix B, part 2**.

The value for a current network, N_{Cont}, can be approximated by knowing the maximum spatial reuse factor (SRF_{MAX}), which is an upper-bound indication, of the average number of simultaneous transmissions that could take place within the deployed network of area, ||A|| m^2 [116]. Assuming nodes, which are $2R_T$ from each other, can engage in simultaneous transmissions, the SRF_{MAX} is then estimated by calculating the number of disjoint non-interfering disks, of radius εR_T that can be included within the corresponding network area ||A||, where ε corresponds to the carrier sensing to communication range ratio.

Throughput Parameters for (7.19)	**Value**
E[P] – Average Packet Load Size	E[P] = Payload / Data-Rate
N_{Cont} – Number of Channel Contending Nodes	$N_{Cont} \approx (E_{Nodes} / SRF_{MAX}) - 1$
τ – Slot Transmission Probability	$\tau \approx (2 / W_{min} + 1) * (L / SRF_{MAX})$ [37]
σ – Slot Time	20μs
T_S – Time Channel is Sensed Busy	$T_S = DIFS + SIFS + E[P] + Y_T + 2\delta$
T_C - Time Channel is Sensed Busy During Collision	$T_C = DIFS + E[P] + Y_C + \delta$
IEEE 802.11b Parameters	**Value**
Payload	125 Bytes
Data-Rate	2 Mbits /sec
W_{min} – Minimum Contention Window Size	W = 32
DIFS – DCF Inter-frame Space	128μs
SIFS – Short Inter-frame Space	28μs
Y_T – Basic Access Mode Delay	$Y_T = (PHY_{hdr} + MAC_{hdr} + ACK) / Data\text{-}Rate$
Y_C – Packet Header Duration	$Y_C = (PHY_{hdr} + MAC_{hdr}) / Data\text{-}Rate$
PHY_{hdr} – Physical Header Size	192 bits
MAC_{hdr} – MAC Header Size	272 bits
ACK – Acknowledgement Packet Size	PHY_{hdr} + 112 Bits
δ – Propagation Delay	1μs

Table 7.1: Parameters used for Throughput Calculation in (7.19)

By setting a carrier sensing to communication range ratio of $\varepsilon = 1$ (i.e. carrier sensing radius = R_T), the SRF_{MAX} can be approximated, for the maximum σ_{xr} bound given in (7.12), as shown in (7.20).

$$SRF_{Max} = \left[\frac{||A||}{\pi(R_T)^2} \right] \tag{7.20}$$

For the minimum σ_{xr} bound outlined in (7.18), the average number of simultaneous transmissions that can occur increases, due to a lower Gaussian plume area, ||A||, thus increasing the SRF_{MAX} which can be approximated, as shown in (7.21).

$$SRF_{Max} = \left[\frac{A - ||A||}{\pi(R_T)^2} \right] \tag{7.21}$$

To estimate the throughput of a multi-hop network also requires us finding the average path length, *L*, in terms of the approximate number of hops that a packet has to traverse, in order to reach its intended destination, as shown in (7.22).

$$L = \frac{\sqrt{(x_0 - x_{sink})^2 + (y_0 - y_{sink})^2}}{E(\Delta i)} \tag{7.22}$$

$$With,\ E(\Delta i) = \left[R_T \int_{\Delta i=0}^{R_T} f(\Delta i)\, d(\Delta i) \right] \times P(Random\ Node\ in\ ||A|| \geq k\ Neighbours)$$

$$= [R_T (1 - e^{-\lambda \pi R_T^2})] \times [1 - \sum_{n=0}^{k-1} \frac{(\lambda \pi R_T^2)^n}{n!} \times e^{-\lambda \pi R_T^2}]$$

$E(\Delta i)$, in (7.22) represents the average *k-connectivity* link distance between two random *PPP* nodes, with $f(\Delta i)$ as detailed in (7.8), representing the *PDF* between two random *PPP* nodes. The one-hop saturated throughput model, as shown in (7.19), can then be used to approximate the saturated throughput performance for a multi-hop network scenario, *S*, within a network defined region ||A||, as shown in (7.23) [116].

$$S = S(N_{1-Hop}) \times \frac{SRF_{Max}}{L} \quad (7.23)$$

A simulation run was conducted to provide confirmation of the validity of our virtual Gaussian topology control model, for the network scenario shown in figure 7.8, described earlier in section 7.2.1. The simulation is run for a length of time for the network to become saturated and in order for results to converge. Preliminary simulation results are ignored when the network is in initial stages since these do not represent values under saturated conditions.

Validity of our model can be confirmed by measuring *S*, achieved at the centre of the ROI and comparing this with analytical results from our model, given in (7.23). For confirmation of (7.23) to be accurate and to match closely with simulation results, it requires use of the correct E_{Nodes} value. Figures 7.14 to 7.16, show results of the validation exercise against network density, under various *k-connectivity* conditions, with R_T set to 100m, within a network region of $A = 1x10^6$ m^2.

From figures 7.14 to 7.16, the analytical results show a good match with our simulation results to within an average loss in accuracy of 3.5% across the different network densities, for each *k-connectivity* condition. The figures, however, also do confirm that (7.23) is an appropriate relationship, which can be applied to approximate the multi-hop saturated network throughput, *S*, performance, under different network densities, for various *SWOB* topology control *k-connectivity* conditions.

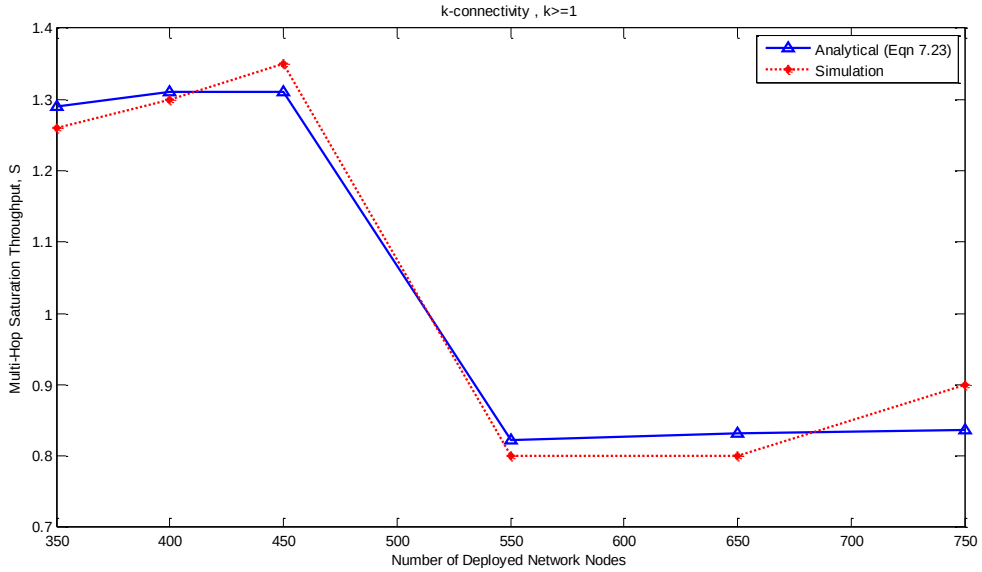

Figure 7.14: Validation of SWOB topology control model, for k-connectivity, k >=1

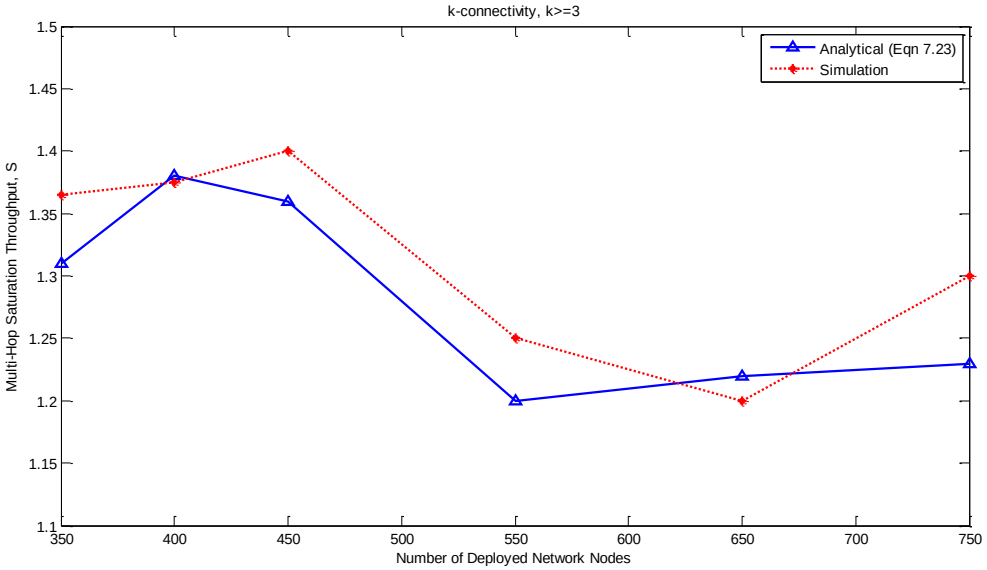

Figure 7.15: Validation of SWOB topology control model, for k-connectivity, k >=3

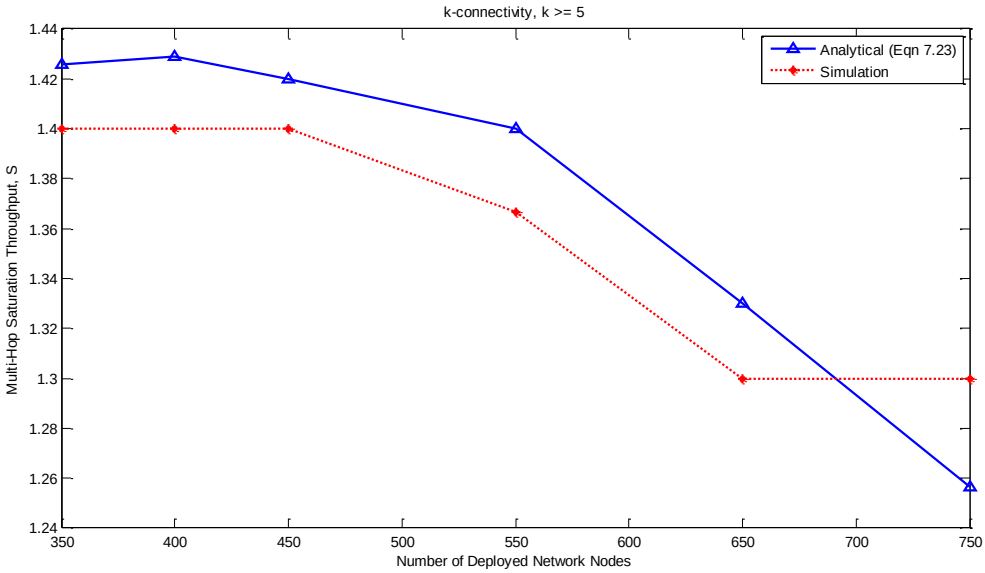

Figure 7.16: Validation of SWOB topology control model, for k-connectivity, k >=5

In 7.2.3, an overall description of the *SWOB* geographic routing methodology is given, which brings together the virtual Gaussian plume model described in section 7.2.1 and the analysis for *k-connectivity* topology control purposes made here in 7.2.2.

7.2.3 Overall Swarm Intelligent Odour Based Routing Algorithm

SWOB geographic routing relies on a two-fold strategy. Firstly a source based technique, similarly to *TBF* where the trajectory towards an intended destination, can be pre-defined initially at the source (gateway node), with regards to influencing and guiding IQ route direction. The intended trajectory model used in *SWOB* has already been described in 7.2.1 and how such a trajectory model can be influenced to reflect on a desired *k-connectivity*, is highlighted in 7.2.2. By definition, the operation shown in **Appendix B, part 2**, would then be performed at a respective gateway node in order to establish the required σ_{xr} topology control value, prior to any forwarding of IQ packets.

Once this is known, the evaluated σ_{xr} value can then be substituted back into (7.4) and rearranged to determine the corresponding σ_y value, as shown in (7.24).

$$\sigma_y = \sqrt{\frac{(R_T)^2}{2\ln\left(\beta/q\right)}} \text{ for } \beta \geq 0.99 \quad \text{and} \quad q = e^{-(R_T)^2/2\sigma_{xr}^2} \tag{7.24}$$

Figure 7.17 illustrates the complete source defined packet, which is broadcast (*publish*) to all neighbouring sensors from the gateway node, in order to begin the *SWOB* routing mechanism. As shown in figure 7.17, corresponding network topology control values $\sigma_{xr,}$ σ_y and ROI destination information (x_0, y_0) are made available to each node, within the received IQ packet and subsequently by neighbouring nodes, as the IQ packet is forwarded.

Header	ROI Centre (x_0, y_0)	Virtual Gaussian Plume Parameters ($\sigma_{xr,}$ σ_y)	IQ Agent (Mission Objective Type)

Figure 7.17: Source defined data centric address packet used for SWOB routing

Secondly, *SWOB* routing employs a *greedy mode* approach, in order to make decisions as to which neighbour to forward an IQ packet to. Such a decision is based only on the location of the ROI destination and its local neighbourhood virtual odour concentration levels *C(x, y)*, as calculated in (7.2). Upon receiving an IQ packet (*subscribe*), as shown in figure 7.17, a node behaves in *greedy mode*, where the node with the highest virtual odour concentration level within a forwarding nodes neighbourhood is selected for IQ forwarding, as illustrated previously in figures 7.6 and 7.8.As shown in figure 7.17, the *geographic scoping content* of the packet would entail the ROI centre coordinates, coupled with the topology control values $\sigma_{xr,}$ σ_y.

Using such an alternative can assist in further reductions in both the overall IQ packet delivery time to the ROI, communication overhead and energy expenditure, since nodes found to be outside the virtual Gaussian plume (i.e. outside the scope of the geographic content message), will not take part in the *SWOB* routing process. The overall *SWOB* geographic routing algorithm, which can be applied by any distributed *UGS* node to determine next hop forwarding within the restricted $x_0 \pm \sigma_{xr}$ virtual Gaussian plume, is detailed further in **Appendix B, part 3**.

Relative *(x, y)* coordinates can be provided, if *UGS* nodes are equipped with small low power GPS receivers, in order to discover their own absolute position within the deployed network field. Such a mechanism is beneficial for surveillance operations since, this will allow for network scalability and *tactical* reach, which are important attributes needed for *C2ISR* providing type networks, such as *UGS* sensor networks [81] [84]. Relative *(x, y)* coordinates of neighbouring nodes, can therefore be exchanged initially within the, R_T neighbourhood and stored in a local table, in order to fulfil the *SWOB* geographic routing algorithm detailed in **Appendix B, part 3**.

7.3 Swarm Intelligence Odour Based Routing Performance

SWOB geographic routing is primarily aimed at maintaining *UGS* network operational longevity and supporting delay sensitive surveillance missions. IQ packets sent to inquire and obtain information about a particular surveillance observation, should be transmitted reliably with low latency and equally to have conservation of communication energy consumption in mind. Our aim is therefore to achieve performance gains that can exhibit both low latency and achieve high throughput, but with low communication energy consumption. Conducting simulations to measure *SWOB* geographic routing performance against these criteria, is therefore imperative. In addition, we are interested in measuring

performance against increasing network node densities conditions, in order to gauge the benefits of integrating topology control within geographic routing.

For the purpose of comparison, the following alternative geographic routing strategies are considered, since these alternatives can also be easily applied to a geographic surveillance scenario, as illustrated in figure 7.1:

- Most forward progress (MFP) towards the destination, within R_T, as already described in 7.1.1, when considering the first strategy as shown, in figure 7.2.
- Restricted directional flooding (RDF) using the adaptive distance scheme, as already described in 7.1.2 and shown in figure 7.3 (b).
- Trajectory Based Forwarding (TBF), which also employs topology control within geographic routing, as already described in 7.1.3 and shown in figure 7.4.
- Geographic random forwarding (GeRAF) [121-122]. GeRAF utilises geographical routing on a best-effort basis, where the actual forwarding node is not known *a-priori* by the sender, but rather is decided after the transmission has taken place. Forwarding in this sense then relies on the broadcast nature of the wireless environment. This allows multiple nodes to receive a packet and for each node being able to decide and assess their own priority, as to acting as a forwarding node, in terms of how close they are to the destination. In essence, GeRAF utilises a broadcast forwarding strategy, with the MFP strategy used as the mechanism for deciding forwarding, node priority selection. Nodes, which therefore receive packets, firstly calculate their respective Euclidean distance to the destination (MFP) and compare this directly with their neighbours, as a way of identifying whether they are the node closest towards the destination (priority selection). If not, nodes drop their packets since an alternative neighbour is identified as being the closest node in the R_T neighbourhood. Prioritising

selection in this manner can subsequently assist in providing further communication energy and bandwidth consumption savings.

Simulations are performed using the OMNeT++ network modeller tool [63] for a number of different network topologies (>50), each with $\boldsymbol{N}$ randomly deployed nodes according to the *PPP*, within a network region area, $A = 1\text{x}10^6$ m^2, with node $R_T = 100$m and using the IEEE 802.11b MAC protocol, under lossless channel conditions. Simulations are run for a duration, which entails the gateway node sending a total of 100 packets, of packet length, as shown in table 7.1. The same network gateway and ROI centre coordinates are used, as described in 7.2.1. Headings 7.3.1 to 7.3.4 describe the various metrics used, to measure and gauge performance of the *SWOB* geographic routing protocol against the comparisons listed above.

7.3.1 Latency Performance

Latency is a *QoS* metric used within packet-switched networks and is typically measured as the *one-way* delay time, from the source sending an initial packet, to the destination receiving it [41]. In our evaluation, latency is therefore measured as the time between the generation of an initial IQ packet at the gateway node and the delivery of that IQ packet to the destination (centre of the ROI). Latency measured in this sense, becomes a direct reflection on the delay sensitivity of the routing strategy employed since transporting the initial IQ packet towards the destination with minimum time, is a key requirement, when considering the nature of surveillance missions. Figure 7.18, shows *SWOB* latency performance, with $\boldsymbol{N}$, against the comparisons listed above.

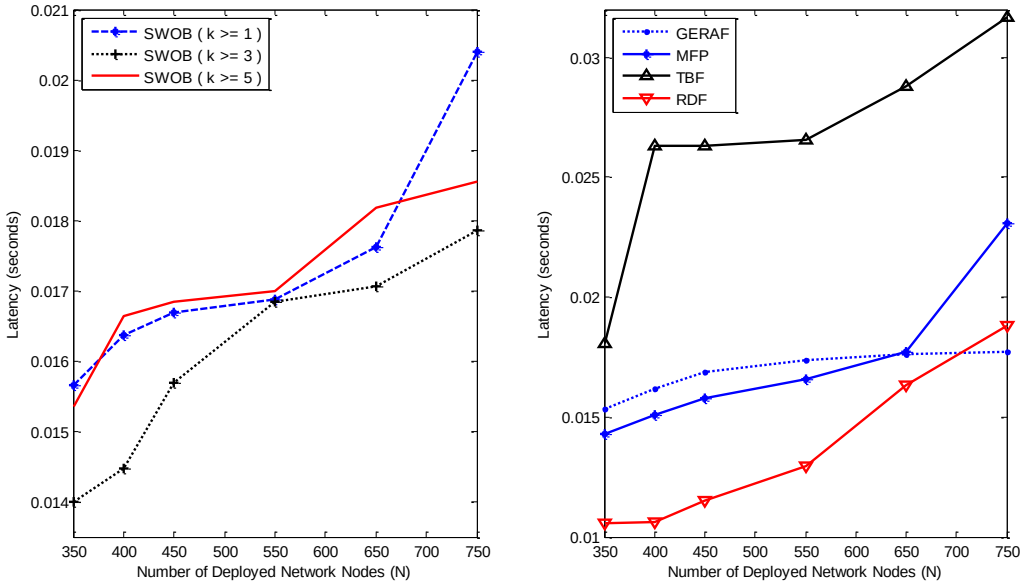

Figure 7.18: SWOB one-way message latency performance and comparison

From figure 7.18, *SWOB* one-way (i.e. gateway node to ROI) message latency is shown and as indicated this increases with network node density. The same effect for increased message latency with network node density also applies to the measured alternatives. Latency increases with network node density primarily because more nodes are available for packet forwarding and as a result, are contending for channel access, which increases packet forwarding delay. *SWOB* through applying the requirement for greater topology control in terms of increasing the required *k-connectivity*, can help to improve on IQ message latency performance, over the measured alternatives. Results indicate for the simulated scenario that *SWOB* ($k \geq 3$) achieves the most improved performance (lower latency delay). The same case is also found with *SWOB* ($k \geq 5$), which does have a slightly increased latency performance over *SWOB* ($k \geq 3$) by 10%, but still provides a more consistent performance, when compared with *SWOB* ($k \geq 1$), under higher network node densities.

This is primarily because setting a higher *k-connectivity* requirement increases the Gaussian plume standard deviation (σ_{xr}), as shown in figure 7.13, which provides a broader plume breadth and therefore to a greater extent more options for route selection towards

the ROI become available. In addition, the plume breadth (σ_{xr}) reduces with network density, as shown in figure 7.13, in accordance with algorithm detailed in **Appendix B, part 2**. As a result of this a greater number of deployed nodes become less involved in packet forwarding under higher network densities, since they are found outside the Gaussian plume shape. This helps to provide a more consistent latency performance, which does not increase dramatically, as the case with TBF, RDF and MFP under higher node density conditions. In TBF the topology control is fixed and does not adapt to network density conditions or incorporate a *k-connectivity* requirement, which results in latency increasing with network density, as shown in figure 7.18.

Comparing *SWOB (k ≥ 3)* to the other measured alternatives shows it can indeed provide improved performance over MFP by some 25% and has comparable performance with GeRAF, under the given network scenario. RDF provides the best performance under lower network density conditions, which indicates a broadcast strategy is beneficial in routing an initial IQ quicker in these circumstances, than compared to unicast forwarding schemes (i.e. *SWOB*, TBF and GeRAF), which tend to utilise more forwarding hops and incorporate less route diversity through *greedy based forwarding* (i.e. unicast and not broadcast) . Under higher network densities using RDF for improved latency performance does not hold. Using *SWOB*, however, provides a more consistent and controlled latency performance across all deployed network node densities because of its ability to provide topology control, which adapts to the current deployed network node density conditions through the Gaussian plume standard deviation (σ_{xr}), according to a desired *k-connectivity* requirement.

7.3.2 Throughput Performance

To measure overall network bandwidth utilisation efficiency during a simulation run it is best to capture this, in terms of the number of packets (*bits*) that can be sent per second, namely throughput. Measured in this way, throughput become a direct reflection on how efficient the *SWOB* geographic routing methodology is as detailed in **Appendix B, part 3,** and the comparison alternatives are towards utilising and re-using communication bandwidth. Figure 7.19, shows *SWOB* throughput performance with ***N***, against the comparisons listed above, in the opening section.

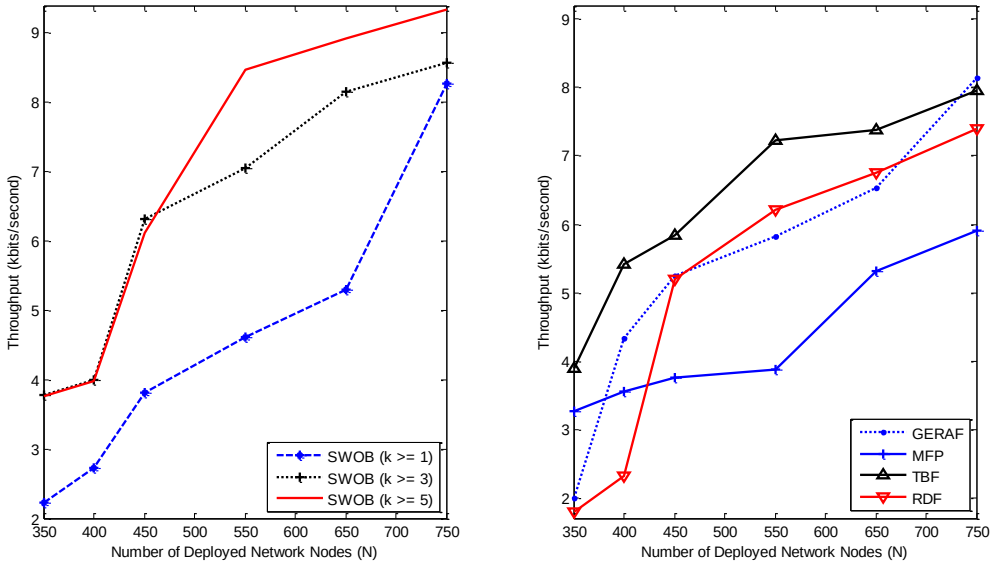

Figure 7.19: SWOB throughput performance and comparison

From figure 7.19, *SWOB* throughput performance as shown increases with network density. This is primarily due to the greater availability of deployed nodes to participate in packet forwarding and subsequently, contribute to the overall network throughput. By increasing the requirement for topology control, in terms of the required *k-connectivity*, *SWOB* can again help to improve on throughput performance over TBF, which incorporates topology control in terms of the **sin** function, but does not adapt the control function according to the deployed network density conditions. Results indicate incorporating a *k-connectivity* restriction for topology control purposes, can achieve

improved throughput performance for the given network scenario. This is primarily because setting a higher *SWOB k-connectivity* requirement varies the Gaussian plume standard deviation (σ_{xr}), according to the *min-max k-connectivity* relationship, as detailed in **Appendix B, part 2** and as shown in figure 7.13.

As a result of this relationship *SWOB*, *C(x, y)*, concentration values given in (7.2), which dictate route selection (i.e. packet forwarding node selection) become more focused with network density, as a result of a lower σ_{xr} value. This in turn provides better geographic directivity for IQ routing to the ROI under higher network densities. As a result, a lower σ_{xr} value under higher network density conditions can achieve higher bandwidth utilisation, since a larger proportion of deployed nodes become less involved in packet forwarding (i.e. more nodes lie outside the virtual Gaussian plume shape and do not participate in packet forwarding) for improved throughput performance. Since throughput forms a direct reflection on channel bandwidth utilisation efficiency, *SWOB* can outperform the measured alternatives under higher network densities ($\boldsymbol{N} \geq 600$).

Advancing a packet as to minimise the number of hops a packet has to traverse, as shown in MFP, does not promote bandwidth efficiency under a majority of network node densities, hence it achieves lower throughput performance by some 60% when compared with *SWOB*. Again broadcast strategies through GeRAF and RDF do not promote bandwidth utilisation efficiency and as a result, achieve lower throughput. *SWOB* through the use of its topology control mechanism can, as a result, provide greater flexibility towards route selection and facilitate a better spatial bandwidth re-usability factor, under higher network density conditions for improved throughput performance.

7.3.3 Energy Efficiency Performance

Energy is a precious resource in *UGS* networks and so conserving on energy expenditure, wherever possible becomes a priority. Energy efficiency is a way of measuring how well a routing system can conserve on energy consumption, while still completing its packet forwarding tasks. From a geographic routing perspective, energy efficiency would entail putting the delivered network throughput, in *bits* and the communication energy expenditure required to do so into perspective. Defined in this way, energy efficiency for *SWOB* geographic routing performance is determined as the total network communication energy consumed, to transport one packet of received payload information from the gateway node to the destination (centre of ROI), as shown in (7.24). The same communication energy consumption model is used, as already described in section 1, under heading 4.4.3.

$$Energy\ Efficiency = \frac{Total\ Network\ Communication\ Energy\ Expenditure\ (Joules)}{Total\ Network\ Packets\ Received\ (bits)} \qquad (7.24)$$

As shown in (7.24), routing schemes which promote lower energy expenditure in order to transport more packets of a certain length in *bits* are ideal and therefore, more energy efficient. Figure 7.20, shows *SWOB* energy efficiency performance with $\boldsymbol{N}$, against the comparisons described earlier in the opening of 7.3.

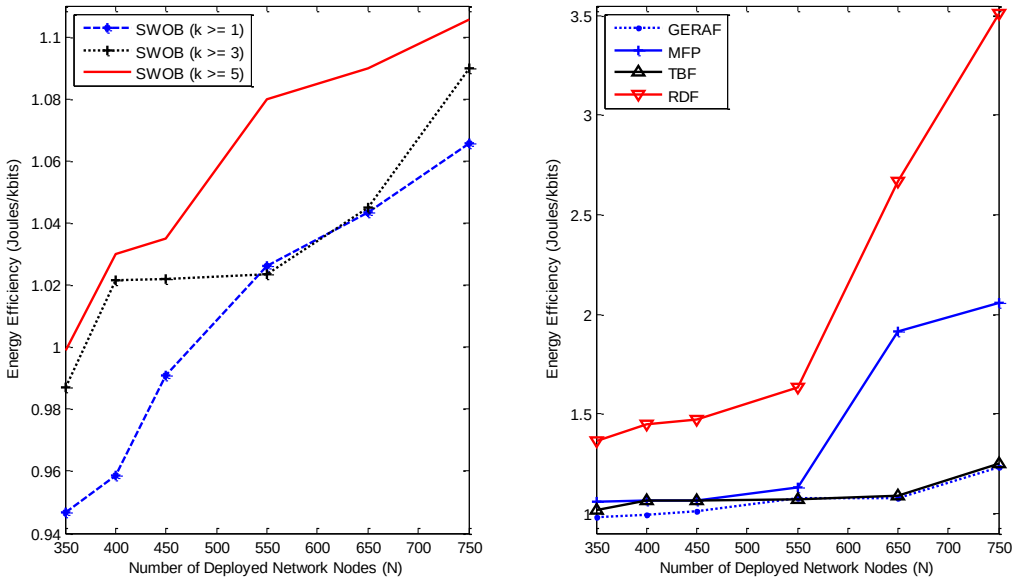

Figure 7.20: SWOB energy efficiency performance and comparison

From figure 7.20, *SWOB* energy efficiency is improved by setting a lower *k-connectivity* requirement (i.e. $k \geq 1$), across the range of network densities. This result is expected since imposing less topology control (i.e. a lower σ_{xr}) through the required number of *k* direct neighbours, reduces the number of forwarding nodes and as a result, reduces the energy expenditure requirement. Increasing topology control (i.e. *SWOB* $k \geq 5$) increases the number of forwarding nodes and as a result we achieve greater energy expenditure, resulting in a slightly lower energy efficiency performance.

Figure 7.20, also indicates the advantage for geographic routing schemes that incorporate directionality through trajectory guidance (control) towards a destination, in terms of a pre-defined route (source defined route) to improve on energy efficiency performance. This can indeed provide better energy efficiency performance under increasing network node density conditions, as indicated through *SWOB* and TBF over MFP. *SWOB* provides directionality and guidance (control) according to the source (i.e.

gateway node) defined virtual Gaussian plume (i.e. σ_{xr} and σ_y), while TBF does the same through the sin function given in (7.1).

In GeRAF directionality is assisted differently by increasing route diversity for *greedy based forwarding* on a per hop basis, through broadcasting towards the destination. Nodes, which therefore receive packets, firstly calculate their respective Euclidean distance to the destination (ROI) and compare this directly with their neighbours, as a way of identifying whether they are the node closest towards the destination (priority selection). Nodes that do not meet this priority selection requirement subsequently drop packets. This can assist in achieving a more consistent energy efficiency performance with increasing network node density. MFP does not provide any means for a source defined route capability within its routing operation and as a result, energy efficiency reduces with network density by some 45% when compared with *SWOB*. This is also because nodes over larger hop distances are primarily preferred, which can increase energy consumption.

Energy efficiency is also poor for RDF, which provides limited guidance through restricting the number of forwarding nodes according to a static zone, as shown in figure 7.3 (a). In wide area surveillance scenarios the static forwarding zone can become large and so the number of actively employed nodes used for packet forwarding, increases with network density. Without using further guidance and topology control towards an intended destination (i.e. ROI) within the static forwarding zone, every node found within the zone, can become a potential packet forwarding node and as a result, expend energy. This explains why energy efficiency reduces quite considerably for RDF, as network node density conditions increase.

7.3.4 Network Load Balancing Performance

Maximising the lifetime of the deployed *UGS* network is also an important attribute, since *UGS* devices are inherently limited by their battery energy reserves. Consumption of

communication energy and the balancing of the load in terms of throughput, which is placed on the network both become crucial and can assist in extending, the overall operational longevity of the deployed *UGS* network field. Network load balancing from a geographic routing perspective therefore encompasses being able to transport packets efficiently, across the number of forwarding nodes required to do so. Defined in this sense, network load balancing is a direct reflection on the energy efficiency from (7.24), consumed across the total number of forwarding nodes used to deliver the packets, $N_{Forward}$, which can only be determined by the routing strategy employed, as shown in (7.25).

$$Network\ \ Load\ \ Balancing = \frac{Energy\ \ Efficiency\,(\,Joules/bits\,)}{N_{Forward}} \tag{7.25}$$

From (7.25), a geographic routing scheme which can provide less communication energy expenditure for transporting packets, while also maintaining a consistent $N_{Forward}$ set as the network density increases, can achieve better network load balancing performance. Geographic routing schemes, which can therefore reduce (7.25) or provide a more consistent level of network load balancing performance as network node density conditions increase, can appropriately assist towards achieving greater operational longevity. Figure 7.21, shows *SWOB* network load balancing performance with $\boldsymbol{N}$, against the comparisons listed above in the opening section.

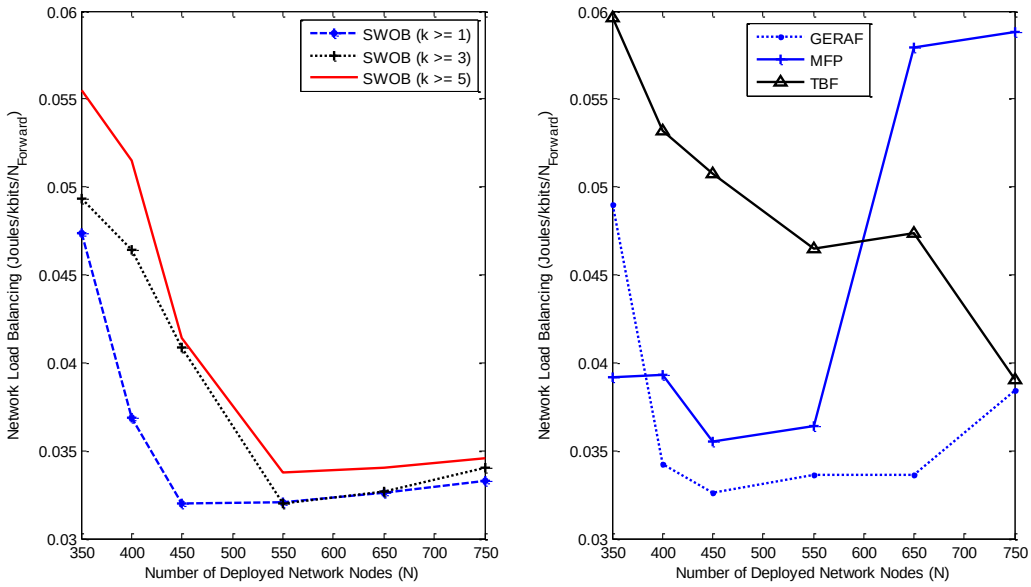

Figure 7.21: SWOB network load balancing performance and comparison

The energy efficiency credentials of *SWOB* is again reaffirmed in figure 7.21 by achieving a lower and more consistent load balancing performance, primarily through maintaining a consistent forwarding set ($N_{Forward}$) across all network node densities. This is possible as a result of the topology control scheme used, as detailed in 7.2.2 and shown in **Appendix B, part 2**. Results from figure 7.21, indicate having a *k-connectivity* restriction of $k \geq 1$, encourages a lower network load balancing performance across the majority of network densities, when compared with *k-connectivity* restriction of $k \geq 3$ or $k \geq 5$. This result is expected, since forcing a requirement for less k direct neighbours to communicate with, inherently implies a lower selection of forwarding nodes, which leads to having an overall lower $N_{Forward}$ figure and energy efficiency value.

Figure 7.21, also shows those geographic routing schemes that employ guidance and topology control towards an intended destination, as the case with *SWOB*, TBF and GeRAF can reduce network load balancing further, as network node density increases. Figure 7.21, also indicates that minimising on the hop count through MFP will typically not mean better network load balancing or energy efficiency performance and as shown,

this increases with network node density. The MFP strategy is designed to use fewer hops, but with similar implications described earlier will require increased communication energy expenditure, in order to cover the larger hop distances and as a result, an increased forwarding set, $N_{Forward}$ and lower energy efficiency value.

CHAPTER 8

Section 2: Summary and Conclusions

Distributed surveillance operations can be assisted if the relevant *UGS's* are utilised, in order to verify both threat observations and fulfil current mission objectives. As shown in figure 7.1, this can be assisted through using *UAV's*, which would typically survey a surveillance region and then communicate potential threat coordinates to a gateway node. Subsequently, a gateway node would generate the relevant information queries (IQs) to verify this potential threat within an identified ROI, using the coordinates provided by the *UAV* collaborator.

The basis of section 2 was to investigate strategies for allowing IQs to be routed to the identified ROI, as shown in figure 7.1, from a gateway node located in the far region of the surveillance field efficiently, within both communication energy and bandwidth constraints. Routing protocols, which can facilitate this functionality, are generally classified as geographic routing protocols, with their primary goal to keep communication overhead small by exploiting the underlying geometry of node positions.

In chapter 7, we began by giving an explanation concerning both the nature of geographic routing and the common packet forwarding strategies engaged to support geographic routing. Geographic routing is an efficient technique, which requires minimal direct use of routing tables, except for the location of the destination and local neighbourhood *UGS* node positions, making it ideal for distributed surveillance operations.

In 7.1.4, a presentation of an alternative strategy with regards to forwarding of IQ packets towards an identified ROI is given. In general, this section outlines the principles, which social insect's use to route towards particular sources of interest. Strategies derived from the social insect natural world, can be broadly classified under the category called

"*Swarm Intelligence*" and in 7.1.5, we explained how such a strategy can be applied and transferred to our intended surveillance scenario, as illustrated in figure 7.1.

The work presented in 7.2, forms the main contribution of this section, where we apply some of the biological principles, described in 7.1.5, towards developing our own biological inspired geographic routing strategy. Our geographic routing protocol named *SWOB* utilises both source based techniques, which allows route discovery mechanisms to be avoided and *greedy based forwarding*, in order to allow packets to make much advancement towards the destination (low latency). Subsequently, a source defined trajectory model based on the natural odour dispersion effects found in nature was developed, providing the necessary guidance for IQ forwarding towards the ROI destination. Our developed source-defined trajectory model contains the following features:

- A Gaussian function model is used to sufficiently portray the real-world odour diffusion plume characteristics found in nature, as illustrated in figures 7.6 and 7.8. The characteristics of the Gaussian function allow us a mechanism to artificially construct odour concentration levels according to *UGS* node geographic position, relative to the ROI, in order to facilitate IQ forwarding. As a result of this, the following potential advantages can then be used:
    - The virtual Gaussian plume model and resulting contour map reveals that not all deployed *UGS* nodes are typically found geographically inside the Gaussian plume shape and resulting contour map, as shown in figure 7.8.
    - Subsequently, using a virtual Gaussian plume model allows forwarding and eventual IQ routing to be controlled within the bounds of the plume shape.

Based on the notion of using a virtual Gaussian plume model to control and restrict IQ forwarding within the deployed *UGS* network, in 7.2.2, we defined a topology control

relationship to reflect on the degree of control (restriction) required. A reliable way of achieving and establishing control, is to vary the required Gaussian plume breadth shape according to, a probabilistic relationship that ensures any deployed node found within the Gaussian plume, can still have a certain number of *k*-direct neighbours to communicate with. This requires a methodology involving the following attributes:

- Firstly, a probabilistic model to describe the random location of *UGS* nodes found within the network region, as described in 7.2.2.1 and 7.2.2.2.
- Secondly, relating node location to a desired network *k-connectivity*, in order to ensure direct restricted communication is possible, while also avoiding the condition for *UGS* node isolation, as described in 7.2.2.3.

A validation of our virtual Gaussian plume topology mechanism is then given primarily through, measuring the approximate saturated multi-hop throughput performance achieved, using the IEEE 802.11b MAC protocol and a confirmation of this approximation, is shown in figures 7.14 to 7.16. In 7.2.3, a complete description of *SWOB* routing algorithm is given, including an explanation, as to the *greedy based forwarding* method employed within *SWOB* routing.

In 7.3, we provide *SWOB* routing performance and gauge this against deployed network node density. Alternative geographic forwarding strategies are also used for *SWOB* comparison purposes. *SWOB* geographic routing is primarily aimed at supporting delay sensitive surveillance missions. IQ packets sent to inquire and obtain information about a particular surveillance observation, should be transmitted reliably with low latency and equally to have conservation of communication energy consumption, in mind. Our aim is therefore to achieve performance gains that can exhibit low latency, high throughput and low communication energy consumption making it imperative to appraise *SWOB* geographic routing performance, against these criteria. From the simulations conducted,

using the deployed network conditions described in 7.3, the following points can be made:

- *SWOB* indicates that both network latency and throughput performance can be improved by incorporating topology control within geographic routing functionality, especially in conditions with increasing network node density. *SWOB* provides a more consistent and controlled latency and throughput performance across all deployed network node densities because of its ability to provide topology control, which adapts to the current deployed network node density conditions through the Gaussian plume standard deviation (σ_{xr}), according to a desired *k-connectivity* requirement. In TBF the topology control is fixed and does not adapt to network density conditions or incorporate a *k-connectivity* requirement, which results in latency increasing and a lower throughput performance being achieved under higher network node density conditions, as shown in figures 7.18 and 7.19.
- Figure 7.21, shows those geographic routing schemes that employ directivity guidance towards an intended destination (i.e. ROI), as shown with *SWOB*, TBF and GeRAF can reduce network load balancing and increase energy efficiency performance further, as network node density increases. For *SWOB* guidance is achieved through the Gaussian plume function (i.e. σ_{xr} and σ_y). In TBF guidance is achieved in terms of the **sin** function given in (7.1), while GeRAF provides guidance by allowing nodes to measure their Euclidean distance towards an intended destination for priority selection, within a broadcast transmission range of R_T.

In summary, the results in figures 7.18 to 7.21 lead us to conclude that utilising a Gaussian plume model to guide *SWOB* IQ forwarding, can therefore assist in providing the following advantages:

- A distributed and scalable surveillance mode of operation. Deployed *UGS* nodes need only to know their geographic position and the ROI centre coordinates and apply the *SWOB* routing methodology, as detailed in **Appendix B, part 3**.
- Supporting the notion of maintaining bandwidth and communication energy consumption savings, through an integrated geographic routing and topology control approach.

It is also worth noting that the performance results for *SWOB* have also been conducted under loss free channel conditions, which in reality is not the case from a wireless *UGS* network point of view. In section 4, we do indeed consider *SWOB* performance under different error prone channel environments. Before we can consider this, in section 3, we aim first to analyse the error prone wireless channel environment, with view towards assisting packet forwarding decisions and further go onto present our own decision making mechanism, to provide reliable packet forwarding node selection under dynamic channel conditions. In section 4, we investigate whether the findings in section 3, can help to improve on fault-tolerant *SWOB* routing performance under a dynamic channel environment setting.

SECTION 3

Channel Aware Packet Forwarding

Introduction

UGS networks typically operate in wireless environments, which can vary considerably in both space and time, due to multi-path propagation effects. Such propagation effects determine the probability of successful packet reception, which, as a result, can influence communication link reliability between node pairs and overall network throughput. Where harsh conditions are prevalent, resulting in channel fading (received signal amplitude fluctuations) or if protocols designed to mitigate these effects by periodically shutting down their communication links, in order to conserve on energy are in operation, this results in link disruption (intermittent connectivity) [123]. Subsequently, intermittent connectivity due to the dynamic wireless transmission environment can create unreliable paths to exist between nodes at any given point in time, resulting in network partitioning and local topological changes to occur, as illustrated in figure 9.1.

The highly dynamic and loss nature of the wireless medium is a challenging problem and becomes a key factor, in support of upper layer operations (i.e. application and network layers), therefore influencing overall distributed networking performance. Adapting well to the dynamic wireless environment where packet transmission failures can occur frequently is imperative, in order to avoid excessive link-level packet retransmissions and unnecessary consumption of network resources [124]. However, selecting nodes to support packet forwarding of mission critical surveillance information can be made robust, by allowing deployed UGS nodes to evaluate their local

neighbourhood link reliability, for example, in terms of the probability in successfully receiving a packet, on a particular link.

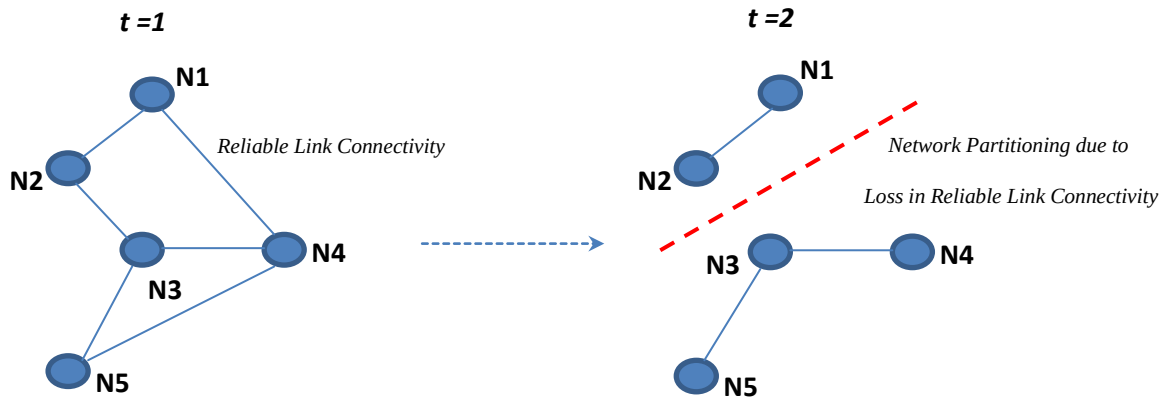

Figure 9.1: Network partitioning due to the unreliable wireless transmission environment at two time interval (t) instants

Our primary goal for section 3 is therefore to, evaluate and analyse link reliability metrics that can assist in avoiding unreliable links and subsequently, provide a basis for a self-managing forwarding node selection capability. Such a capability can assist *UGS's* to avoid nodes, which have a high chance of packet loss and thus, potentially improve their decision making performance with regards to packet forwarding.

In this section, chapter 9 begins by modelling the dynamic wireless environment as detailed in 9.1. In 9.2, we then quantify the unreliable wireless channel environment in terms of the known transitional region coefficient (*TRC*) metric. A presentation of our key analytical findings on the effects and benefits this coefficient can have for both link reliability and performance of a well-studied link quality metric, which is used extensively in many routing protocol schemes for *WSNs*, then follows. In 9.3, we further expand both our use of the *TRC* and our findings about the effects of the *TRC*, within a realistic broadcast channel environment setting. Based on our analysis made in 9.2 and 9.3, we then outline our designed decision making mechanism, for identifying reliable packet forwarding paths in a distributed manner, as detailed in chapter 10. Finally in chapter 11, we summarise and conclude our main contributions of this section.

CHAPTER 9

Impact of the Wireless Channel Environment

9.1 Modelling the Wireless Channel Environment

Understanding the impact that the wireless medium has on link reliability, stems from how we can realistically model the channel environment, in a simulation setting. Due to the complexity of real wireless channels, stochastic models are mostly used [125]. Signals propagating in a wireless channel environment are commonly subject to a distance-dependent loss of power (attenuation), path loss (*PL*), which is defined as the ratio in decibel (*dB*) between the transmitted power (P_{TX}) and received power (P_{RX}) in Watts (*W*), as shown in (9.1).

$$PL(dB) = 10\log_{10}\frac{P_{TX}}{P_{RX}} \tag{9.1}$$

If the wireless channel propagation characteristics are not specified, it is usual to infer that signal propagation takes place over an ideal free space environment, $PL_{Free\text{-}Space}$, in *dB* forming a line of sight (*LOS*) channel [126] and can be expressed, as shown in (9.2).

$$PL_{Free-Space}(d)\ (dB) = 10\log_{10}\frac{(4\pi d)^2}{(G_l\lambda)^2} \tag{9.2}$$

In (9.2), G_l is the product of transmit and receive antenna field radiation patterns in the *LOS* direction, d is the distance between the transmitter-receiver pair and λ is the wavelength of the propagating signal.

The *PL* model of free space treats the wireless channel environment as being free of all objects that might absorb, reflect and scatter transmission signal energy. However, in realistic wireless environments, it is also well known that signal propagation includes

intrinsic effects such as shadowing (large scale fading) and multipath (small scale fading), inducing dynamic and random received signal strength behaviour, which is relevant, when modelling realistic wireless *UGS* network environments.

9.1.1 Large-Scale Fading

The mean path loss, PL_{mean}, as a function of distance, *d*, is proportional to an *nth* power of *d* relative to a reference distance d_0, as shown in (9.3) with mean received signal power $P_{RX\text{-}Mean}$, given in (9.4).

$$PL_{Mean}(d)\,(dB) = PL_{Free-space}(d_0) + 10n\log_{10}(\frac{d}{d_0}) \tag{9.3}$$

$$P_{RX-Mean}\,(d)\,(dB) = P_{TX}\,(dB) - PL_{Mean}\,(d)\,(dB) \tag{9.4}$$

Equation (9.3) is usually referred to as the log-distance path loss model with *n*, the path-loss exponent, reflecting the rate at which the signal decays with respect to *d*. The path-loss exponent typically varies between 2 (free-space path loss) and 4 to 6 (shadowed areas and obstructions due to urban building scenarios) [127]. The reference distance d_0 corresponds to a point located in the far field of the antenna and for short range systems such as *WLANS*, similar to *UGS* network deployments, can have a value between 1-10m [127].

Empirical studies have shown however that for any value of *d*, the *PL* is a random variable having a log-normal distribution about the mean distant dependent value, PL_{mean} [128-129]. A common channel model using a combination of analytical and empirical methods to describe the effect of large-scale fading, in the presence of obstacles, is the log-normal path loss model, as shown in (9.5).

$$PL_{Large-Scale}(d)\,(dB) = PL_{mean}(d)\,(dB) + X_{\sigma} \tag{9.5}$$

As shown in (9.5), X_{σ} is a zero-mean Gaussian random variable in *dB*, with standard deviation σ_{shadow}, due to shadowing effects, also in *dB*. Equation (9.5) depicts the channel

environment in which significant variations in *d*, or the movement beyond obstacles lead to variations of the long-term mean signal strength at the receiver, referred to as "slow" fading. In our simulation studies we model X_σ as a constant random variable over time for a particular link. In large-scale fading, the received power, $P_{RX\text{-}Large\text{-}Scale}$, is shown in (9.6).

$$P_{RX-Large-Scale}(d)\,(dB) = P_{TX}\,(dB) - PL_{Large-Scale}(d)\,(dB) \tag{9.6}$$

9.1.2 Large-Small Scale Fading

In realistic channel propagation environments, a number of signal copies with stochastically independent signal amplitudes of the same mean value can overlap at the receiver. This implies, the received signal power will also show fading consisting of rapid amplitude fluctuations (small-scale fading) around the mean signal level, superimposed on relatively slow variations (large-scale fading) of the mean level. Rapid amplitude fluctuations are mostly caused by local multipath propagation effects and it is well known that the amplitude distribution of the received signal power can be approximated by a Rayleigh distribution [130]. The Rayleigh *PDF*, used to model just small-scale fading scenarios, is shown in (9.7).

$$P(x) = \frac{x}{x_o} e^{-x^2/2x_0} \tag{9.7}$$

As shown in (9.7), x is the amplitude of the received signal envelope and x_0 the mean received power. Incorporating the effects due to large scale-fading into the Rayleigh distribution, the instantaneous power of the received signal, $P_{RX\text{-}Large\text{-}Small\text{-}Scale}$, can be approximated, as shown in (9.8) [130].

$$P_{RX-Large-Small-Scale}(d)\,(dB) = \frac{1}{P_{RX-Mean}} e^{-(P_{RX-Large-Scale}\,/\,P_{RX-Mean})} \tag{9.8}$$

Where, $P_{RX\text{-}Mean}$ and $P_{RX\text{-}Large\text{-}Scale}$, are calculated as shown in (9.4) and (9.6). The resulting expression in (9.8) represents the worst case of fading, per mean received power, for a single communication link. Figure 9.2, illustrates received power characteristics for the wireless channel fading models described in this section.

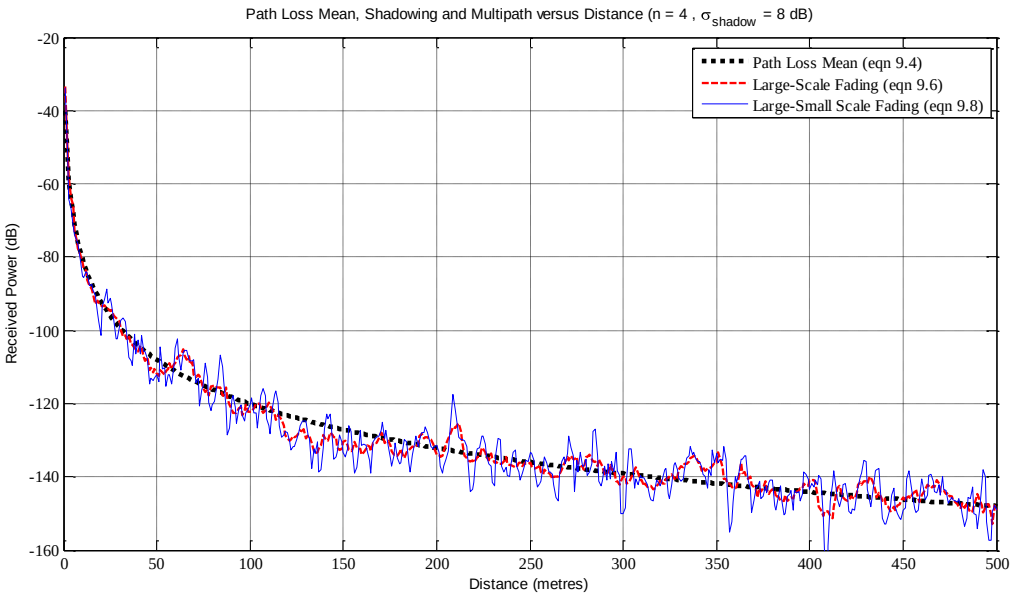

Figure 9.2: Receiver power characteristics for channel conditions, P_{TX} = 10mW, d_0 = 1m, λ = 0.125m, G_l =1

In this chapter, we assume that channel fading due to large and small scale effects are "frequency-non-selective", implying that received signal amplitudes are strongly uncorrelated [131]. We can make this assumption, since *UGS* nodes are usually deployed using fixed positions within the monitoring field, making them static in nature and therefore transmitter-receiver pairs will be rarely moving relative to each other. We also take the view that packet errors are primarily caused by the channel environment and not due to interference of other nodes deployed within the network, when evaluating communication link reliability.

9.1.3 Evaluating Communication Link Reliability

The importance of fading is its impact on the receiver since a minimum level of received signal strength is required in order to have a chance for proper demodulation. A fade with

its resulting drop in received signal strength, therefore becomes a source of packet errors on a particular communication link. One way to characterise this source of error, is the probability of receiving a packet over a link, which subsequently can act as an evaluation of communication link reliability for packet forwarding purposes. The Packet Reception Rate (*PRR*), measures the probability of successfully receiving a packet, by firstly considering the particular encoding scheme employed for a specific transmitter-receiver pair distance and secondly including the effects of the propagation environment. For a standard transceiver, using Non-Return-to-Zero (*NRZ*) encoding, the *PRR* can be calculated, as shown in (9.9) [132].

$$PRR(d) = (1 - P_e)^{8l}(1 - P_e)^{8(f-l)} = (1 - P_e)^{8f} \tag{9.9}$$

From (9.9), f is the frame size in bytes and P_e is the probability of bit error, which is dependent on the modulation scheme used and can be calculated for a transceiver, using Differential Phase-Shift Keying (*DPSK*) modulation, as shown in (9.10) [132].

$$P_e = \frac{1}{2}\exp^{-\gamma(d)\frac{B_N}{R}} \tag{9.10}$$

From (9.10), $\gamma(d)$ is the *SNR*, equal to $10^{\frac{\gamma_{dB}(d)}{10}}$, where $\gamma_{dB}(d) = P_{RX}(d)\,(dB) - P_n\,(dB)$, with P_n the noise floor, B_N the noise bandwidth and R the data rate in bits per second (*bps*). The $P_{RX}(d)\,(dB)$ values for $\gamma_{dB}(d)$ calculation, can be inserted for either large-scale or large-small-scale fading propagation environments, as shown in (9.6) or (9.8). In our simulation study, we base our channel model on static interference-free environments and assume small changes in temperature; therefore P_n is only given by thermal noise and is constant. Table 9.1 summarises the channel model parameters used in this section and based on the analysis made, values undertaken for simulation purposes in the remainder of this chapter.

Channel Model Parameter	***Value***
λ, Propagating Signal	0.125m (frequency = 2.4 GHz)
P_{TX}, Transmission Power	10mW
d_{max}, Node Transmission Range	500m
G_l, (eqn. 9.2)	1
d_0 , reference distance (eqn. 9.3)	10m
$X_\sigma \sim N(0, \sigma_{shadow})$ (eqn. 9.5)	σ_{shadow} = 2,4,6,8,10 dB
f, frame size (eqn. 9.9)	125 Bytes
P_n, noise floor (eqn. 9.10)	-130dB
$B_{N,}$ Noise Bandwidth (eqn. 9.10)	20MHz [132]
R, Data Rate (eqn. 9.10)	2Mbps [132]
Medium Access Control (MAC)	IEEE 802.11b

Table 9.1 Parameters used for communication link reliability performance evaluation

9.2 Impact of the Channel Environment on Link Reliability

Empirical studies have revealed the existence of three distinct reception regions in a wireless link, these being connected, transitional and disconnected [133-134]. In the connected region, links are often of good quality, stable and symmetric and the disconnected region has no practical links for transmission. By contrast, the transitional region is crucial to link reliability since it is characterised by high variance in *PRR* and asymmetric connectivity, which grows with distance and is often quite significant in size, as shown in figure 9.3. In 9.2.1, we begin to define the transitional region and quantify its size in terms of a transitional region coefficient (*TRC*) metric, for different channel environments.

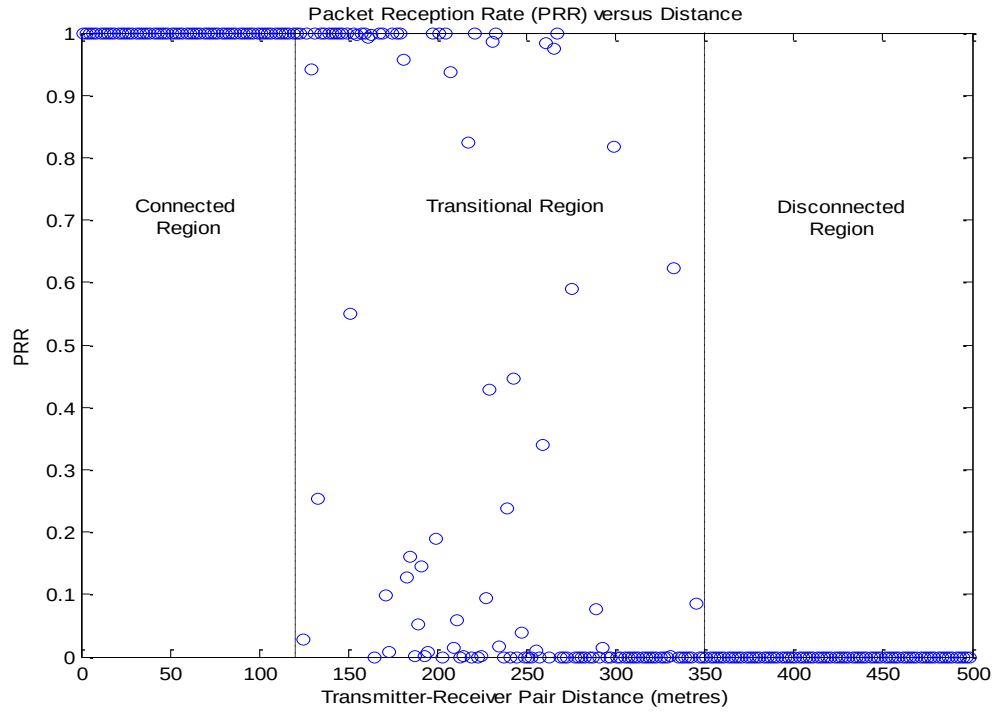

Figure 9.3: PRR characteristics demonstrating three distinct reception regions

9.2.1 Defining the Transitional Region

The extent of the transitional region can be quantified by specifying the desired level in *PRR*, in order to insure high link reliability. This implies bounding the connected and disconnected regions in terms of specific desirable *SNR* values, $\gamma_{dB.}$ Defining high link reliability to be with $PRR > P_{h,}$ and low link reliability with $PRR < P_l$, the upper *SNR* value, $\gamma_{\text{-}Upper\text{-}dB}$, and lower *SNR* value, $\gamma_{\text{-}Lower\text{-}dB}$, can be calculated using (9.10), as shown in (9.11).

$$\gamma_{-Upper-dB} = 10log_{10}((-R/B_N)\times ln(2(1-P_h^{1/8f}))) \tag{9.11}$$

$$\gamma_{-Lower-dB} = 10log_{10}((-R/B_N)\times ln(2(1-P_l^{1/8f})))$$

Figure 9.4, shows a *PRR* curve, with various P_h and P_l values and the impact which this has on the transitional region. Figure 9.4, illustrates by reducing P_l for the disconnected region and increasing P_h for the connected region, can have the effect of increasing the

transitional region and therefore the possibility of a higher chance in unreliable links occurring, for packet forwarding.

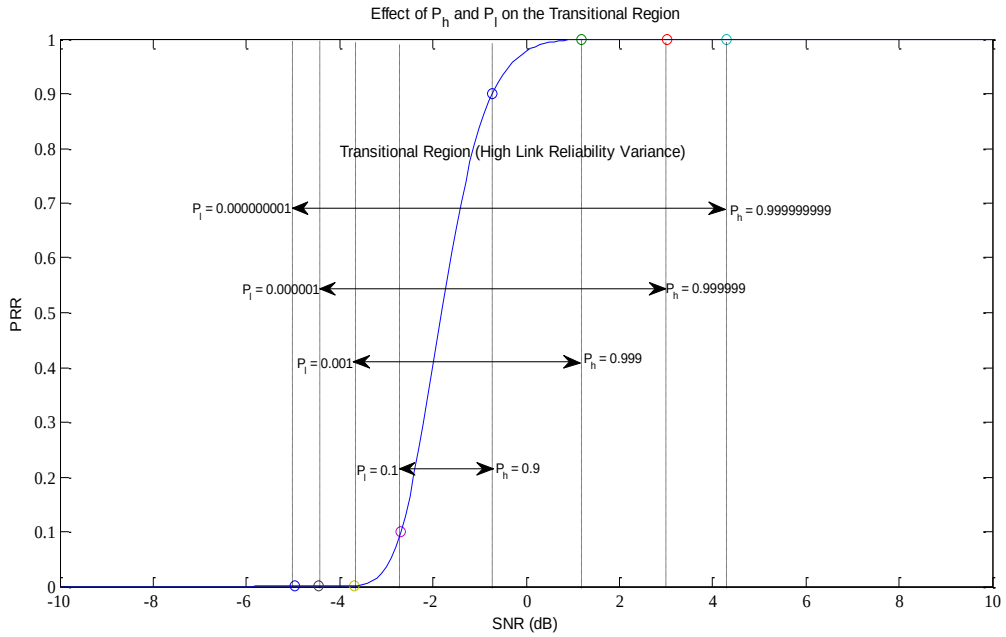

Figure 9.4: Transitional region dynamics for various P_h and P_l values

Both γ-$_{Upper\text{-}dB}$ and $\gamma_{\text{-}Lower\text{-}dB}$ values as shown in (9.11), can be translated into terms of communication link reliability regions. To define this we use the Gaussian characteristics for both large and large-small scale fading propagation environments to help characterise and bound the received signal strength, within $\pm 2\sigma_{Shadow}$, which implies that $p(PL_{mean}\ (d)\ (dB) - 2\sigma_{Shadow} < P_{RX}\ (d)\ (dB) < PL_{mean}\ (d)\ (dB) + 2\sigma_{Shadow}) = 0.955$ [134] and can be expanded as shown in (9.12).

$$P_{RX-Upper}(d)(dB) = P_{TX}(dB) - PL_{Mean}(d)(dB) + 2\sigma_{Shadow} \tag{9.12}$$

$$P_{RX-Lower}(d)(dB) = P_{TX}(dB) - PL_{Mean}(d)(dB) - 2\sigma_{Shadow}$$

From (9.12), the transitional region can be formulated in terms of *SNR*, which begins at $P_{RX\text{-}Transitional\text{-}Begin} = \gamma\text{-}_{Upper\text{-}dB} + P_n$ and ends at $P_{RX\text{-}Transitional\text{-}End} = \gamma\text{-}_{Lower\text{-}dB} + P_n$. Rearranging (9.12) to express communication link reliability, in terms of the beginning and end of the transitional region, $d_{Transitional\text{-}Begin}$, and $d_{Transitional\text{-}End}$, in metres, these are given in (9.13).

$$d_{Transitional-Begin} = 10^{\frac{P_n + \gamma_{-Upper-dB} - P_{TX} + PL_{Free-Space}(d_0) + 2\sigma_{Shadow}}{-10n}} \quad (9.13)$$

$$d_{Transitional-End} = 10^{\frac{P_n + \gamma_{-Lower-dB} - P_{TX} + PL_{Free-Space}(d_0) - 2\sigma_{Shadow}}{-10n}}$$

The impact of the channel environment on the transitional region is neatly described through (9.13) and figure 9.5. As shown in figure 9.5, increasing σ_{Shadow} has the effect of increasing the transitional region, while increasing the path loss exponent *n*, due to faster decay of received signal strength, has the effect of reducing it. From figure 9.5, channel conditions with a high path loss exponent *n*, and low σ_{Shadow}, therefore reduce size of the transitional region. A ratio, which brings together $d_{Transitional-Begin}$ and $d_{Transitional-End}$, in order to describe the relative size of the transitional region, can be derived in terms of the Transitional Region Coefficient (*TRC*), as shown in (9.14) [134-135].

$$TRC = \frac{d_{Transitional-End} - d_{Transitional-Begin}}{d_{Transitional-Begin}} = \left(10^{\frac{(\gamma_{-Upper-dB} - \gamma_{-Lower\_dB}) + 4\sigma_{Shadow}}{10n}}\right) - 1 \quad (9.14)$$

As shown in (9.14), *TRC* represents a value of merit in link reliability giving an indication of the extent of the transitional region to connected region parts of a network, which are independent of P_n and P_{TX}. According to (9.14), achieving a lower *TRC* is therefore better, since this implies a larger connected region compared to a transitional one.

However, as detailed in 9.2.2, increasing the size of the transitional region (higher *TRC*) for a fixed *PRR* curve can help to achieve an improved optimal link forwarding distance, for a defined path loss exponent *n* and σ_{Shadow} channel environment. Evaluating the optimal link forwarding distance with respect to the transitional region is important since, this enables us to establish how link reliability might behave within an unreliable channel environment, across a range of potential communication link distances present within a deployed network. In addition, knowing how the optimal link forwarding distance

behaves in different channel environments can further assist towards developing strategies in managing node selection efficiently, for reliable packet transmission.

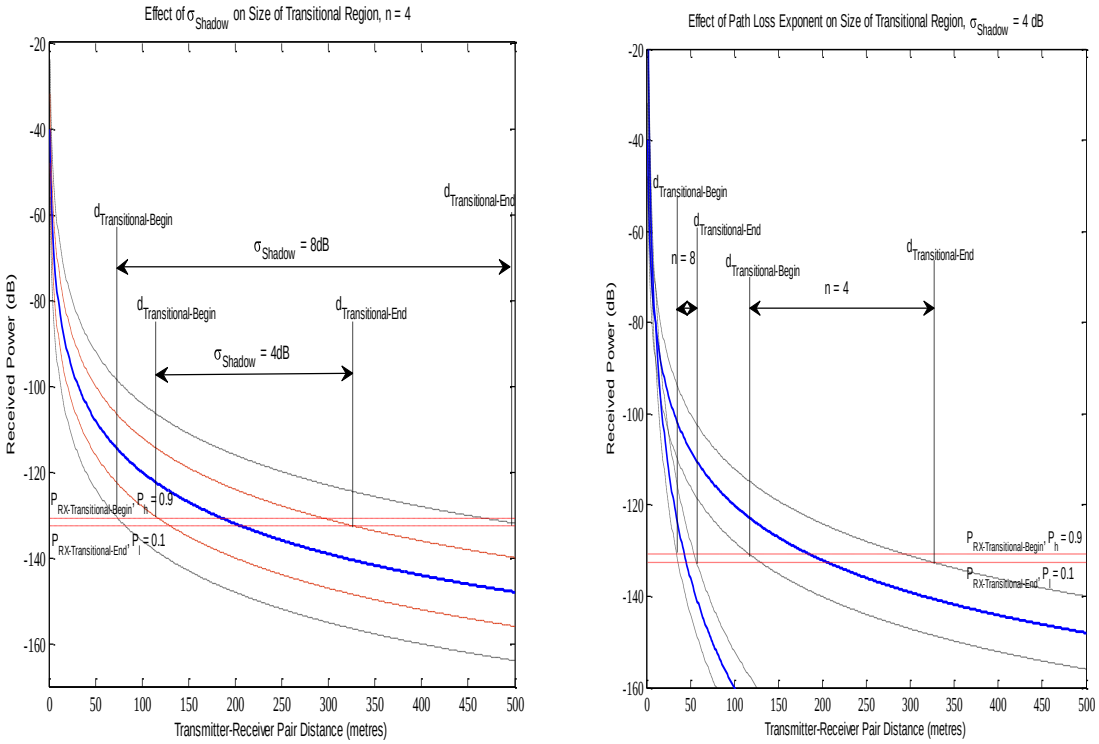

Figure 9.5: Impact of channel parameter conditions on size of transitional region. Solid lines represent $P_{RX\text{-}Mean}$

9.2.2 Impact of Transitional Region on the Optimal Forwarding Distance

The average forwarding distance ($d_{Average}$), to achieve a particular link reliability in terms of *PRR*, can be defined as the distance traversed in a communication link hop, *d*, multiplied by the Expected *PRR*, *E [PRR]* (first moment), as shown in (9.15).

$$d_{Average} = d \times E\,[PRR] \tag{9.15}$$

E [PRR] depends on both the receiver response curve given in (9.9), illustrated in figure 9.4 and the *PDF* of the *SNR* for a given distance *d*, $\gamma_{dB}(d)$, as shown in (9.16).

$$E[PRR] = \int_{-\infty}^{\infty} PRR(\gamma_{dB}(d))\, f(\gamma_{dB}, d)\, d\gamma_{dB} \tag{9.16}$$

As shown in (9.16), $f(\gamma_{dB}, d)$ represents the *SNR PDF*, which is given by $SNR \sim N(\gamma_{dB\text{-}Mean}, \sigma_{Shadow})$, where $\gamma_{dB\text{-}Mean} = P_{RX\text{-}Mean} - P_n$. Due to the complexity in solving (9.16), we can estimate and represent the receiver response curve, by using a linear function, in order to derive an approximate expression to *E [PRR]*. Firstly, defining the limits of the integral, in terms of the transitional region, we obtain *E [PRR]* as shown in (9.17), where *Q (.)*, is defined as the tail integral of a unit Gaussian (*Q*-function).

$$E[PRR] \approx \int_{\gamma_{-Lower-dB}}^{\infty} PRR(\gamma_{dB}(d)) f(\gamma_{dB}, d)\, d\gamma_{dB} \tag{9.17}$$

$$E[PRR] \approx \int_{\gamma_{-Lower-dB}}^{\gamma_{-Upper-dB}} (T_e \gamma_{dB} + h_e) f(\gamma_{dB}, d)\, d\gamma_{dB} + \int_{\gamma_{-Upper-dB}}^{\infty} f(\gamma_{dB}, d)\, d\gamma_{dB}$$

$$E[PRR] \approx \left[(T_e \gamma_{dB} + h_e) \times \left(Q\left(\frac{\gamma_{-Lower-dB} - \gamma_{dB-Mean}}{\sigma_{Shadow}}\right) - Q\left(\frac{\gamma_{-Upper-dB} - \gamma_{dB-Mean}}{\sigma_{Shadow}}\right) \right) \right] + Q\left(\frac{\gamma_{-Upper-dB} - \gamma_{dB-Mean}}{\sigma_{Shadow}}\right)$$

As shown in (9.17), $PRR(\gamma_{dB}(d))$ has been approximated by a linear function within the limits, $\gamma_{Lower\text{-}dB} \geq \gamma_{dB} \leq \gamma_{Upper\text{-}dB}$, where $T_e = \frac{P_h - P_l}{(\gamma_{-Upper-dB} - \gamma_{-Lower-dB})}$ and $h_e = \frac{((P_l \times \gamma_{-Upper-dB}) - (P_h \times \gamma_{-Lower-dB}))}{(\gamma_{-Upper-dB} - \gamma_{-Lower-dB})}$, with $\gamma_{Upper\text{-}dB}$ and $\gamma_{Lower\text{-}dB}$ calculated, as shown in (9.11). It is also assumed from (9.17) that *E [PRR]* = 0 for, $\gamma_{dB} < \gamma_{Lower\text{-}dB}$ and *E [PRR]* = 1 for, $\gamma_{dB} > \gamma_{Upper\text{-}dB}$. The optimal forwarding distance (d_{opt}) can therefore be formulated as the link distance, which maximises the average forwarding distance ($d_{Average}$). This implies maximising *E [PRR]*, for all φ, where φ is defined as ($1 \geq \varphi \leq d_{max}$), and d_{max} being the maximum node transmission range, as shown in (9.18) and is illustrated, as shown in figure 9.6, with d_{max} set to 500m.

$$d_{opt} = arg \max_{d \in \varphi}(d_{average}) = arg \max_{d \in \varphi}(E[PRR]) \tag{9.18}$$

As shown in figure 9.6, increasing the *TRC*, has the effect of increasing d_{opt} for a set channel environment. For different channel environments, as shown in figure 9.7 (a), the path loss exponent *n*, has the effect of reducing d_{opt} by shifting it to the left, since as expected this represents a greater decay in received signal strength. As shown in figure 9.7(b), decreasing σ_{Shadow} however increases d_{opt}. Figure 9.7(b) also indicates that channel conditions with a higher σ_{Shadow} value, coupled with setting a high *TRC* value of 9.8, as indicated in figure 9.6, can increase the probability of achieving better communication link reliability further away from the transmitter, due to there being a larger expectation range from d_{opt} to d_{max} (500 m). This can assist the chances of a packet being successfully received, in conditions where larger transmitter-receiver pair link distances exist, within a deployed UGS network (i.e. low node density conditions). It is important to note that since *n* and σ_{Shadow} have a direct effect on the dynamics of the transitional region, as illustrated in figure 9.5, the optimal link forwarding distance is always found within it.

With this in mind utilising links with a higher *TRC* value could potentially compensate for an unreliable wireless transmission environment, through achieving a better *E [PRR]* range along with a lower decay rate from d_{opt} to d_{max}. Utilising such a potential characteristic could also assist in increasing the scope in which nodes can be selected for packet forwarding, over larger transmitter-receiver pair link distances.

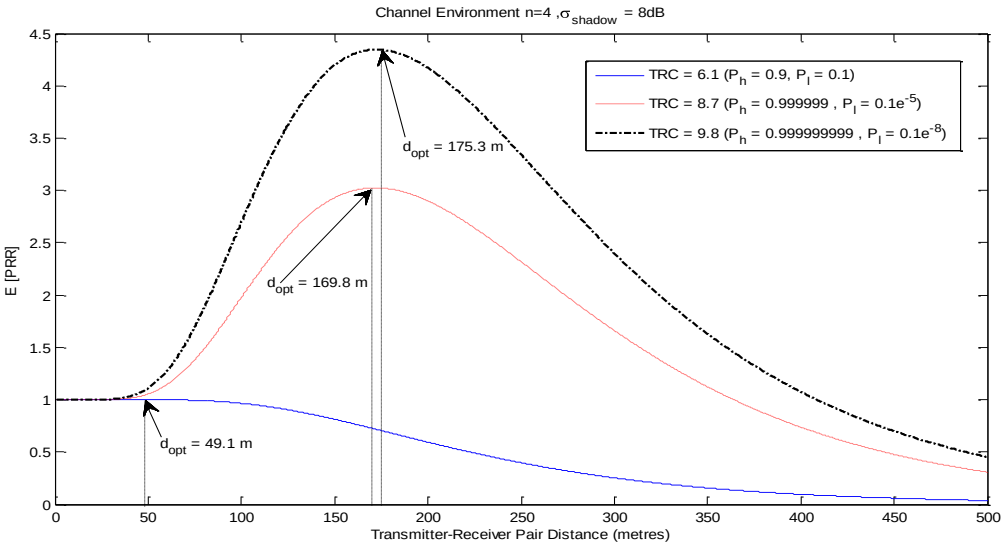

Figure 9.6: Impact of increasing the TRC on d_{opt}

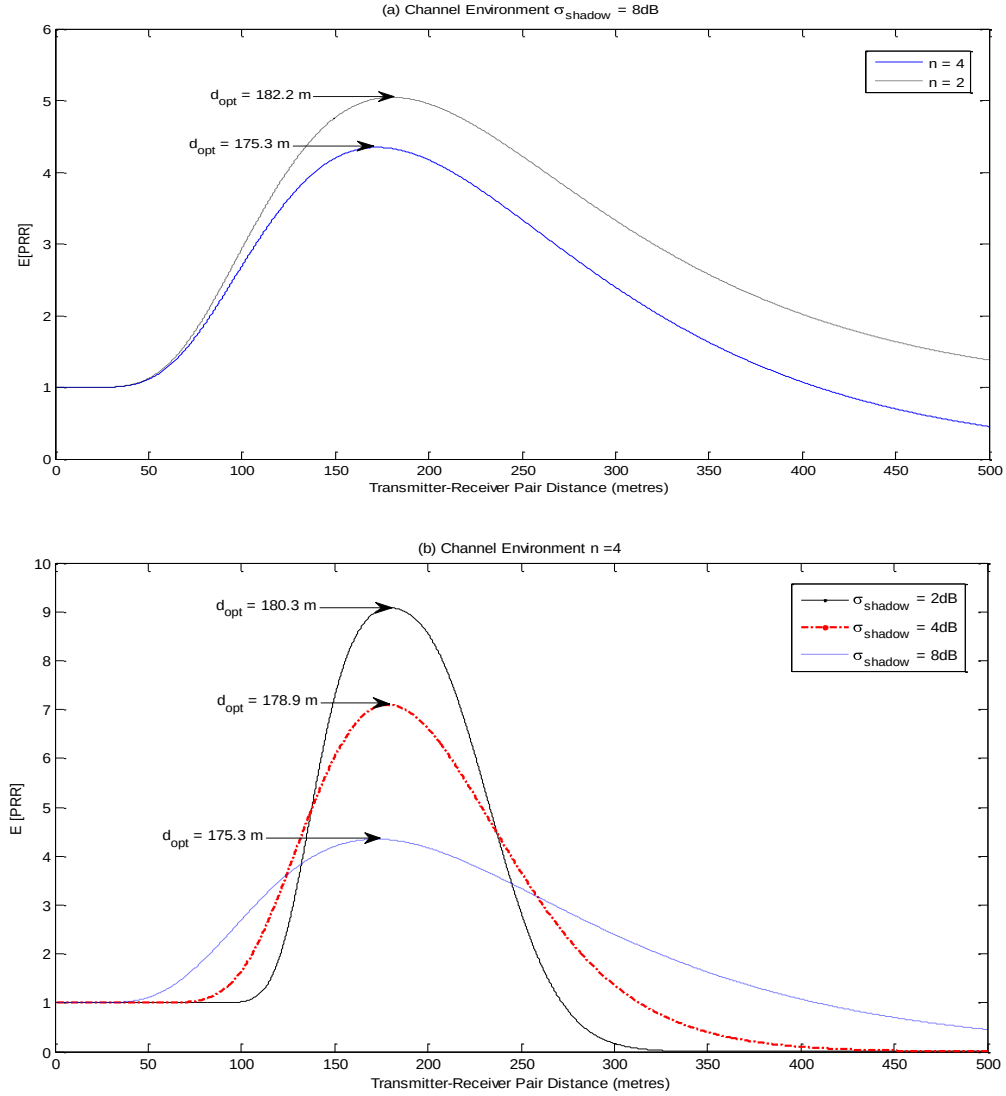

Figure 9.7: Effect of channel environment on d_{opt} for different (a) n and (b) σ_{Shadow} with TRC = 9.8

In 9.2.3, we seek to further explore whether utilising a higher *TRC* value can also offer benefits in achieving better transmission reliability.

9.2.3 Impact of the Transitional Region on Transmission Reliability

Within large-scale and small-scale fading environments, packet transmissions on a particular communication link occur with a certain fixed error probability and packet errors occur independently of each transmission attempt made. Subsequently, this implies firstly that *PRR* values do not depend on the number of transmission made and secondly that packet errors are usually random in nature [136]. A popular and widely used model, describing the transmission reliability over a single hop, which takes into consideration and distinguishes the alternation between deep fades and good periods of a fading channel, is the "Gilbert-Elliot" model [137-138]. The "Gilbert-Elliot" model is a two-state Markov chain, with each state of the chain corresponding to a link reliability level, therefore capturing the tendency of fading channel environments to inflict bursty packet errors, as shown in figure 9.8. The state transition matrix (*A*) governing figure 9.8 is shown in (9.19).

$$A = \begin{bmatrix} 1-P_1 & P_1 \\ P_2 & 1-P_2 \end{bmatrix} \tag{9.19}$$

As shown in figure 9.8 and (9.19), P_1 represents the transition probability of going from a non-loss state to a loss state and P_2 is the transition probability of going from a loss state to a non-loss state. Defining the transmission reliability (no-loss state) in terms of the transitional region to be high, if $PRR \geq P_h$ and low (loss state), if $PRR \leq P_l$, P_1, P_2 are shown in (9.20).

$$P_1 = p(PRR \le P_h) = 1 - Q\left(\frac{\gamma_{-Upper-dB} - \gamma_{dB-Mean}}{\sigma_{Shadow}}\right) \quad (9.20)$$

$$P_2 = p(PRR \ge P_l) = Q\left(\frac{\gamma_{-Lower-dB} - \gamma_{dB-Mean}}{\sigma_{Shadow}}\right)$$

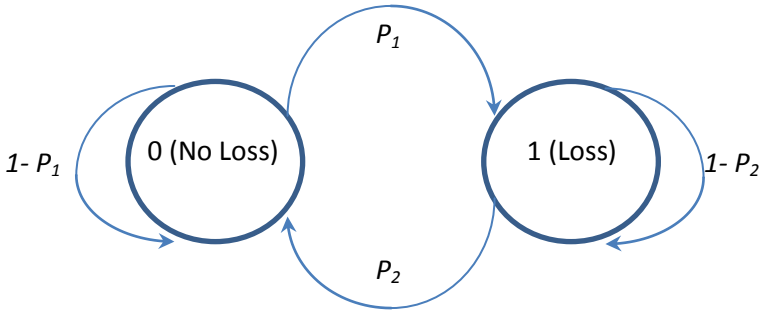

Figure 9.8: "Gilbert-Elliot Model: A two state Markov channel

As shown in (9.20), P_1 and P_2 signify state transition probabilities within the defined size of the transitional region, given by $\gamma_{-Upper-dB}$ and $\gamma_{-Lower-dB}$. From A, as shown in (9.19), the stationary state probabilities, π_0 for state 0 and π_1 for state 1 can be calculated as shown in (9.21).

$$\pi_0 = \frac{P_2}{P_1 + P_2}, \pi_1 = \frac{P_1}{P_1 + P_2} \quad (9.21)$$

As shown in (9.21), π_0 represents the average arrival probability and π_1 represents the mean loss probability. We define transmission reliability, over a single communication hop link, to be π_0, as shown in figure 9.8. Figure 9.9, shows the impact on transmission reliability through increasing the *TRC* metric.

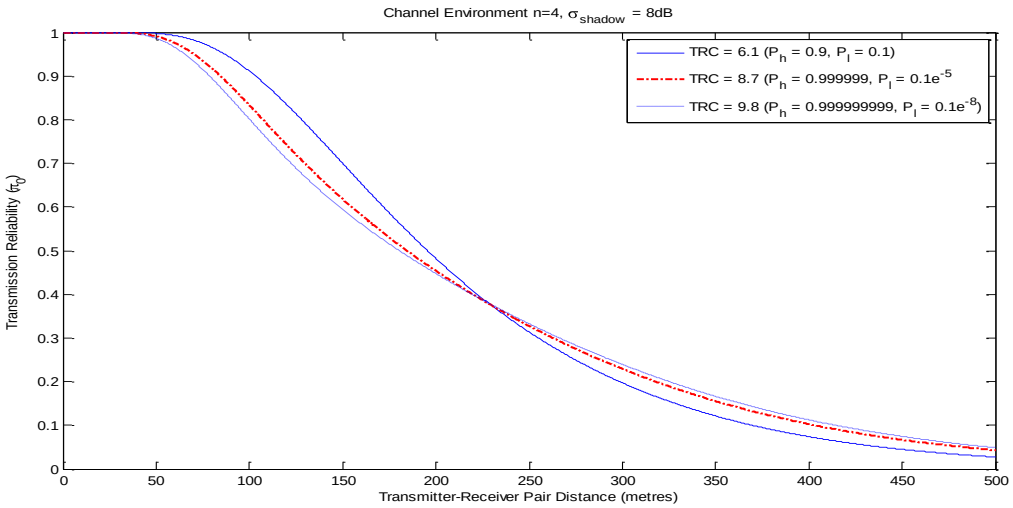

Figure 9.9: Impact of increasing the TRC on transmission reliability (π_0)

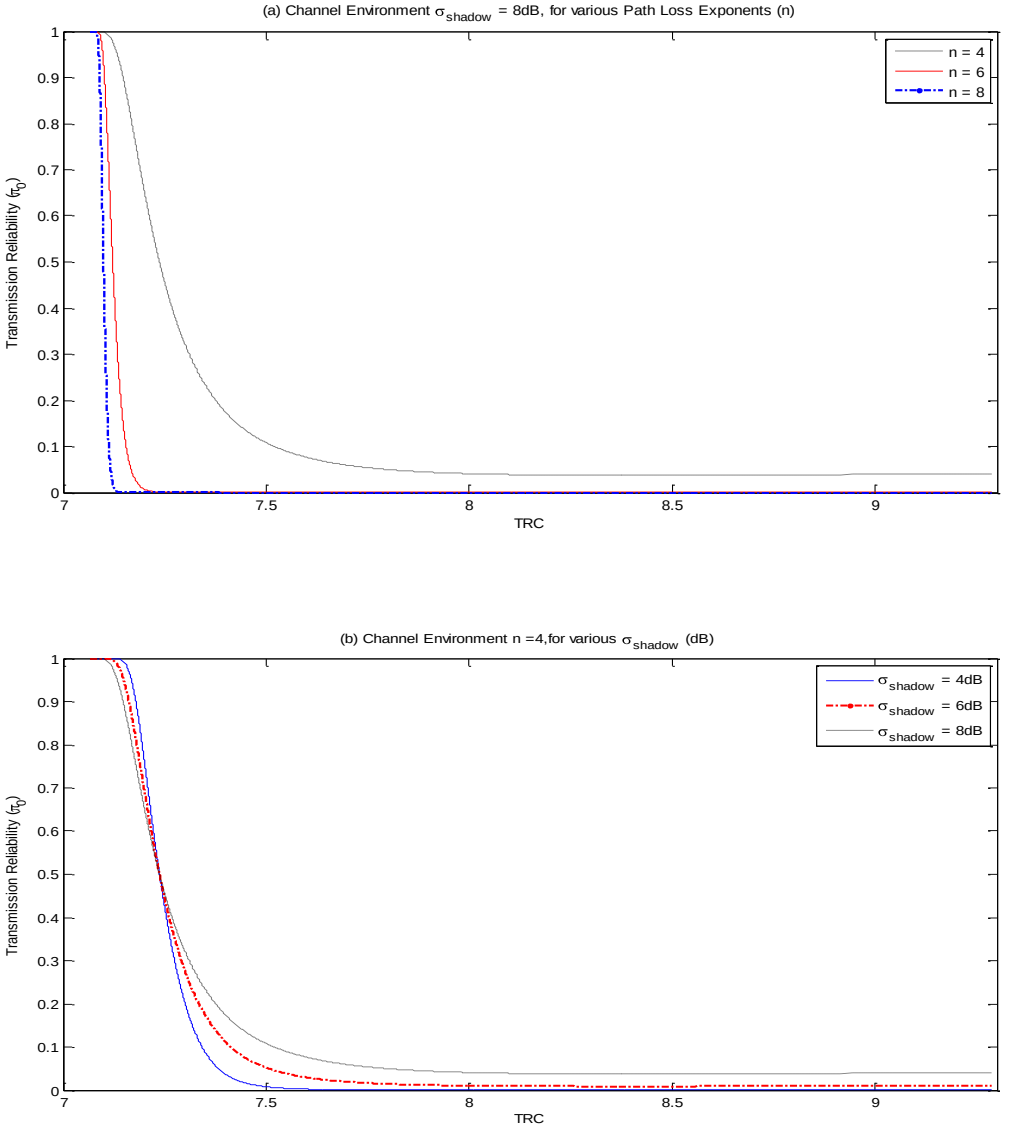

Figure 9.10: Effect of TRC on transmission reliability for channel conditions with different (a) n and (b) σ_{Shadow}

From figure 9.9, defining a lower *TRC* value, achieves a better transmission reliability performance over shorter communication link distances, however utilising a higher *TRC* value is more beneficial over larger single hop communication link distances. This is expected since a higher *TRC* value, as indicated in figure 9.6, can increase the *E [PRR]* range and therefore the chances of reliable packet reception over larger hop distances, which might be the case within a realistic *UGS* network deployment setting. As shown in figure 9.10(a), increasing *TRC* has no effect on improving transmission reliability performance, in channel conditions with increasing *n*. As shown in figure 9.10(b) and initially verified through figure 9.9, defining a higher *TRC* value is again only beneficial in channel environments with a fixed *n* but varying σ_{Shadow}.

The transmission reliability however, as a value of merit only reflects the average packet arrival probability and does not give an indication, as to the number of transmissions required to achieve a desired transmission reliability. The number of packet transmission attempts required to successfully deliver a packet, ultimately reflects on the amount of energy consumed over a particular link and so must be actively considered. Identifying forwarding nodes, which minimise the expected total number of link packet transmission attempts, is therefore crucial and in 9.2.4, we explore whether utilising a higher *TRC* value has any bearing on this.

9.2.4 Impact of Transitional Region on the Expected Transmission Count

So far our analysis concerning the impact of the channel environment (*TRC*) on communication reliability has not considered using link quality performance metrics, as a potential way towards identifying reliable packet forwarding nodes. An initial indication has been given to this, in 9.2.2, by restricting packet forwarding to nodes with hop distances that can maximise $d_{average}$, given in (9.18), which can primarily be achieved through using links with a higher *TRC*, as shown in figure 9.6. An additional way of

identifying reliable packet forwarding nodes is to use communication links, which can minimise on the expected number of transmissions required for successful packet delivery [139]. This can therefore help to achieve higher link throughput rates, but most importantly lower communication energy expenditure.

The authors of [139] argue that traditional routing protocols such as DSR and DSDV are more focused on identifying nodes in rapidly changing topology environments and scalability issues, rather than identifying high-quality links, within an unreliable wireless channel environment. As with the case in DSR and DSDV type protocols, identifying routing paths which minimise on hop-count can maximise the distance travelled by a packet towards its destination to achieve better *QoS* (message latency), but is likely to induce lower received packet signal strength, increasing the chance for higher packet loss ratios (lower transmission reliability).

The derivation of the expected number of transmissions (*ETX*) link quality metric starts with first measuring the underlying *PRR* in both the forward (P_F) and reverse (P_R) directions, in order to handle the asymmetric nature of bi-directional links, through incorporating the *PRR* in each direction. By denoting *P*, as the probability that a packet transmission across an arbitrary bi-directional link is not successful, this is given in (9.22).

$$P = 1 - [\,(P_F) \times (P_R)\,] \tag{9.22}$$

For analysis purposes, we assume that both P_F and P_R for an arbitrary link share the same *PRR* characteristics, as shown in figure 9.4. Defined in this way, allows us to further simplify *P*, so that it can be formulated in terms of the lower limit of the transitional region, as shown in (9.23).

$$P = 1 - [\, p(PRR \geq P_l)\,] = 1 - [\, Q(\frac{\gamma_{-Lower-dB} - \gamma_{dB-Mean}}{\sigma_{Shadow}})\,] \tag{9.23}$$

As shown in (9.23), we assume P_R = 1 and therefore (9.23) represents the probability of unsuccessful packet transmission, in terms of the lower transitional region size limit in the P_F direction. In addition, we expect that the link-layer operation (MAC) will always retransmit a packet whose transmission was not successful. In [139] this consideration is denoted by firstly, assuming a Bernoulli trial and then formulating the probability that the packet will be successfully delivered for an arbitrary link after *c* attempts, T_c, as shown in (9.24).

$$T_c = P^{c-1} \times (1 - P) \tag{9.24}$$

Finally, the *ETX* required to successfully deliver a packet on an arbitrary link is given in (9.25). As shown in (9.25), in order to establish and identify reliable links it requires us to minimise *ETX*, which implies minimising on *P* through utilising the known condition that if $P \geq 0$, then *ETX* is always greater than 1.

$$ETX = \sum_{c=1}^{\infty} c \times T_c = \frac{1}{1 - P} \tag{9.25}$$

Figure 9.11, shows that by decreasing the lower limit of the transitional region, $\gamma_{\text{-}Lower\text{-}dB}$ and thus increasing the *TRC* by maintaining a fixed $\gamma_{\text{-}Upper\text{-}dB}$ value , can minimise *ETX* further, using fixed channel conditions. Figure 9.11, indicates that over shorter hop-distances, using various $\gamma_{\text{-}Lower\text{-}dB}$ values is comparable, in order to maintain an ideal *ETX* but also indicates that keeping a lower $\gamma_{\text{-}Lower\text{-}dB}$ value (higher *TRC*) becomes more apparent over longer hop-distances, in minimising on *ETX* further. This suggests that in low node density network environments, such as *UGS* networks where hop-distances can be large, identifying links that achieve a higher *TRC* could help to improve on potential communication energy expenditure, through better *ETX* performance.

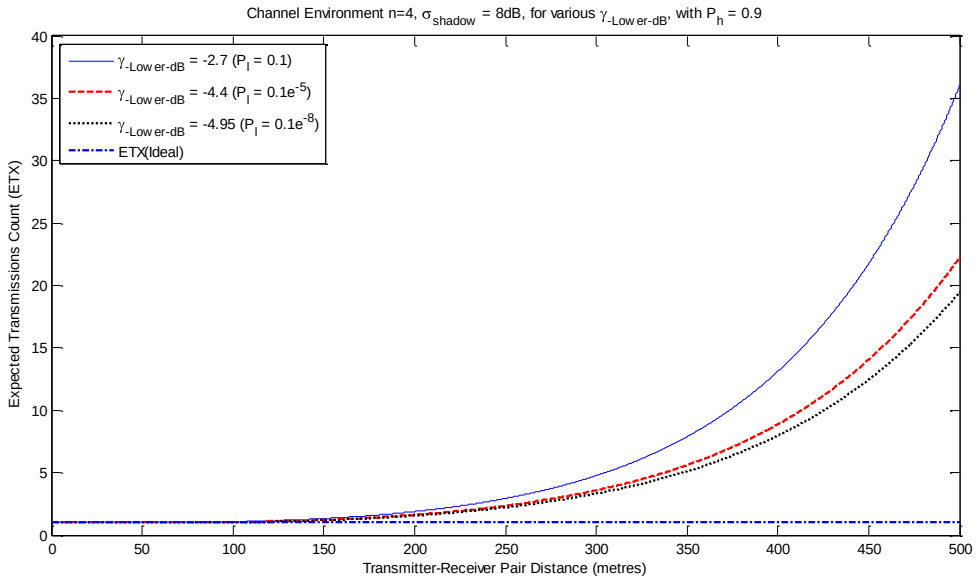

Figure 9.11: Impact of the TRC on ETX, with a fixed $\gamma_{\text{-Upper-dB}}$ value using P_h =0.9

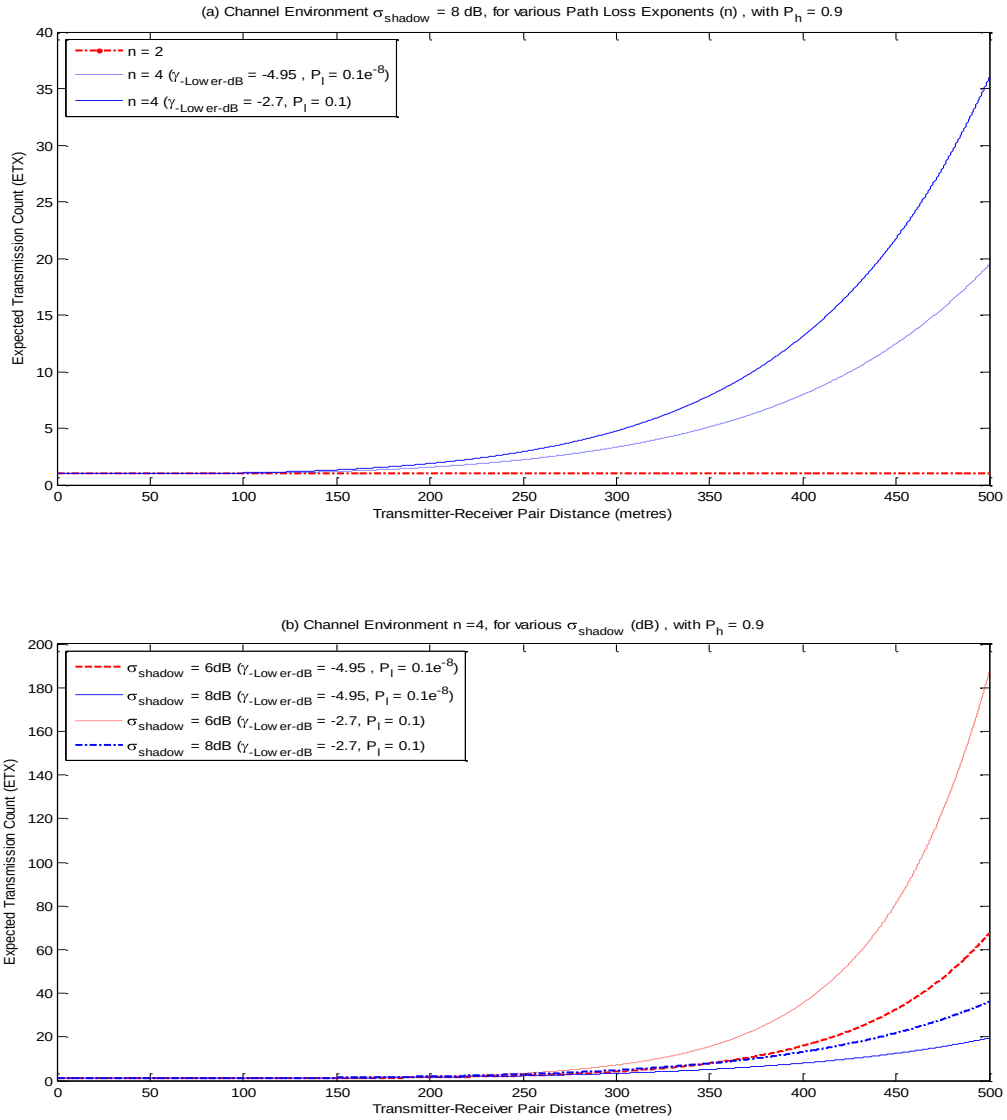

Figure 9.12: Effect of TRC on ETX for channel conditions with different (a) n and (b) σ_{Shadow}

Figures 9.12 (a) and (b) illustrate the effect that the channel environment has on *ETX*. In figure 9.12 (a) increasing the path loss exponent has the effect of increasing *ETX*, while increasing σ_{Shadow} has the effect of reducing *ETX* over larger hop-distances. As shown in figures 9.12 (a) and (b) increasing the *TRC*, through setting a lower $\gamma_{\text{-}Lower\text{-}dB}$ value can minimise *ETX*, within both an increasing *n* and σ_{Shadow} channel environment. This gives both a reason to believe and an indication, as to the benefit in increasing the *TRC* , in order to mitigate on *n* and σ_{shadow} channel conditions further, thus improving on overall *ETX* performance.

9.3 Broadcast Nature of the Wireless Channel Environment

Packet forwarding in wireless networks have traditionally focused on identifying nodes, which satisfy the best-path (i.e. minimum number of hops to a destination with favourable link reliability) criteria between nodes. While best-path forwarding is suitable for wireless environments with relatively stable and reliable point-to-point links, it is not an ideal approach in realistic wireless environments that express time varying qualities over larger hop-distances, as detailed in 9.1. As a result, best-path routing in this scenario, will require higher packet retransmissions and more frequent path rediscoveries. With a view to further improving on packet retransmissions, the impact of the error prone channel environment on packet forwarding can be further mitigated by exploiting the broadcast nature of wireless transmissions (*opportunistic forwarding*) and many schemes have been proposed, which the major ones are detailed and surveyed in [140-142].

Utilising an opportunistic forwarding strategy, allows nodes to maximise the progress a packet makes towards the destination that each received broadcast transmission may provide. Thus, in contrast to best-path packet forwarding where a packet is unicast to the predetermined next-hop, under opportunistic forwarding, a next-hop is determined per-packet after its broadcast transmission has been received. Primarily, all opportunistic

forwarding schemes operate by actively involving multiple neighbouring nodes (*forwarding candidates*) for each packet relay in order to firstly, make the forwarding task insensitive to link quality variations and secondly further improve on network throughput, as surveyed in [142-143]. As shown in [142-143] *opportunistic forwarding* schemes differ mainly on how they improve on selecting forwarding candidates, in order to avoid packet duplication at the destination. Many of the surveyed schemes predominantly rely on the *ETX* metric or maximising the geo-graphical distance on a hop-by-hop basis towards the destination, as their prioritisation selection mechanisms.

In 9.3, we do not propose a new protocol for *opportunistic forwarding* but analyse the impact of the channel environment (*TRC*) on the expected any-path transmission (*EAX*) link quality metric [144]. *EAX*, which builds on the *ETX* format, is a link quality metric, which neatly captures the *ETX* between a node pair, under an *opportunistic forwarding* environment. By employing the *EAX* metric, within an opportunistic any-path forwarding (*OAPF*) environment, as detailed in [144-145], we seek to inquire whether we can indeed reduce the required number of transmissions further, in order to achieve reliable delivery of a packet to its destination.

9.3.1 The Expected any Path Transmission Link Quality Metric

We now define the *EAX* for a source ***s*** and destination ***d*** pair, given a simple arbitrary static network topology. Let $C^{s,\ d}$, denote the potential set of forwarding candidates ($f_{1,\ldots,}\ f_i$), between ***s*** and ***d***, where $i \leq C^{s,\ d}$, and let $C_i^{\ s,d}$ be the i^{th} forwarding candidate, within d_{max} (Table 9.1) of ***s***. We denote the underlying probability of delivery success considering both P_F and P_R, as introduced in 9.2.4, from ***s*** to $C_t^{s,\ d}$ as $\boldsymbol{p_i}$. As defined in [145], the *EAX* needed for reliable delivery of a packet from a source ***s*** to a destination ***d***, given the $C^{s,\ d}$ and assuming $P_R = 1$, is shown in (9.26).

$$EAX(s,d) = S(s,d) + Z(s,d) \tag{9.26}$$

Where, $S(s,d) = \frac{1}{1 - \prod_{i}(1 - p_i)}$ and $Z(s,d) = \sum_{i} EAX(C_i^{s,d}, d)\, p_i \prod_{j=1}^{i-1}(1 - p_j)$.

By doing a direct comparison between (9.25) and (9.26), we can see that using (9.25) merely considers a best path scenario from each node in the network, in terms of *ETX*. As shown in (9.26), the opportunistic forwarding framework is neatly captured by *S(s, d)*, which describes the *ETX* for successfully transmitting a packet from source ***s***, to at least one of the next hop forwarding candidates $C_i^{s,d}$ and *Z(s, d)*, which captures the *ETX* for delivering the packet in turn from those candidates to a destination, ***d***.

9.3.2 Impact of Transitional Region on the EAX Metric

The *TRC* in it's own right can serve as a value of merit for current link reliability, by giving an indication of the extent of the transitional region to connected region, associated with a single communication link. By considering the transistional region defined by the *TRC* as a potential way of mitgating link unreliabilty within an *OAPF* environment, we analyse if this has any effect on *EAX* performance, within a 2-hop scenerio (i.e. the set of forwarding candidates, $C^{s,d}$, are the first hop nodes to a destination ***d***). We also assume for the purposes of analysis that $C^{s,d}$ nodes all have equal priority, for packet forwarding selection. Figure 9.13, shows the effect of increasing *TRC* on *EAX* performance, while maintaining a fixed P_h ($\gamma_{\text{-Upper-dB}}$) value. By increasing the *TRC*, it is shown through the *EAX* metric that we can further reduce the number of transmissions required for sucessful packet delivery.

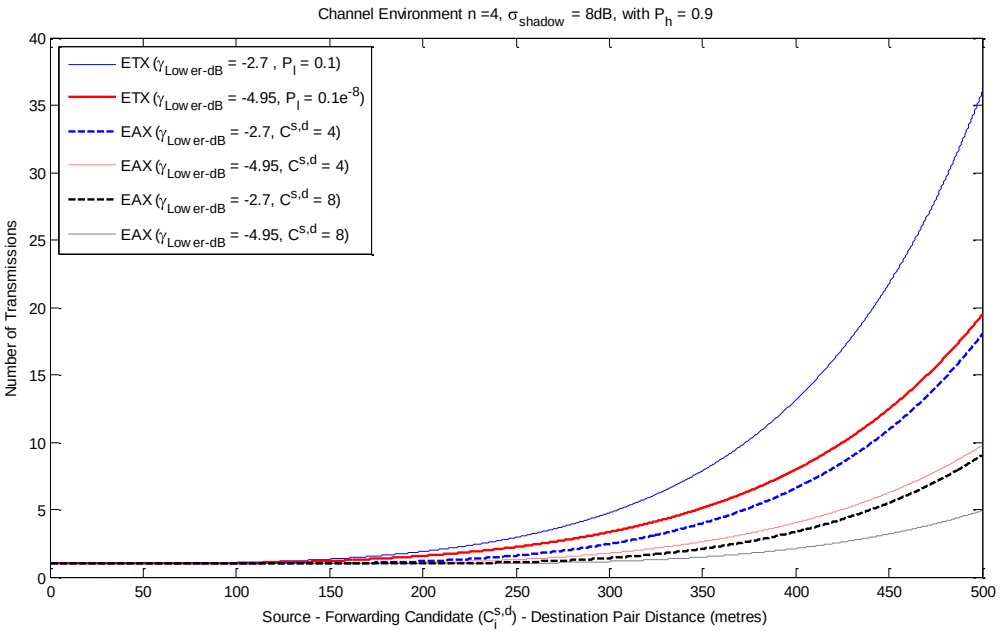

Figure 9.13: Effect of TRC on EAX and improvements possible over ETX

In addition, figure 9.13 highlights the difference between the *ETX* and *EAX* performance lines, which gives an indication as to the extent of gain possible with opportunistic packet forwarding, when compared with just utilising *ETX* best-path packet forwarding, within a fixed channel environment. The extent of gain is possible because of the probability a packet is successfully received by at least one of the next-hop forwarding candidates $C_i^{s,d}$ through *S(s, d)* and *Z(s, d)* operations, as shown in (9.27) increases. Figure 9.13 also shows increasing the selection diversity, achieved by setting the number of candiadates in a potential packet forwarding set, $C^{s,d}$, can also help to reduce the number of transmissions required for successful packet delivery to a destination. This finding suggests that permitting nodes to decide, in a distributed manner, packet forwarding actions based on link reliability knowledge of multiple relay paths can assist in mitigating communication link unreliability. Increasing the packet forwarding set, $C^{s,d}$, does however create implications for *UGS* operations, since this would imply both packet overhead (bandwidth efficiency) and communication energy expenditure would increase with a larger $C^{s,d}$ set and therefore must be viewed as a potential trade-off against required packet delivery success performance.

CHAPTER 10

Development of a Channel Aware Hop Selection Scheme

10.1 Channel Aware Fuzzy Logic Hop Selection Scheme

As detailed in chapter 9, in sections 9.2 and 9.3, we have studied how the *TRC* can affect both link reliability and known link quality metrics, such as *ETX* and *EAX*. In section 9.3, it is also shown how the packet forwarding task can be improved, in a distributed manner, through using the *TRC* within an *OAPF* environment. In this chapter, we highlight our decision making mechanism based on the benefits we have discovered and knowledge gained about the *TRC*, as a potential metric to achieve improved packet forwarding performance within a dynamic channel environment.

A decision mechanism of this kind would serve *UGS* nodes the advantage and ability to self-manage their own packet forwarding tasks on a per hop basis, based solely on the *TRC* information gained from the channel environment, in a distributed and opportunistic manner. Since the uncertainty associated with the dynamic channel environment is a key factor towards data packets being successfully received, controlling node selection for packet forwarding efficiently, according to current channel conditions (channel awareness), becomes a key design requirement. In this section, we propose to use a Fuzzy Logic System (*FLS*) as our control implementation for packet forwarding, utilising the current received *TRC*, as its control input source.

Fuzzy Logic (*FL*) has the potential to deal with conflicting real-world uncertainties without needing complex mathematical modelling, through using heuristic reasoning [146]. Such a *FLS* scheme can be applied to hop node selection for data forwarding in varying channel conditions. In addition, our other reason for applying a *FLS* decision making capability is to see if any advantages can be achieved in allowing nodes to improve

their node selection capability against techniques, which currently rely on defined metrics, as detailed in [147-148]. Defined metrics have the disadvantage of not promoting adaptive behaviour towards packet forwarding links, which can become unreliable and result in changes to local network topology. We begin initially in 10.1.1, by giving an overview to *FL*. In 10.1.2, we then introduce the building blocks associated with a *FLS* and based on this introduce our proposed *FLS* design in heading 10.1.3. In 10.1.4, we perform simulations for large-scale and large-small scale fading channel environments using our proposed *FLS* approach against other common packet forwarding strategies.

10.1.1 Overview of Fuzzy Logic

The principles of *FL* and its application to real-world engineering problems have been well reviewed and studied [149-151], since being initially established as a field of genuine study, by L.Zadeh [152-153]. In [152-153], L.Zadeh argued that the majority of real-world decision making problems could not be assisted by completely formulating problems using either objective (i.e. use of mathematical models) or subjective (i.e. use of linguistic based rule systems) techniques, but that a combination of both methods of problem solving should be incorporated and utilised effectively. An example of this might be temperature control in a room, which could be objectively modelled but also subjectively perceived as being either “warm”, “hot” or “cool”.

In essence, *FL* principles [152-153] allow a logical and rational way in which both forms of problem solving can be coordinated jointly and effectively, in order to provide assistance in a decision making process to a realistic problem. The ability to map the objective world to the subjective way of thinking has been the key driver towards *FL* being adopted and used as decision making capability for a wide range of scenarios. In terms of our proposed decision making mechanism, the *TRC* metric and our subsequent analysis made on communication link reliability has so far been modelled objectively. However, the

behaviour of the realistic dynamic channel environment in real world terms could also be summarised subjectively. The mapping of this situation into a complete *FLS* for packet forwarding decision making can be neatly illustrated, as shown in figure 10.1. From figure 10.1, a *FLS* basically consists of three parts: *fuzzifier*, *rules-inference engine* and *defuzzifier* and an explanation of these operations is further expanded, in 10.1.2.

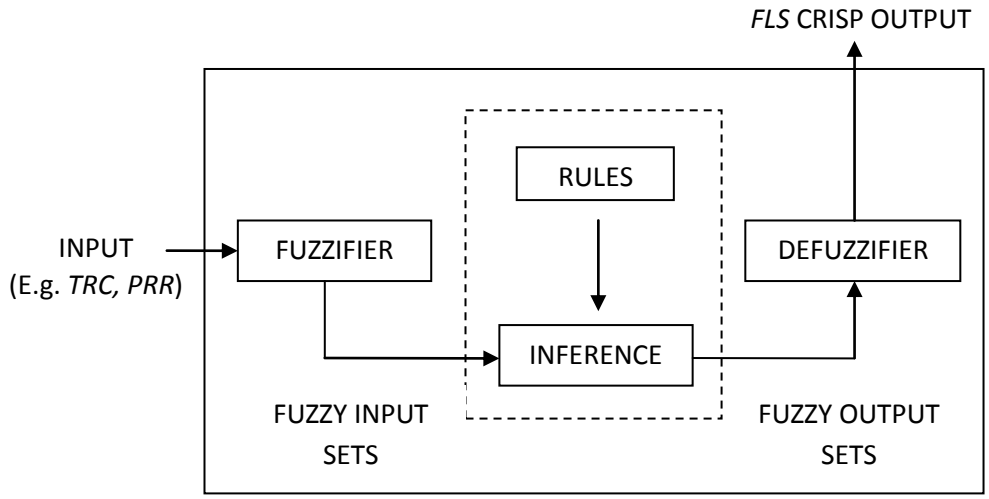

Figure 10.1: Fuzzy Logic System Architecture

10.1.2 Building Blocks of a Fuzzy Logic System

Here we detail the building blocks associated with using a *FLS* based decision making mechanism. As shown in figure 10.1, the *FLS* maps crisp inputs into crisp outputs. When a crisp input is applied to a *FLS*, the *inference engine* computes the output set corresponding to each *rule*. Rules form the heart of a *FLS* and maybe provided by experts or extracted from numerical data. Rules can be simply expressed as a collection of *IF-THEN* statements, forming an overall rule–base. The **IF**- part of a rule is its *antecedent* and the **THEN**- part of a rule is its *consequent*. Consider a type-1 *FLS* [151], having ***p'*** inputs and one output. Suppose that it has *M* rules, the l^{th} rule can then be expressed, as shown in (10.1).

$$\mathbf{R^l: IF\ x_1\ is\ F^l_1\ and\ x_2\ is\ F^l_2\ and\ ....and\ x_{p'}\ is\ F^l_p \quad THEN\ y\ is\ G^l,\ with\ } l = 1,.,M \qquad (10.1)$$

As shown in (10.1), $x_1 \ldots x_p$, are crisp inputs, representing the objective space while $F^l_1 \ldots F^l_p$ are linguistic variables representing the subjective space. G^l represents the subjective consequent of the eventual decision. All the rules are processed in a parallel manner by the inference engine. Any rule that fires, contributes to the final *FLS* decision solution space.

The degree of uncertainty associated with a received channel input is evaluated by the *fuzzification* process. A common *fuzzification* process used in *FLS's* is *singleton fuzzification* [152-153]. The uncertainty (fuzziness) is essentially characterised by fuzzy sets or *membership functions* (*MFs*), taking on values (degrees of membership) in the interval [0, 1]. Fuzzy sets, through its *MFs* are the mechanism through which the *FLS* interfaces with the outside world. The rule base then relates the input fuzzy variables with the output fuzzy variables using linguistic variables, each of which is described by a fuzzy set (*MF*) and a fuzzy implication operator (i.e. AND, OR etc.). The nature of the rule base determines how and which consequent output fuzzy set is then copied to the final fuzzy solution space (final decision outcome).

Defuzzification is the last process in a *FLS* and finds a crisp output value from the fuzzy output solution space, in order to determine the combined truth of the *antecedent* using *MINIMUM* or *MAXIMUM* functions. Common *defuzzification* methods include maximum, mean-of-maxima, centroid, centre-of-sums and centre-of-sets [154]. In our proposed design we focus on simplicity and therefore undertake *singleton defuzzification*, (centre of singleton method), which implies that the output fuzzy sets (*MFs*) are represented by single spikes (zero-order Sugeno fuzzy model) [154]. Therefore in this sense, each output *MF* assigns the value 1 to a single point and 0, to all other points. We consider this method since, it is both computational quicker and simpler to implement than the methods listed above, which is an added benefit operating within a varying channel environment.

The final crisp output (weighted average) to be used for the decision making process is calculated, as shown in (10.2).

$$\frac{\sum_{i=1}^{n} \mu(k_i) \times k_i}{\sum_{i=1}^{n} \mu(k_i)} \tag{10.2}$$

As shown in (10.2), n is the number of rules which are activated, $\mu\ (k_i)$ the specific maximum value of the input fuzzy set (*MF*) that has been activated by the rule base and k_i, the activated output rule singleton consequent value. The final crisp output given by the *FLS* after *defuzzification*, serves as a current reflection of the channel environment, for the purposes of facilitating packet forwarding decision making.

10.1.3 Channel Aware Fuzzy Logic Node Selection

In our proposed *FLS*, we setup fuzzy rules for adjusting hop node selection based on the following two channel aware *antecedents*:

1) ***Antecedent 1***. *TRC* (A measure of link reliability and quality as analysed in chapter 9, 9.2 and 9.3).
2) ***Antecedent 2***. *PRR* (A measure of only link reliability)

The linguistic variables used to represent the three distinct reception regions, both for the *TRC* and *PRR* input fuzzy sets are divided into three levels: ***low***, ***moderate*** and ***high***. A typical choice for input fuzzy sets are piecewise linear trapezoidal *MFs* to represent ***low*** and ***high*** and triangle *MFs* to represent ***moderate***, in the fuzzification process [154], as shown in figure 10.2. Figure 10.2, shows the domain of possible values that can be taken for either the *TRC* and *PRR*, determined by the channel parameters used in this section, as defined in table 9.1 and the analysis of the *TRC* made in chapter 9. In figure 10.2(a), $TRC_{Current}$ is calculated in the same way, as shown in (9.14) with $\gamma_{\text{-}Lower\text{-}dB}$ being replaced with the current received channel *SNR*, given by $\gamma_{dB}\ (d)$ calculation, as shown in (9.10).

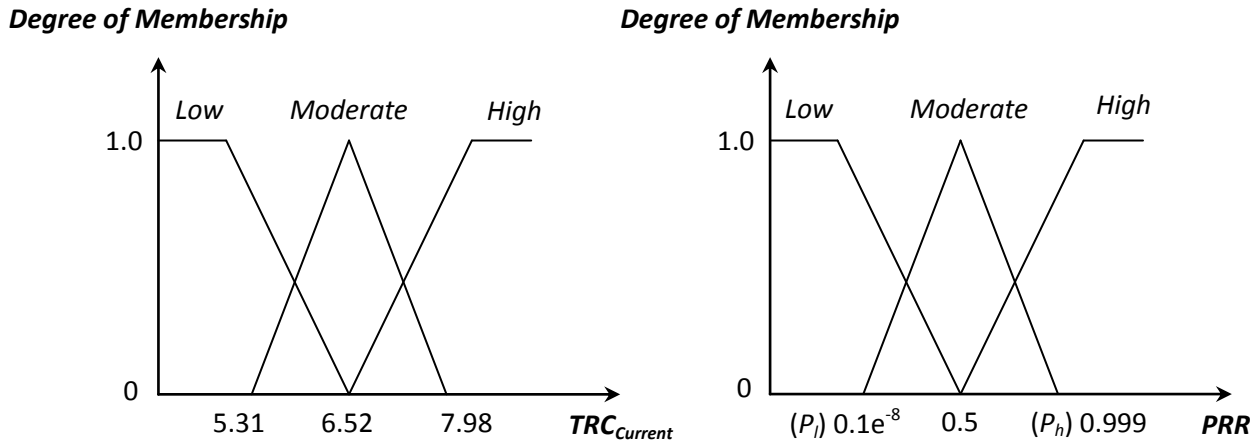

Figure 10.2: Membership Functions for (a) Antecedent 1 and (b) Antecedent 2

The output fuzzy *singleton consequent* sets, defining the possibility of a node being selected for packet forwarding, are divided into 5 levels, ***Very High***, ***High***, ***Medium***, ***Low*** and ***Very Low***. The overall rule base therefore needs to be setup with 9 rules (3^2), for the *FLS* because every antecedent has 3 fuzzy sets (*MFs*).

The design of the overall rule base is constructed utilising rules such as shown below:

IF *TRC is* ***High*** *and PRR is* ***Low***, ***THEN*** *Possibility for this node being selected is* _____.

As indicated in 9.2.2, our analytical observations suggest it is best to segregate the network according to link distance, in terms of d_{opt}, which is ultimately defined by the conditions of the operating channel environment (n and σ_{Shadow}). As suggested in 9.2.2, link distances, which are $\leq d_{opt}$ are best utilised if they can achieve a lower *TRC* and vice versa for link distances, which are $\geq d_{opt}$, in order to compensate for an increasing n and σ_{Shadow} channel environment. To address this leads us to draw up *consequents*, which reflect this channel environment defined condition, as summarised in table 10.1. Table 10.1, indicates our proposed rule base, in terms of individual *rules* and *consequents* used for packet forwarding node selection, based on d_{opt} and the *TRC* analysis made in chapter

9. As shown in table 10.1, an ideal desired node to be selected for packet forwarding should have a ***Low*** TRC and ***High*** PRR, for link distances $\leq d_{opt}$ and ***High*** TRC and ***High*** PRR, for link distances $\geq d_{opt}$.

Antecedent 1	***Antecedent 2***	***Consequent*** $\leq d_{opt}$	***Consequent*** $\geq d_{opt}$
Low	High	Very High	High
Low	Moderate	Medium	Medium
Low	Low	Low	Very Low
Moderate	High	High	High
Moderate	Moderate	Medium	Medium
Moderate	Low	Low	Low
High	High	High	Very High
High	Moderate	Medium	High
High	Low	Very Low	Low

Table 10.1: A summary of rules and consequents for packet forwarding node selection

Consequent output fuzzy set singleton values, as shown in table 10.1, are defined in terms of a percentage (%) and are assigned as follows: ***Very High*** (90), ***High*** (70), ***Medium*** (50), ***Low*** (30) and ***Very Low*** (10). Consequent output fuzzy set singleton values viewed in this sense implies for example, a node with a ***Low*** *TRC* and ***High*** *PRR* has a defined 90% possibility of being selected for packet forwarding, as detailed in table 10.1, for link distances $\leq d_{opt}$.

10.1.4 Channel Aware Fuzzy Logic System Performance

Simulations have been conducted in order to show the benefits, which can be achieved using our proposed channel aware *FLS* decision making mechanism. Performance of our proposed *FLS* design is evaluated in terms of *throughput* (packets received at destination/simulation time (sec)) and average communication energy consumption (Total energy consumed/number of deployed nodes). Simulations are conducted using the OMNeT++ network modeller tool [63]. To simulate a realistic wide area *UGS* surveillance setting, a 1km by 1km simulation region is specified, with nodes being randomly deployed according to a uniform distribution.

As part of our evaluation we do not consider the effects of increasing node density on throughput and communication energy consumption performance and so for the purposes of simulation, an arbitrary total of **40** nodes are used, with communication parameters as specified in table 9.1. We assume that each node is aware of their and neighbour geographic position coordinates. Simulations are conducted using a multi-hop network scenario, with a single source-destination pair. The source node generates packets to be forwarded according to a Bernoulli trial, with a set constant probability of success, *Bernoulli-p*, meaning that each trial outcome is 1 for *Bernoulli-p* and 0 for (1 – *Bernoulli-p*).

To provide up to date route maintenance and relevant channel aware link reliability readings for the *FLS*, a local refresh mechanism is adopted, where each node broadcasts a **HELLO** message at regular intervals. **HELLO** messages are used in order to serve as a refresh mechanism, concerning the changing topology of the network, so that relevant decisions on node selection for packet forwarding can be made. Node selection however, brings to the fore the concept of neighbour classification based on the *FLS* crisp output. In this sense, some neighbours may be more favourable to choose than others; therefore using schemes such as *blacklisting* (*neighbour selection*) [155] may be needed to avoid "weak links".

A possible way of making a distinction between "weak" and "good" is to utilise only *FLS* output values, which are greater than a certain threshold (*Blacklist Value*). To discover the possibilities of *blacklisting*, for the channel environment studied, simulations for a high traffic scenario (high *Bernoulli-p* value) are conducted, with respect to a set *Blacklist Value*, as shown in figure 10.3. Simulations are run for a total of 200 Bernoulli trials, with random node topology configurations, *Bernoulli-p* = 0.9, n = 4 and σ_{Shadow} = 4dB channel conditions.

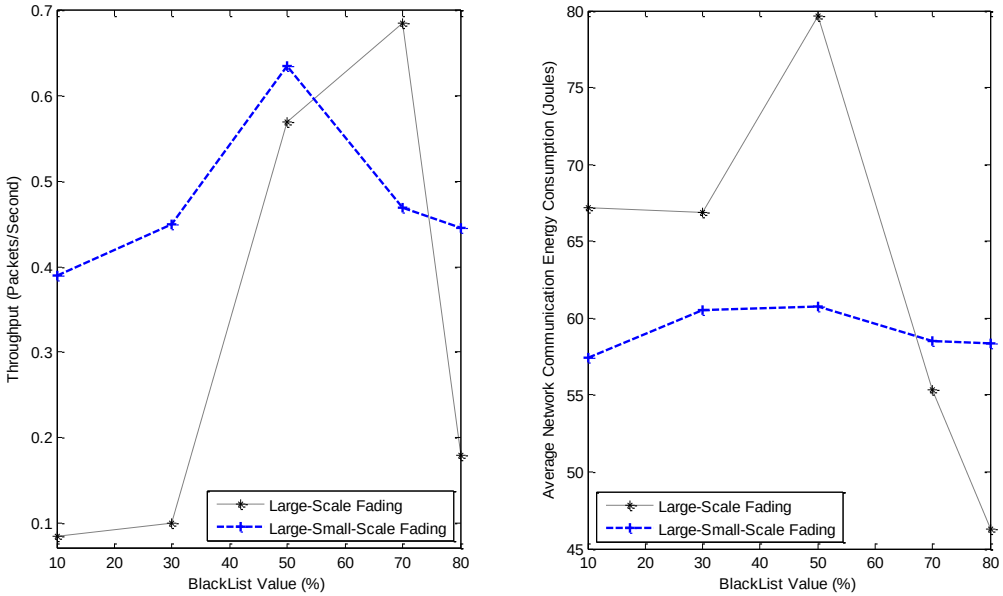

Figure 10.3: The effect of blacklisting on throughput and average network communication energy consumption

As can be seen from figure 10.3, the throughput of packets being received at the destination can be increased as a higher *Blacklist Value* is set, but only up to a certain value. For the large-small-scale channel fading propagation environment, figure 10.3 suggests *FLS* crisp output values > 50% could be used, while for the large-scale fading environments *FLS* crisp output values > 70% could be considered. Rather than *Blacklist FLS* crisp output values based on a single value, a range of values should be considered, in order to appropriately fit both types of channel propagation environments. Node selection for packet forwarding purposes, therefore should be made on the basis of *FLS* crisp outputs which are > 50% (lower limit) but are < 80% (upper limit), in order to achieve better throughput and minimise on communication energy consumption, as indicated in figure 10.3.

For the purposes of comparing our proposed *FLS* approach, we rely on simple packet forwarding strategies which are either distant based or reception based techniques. In distance-based policies, nodes need to know only the distance to their neighbours. In reception-based policies, in addition to the link distance, nodes need to know also the *PRR*

or *SNR* of their neighbour link states. Two common schemes, which cover the simple packet forwarding techniques discussed above and used for comparison purposes, are detailed below:

- Most Forward with Fixed Radius *(MFR)* [156]. *MFR* is a pragmatic single path packet forwarding strategy relying on neighbouring nodes which are only closest to the destination. In this sense *MFR* is a shortest path scheme using a strategy on minimising the number of hops required to the destination, in order to ensure high spatial reuse (bandwidth) efficiency.
- Nearest with Forward Progress *(NFP)* [157]. *NFP* is a simple best reception neighbour strategy, where each node forwards to the neighbour that has the highest *PRR* and is closer to the destination. *NFP* is again a shortest path scheme but incorporates a simple path loss link reliability dependent metric, within its decision making routine.

All the techniques discussed above rely on packet forwarding to the node closest to the destination, among their remaining neighbours, with *MFR* however being the most aggressive, but not including any channel aware metrics. To evaluate our proposed *FLS* design, it is also integrated within the *NFP* strategy, in order to substantiate whether any improvements can be gained over just using a simple *PRR* metric. An evaluation is also considered against the *ETX* metric, introduced in chapter 9, whose analysis under different channel environments using the *TRC* metric formed the basis towards our eventual proposed *FLS* design. This evaluation will hopefully seek to insure whether the analytical observations made in 9.2.4, which have been incorporated into our *FLS* design, are indeed correct. The overall flow chart algorithm illustrating the *FLS* strategy in selecting nodes for packet forwarding, is detailed in, **Appendix C, part 1**. In figures 10.4 and 10.5, the throughput and communication energy consumption performance for the above mentioned schemes and our *FLS* system are shown. The same energy consumption model is used as already described in section 1, under heading 4.4.3.

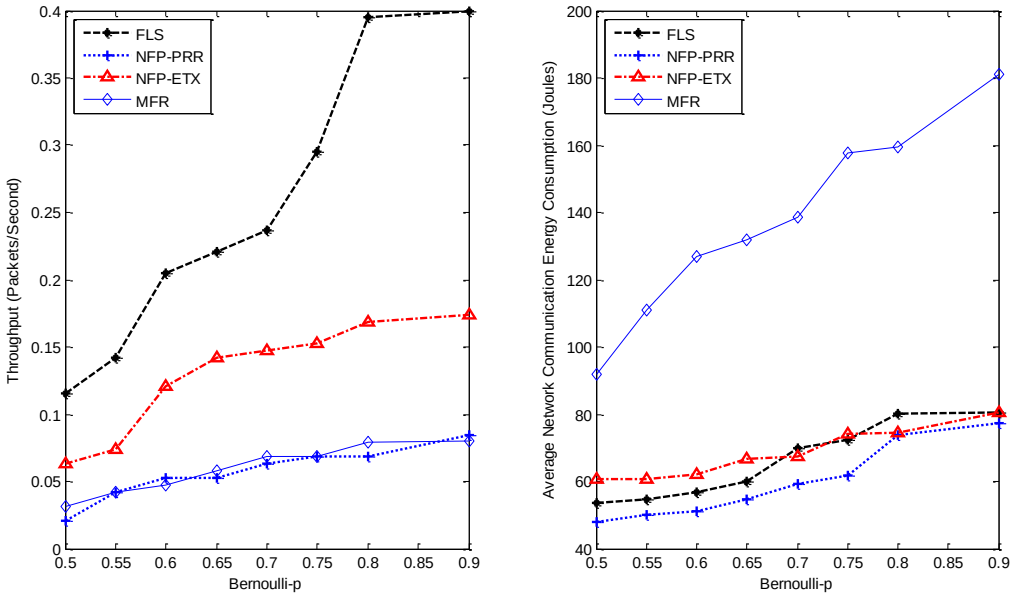

Figure 10.4: Large-scale fading, channel environment conditions n =4, σ_{Shadow} = 4dB

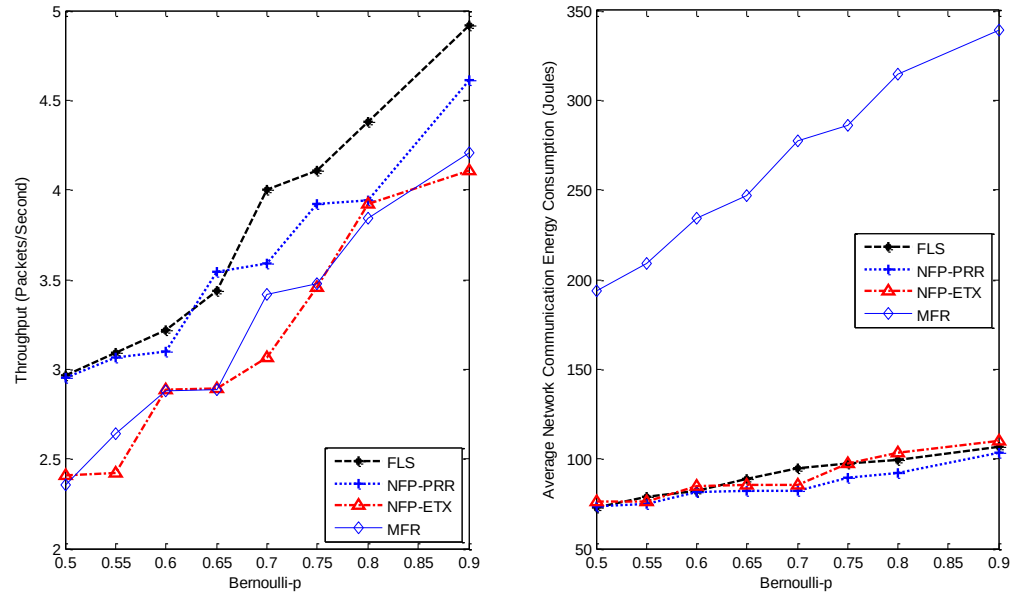

Figure 10.5: Large-small-scale fading, channel environment conditions n =4, σ_{Shadow} = 8dB

Figures 10.4 and 10.5 indicate that packet forwarding strategies, which incorporate knowledge of the communication link environment, as shown with our *FLS*, *NFP-PRR* and *NFP-ETX* can provide improved throughput and communication energy performance under different channel fading scenarios. As expected the *MFR* strategy performs the worst in both types of channel fading scenarios, when compared with all packet forwarding

strategies, as shown in figures 10.4 and 10.5. This is primarily because minimising on hop count entails using forwarding nodes, which are over longer communication link distances and therefore become more susceptible to channel variations, resulting in increased packet retransmissions and increased communication energy expenditure, with traffic intensity.

From figures 10.4 and 10.5, *FLS*, *NFP-PRR* and *NFP-ETX* all have similar communication energy expenditure profiles, for the different traffic condition scenarios (Bernoulli-p) used. The *FLS* strategy however, outperforms on throughput performance against the alternative forwarding schemes in all cases, as shown in figures 10.4 and 10.5. An efficient *UGS* network is also one in that can pass as many packets as possible (higher throughput), while minimising the energy consumption burden. From figures 10.4 and 10.5 for conditions with Bernoulli-p > 0.7, our proposed *FLS* scheme can increase the throughput performance whilst maintain a consistent communication energy consumption performance under the simulated channel environment scenario. This leads us to suggest that our proposed *FLS* strategy, under the simulated scenario, can support the throughput-energy efficiency requirement.

There are two reasons for this. Firstly, the *FLS* strategy utilises the broadcast medium to encourage opportunistic forwarding, thus increasing the chance a packet is received at the destination via diversification of routes used (selection diversity), which assists on increasing throughput and reducing the need for consuming further communication energy. Secondly, by segregating the network according to d_{opt} and incorporating both the *TRC* metric and *PRR*, as shown in table 10.1, the *FLS* strategy can increase a nodes ability to make better decisions as to selecting nodes for packet forwarding. In addition, it is also worth noting how all strategies can achieve better throughput performance levels, in channel environments with a higher σ_{Shadow}. This result seems to agree with the analysis made in chapter 9, under 9.2.2 and also, as shown in figure 9.7 (b).

10.2 Genetic Adaptive Fuzzy Logic Hop Selection Scheme

One of the most important considerations to be made in the application and use of *FL* is the accurate derivation of both the rules to be used in the rule base and their corresponding *MFs*. Both play a crucial role in overall *FLS* performance, so it becomes important to both derive and adjust these parameters accurately to the process being controlled, which in our scenario entails ensuring the best decision, as to node selection for packet forwarding, is achieved.

The derivation of *FLS* rule base parameters can be commonly performed using learning based techniques [149] [151], while the adjustments of *MF* parameters are best performed using tuning based techniques [158]. In a learning process, rules and corresponding *MF's* are directly obtained by learning from available measurement data concerning the control process. Tuning based processes assume there is already an existing rule base and *MF* definition present. Our proposed *FLS* design highlighted in 10.1 uses rules and *MF's* that have been defined by us, as shown in table 10.1 and figure 10.1, which has been made possible, based on the analysis made in chapter 9. In this sense, our proposed *FLS* is typically classified as an expert based system and so a prime candidate for a tuning process where parameters of the rule base and corresponding *MFs* can be adjusted, in order to improve on overall *FLS* control performance [159].

In 10.2, an improvement on our initial *FLS* detailed in 10.1 is considered, in order to allow the *FLS* to automatically adapt their *MF* parameters by means of a genetic algorithm (*GA*) according to, the current channel environment. The tuning of input *MF's*, as illustrated in figure 10.2, is important since these serve as an interface to and representation of the channel environment dynamics, for our *FLS* inference engine. Adjusting the *MF's* would therefore improve on the overall *fuzzification* process whose primary operation as discussed earlier, is to determine the degree of uncertainty present within the channel

environment, so that decisions concerning the most reliable node for packet forwarding can be made and selected. In 10.2.1, we begin by providing an overview to *GAs* and their functionality. In 10.2.2, we then introduce our proposed genetic adaptive *FLS* architecture and in 10.2.3, we again perform simulations for large-scale and large-small scale fading channel environments using our proposed genetic adaptive *FLS* approach and compare this against, our non-genetic adaptive *FLS* operation.

10.2.1 Genetic Algorithms

The tuning of *FLS MF's* can be considered as an optimisation or search process. A *GA* is a search algorithm, widely known to be capable of finding near optimal solutions in complex search spaces [159-160]. *Genetic algorithms* use operations found in natural genetics, which guide the process through a search space. The use of natural genetic techniques follows the "*survival of the fittest strategy*", whereby the fittest individuals of any population tend to reproduce and survive to the next generation, thus improving on the quality of successive generations [159]. The main components involved in a *GA* are the *initial population, fitness function, selection, reproduction* each of which is expanded below:

- *Initial Population* represents the initial set of randomly generated solutions after which these will be recombined to obtain further new generations. A random initial population set assures diversity and avoids bias. In our case, the initial population is randomly generated according to the initial *MF* parameters being used, as shown in figure 10.2. An individual population member is labelled as a *chromosome* and is used to reflect a set of possible initial *MF* parameter values that have been undertaken within a population set.

- *Fitness Function* is used to determine a fitness value for each respective *chromosome* within the initial population set. Determining a fitness function value allows the *selection* process to choose *chromosomes*, which should be used to form further new generations. In our case the fitness value for each chromosome is calculated using the common absolute square error (*ASE*) measure, as shown in (10.3), where $F(x^l)$ is the crisp output value obtained from the *FLS*, when the l^{th} chromosome is considered, using the current received channel reliability values (*TRC* and *PRR*) and y^l being the known desired output.

$$ASE_l = (F(x^l) - y^l)^2 \tag{10.3}$$

- *Selection* of a *chromosome* to produce successive generations plays an extremely important role in a *GA*, since this allows fitter generations to be achieved. A common selection approach is to assign a probability of selection, P_j, to each respective *chromosome*, as shown in (10.4) [162].

$$P_j = \frac{ASE_l}{\sum_{l}^{N} ASE_l} \tag{10.4}$$

As shown in (10.4), P_j is a ratio measure of a *chromosome's* own calculated fitness value, compared with the whole population of size *N* (fitness proportionate selection). A *chromosome* that has the most minimum value (i.e. lowest error) within the population set would then be selected, since this represents the current fittest *MF* parameter values, within a current generation. In order to avoid the local minima condition, only the two fittest *chromosomes* are selected for the *reproduction* operation.

- *Reproduction* entails both a *crossover* and *mutation* operation. The two fittest *chromosomes*, which have been selected, are crossed over in order to generate new *chromosomes* for the next generation. Several types of *crossover* operators can be used [39-40] but in our design we employ a one-point *crossover* operation, implying each

chromosome is split from its middle point, with the latter half being swapped between each *chromosome*. *Mutation* is used to provide increased diversity within the new chromosome, so that the *GA* may search broader spaces. This prevents *chromosomes* becoming too similar to each other, avoiding local minima, which can limit further evolution. Mutation in our case means adding a small random value to each *MF* parameter value, contained within the new *chromosome*.

The complete *GA* process for searching optimal input *MF* parameters is shown in **Appendix C, part 2**. The decision to terminate the *GA* is usually defined after a fixed number of generations have passed. Subsequently, the best *chromosome* is then selected containing the final input *MF* parameters to be used by the *FLS*, as described above using (10.4).

10.2.2 Genetic Adaptive Channel Aware Node Selection

The overall genetic adaptive *FLS (GAFLS)* for selecting packet forwarding nodes is shown in figure 10.6. From figure 10.6, the *GA* operation works as a stand-alone module providing adjusted *MF* parameters to be used by the inference engine. For the purposes of selecting nodes for packet forwarding the *GA* functionality module works in an offline manner. This means the *GA* searches for optimal *MF's* parameters according to current received channel reliability metrics (*TRC* and *PRR*), whilst applying the normal *FLS* operation. Upon termination, the *GA* comes back online in order to provide the final adjusted *MF* parameters to the inference engine, so that a node selection decision can be made.

The adjusted parameters thus vary the shape of the input *MF's* to reflect on current received channel reliability and as such influencing overall *FLS* performance. As shown in (10.3) calculating the fitness function value for each respective *chromosome* requires the *ASE* function to have a known desired output. For the purposes of node selection the

desired output y^l, is evaluated in terms of the three distinct reception regions (Disconnected, Transitional, and Connected) and the *TRC* metric, as outlined further in **Appendix C, part 3.**

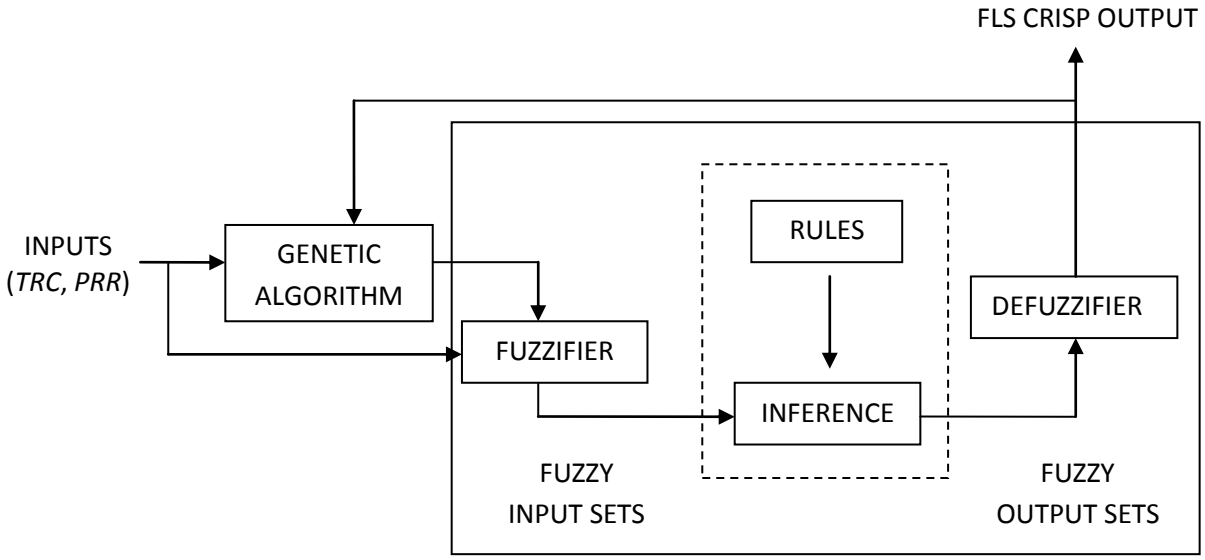

Figure 10.6: Genetic Adaptive FLS Architecture

10.2.3 Channel Aware Genetic Adaptive Fuzzy Logic System Performance

For the purposes of evaluating our genetic adaptive fuzzy logic system the same setup as described in 10.1.4 is used, with a direct comparison made with non-genetic adaptive *FLS* operation, in order to gauge the level of improvement in throughput and communication energy consumption that can be achieved. Again we do not consider the effects of node density, but we are interested in how the *FLS* and genetic adaptive *FLS* perform, within a large-scale and large-small-scale fading setting, under similar n and different σ_{Shadow} channel environments. The focus is on *FLS* and genetic adaptive *FLS* performance in different channel environments, which can help to ascertain if adapting *FLS MF's* to current channel characteristics can indeed improve performance. The energy packet delivery consumption (*EPDC*) is considered as the main performance metric in evaluating performance. The *EPDC* metric can help to establish the average

amount of network communication energy consumed for every packet received at the destination. This is useful, in order to consolidate both throughput and energy consumption performances into a single metric, as shown in (10.5).

$$EPDC = \frac{Average\ Network\ Communication\ Energy\ Consumed}{Total\ Packets\ Received} \tag{10.5}$$

As shown in (10.5), a lower *EPDC* value would therefore imply a better and more energy efficient performance gain, since less communication energy is being consumed for delivering more packets to a destination.

For the *GA* operation, having too large an initial population set can give rise to longer computation periods, since the fitness function and genetic operator's would have to be evaluated at each generation [162]. For our performance evaluation we limit the initial population set to just 50 *chromosome* members. In addition, since *genetic algorithms* normally show very fast initial convergence, followed by progressively smaller improvements [162], the decision to terminate the *GA* is placed after completing only 50 generation cycles. Figures 10.7 to 10.12 illustrate throughput and *EPDC* performances for our *FLS* and genetic adaptive *FLS* operations respectively.

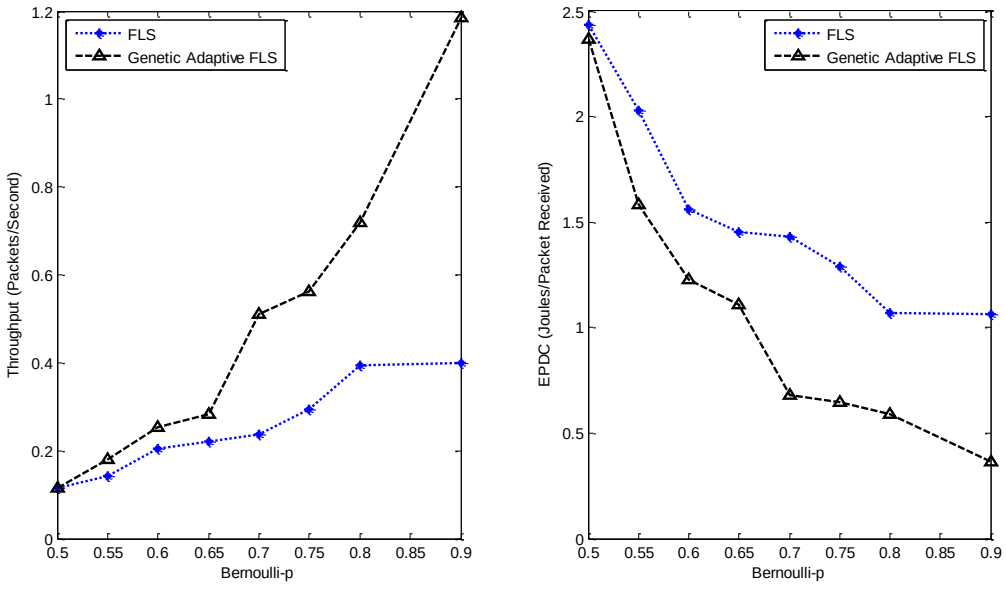

Figure 10.7: Large-scale fading, channel environment conditions n =4, σ_{Shadow} = 4dB

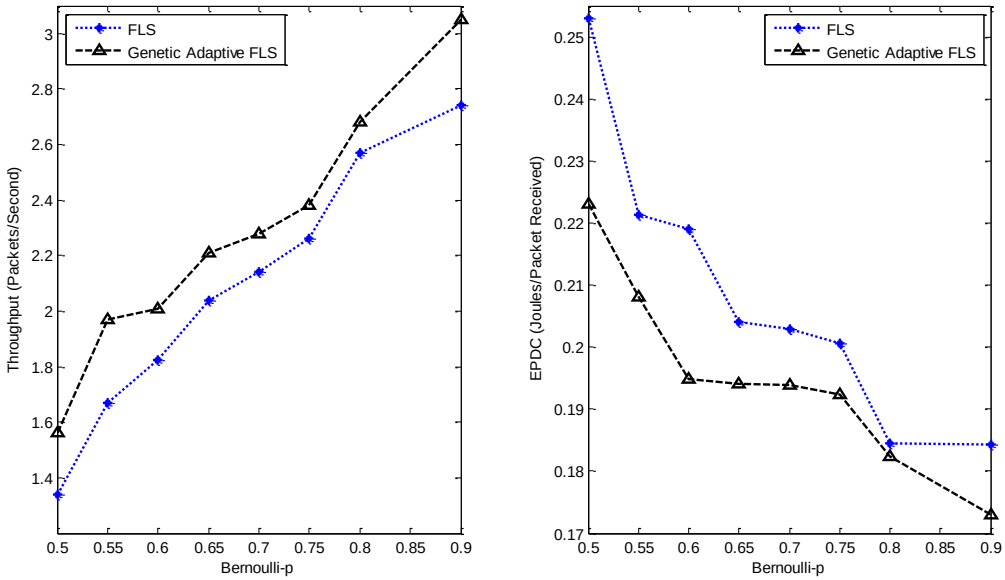

Figure 10.8: Large-small-scale fading, channel environment conditions n=4, σ_{Shadow} = 4dB

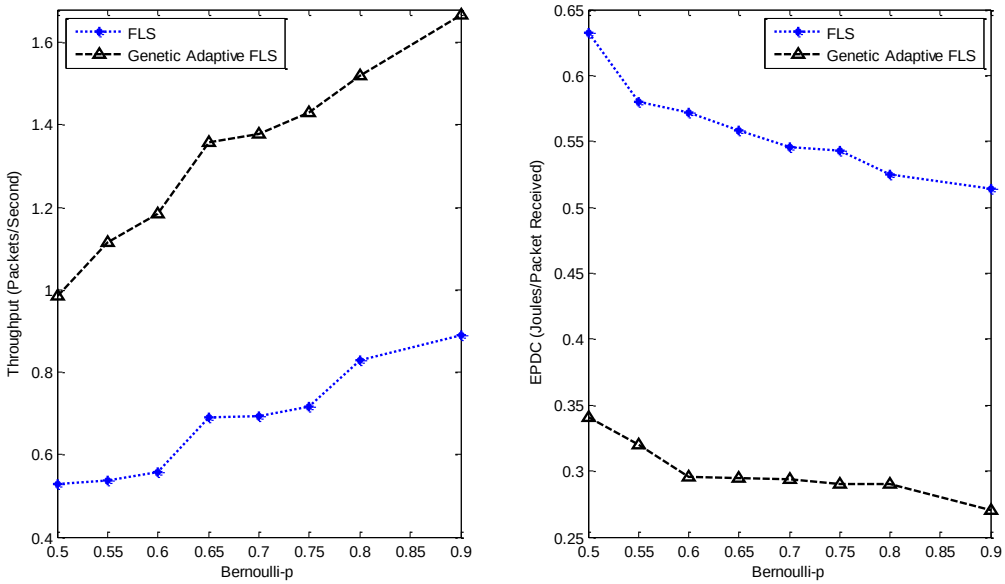

Figure 10.9: Large-scale fading, channel environment conditions n =4, σ_{Shadow} = 8dB

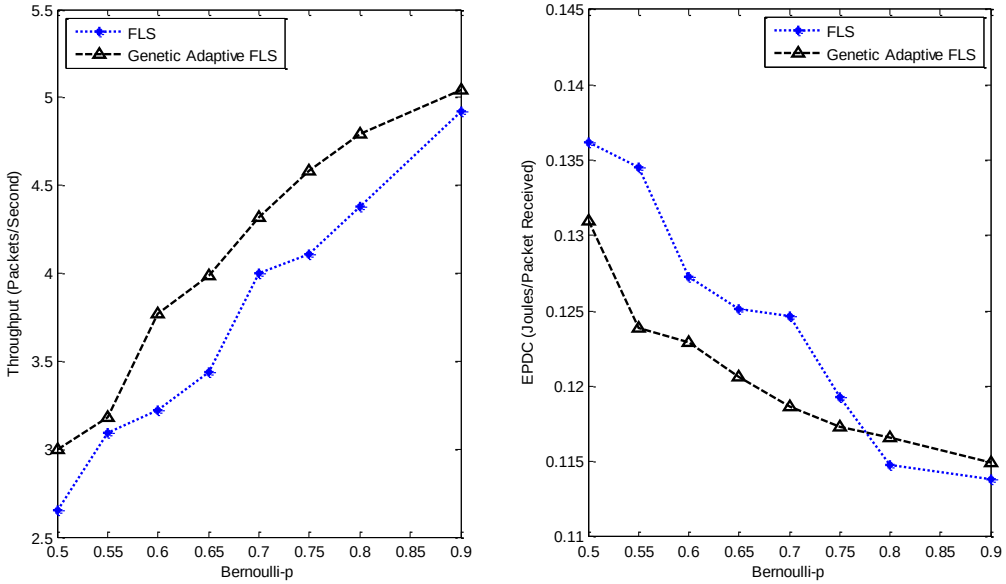

Figure 10.10: Large-small-scale fading, channel environment conditions n =4, σ_{Shadow} = 8dB

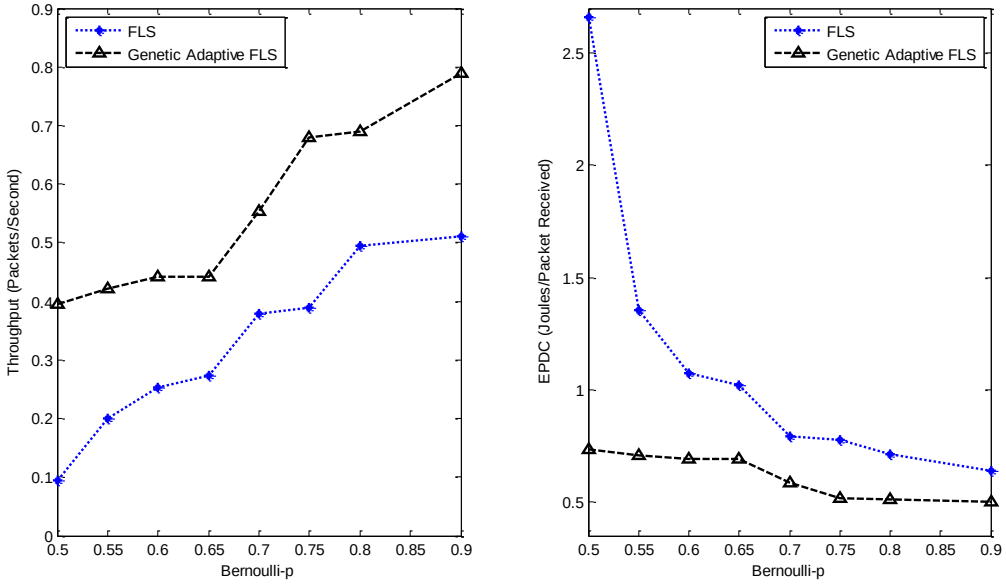

Figure 10.11: Large-scale fading, channel environment conditions n =4.5, σ_{Shadow} = 4dB

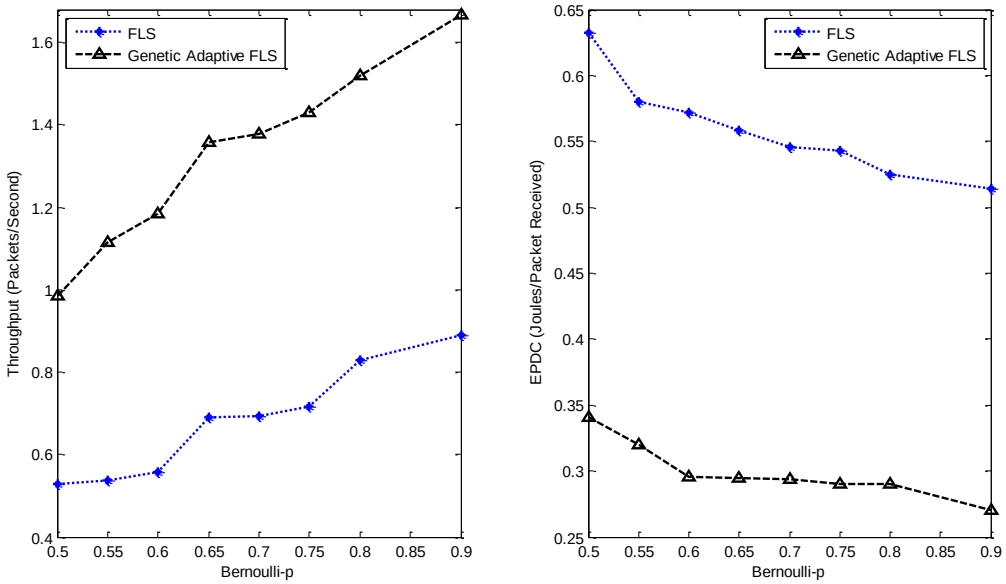

Figure 10.12: Large-small-scale fading, channel environment conditions n =4.5, σ_{Shadow} = 8dB

As shown in figures 10.7 to 10.10, under different channel fading propagation environments but with the same *n* and σ_{Shadow}, the genetic adaptive *FLS* system can achieve a better performance over normal *FLS* operation, in terms of throughput and *EPDC*. This indicates a genetic adaptive *FLS* system, has potential to improve a nodes decision making capability and adaptability towards a varying, uncertain channel environment, under various traffic intensity conditions. This is confirmed again when using a different path loss exponent of *n* = 4.5 and σ_{Shadow} values, as shown in figures 10.11 and 10.12.

From figures 10.7 to 10.12, results indicate that applying a *GA* to search for optimal *MF* parameters according to current received channel reliability metrics (*TRC* and *PRR*), whilst continuing the normal *FLS* operation, can further improve on both throughput (transmission reliability) and *EPDC* performance. In addition, the genetic adaptive *FLS* would also continue to segregate communication links according to d_{opt}, as shown in table

10.1. This leads us to consider when combining both a genetic adaptive capability to vary *FLS MF* parameters and to enforce node selection according to d_{opt}, can support better throughput and *EPDC* performance. Figures 10.7 to 10.12 also show that a genetic adaptive *FLS* can increase throughput performance and at the same time consume on average less energy for every packet received, as traffic intensity conditions increase, when compared with normal *FLS* operation by some 44%. For the simulated network scenario, this indicates that the genetic adaptive *FLS* system can achieve improved energy-load balancing. Improvement in energy-load balancing is possible since, a genetic adaptive *FLS* system would actively seek to identify links opportunistically, which exhibit a higher *TRC* according to its adapted *MF's*, to increase performance over normal *FLS* operation.

An additional observation from figures 10.10, 10.11 and 10.12, when compared with figures 10.7, 10.8 and 10.9, shows the effect of the large-small-scale channel fading environment on improving throughput on average by 17% and *EPDC* performance on average by 40%. Operating in a large-small-scale channel fading environment, which would typically be a similar wireless environment to be found in a realistic *UGS* surveillance setting, can assist in increasing throughput and reducing *EPDC* further. The effects of a large-small-scale channel fading environment suggests it can naturally encourage better *opportunistic* forwarding selection and therefore, encourage a higher chance of successful packet reception, but without some further investigation this finding cannot be made completely conclusive.

CHAPTER 11

Section 3: Summary and Conclusions

UGS networks typically operate in wireless environments, which can vary considerably in both space and time, due to channel fading propagation effects. Chapter 9 began by quantifying the channel fading propagation effects, in terms of being either large-scale or large-small-scale fading. Channel fading effects can determine the success in packet reception, which as a result can influence communication link reliability between node pairs, communication energy consumption and overall network throughput. It is also shown that mitigating on the effects of communication link unreliability can be assisted by dividing packet reception into three distinct reception regions, these being connected, transitional and disconnected, according to link distance.

In 9.2, we then introduced the transitional region, which is characterised by asymmetric connectivity with high variance in *PRR*. We then quantified the size of the transitional region by defining a known metric called the *TRC*. The *TRC* in its own right can serve as a value of merit for current link reliability, by giving an indication of the extent of the transitional to connected region parts of a communication link. The *TRC*, as expected is effected by the channel environment conditions, with σ_{shadow} increasing *TRC* and *n* reducing the *TRC*, as shown in figure 9.5.

One of the main contributions of this chapter was then to study, understand and examine what impact the *TRC* might have on communication link reliability, in terms of the optimal packet forwarding distance (d_{opt}), transmission reliability and *ETX*, within different channel fading environments. In headings 9.2.2 to 9.2.4, we analysed how communication link reliability and link quality (*ETX* metric) performance can be affected

by the *TRC* within different channel environments, which the main findings are summarised as follows:

- In 9.2.2, a higher *TRC* can increase d_{opt} by maximising *E [PRR]* for a set channel environment, as shown in figure 9.6 and for various σ_{shadow}, as shown in figure 9.7(b). These findings indicate that a higher *TRC* could potentially compensate for an unreliable wireless environment, through achieving a better *E [PRR]* range, with a lower decay rate from d_{opt} to d_{max}, as shown in figure 9.7 (b).

- In 9.2.3, a lower *TRC* achieves better transmission reliability performance over shorter communication link distances and this is reversed for a small gain in performance over larger distances, as shown in figure 9.9. A lower *TRC* should be used for channel environments with an increasing *n* and higher *TRC* for increasing σ_{shadow}, as shown in figure 9.10.

- In 9.2.4, a higher *TRC* value can minimise on *ETX*, over larger communication link distances through maintaining the same P_h ($\gamma_{\text{-Upper-dB}}$) value and lowering the P_l ($\gamma_{\text{-Lower-dB}}$) value. Over shorter hop-distances increasing the *TRC* has no effect on minimising *ETX*, but remains in an ideal state. Figure 9.12, also indicates that increasing the *TRC* can however mitigate on channel environment conditions with increasing *n* and σ_{shadow}, over longer hop-distances for improved *ETX* performance.

The findings from above lead us to suggest that potential packet forwarding nodes can be best achieved through identifying links with a higher *TRC* value, due to a higher *E[PRR]* range and better *ETX* performance (whilst maintaining a fixed P_h value). However over shorter hop distances ($\leq d_{opt}$), we conclude that identifying links with a lower *TRC* are given priority since this achieves better transmission reliability, while maintaining an ideal *ETX*.

As a matter of further reassurance in 9.3, the impact of the *TRC* on further reducing the number of transmissions required for successful packet delivery within a realistic wireless broadcast environment is detailed. We considered the broadcast environment since this has the advantage of allowing multiple paths (diversity) from a source towards a destination to exist. In 9.3, we explored the idea behind *OAPF* as a potential way to further reducing the number of transmissions required for successful packet reception and therefore as a means of mitigating against the unreliable channel environment, to inflict changes on local topology. *OAPF*, through the *EAX* metric, considers the broadcast nature of wireless channel transmissions as opportunities that can be taken advantage of in a distributed manner, so as to increase the chance a packet is received successfully towards its destination. Utilising a distributed hop-by-hop strategy for packet forwarding in this manner can also offer advantages by firstly, being easier to implement and secondly in achieving network scalability, which are important attributes required for *UGS* surveillance operations. The main findings of whether combining the *TRC* within an *OAPF* environment can affect the number of transmissions required for successful packet delivery for a 2-hop scenario, are summarised below:

- Our analytical findings indicate that utilising a higher *TRC* through varying P_l ($\gamma_{\text{-Lower-dB}}$) with a set P_h ($\gamma_{\text{-Upper-dB}}$) value within an *OAPF* environment, can indeed achieve better *ETX* performance.
- We also conclude that the number of transmissions required for a successful packet delivery is improved within an *OAPF* (*EAX* metric) environment against *ETX* over higher transmission ranges, as shown in figure 9.13.
- Increasing the forwarding selection diversity (number of nodes deployed between a source and destination), can also help to reduce the number of transmissions required for successful packet delivery. This finding suggests that permitting nodes to decide, packet forwarding actions based on link reliability knowledge of multiple relay paths,

in a distributed manner, can assist in providing robustness against communication link unreliability.

In general, utilising the broadcast transmission channel to select nodes opportunistically assists in reducing the number of transmissions required for successful packet reception and subsequently, can help to mitigate the effects of communication link unreliability further.

Based on the *TRC* study made in chapter 9, under 9.3 and 9.4, the second main contribution of this chapter was to bring these findings together into an overall decision making mechanism, in order to cater against the effects of the channel fading environment. Such a mechanism would then allow *UGS* nodes to evaluate and select nodes for reliable packet forwarding, in a distributed manner. For this purpose a *FLS* system is used and deemed suitable because of its ability to assist in making decisions within high uncertainty environments, similar to channel fading, as described in chapter 10, under 10.1.

Normal *FLS* operation performance can also be improved by providing a mechanism, which can adjust to the channel environment, in order to make decision making relevant to a current underlying channel environment. For this purpose a *GA* is implemented and integrated within normal *FLS* operation, in order to provide adaptability to the channel environment, as detailed in section 4.6 and shown in figure 10.6. Simulation results conducted under different channel fading environments indicate that for a Genetic adaptive *FLS* operation an improvement is indeed made, in terms of throughput and *EDPC* over normal *FLS* operation. An improvement is possible since, a genetic adaptive *FLS* system would actively seek to identify links opportunistically, which exhibit either a lower *TRC* (if $\leq d_{opt}$) or higher *TRC* (if $\geq d_{opt}$) according to its adapted *MF's*, to increase performance over normal *FLS* operation.

In summary, results for the simulated network scenario made in 10.2.3, suggest utilising a genetic adaptive *FLS* has potential to provide the following advantages:

- A fully distributed approach, where each *UGS* node only needs to evaluate its network link quality values (*TRC* and *PRR*) and apply the genetic adaptive *FLS* system, for packet forwarding node selection.
- A genetic adaptive *FLS* can therefore allow *UGS* nodes to make relevant self-managed decisions on, which one-hop neighbour should be chosen for reliable packet forwarding at discrete points in time.

In addition, findings from this section show that a genetic adaptive *FLS* scheme has potential to improve distributed surveillance missions by allowing it to be integrated with, upper-layer operations. In this way, advantages within an unreliable communication environment can be achieved in the following way:

- Only a reduced number of nodes (**those with good channel reliability**) will be competing for available bandwidth, which can help to increase network throughput, but with lower communication energy consumption.

It is important to also note that the computational expense of applying a genetic adaptive *FLS* on every packet received has not been evaluated. This of course will be very high given the nature of using a genetic optimiser [162] and as a result, will contribute towards increasing overall energy consumption and a reduction in network longevity which may prove to be impractical, given the nature of *UGS* deployment.

In section 4, however, we continue to investigate whether the use of channel reliability information from the physical layer that is processed using our genetic adaptive *FLS* scheme and then shared with both the application (VIGILANT^{+}) and network layers (*SWOB* geographic routing), can assist their respective procedures and improve on overall distributed operation within an unreliable wireless channel environment.

SECTION 4

Integrated System Performance

Introduction

Unattended ground sensor (*UGS*) networks are classified as distributed systems, capable of supporting mission objectives such as, threat presence detection and geo-location within a security-sensitive region. Our performance appraisals concerning distributed mission objective operation, as detailed in sections 1 and 2 have, thus far, been evaluated under error free wireless channel conditions (physical environment). For an overall performance viewpoint, *UGS* networks should ultimately be assessed as distributed systems, operating within both their deployed surveillance and physical environment. *UGS* networks, which are assessed in this manner, are commonly referred to as mission orientated sensor networks (MOSN) [163]. A mission orientated capability is an important attribute to have, since, the notion of self-reconfigurable *UGS* networks capable of fulfilling mission objective requirements within an uncertain physical environment, is supported [163-166]. As a result of mission orientated operation, *UGS* networks can ensure that a dependable infrastructure for information collection is available.

The purpose of section 4, is to evaluate a potential mission orientation capability, through the integration of our genetic adaptive fuzzy logic system (*GAFLS*), detailed in section 3, with VIGILANT^{+}, detailed in section 1 and *SWOB*, detailed in section 2. Our proposed mission orientated approach can be summarised, as shown in figure 12.1. From figure 12.1, a potential cross-layer approach towards enabling *UGS* surveillance operations within a dynamic mission-orientated environment, is illustrated. In essence, the *GAFLS* mechanism is responsible for providing reliable forwarding node selection knowledge to

support both VIGILANT^{+} and *SWOB* functionalities. In this way, our aim for this section is to assess whether our *GAFLS* can indeed provide the necessary adaption towards an unreliable wireless channel environment, in order to ensure dependable mission objective information collection and reliable information query routing.

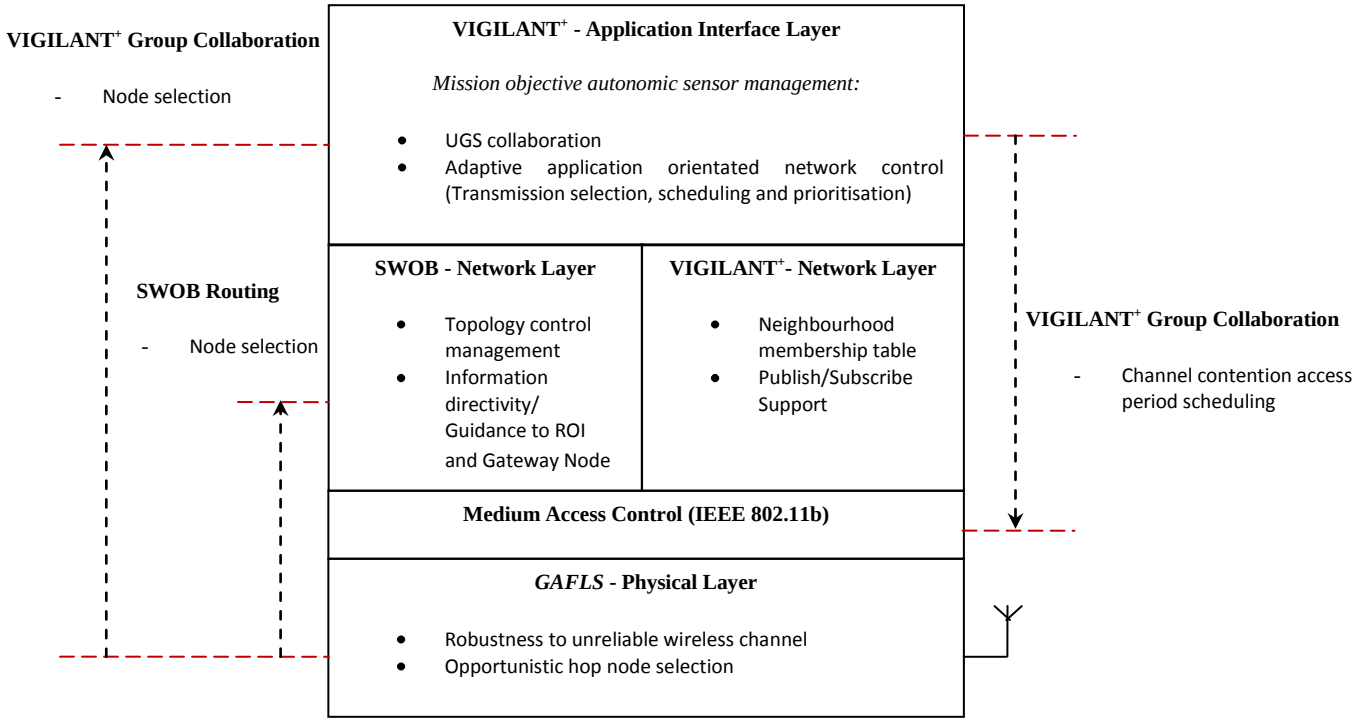

Figure 12.1: Proposed mission orientated capability for UGS surveillance operations

In this section, chapter 12 provides performance results of our proposed mission orientated capability, as shown in figure 12.1, within a dynamic threat monitoring and wireless channel environment, as follows:

- In 12.1, we highlight the performance results of our joint VIGILANT^{+} and *GAFLS* functionality, within a dynamic threat situation, for different large-scale and large-small-scale channel fading settings. In 12.3, our aim is therefore to assess whether our *GAFLS* can indeed provide the necessary adaption towards the unreliable wireless

channel environment, in order to ensure dependable mission objective information collection.

- In 12.2, a similar exercise is repeated for *SWOB* but only for different large-scale and large-small-scale channel fading settings. In 12.2, our aim is to assess whether our *GAFLS* can indeed provide the necessary adaption towards the unreliable wireless channel environment, in order to ensure reliable information query routing to a designated ROI.
- In 12.3, we then summarise and conclude the main contributions of this section.

CHAPTER 12

Mission Orientated Sensor Surveillance

12.1 VIGILANT^{+} Mission Orientated Performance

Simulations are conducted using the OMNeT++ network modeller tool [63]. To simulate a realistic wide area *UGS* surveillance setting, a 1km by 1km simulation region is specified, with nodes being randomly deployed according to a uniform distribution. Simulations are run using a number of random deployments (>50), each with duration of 100 detectable events. As part of our evaluation we do not consider the effects of increasing node density on VIGILANT^{+} mission orientated performance and so for the purposes of simulation, an arbitrary total of **20** nodes are used with communication parameters, as specified in table 9.1, from section 3, chapter 9. We do not consider the effects of increasing node density, since, in this section our evaluation is primarily concerned with VIGILANT^{+} performance within an uncertain and variable wireless channel environment setting.

Threat mobility characteristics are again simulated using the random waypoint (RWP) model, with a dynamic velocity (m/s) set from a uniform distribution, *uniform* (0, v_{max}). A RWP simulation model is again considered because of its extensive use within surveillance type evaluations, in order to mimic the random movement characteristics of a realistic monitored threat [78-79]. For the purposes of VIGILANT^{+} performance, we only simulate for a single v_{max} condition. In addition, the effects of threat velocity have already been discussed in section 1, chapter 5, under heading 5.4. We also assume that deployed sensors have accurate knowledge concerning a threat presence and therefore, we operate in a low false alarm surveillance environment (i.e. Threat Observation Certainty (TOC) = 0.9). We consider this condition, since the effects of the false alarm environment on

VIGILANT^{+} performance has already been discussed in section 1, chapter 5, under heading 5.3.

For the purposes of providing a refresh mechanism concerning current communication link status and to enable *GAFLS* evaluation within the distributed neighbourhood, we utilise the same mechanism detailed earlier in section 1, chapter 5, under heading 5.3. As outlined, a distributed node would only start to initiate sending updates (i.e. refresh packets) once the confidence in a current threat, is less than the previous evaluated confidence measure. Providing the distributed neighbourhood with updated link state information in this way, ensures the network is able to make channel aware forwarding decisions according to the dynamics of a threat situation and can also ensure that the most relevant nodes within the deployed network are utilised, for packet forwarding purposes. In addition, this can also prevent link status updates being made on a continuous basis, which can consume network resource consumption unnecessarily and further, is not tailored towards the objectives of a mission.

For purposes of illustration, we evaluate VIGILANT^{+} using the MDP and POMDP methodologies, which were described earlier in, section 1, chapter 5, under heading 5.2. Evaluating VIGILANT^{+} under these two scenarios will assess whether a centralised (MDP) or distributed (POMDP) mode of operation, is more effective under uncertain channel environment settings. As discussed in section 1, under heading 5.4, different decision epoch control strategies for the POMDP methodology were also considered and evaluated. From this study, we found strategy 1 was more beneficial in improving CEP performance for *M2* scenarios, while strategy 3 provided the most improved *M1* QoSI performance out of strategies 1 and 2. For POMDP operation, we thus utilise strategy 3 for *M1* scenarios and strategy 1 for *M2* scenarios. We utilise the IDSQ scheme for bench-mark comparison purposes, which incorporates just a SNR channel aware operation, when

selecting and forwarding information to local neighbours. Figures 12.2 to 12.5 show VIGILANT^{+} mission orientated performance for *M1* and *M2* scenarios against σ_{Shadow} (shadowing effects), under different *n* (path loss exponent) for both large-scale and large-small-scale fading channel environments.

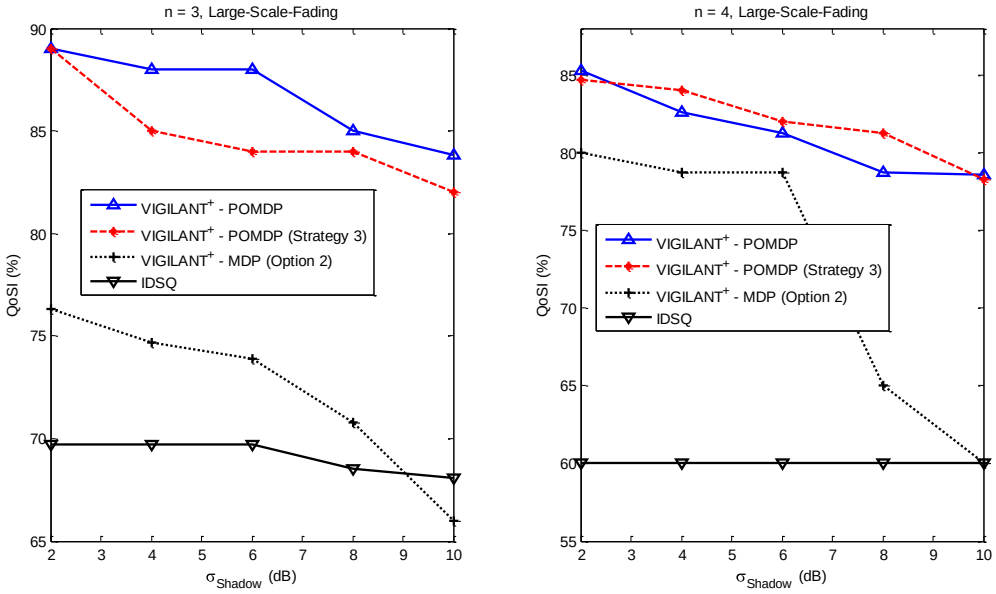

Figure 12.2: VIGILANT^{+} mission orientated QoSI performance (M1), large-scale-fading

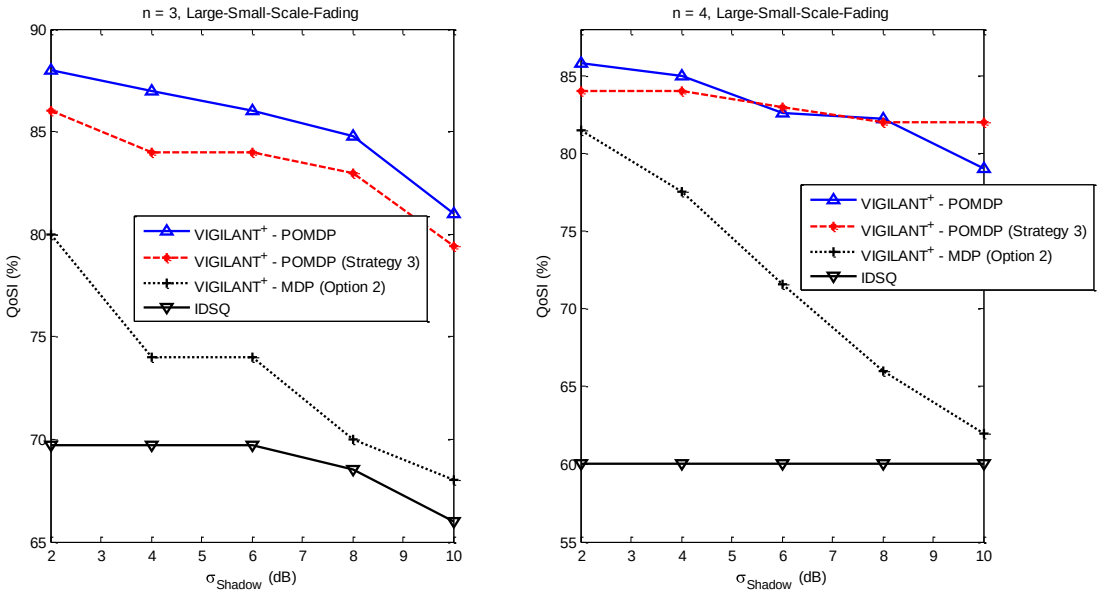

Figure 12.3: VIGILANT^{+} mission orientated QoSI performance (M1), large-small-scale-fading

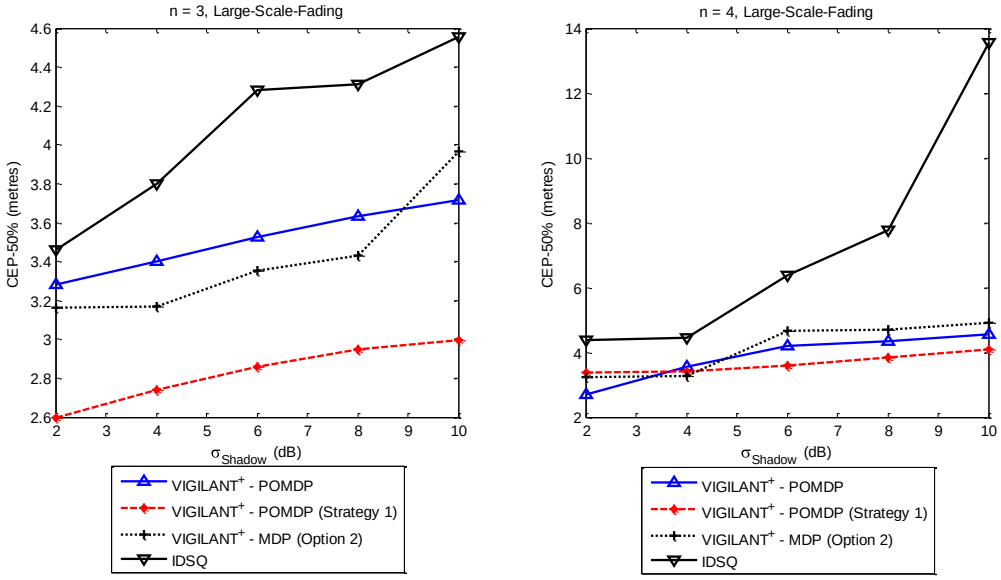

Figure 12.4: VIGILANT^{+} mission orientated CEP performance (M2), large-scale fading

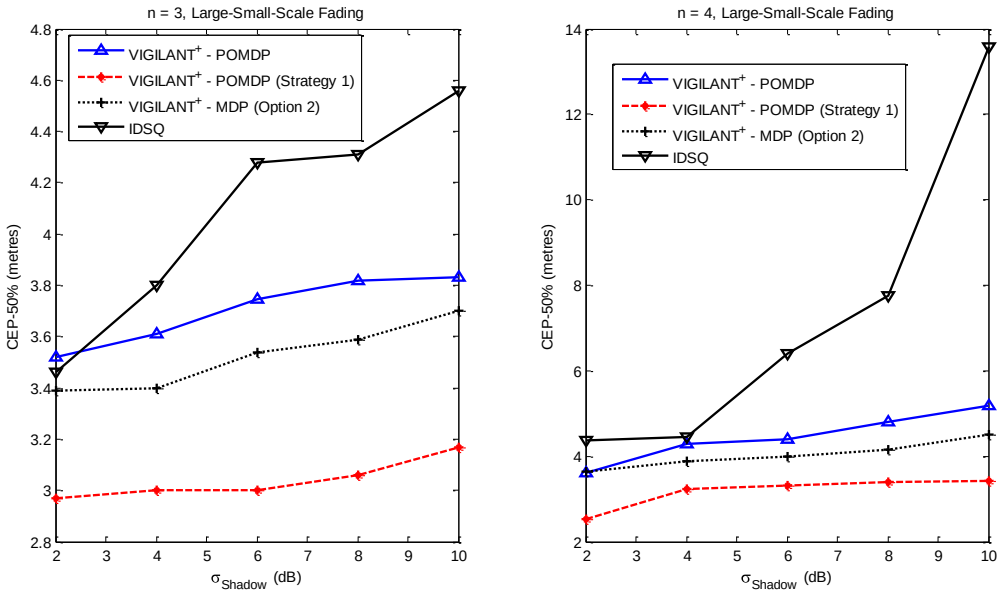

Figure 12.5: VIGILANT^{+} mission orientated CEP performance (M2), large-small-scale fading

Figures 12.2 to 12.5 show VIGILANT^{+} *M1* and *M2* performance, in terms of QoSI and CEP, for different, σ_{Shadow}, values in dB. As shown for both channel fading environments increasing the shadowing effects present within the channel, decreases the reported QoSI and threat geo-location accuracy possible, for both VIGILANT^{+} and IDSQ. As expected increasing *n*, also reduces the QoSI under both channel fading environments,

since, the chances of packet loss increases and so, reported QoSI and CEP performance reduces.

In 12.1, our main aim is to assess whether our *GAFLS* can indeed provide the necessary adaption towards the unreliable wireless channel environment, in order to ensure dependable mission objective information collection. From figures 12.2 and 12.3, VIGILANT^{+} which integrates *GAFLS* functionality does indicate dependable mission objective information collection and as shown, for the simulated conditions, can improve *M1* QoSI performance over IDSQ by some 20%. The same is also true for *M2* CEP performance and from figures 12.4 and 12.5 results indicate, VIGILANT^{+} improves CEP performance over IDSQ by some 30% under large-scale channel fading and by some 40% under large-small-scale channel fading environments. IDSQ incorporates just a SNR channel aware operation, when selecting and forwarding information to local neighbours and figures 12.2 to 12.5 show that this reduces both QoSI and CEP performance. Results from this evaluation clearly show that using a single channel aware metric (i.e. SNR) is not adequate enough to provide the necessary adaption to the unreliable error prone channel environment. Our *GAFLS* on the other hand evaluates the channel environment using both the *TRC* and *PRR* metrics and in addition, provides adaptability to the error prone channel by ensuring that its membership functions, which are used for forwarding node selection inference, reflect the status of the current channel conditions.

Part of the evaluation made in 12.1 was to also assess whether a VIGILANT^{+} centralised (MDP) or distributed (POMDP) mode of operation, is more effective under uncertain channel environment settings. From figures 12.2 to 12.5, it is clearly evident that a fully distributed mode of operation through VIGILANT^{+} - POMDP is more effective. Results from figures 12.2 to 12.5 indicate for the simulated scenario that a POMDP (strategy 3) mode of operation can improve QoSI performance by some 15% and a

POMDP (strategy 1) mode of operation can improve CEP performance by some 10% over just the MDP mode of operation, when operating under both large-scale channel fading and large-small-scale channel fading environments. The main reason for a performance shortfall, when using a MDP mode of operation is that it forces collaborating nodes to report their respective *M1* and *M2* information reports to the central group initiator (GI).

A central point of focus, limits the possibilities associated with opportunistic node selection. In this case rather than nodes selecting neighbouring nodes opportunistically, which become available due the broadcast transmission environment, nodes are more concerned with ensuring packet forwarding reliability with the GI itself. Opportunistic forwarding can overcome the unreliable wireless transmission environment by taking advantage of the broadcast nature of the wireless medium, as shown by the POMDP mode of operation. A POMDP mode of operation (strategy 1 and 3) would actively encourage the use of *GAFLS* evaluation on every received broadcast packet, in order to select a reliable node opportunistically when forwarding *M1* or *M2* information and as shown in figures 12.2 to 12.5, this provides an overall better and more dependable mission objective information collection approach.

12.2 SWOB Mission Orientated Performance

Simulations are conducted using the OMNeT++ network modeller tool [63]. To simulate a realistic wide area *UGS* surveillance setting, a 1km by 1km simulation region is specified, with nodes being randomly deployed according to a uniform distribution. Specified gateway node and ROI *x-y* coordinates in metres are (500, 0) and (500, 1000) respectively. Simulations are run using a number of random deployments (>50), each for a duration, which entails the gateway node sending a total of 100 packets with communication parameters, as specified in table 9.1, from section 3, chapter 9. As part of our evaluation,

we do not consider the effects of increasing node density on *SWOB* mission orientated performance and so, for the purposes of simulation an arbitrary total of 20 nodes are used. We do not consider the effects of increasing node density, since, our evaluation is primarily again concerned with *SWOB* performance within an uncertain and variable wireless channel environment setting.

We also evaluate *SWOB* mission orientated performance under *opportunistic forwarding* conditions and in this sense, overheard broadcast messages from neighbouring nodes are used for the purposes of providing a refresh mechanism, concerning current communication link status and to enable *GAFLS* evaluation, within the distributed neighbourhood. Providing the distributed neighbourhood with updated link status in this way, ensures the network is able to make channel aware forwarding decisions according to the current dynamics of the channel environment. In addition, this can also prevent link status updates being made on a continuous basis, which can consume network resource consumption unnecessarily.

The main *SWOB* performance evaluation aims conducted in section 2, chapter 7, in 7.3 were to measure throughput and energy efficiency performance. In 12.2, we maintain these two performance criteria's when evaluating *SWOB* under different large-scale and large-small-scale channel fading settings. In this sense, using a throughput metric measures overall network bandwidth utilisation efficiency, while energy efficiency measures how well *SWOB* conserves on energy consumption, in order to complete its forwarding tasks, under an error prone wireless channel environment. The same equation given in section 2, chapter 7, as (7.24) is used to calculate energy efficiency. For *SWOB* comparison purposes, we utilise the GeRAF routing strategy, as detailed earlier in 7.3. GeRAF is used, since it also employs a geographic *opportunistic forwarding* strategy to overcome the drawback of the unreliable transmission environment. Figures 12.6 to 12.9 show *SWOB* mission

orientated performance against σ_{Shadow} (shadowing effects), under different n (path loss exponent) for both large-scale and large-small-scale fading channel environments.

In 12.2, our main aim is to assess whether our *GAFLS* can indeed provide the necessary adaption towards the unreliable wireless channel environment, in order to ensure reliable information query routing to a designated ROI. From figures 12.6 to 12.9, *SWOB* which integrates *GAFLS* functionality can improve on both throughput and energy efficiency performance over GeRAF.

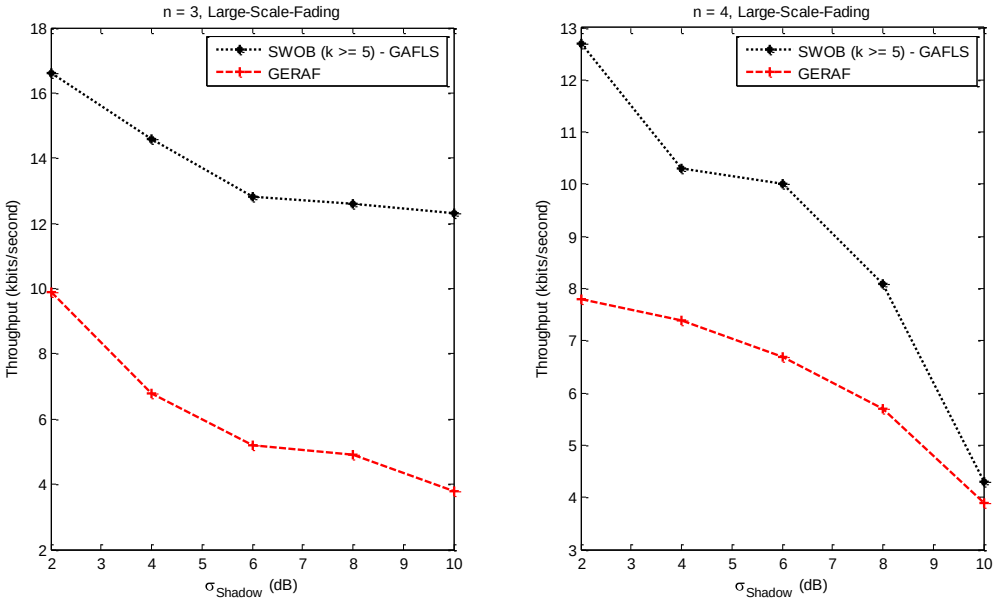

Figure 12.6: SWOB mission orientated throughput and comparison, large-scale-fading

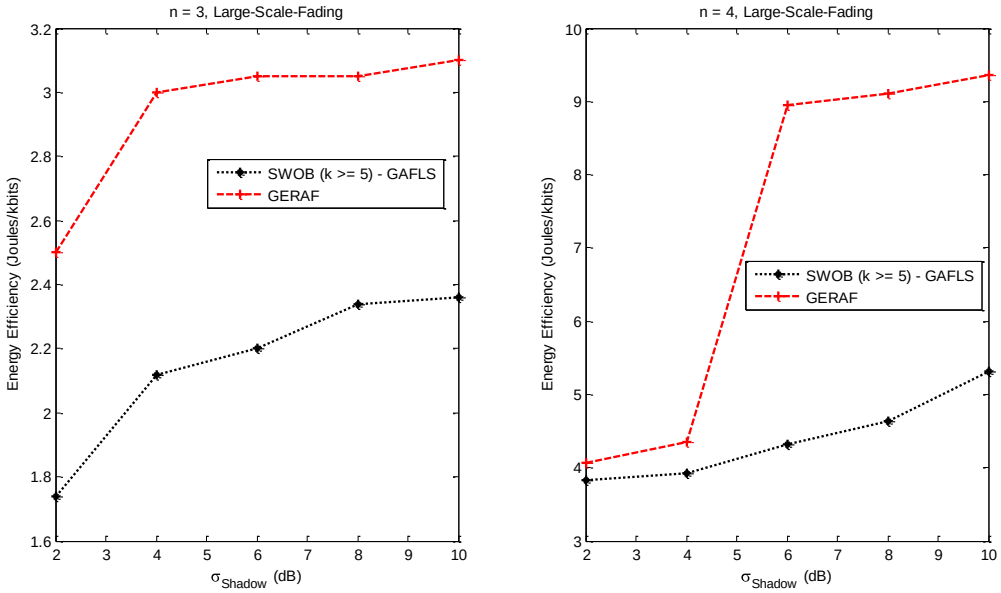

Figure 12.7: SWOB mission orientated energy efficiency and comparison, large-scale-fading

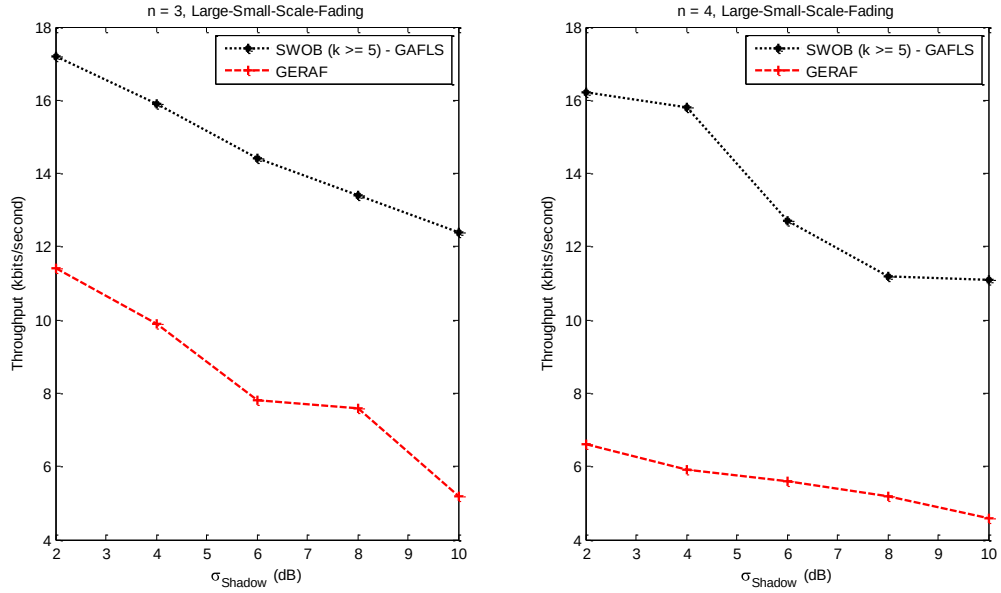

Figure 12.8: SWOB mission orientated throughput and comparison, large-small-scale-fading

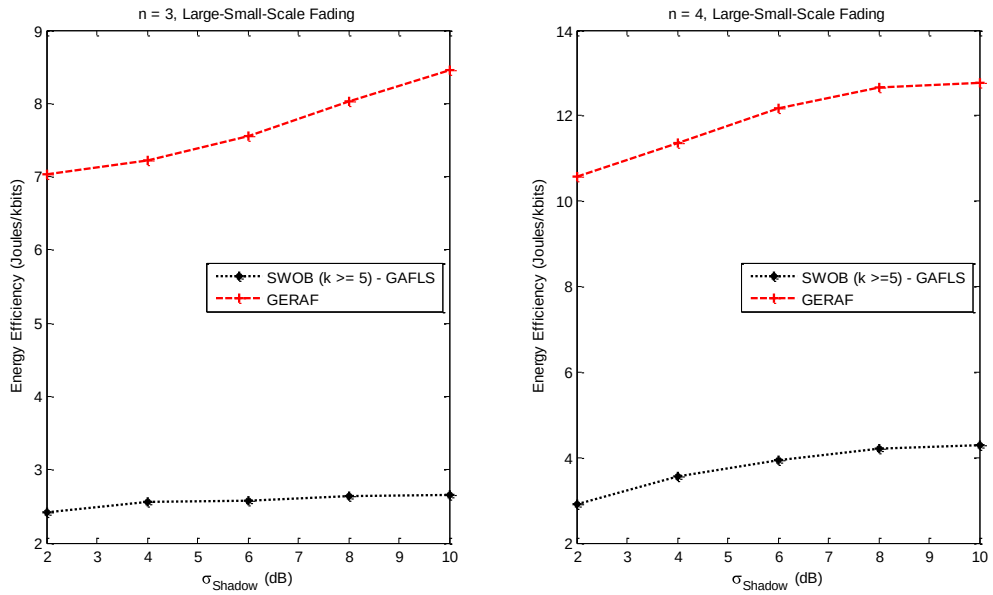

Figure 12.9: SWOB mission orientated energy efficiency and comparison, large-small-scale-fading

The results from figures 12.6 and 12.8, under the simulated scenario, indicate that *SWOB* under the condition of $k \geq 5$ neighbours, can improve throughput performance over GeRAF by some 38% under large-scale and by some 56% under large-small-scale channel fading environments. This indicates that a simple broadcasting forwarding strategy to cater against the error prone channel environment is not bandwidth efficient. For energy efficiency a similar conclusion can be reached, from figures 12.7 and 12.9. As shown, *SWOB* can improve energy efficiency performance over GeRAF by some 35% under large-scale and by some 62% under large-small-scale channel fading environments.

Results from this evaluation study clearly shows that with GeRAF, which just relies on the broadcast nature of wireless transmissions to discover forwarding node selection opportunistically is not reliable, when compared with *SWOB*, which uses a combination of broadcast and channel reliability evaluation (i.e. *GAFLS*) to discover and select forwarding nodes. A GeRAF strategy employs a "best-effort" and "best-path" approach, where nodes

receiving packets judge their forwarding suitability according to, their Euclidean distance to the destination. As shown in figures 12.6 and 12.8, such an approach can result in a very poor packet delivery rate (throughput).

SWOB with *GAFLS* ensures reliable *opportunistic forwarding* node selection. In general *SWOB* on its own would focus on node selection, according to its *greedy based forwarding* algorithm (**Appendix B, part 3**) but, with the addition of a *GAFLS*, alternative forwarding nodes can be selected according to both channel reliability and *greedy based forwarding*. As shown in figures 12.6 to 12.9, such an approach can result in an improved packet delivery rate and energy efficiency performance. In addition, the strategy also employed by GeRAF does not provide any adaption towards the error prone wireless channel environment. A *GAFLS* approach used with *SWOB* can, by ensuring that its membership functions, which are used for forwarding node selection inference, reflect the status of the current channel conditions, to help improve throughput and energy efficiency performance.

12.3 Section 4: Summary and Conclusions

UGS networks should ultimately be assessed as distributed systems, operating within both their deployed surveillance and physical environments. An assessment of this kind refers to *UGS* networks as, mission orientated sensor networks. A Mission orientated capability supports the notion of self-configurable *UGS* networks, capable of fulfilling mission objective requirements within an uncertain physical environment. In this section, we proposed a potential mission orientation capability, which involved the integration of our genetic adaptive fuzzy logic system (*GAFLS*), detailed in section 3, with VIGILANT^{+}, detailed in section 1 and our *SWOB* routing protocol, detailed in section 2, as shown in figure 12.1. We then undertook a performance evaluation of our VIGILANT^{+} system and *SWOB* routing protocol, under an error prone wireless channel environment. The purpose

of our evaluation was to inquire whether the *GAFLS* mechanism can indeed provide reliable forwarding node selection knowledge, to support both VIGILANT^{+} and *SWOB* routing functionalities.

In 12.1, we evaluated VIGILANT^{+} mission orientated performance for *M1* and *M2* scenarios against σ_{Shadow} (shadowing effects in dB), under different *n* (path loss exponent) for both large-scale and large-small-scale fading channel environments. Results show that:

- VIGILANT^{+} with integrated *GAFLS* functionality does indeed provide a dependable mission objective information collection approach and as shown, for the simulated conditions, can improve *M1* and *M2* performance over IDSQ by some 30% under large-scale channel fading and by some 40% under large-small-scale channel fading environments.
- A VIGILANT^{+}- MDP mode of operation forces a centralised point of focus (i.e. GI) for mission objective information collection and as a result, reduces *M1* and *M2* performance. A centralised approach can limit the possibilities associated with *opportunistic forwarding* node selection. In this case, rather than nodes selecting neighbouring nodes opportunistically, which become available due the broadcast transmission environment, nodes are more concerned with ensuring packet forwarding reliability with the GI.
- A VIGILANT^{+}- POMDP mode of operation (strategy 1 and 3) can actively encourage the use of *GAFLS* evaluation on every received broadcast transmission packet, in order to select reliable nodes opportunistically when forwarding *M1* or *M2* information. This provides an overall better and more dependable mission objective information collection approach.

In 12.2, we evaluated *SWOB* mission orientated performance against σ_{Shadow} (shadowing effects), under different *n* (path loss exponent) for both large-scale and large-small-scale fading channel environments. Results show that:

- *SWOB* with integrated *GAFLS* functionality can improve on both throughput and energy efficiency performance over GeRAF. The results indicate that *SWOB* under the condition of $k \geq 5$ neighbours, can improve throughput performance over GeRAF by some 38% under large-scale and by some 56% under large-small-scale channel fading environments. This indicates that a simple broadcast forwarding strategy to cater against the error prone channel environment is not bandwidth or energy efficient.
- *SWOB* with the addition of *GAFLS*, can create alternative forwarding nodes to be selected according to both channel reliability and *greedy based forwarding*. Such an approach can result in an improved packet delivery rate (throughput) and energy efficiency performance. This indicates a combination of both broadcast transmission (*opportunistic forwarding*) and channel reliability evaluation (i.e. *GAFLS*) to discover and select reliable forwarding nodes, can achieve the better performance.

CHAPTER 13

Conclusions

In this thesis, we studied both the application interface and networking technologies required to achieve a network centric capability (NCC), within a distributed unattended ground sensor (*UGS*) surveillance setting. The key research aims presented in this thesis are summarised in table 1.1 and are further developed, with view that *UGS* networks should be able to fulfil their mission objectives and conserve on their network resource consumption, within a dynamic mission-orientated environment. In this thesis, a dynamic mission-orientated environment refers to both a changing threat monitoring situation and underlying wireless channel environment. The thesis is then organised into four relevant sections, in order to address the key research aims outlined in table 1.1.

13.1 Section 1: Distributed Sensor Management

In section 1, the area of work concerned with distributed sensor management is addressed. Here the situation awareness methodology is applied to create the "*context-awareness*" element associated with a, specific mission objective surveillance situation. It is shown that the situation awareness framework can enable sensors to autonomously collaborate, in support of threat presence detection (*M1*) and geo-location (*M2*) mission objectives. This is possible, since, the situation awareness framework ensures that different elements from a current changing threat scenario are integrated (levels 1, 2 and 3) effectively to create new "*context-awareness*", which can then be used to establish relevant *autonomic* decision making outcomes for critical operations such as, distributed surveillance.

The level 1 part of the situation awareness framework entails how deployed sensors can effectively detect and assess, whether a threat is present within the "false alarm" surveillance environment. Simulation performance results of our developed PORTENT system demonstrate that:

- The Neyman-Pearson (NP) detection threshold remains consistent and adapts to the varying "false alarm" uncertainties present within the sensing observation environment, with only a small loss in detection certainty, as shown in figure 3.3. As shown in figure 3.8, through PORTENT-option 1 and 2, adapting the NP detection threshold ensures that relevant threat detection information is captured and aggregated, in terms of QoSI. This assists in maintaining a relevant and accurate picture (i.e. confidence) concerning the threat presence detection surveillance environment.
- PORTENT can reduce threat event detection delay by consolidating both "fast" and "slow" systems. The options developed and presented in this thesis, as part of the "fast-slow" system consolidated approach, are designed to increase the level of a perceived threat being present through further reduction of the NP detection threshold, as shown in figure 3.4. This is made possible through applying feedback on the initial signal level detection criterion used by the "fast" response system, to further improve the detection probability estimate of a threat being present, subject to the current "false alarm". As shown in figure 3.8, PORTENT-option 2 can improve QoSI performance over option 1 by 10% and over normal binary detection by 40%.

Our complete situation awareness enabled system, VIGILANT, integrates PORTENT-option 2, with its level 2 Bayesian Belief Network (BBN). This enables an effective analysis and comprehension to be made of the uncertain surveillance environment. VIGILANT performance results demonstrate that using derived "*context*" can, assist the management of the deployed network in the following ways:

- The dynamic grouping of relevant immediate neighbours (i.e. minimising on outlier contribution), which share the same level of confidence concerning the "*context*" of a threat presence detection situation. This assists in maintaining higher levels in QoSI provision when compared with LEACH, as shown in figure 4.6.
- Evaluating the level of common "*context-awareness*" concerning a threat presence situation allows transmission updating to be adapted according to, the dynamics of a threat. This prevents non-essential communication from occurring, which improves latency and communication energy consumption, as shown in figures 4.9 and 4.10 and at the same time prevents QoSI performance degradation, as shown in figure 4.6.

With VIGILANT it is found that having all "*context*" evaluation features being conducted and evaluated at a central node, results in greater communication energy and bandwidth being consumed. An improvement in this aspect is made from VIGILANT to the VIGILANT^{+} system, which allows sensors to take over more of the management control functionality, in a distributed manner. This is made possible through:

- "*Context*" querying. In this way, distributed nodes are only made aware of the most relevant "*context*" confidence measure concerning a specific mission objective, which can then be used to compare with their own locally derived "*context*".
- Evaluating "*context-awareness*" of a specific mission objective through the incorporation of a Markov Decision Process (MDP) and Partial Observable MDP (POMDP) methodology, which can then be used further to establish distributed *autonomic* transmission control.

VIGILANT^{+} simulation results demonstrate that by incorporating the above system improvements a better combined *M1* and *M2* surveillance utility and network resource consumption performance can be achieved mainly through:

- An integration of a geo-location "*context*" capability through GDOP evaluation leading to a combined improvement of 13%, when compared with VIGILANT, which performs geo-location based only on threat presence "*context*", through QoSI updating, as shown in figures 5.11 and 5.12.
- As shown in figures 5.10, 5.11 and 5.12, results demonstrate that setting a high confidence measure on sensor mission objective "*context*" and utilising a contention-schedule MAC scheme, where access periods are adapted in a distributed manner (e.g. VIGILANT^{+}-POMDP) according to, the level of common *M1* or *M2* "*context-awareness*", promotes reception of *M1* and *M2* update packets in a timely manner. This attribute is again demonstrated with figures 5.15 and 5.16, when compared with more centralised schemes (e.g. VIGILANT / VIGILANT^{+}-MDP) and continuous updating approaches, which adopts a schedule based MAC scheme (e.g. LEACH-TDMA).

VIGILANT^{+} simulation and test bed evaluation trials reveal that a POMDP mode of operation encourages better communication energy and bandwidth consumption, including processing time performance, as shown in figures 5.18 and 5.19. However, as shown in figures 5.11 and 5.12, a normal POMDP framework can induce a lower geo-location performance. This was found to be because a normal POMDP framework does not adapt its decision epoch selection interval according to, the dynamic characteristics of a monitored threat. Results show this can lead to a lower *M2* surveillance utility, since, less frequent *M2 "context"* evaluations are being made accordingly. By improving on this fact, performance results show that:

- Adapting POMDP interval selection according to, a history of physical threat position observations made within a designated time frame window can achieve the most

improved geo-location performance against threat velocity by 22% over normal POMDP operation, as shown in figure 5.25.

The disadvantage of using decision epoch interval selection strategies is felt through QoSI performance, which shows that normal POMDP operation can achieve better and more consistent performance against threat velocity, as shown in figure 5.24. Adapting the decision epoch interval selection by measuring the similarity *"context"* within the combined *M1* and *M2* surveillance environment, however, achieves the most improved combined network resource consumption performance, by 23% on top of normal POMDP operation, as shown in figures 5.22 and 5.23.

13.2 Section 2: Geographic Routing to Support Distributed Surveillance

In section 2, our *SWOB* geographic routing protocol to support distributed surveillance operations is developed. *SWOB* takes its inspiration from how social insects can create routes towards particular odour sources of interest. Subsequently, a source defined trajectory model based on the natural odour dispersion effects found in nature is developed. It is shown that a Gaussian plume model can provide an effective way to guide and create network topology control for IQ forwarding, towards the ROI destination. In our network topology control scheme the required Gaussian plume breadth shape is varied according to, a probabilistic relationship that ensures any deployed node found within the Gaussian plume is still able to have, a certain number of *k*-direct neighbours to communicate with. This relationship is then validated, in terms of saturated throughput performance and as shown in figures 7.14, 7.15 and 7.16, our analytical model provides a good match with our simulation results.

Based on our developed network topology control relationship, *SWOB* routing performance against deployed network node density, demonstrates that:

- Network latency and throughput performance can be improved by 35% over TBF and by 33% over MFP, through incorporating topology control within geographic routing functionality, especially in conditions with increasing network node density, as shown in figures 7.18 and 7.19.
- Employing directivity guidance towards an intended destination (i.e. ROI), in the form of the Gaussian plume model can increase energy efficiency performance further by 47% over MFP and by 70% over RDF, as network node density increases, as shown in figures 7.20 and 7.21.

13.3 Section 3: Channel Aware Packet Forwarding

In section 3, a consideration of the error prone wireless environment is given and a potential decision making mechanism, which adapts to current channel characteristics in order to assist reliable packet forwarding, is highlighted. Our analysis of the *TRC* on communication link reliability, in terms of the optimal packet forwarding distance (d_{opt}), transmission reliability (TR), expected transmission count (*ETX)* and expected-any-path-transmissions count (*EAX*), within different channel fading environments show that:

- A higher *TRC* can increase d_{opt} by maximising the expected packet reception rate (*E [PRR]*) under the same shadowing effect (σ_{shadow}) condition, as shown in figure 9.6.
- A lower *TRC* achieves better TR performance over shorter communication link distances and this is reversed for a small gain in TR performance over larger distances, as shown in figure 9.9.
- A higher *TRC* value can minimise the *ETX*, over larger communication link distances through maintaining the same upper link reliability limit, P_h ($\gamma_{\text{-}Upper\text{-}dB}$) value and setting a lower link reliability limit, P_l ($\gamma_{\text{-}Lower\text{-}dB}$) value, as shown in figure 9.11.

- The number of transmissions required for a successful packet delivery is reduced within an *EAX* environment against *ETX*, over higher transmission ranges (250m-500m), when utilising communication links with a higher *TRC*, as shown in figure 9.13.

Based on the *TRC* analytical study, an overall decision making mechanism, in order to cater against the effects of the channel fading environment is developed. For this purpose an initial fuzzy logic system (*FLS*) system is developed and it is later shown that normal *FLS* performance can be improved by providing a mechanism, which can adjust the *FLS* membership functions (*MFs*) according to, the channel environment. For this purpose, a genetic algorithm (*GA*) is implemented and integrated within normal *FLS* operation, in order to provide this adaptability to the channel environment.

Results for the simulated network scenario, as shown in figures 10.7 to 10.12 demonstrate that utilising a genetic adaptive *FLS* provides a combined improvement in throughput performance by 66% and energy efficiency by 46% over normal *FLS*. An improvement is possible since, a genetic adaptive *FLS* system would actively seek to identify links *opportunistically*, which exhibit either a lower *TRC* (if $\leq d_{opt}$) or higher *TRC* (if $\geq d_{opt}$) according to its adapted membership functions (*MF's*), to increase performance over normal *FLS* operation.

13.4 Section 4: Integrated System Performance

In section 4, a potential mission orientation capability is evaluated through the integration of our genetic adaptive fuzzy logic system (*GAFLS*), detailed in section 3, with VIGILANT^{+}, detailed in section 1 and *SWOB*, detailed in section 2. The integrated system performance results show that:

- VIGILANT^{+} with integrated *GAFLS* functionality does indeed provide a dependable mission objective information collection approach and as shown for the simulated scenario, can improve *M1* and *M2* performance over IDSQ by 34% under large-scale channel fading and by some 40% under large-small-scale channel fading environments, as shown in figures 12.2 to 12.5.
- A VIGILANT^{+}- POMDP mode of operation can actively encourage the use of *GAFLS* evaluation on every received broadcast transmission packet (*opportunistic forwarding*), in order to select reliable nodes when forwarding *M1* or *M2* information. This provides an overall better and more dependable mission objective information collection approach.
- *SWOB* under the condition of $k \geq 5$ neighbours, can improve throughput and energy efficiency performance over GeRAF by 38% under large-scale and by 56% under large-small-scale channel fading environments, as shown in figures 12.6 to 12.9. This indicates that a simple *opportunistic* broadcast forwarding strategy to cater against the error prone channel environment is neither bandwidth nor energy efficient.

13.5 Suggestions for Further Work

The areas of future research comprise mostly practical and theoretical work that may be categorised into the main sections covered in this thesis, as follows.

Section 1 - Distributed Sensor Management

1. An evaluation of VIGILANT^{+} performance using multiple (i.e. more than a single threat scenario) and dynamic threat mobility scenarios are required.
2. The development of our VIGILANT^{+} system assumes that information regarding the presence and geo-location of a threat can be obtained immediately without any loss. In realistic deployment scenarios this may not be the case and indeed there may be

periods during a mission where the "*context-awareness*" regarding the presence or geo-location of a threat is incomplete, affecting the outcomes for relevant *autonomic* decision making (e.g. transmission control). Until recently, information gap theory has been formalised as a means of supporting model-based decisions under severe uncertainty [167]. The uncertainty may be expressed as a value of a parameter, such as, probabilities that a threat is present in each of several possible geographical cells (i.e. positions). An information-gap may then be expressed in the shape of a robustness utility function assessing the greatest tolerable horizon of uncertainty. Through applying a relevant robustness function on top of normal VIGILANT^{+} operation a quantitative answer to the questions: how wrong can we be in our current "*context*" or whether the action we are considering (i.e. transmission selection) will still lead to an acceptable outcome (i.e. QoSI update), can be applied.

3. Currently, the provisioning of "*context*" information in VIGILANT^{+} assumes it is available when it is required. This is invalid if one were to consider that the sources and mechanisms to enable sharing of "*context*" information within the surveillance neighbourhood (e.g. sensors) may fail or become disconnected overtime. It is therefore important to consider an evaluation of VIGILANT^{+} performance under the sensor "failure" condition. A possible way to overcome the sensor "failure" condition is to consider the opportunistic use of sensors within the neighbourhood, or a decision tree preference based method.
4. From a practical evaluation viewpoint and to extend the current test bed environment, VIGILANT^{+} performance should also be conducted within a dynamic threat monitoring experimental scenario. For this, we might envisage a moving audio source within a distributed mobile sensing environment, similar to the one described in **Appendix A, part 3**.

Section 2 - Geographic Routing to Support Distributed Surveillance

1. Again a consideration of evaluating *SWOB* routing performance within a multiple and dynamic threat mobility environment scenario, is also required.
2. In *SWOB*, network topology control and routing directivity provided by use of the Gaussian function, currently does not support rotation. At present, both virtual odour plume concentration calculations and *k-connectivity* evaluations assume the Gaussian function remains central and static, relative to both the gateway node and intended region of interest (ROI). If the ROI coordinates were to change relative to the gateway node, a rotatable Gaussian function, which moves to the new ROI coordinates and maintains the highest odour concentration to be found at the centre of the new identified ROI (i.e. routing directivity), would be required. This can therefore provide a means to support multiple ROI coordinates, which would potentially become available during a changing surveillance mission.
3. Consideration of creating high-priority routes to rapidly send information queries to an ROI and to convey important events within *SWOB* routing is also required. We would envisage both of these routing functions to occur at the same time within a dynamic surveillance mission scenario and so, a possible way to cater for this is to create both high-priority and secondary routes. Different routes could then be selected and matched to forwarding nodes, which can support the priority, required (i.e. forwarding nodes that have similar "*context-awareness*" concerning the presence of a threat or can achieve higher security levels).

Section 3 - Channel Aware Packet Forwarding

- Currently, knowledge about the channel environment is only used to influence forwarding node selection. The knowledge generated could also be used to adapt or influence the packet being forwarded. For example, larger packets can lead to longer

packet transfer times whereas, current channel status processed using the genetic adaptive fuzzy logic system could adapt packet size length (i.e. message fragmentation) accordingly to, suit the current channel. This has potential to further improve the utilisation of bandwidth and increase the connectivity opportunities of the network.

Section 4 - Integrated System Performance

1. For VIGILANT^{+} an intelligent caching mechanism should be considered, in order to enable storage of local mission objective information, when reliable forwarding node selection knowledge becomes unavailable. Currently, an opportunistic forwarding node would be selected to forward information to immediately, which can lead to a performance shortfall. If we were to consider the history of neighbour communication link statuses this could allow us to adopt a cache and forward policy, which ensures that relevant information is only forwarded during periods of reliable connectivity based on historical evidence of specific neighbouring nodes. This has potential to then further increase both *M1* and *M2* surveillance utility performance, within a dynamic mission orientated environment.
2. A complete joint evaluation performance of VIGILANT^{+} and SWOB functions working together within a dynamic, multiple threat mission orientated environment scenario, is also required. An evaluation of this nature would give an overall integrated system performance perspective.

Finally, it is also hoped that the work presented in this thesis will lead to a good appreciation of the role that NCC can play in distributed network management and the potentially new areas of associated research that may be developed.

APPENDICES

The Appendices are organised into three sections:

- Appendix A, lists all of the flow charts for section 1, describing the operations for PORTENT and VIGILANT systems. In Appendix A, part 1, it details PORTENT threat situation assessment operation. In Appendix A, part 2, it details VIGILANT situation awareness system, showing the complete integrated level 1, 2 and 3 functions for QoSI updating. In addition, Appendix A, part 3, details the test bed evaluation experiment setup used for evaluating VIGILANT^{+} performance.
- Appendix B, lists all of the flow charts for section 2, describing SWOB topology control operations to ensure a certain *k-connectivity* requirement is achieved, shown in parts 1 and 2, while the overall *SWOB* routing algorithm, is described in part 3.
- Appendix C, lists all of the flow charts for section 3, describing operations for our *FLS* and *GAFLS*. In part 1, the mechanism for packet forwarding using our *FLS* system is described. In part 2, the Genetic Algorithm (GA) to search for optimal *FLS* input *MF* parameters is given and in part 3, the desired system output in order to tune the GA fitness function, is given. In part 4, the mechanism for packet forwarding using our *GAFLS* is detailed.

APPENDIX A

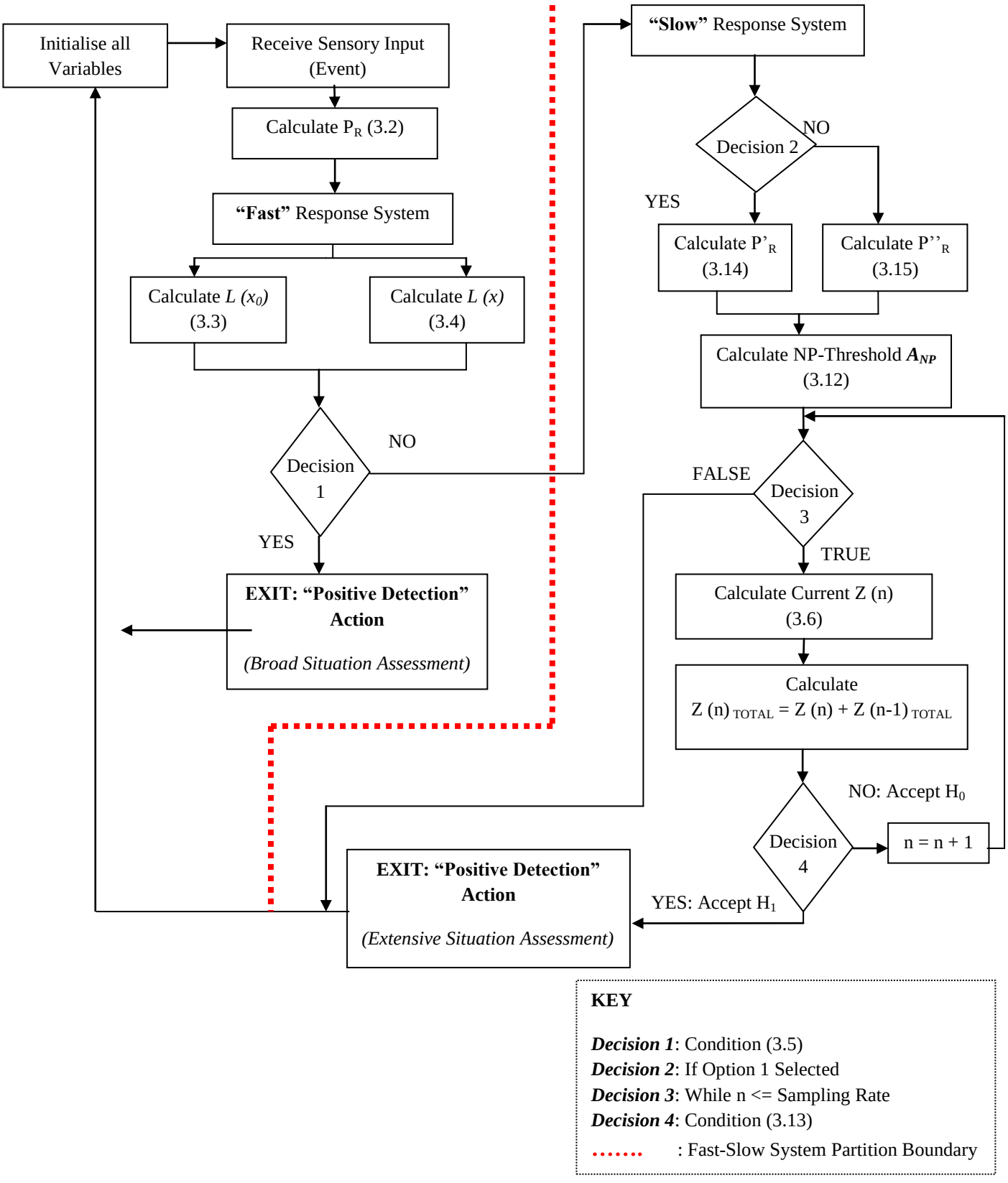

***Part 1**: Level 1 PORTENT threat situation assessment flow chart operation*

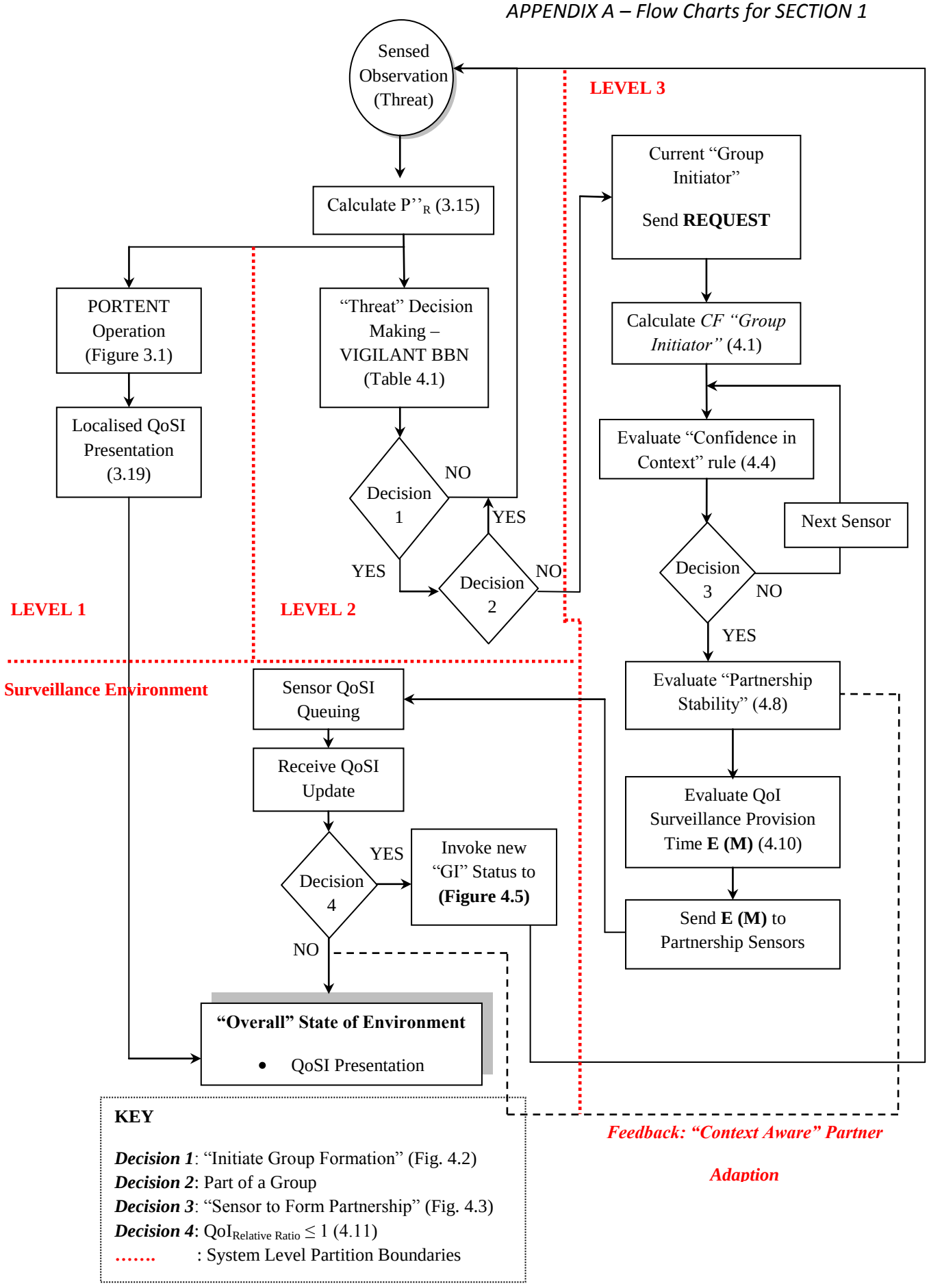

***Part 2**: VIGILANT flow chart operation showing an integrated level 1, 2, 3 process for QoSI updating*

Part 3: VIGILANT+ Test Bed Trial Evaluation

General Background

For the purpose of the test bed trials, we propose the development of a new kind of static sensor network, which consists of a number of deployed *Android*-based smart phones. For test bed trial evaluation purposes, smart phones running the *Android* Operating System (OS) are used.

Android is an open-source software stack that includes an operating System, middleware and key application routines. The readily available *Android* Software Development Kit (SDK) allows anyone to develop their own applications in Java. Android SDK provides all the tools and Application Programming Interfaces (API) that are required for the application development, intended to be run on *Android* phones.

Aim

The main purpose of the trial is to develop the appropriate software using Java, in order to exploit the phones microphone as a "sensor" and test the VIGILANT+ sensor algorithm.

The nature of the experiment is to reduce the sensors energy consumption caused by inter-device communication and at the same time prevent captured QoSI degradation.

Method

Test Bed experimentations are based on correctly perceiving (SA- Level 1) and identifying a fixed audio source generator (SA –Level 2), to mimic a basic static threat detection monitoring scenario and to record how transmissions are being managed (SA- Level 3), for example, total number of transmissions made (i.e. communication overhead).

We adopt a **client-server** architecture, where the **server** represents a potential lead UGS and **clients** represent potential distributed UGS collaborators.

Experimental Setup

Our attempt at constructing a smart phone static sensor network consists of a server phone and six client phones. Each client remains connected to the server exchanging data packets when needed, but clients do not communicate with each other respectively.

The equipment that we used included a speaker that functions as our audio source (static threat), frequency generator to set the audio frequency and an oscilloscope to tune the frequency generator.

We decided to use a sinusoidal wave function with a fixed frequency of 300Hz. The amplitude of the frequency generator was set to 6 Volts since during initial test runs this was found to allow all deployed clients to adequately register, an audio source event.

Experiments were conducted in an enclosed teaching room with length 8.5 meters by 2 meters. Prior to carrying out the actual experiment, it was of vital importance to evaluate the environmental conditions and acquire a suitable value to be used a detection threshold from the accumulated results. The value of the threshold would then be inserted in the application to help us determine the presence of an audio source, needed in PORTENT-"fast" system operation. Based on this initial evaluation clients were deployed accordingly to figure A.1.

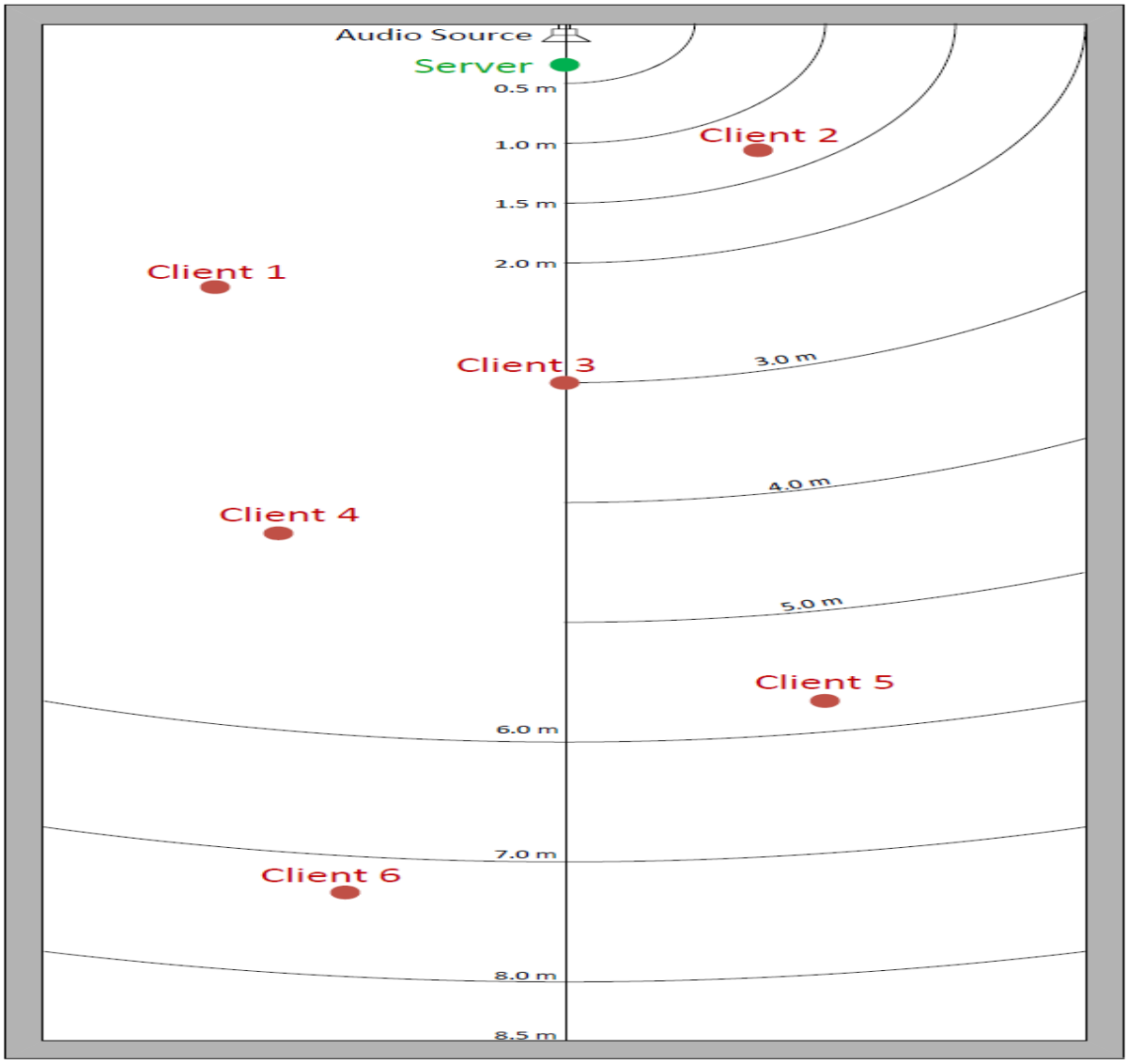

Figure A.1: Experimental test bed evaluation layout

A number of trial runs were conducted with each trial run being conducted for a total of 1000 seconds. Results of the experiment are presented according to the various volume setting levels of the audio source (speaker), with the relative level values set out of maximum setting of 10 levels (i.e. (2/10); (3/10); (4/10); (5/10); (6/10)). The respective unit-less RMS values registered by the microphone register at the server position, as shown in figure A.1, were noted as follows in table A.1. Table A.2, gives the respective average

RMS values registered by the clients deployed accordingly to figure A.1 and measured across the range of volume level settings, as used in table A.1.

Volume Level	RMS Value
2 / 10	15098.64
3 / 10	17651.02
4 / 10	19927.89
5 / 10	21867.37
6 / 10	23596.73

Table A.1: Respective RMS values registered at the server position

Client	Average RMS Value
1	2550.63
2	3720.43
3	2078.72
4	1501.25
5	1149.89
6	841.21

Table A.2: Respective average RMS values registered at each client position

The test-bed evaluations were carried out for comparison purposes using three different system operations:

- **Fully Distributed:** Emphasises more on the distributed client's retrieved local state *"context"* from the microphone sensor after an initial server assumption concerning an event, for transmission control decision making. **(Memory Operation –POMDP)**

- **Semi-Distributed:** Takes into account the need for updated threat (audio source) observations made by both the server and collaborating clients to deduce state *"context"*, for transmission control decision making. **(Memory-less Operation – MDP-Option 1)**

- **Centralised:** Constitutes the server and clients utilising only SA level 1 and ignoring SA levels 2, 3 (i.e. Threat comprehension and Projection). Clients send their updated threat detection information values on every server request, which is sent every time a positive SA-level 1 detection is made. This constitutes as a non-"context aware" approach.

Assumptions

There are some limitations to our approach. The phone's sensing ability is limited to sound-emitting objects only. Taking this into consideration we do not actively consider the effects of background noise and other factors, such as the reflection of sound waves inside the room. These assumptions are important since we do not implement any classification algorithms that can distinguish between our fixed audio source and other audio source anomalies.

Our primary concern is to evaluate how VIGILANT^{+} operation can improve on transmission control decision making and as a result, provide the necessary network resource consumption benefits.

APPENDIX B

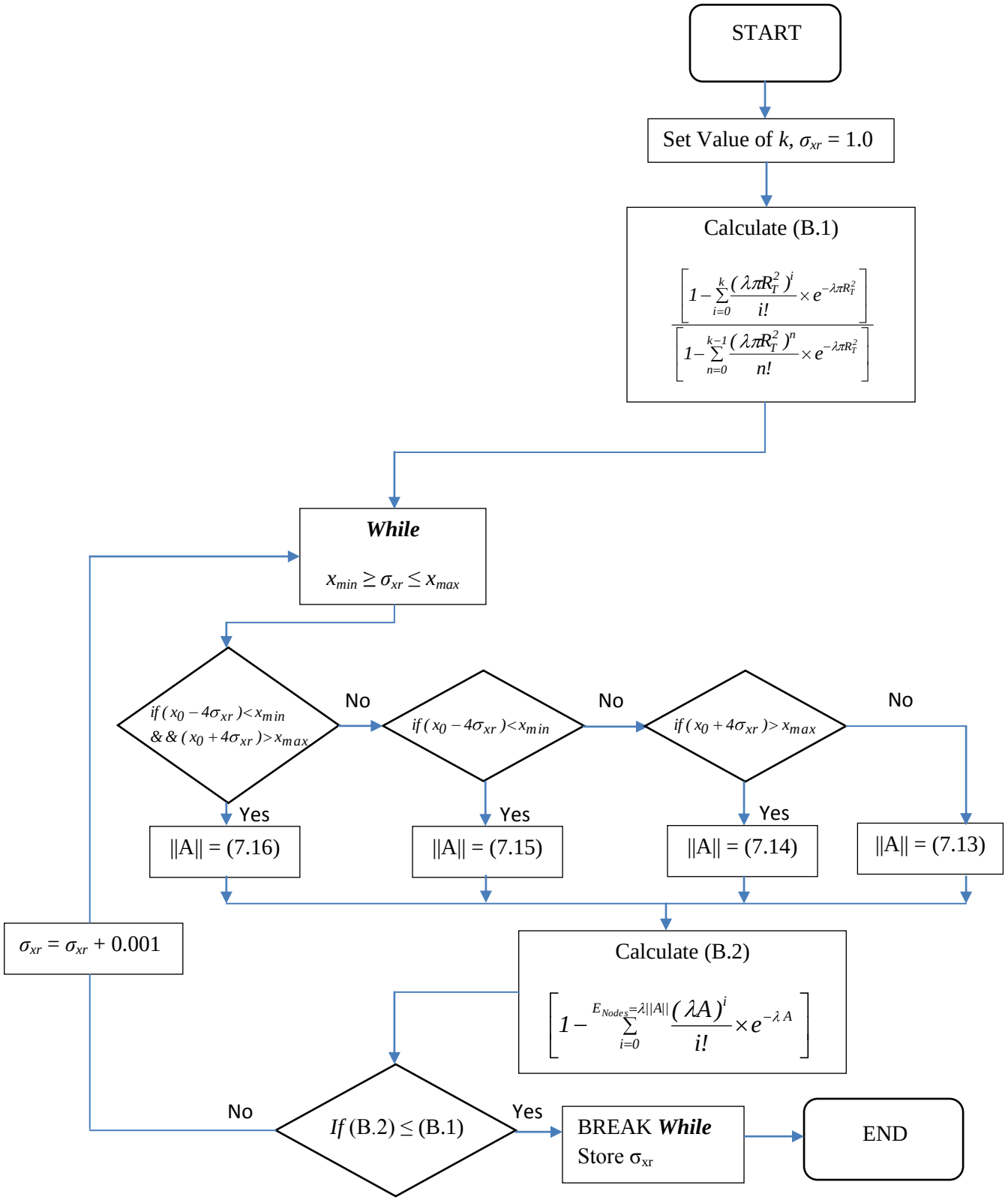

***Part 1**: Calculating the σ_{xr} value to ensure nodes have a desired k-connectivity for SWOB topology control*

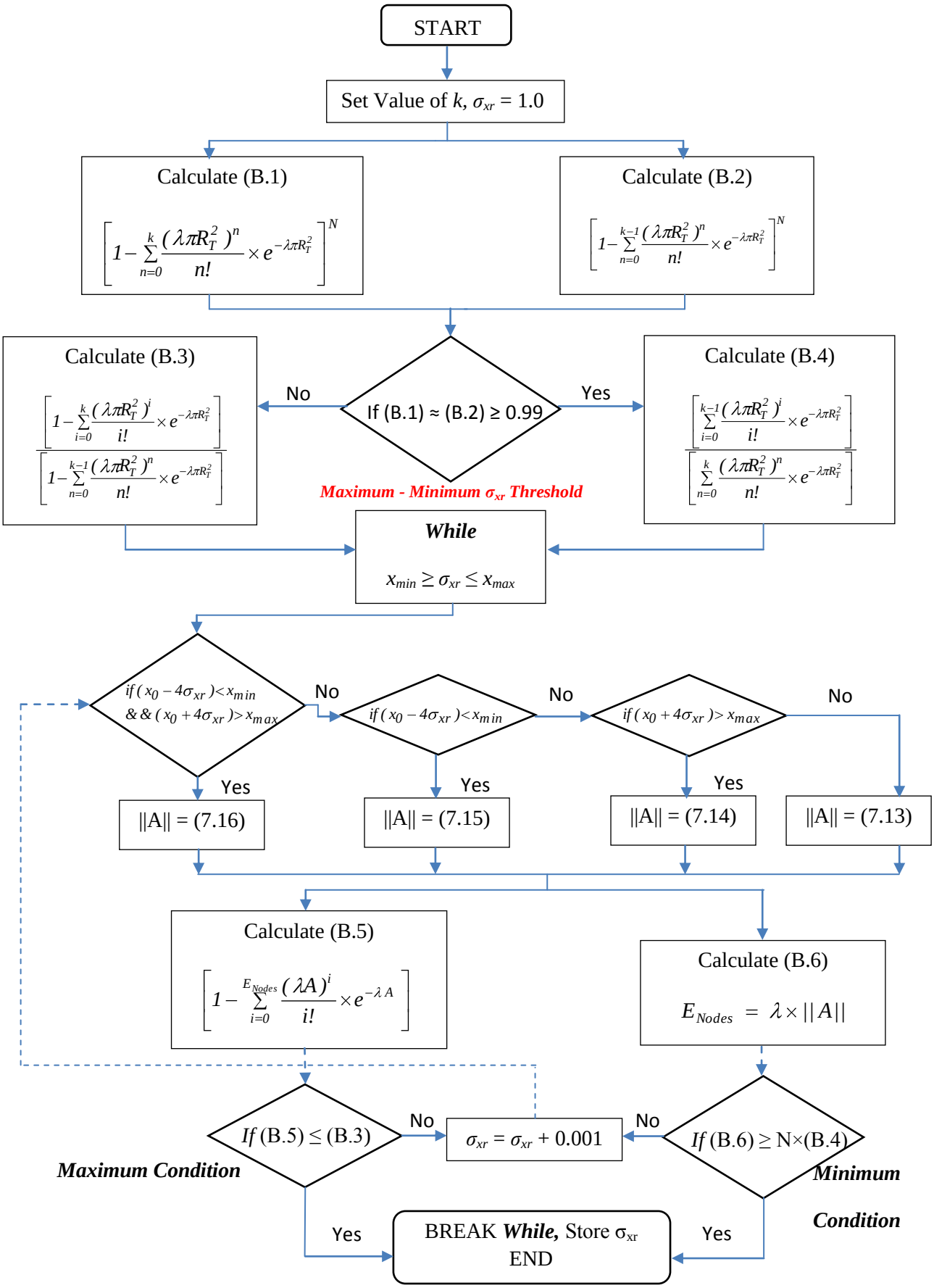

***Part 2**: Calculating a maximum or minimum σ_{xr} value to ensure nodes have desired k-connectivity for SWOB topology control*

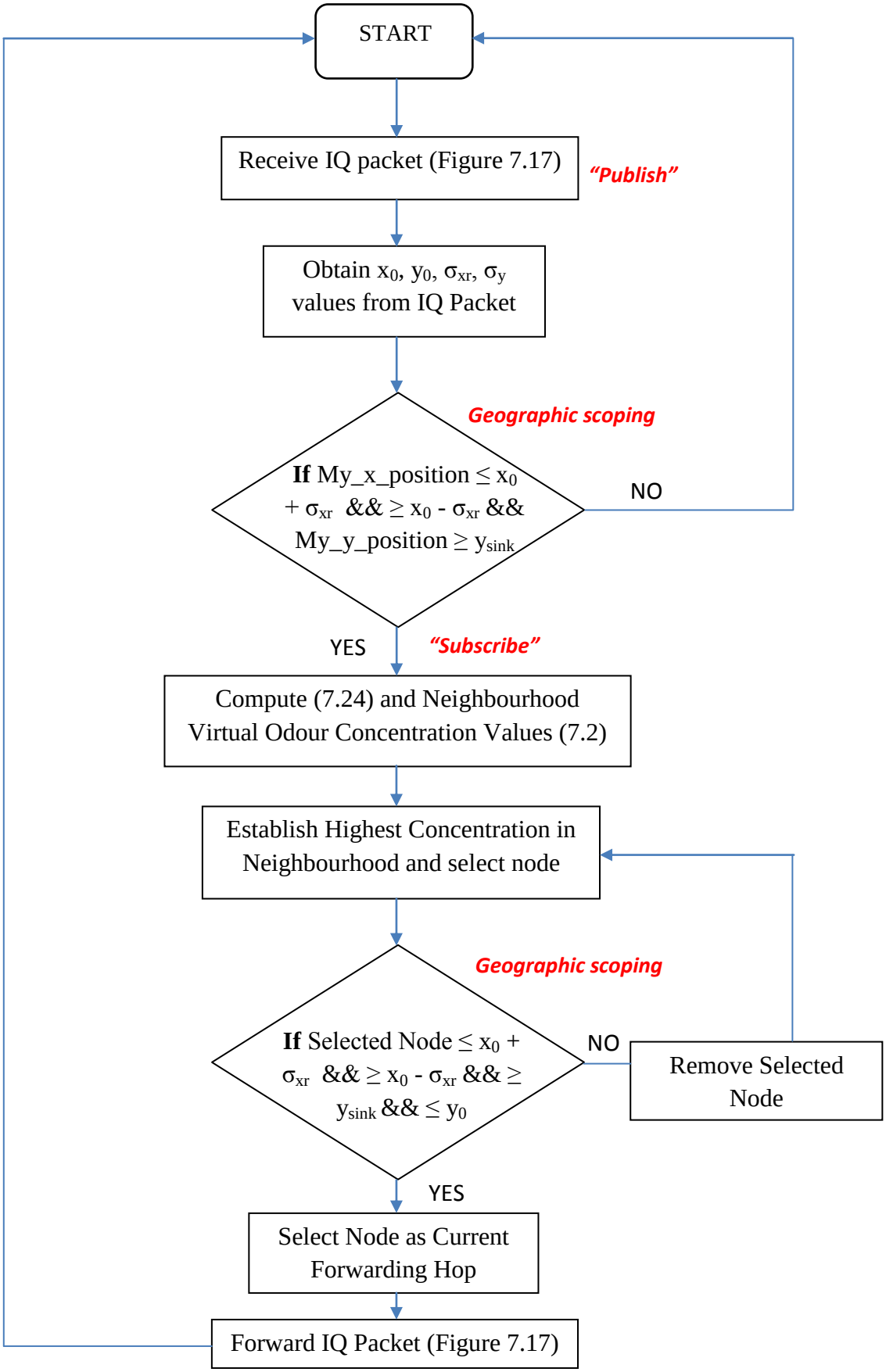

***Part 3**: Overall SWOB geographic routing algorithm*

APPENDIX C

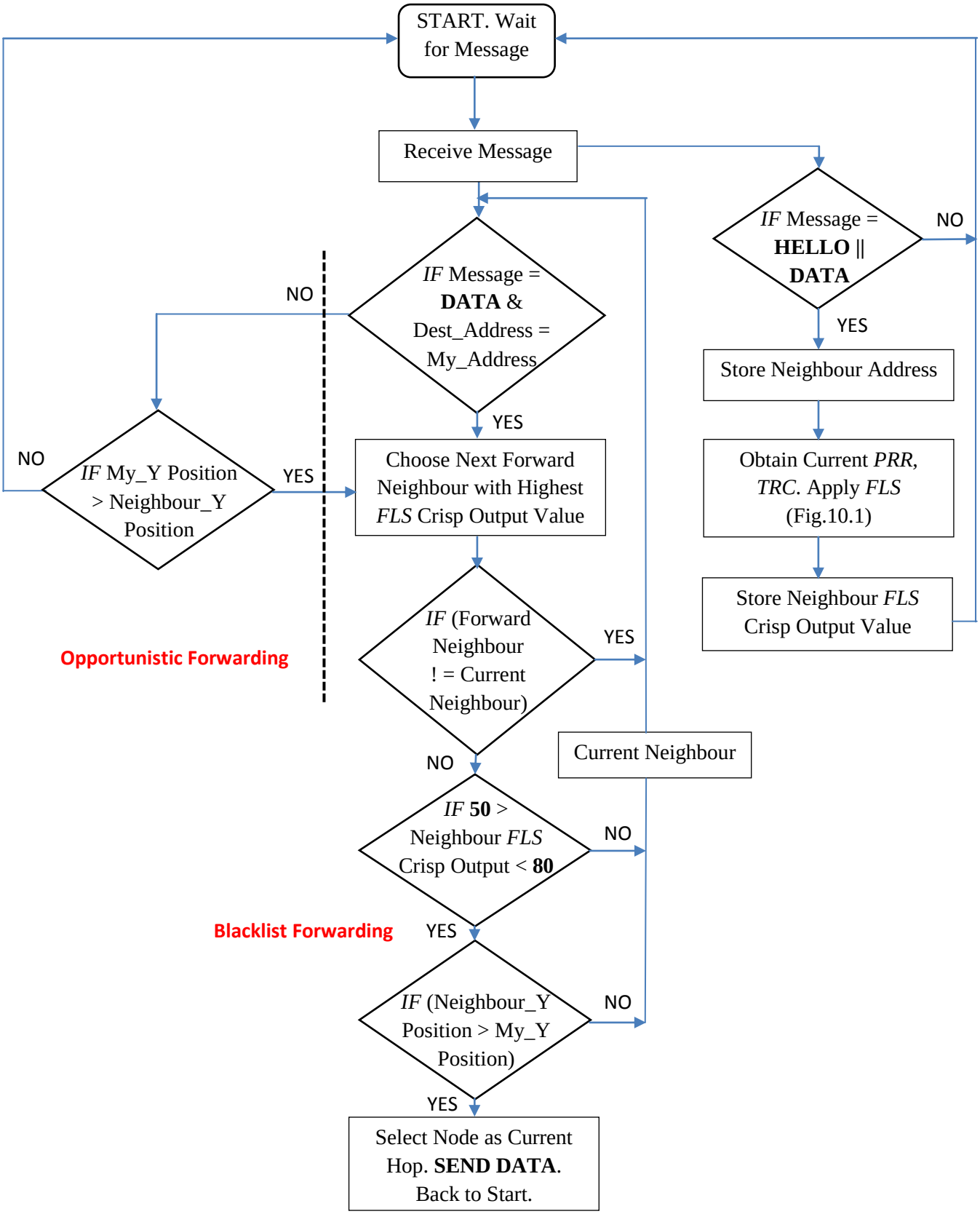

***Part 1**: Overall Algorithm Mechanism for Packet Forwarding using the FLS Based Strategy*

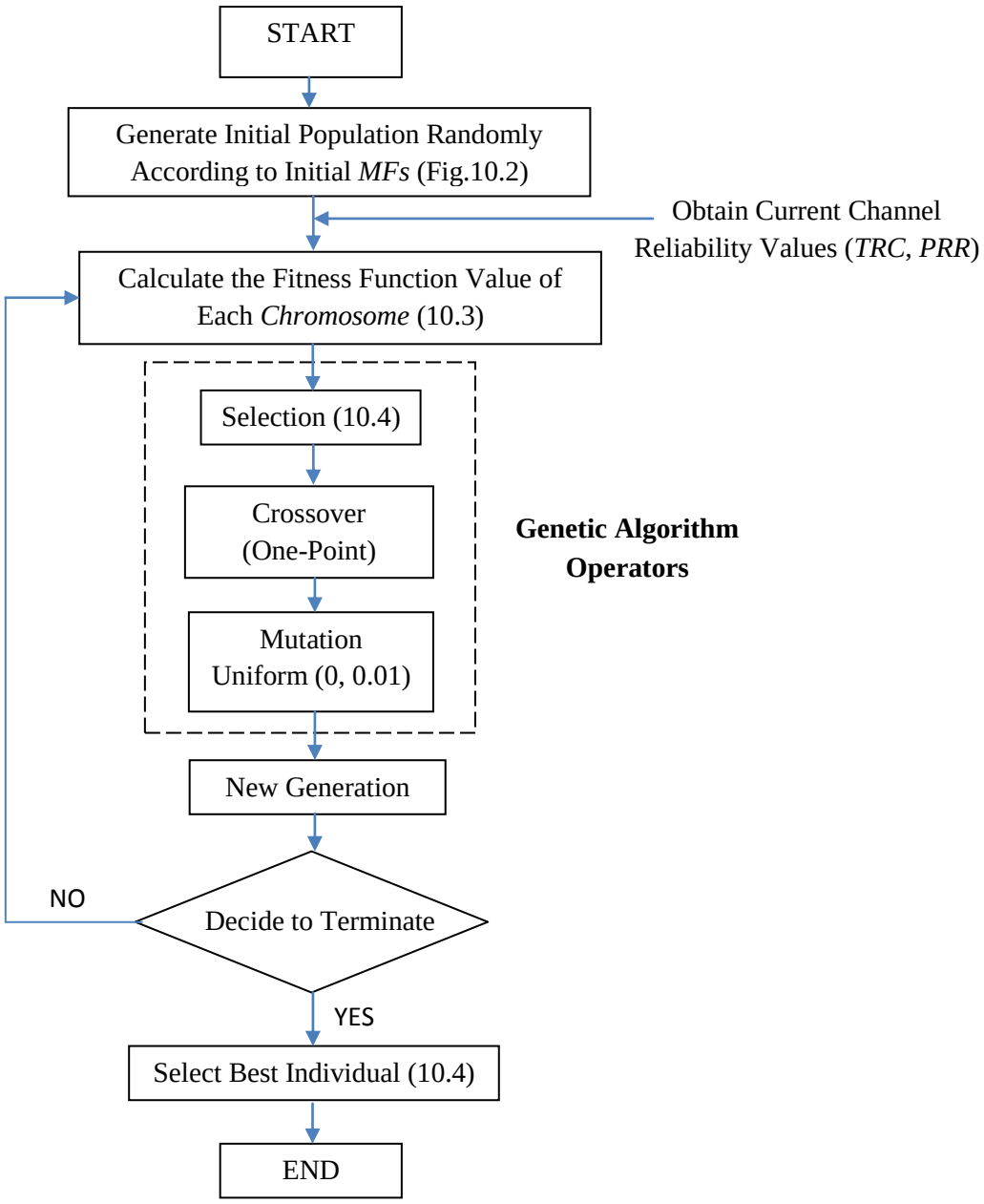

***Part 2**: Genetic Algorithm for Searching Optimal FLS Input MF Parameters*

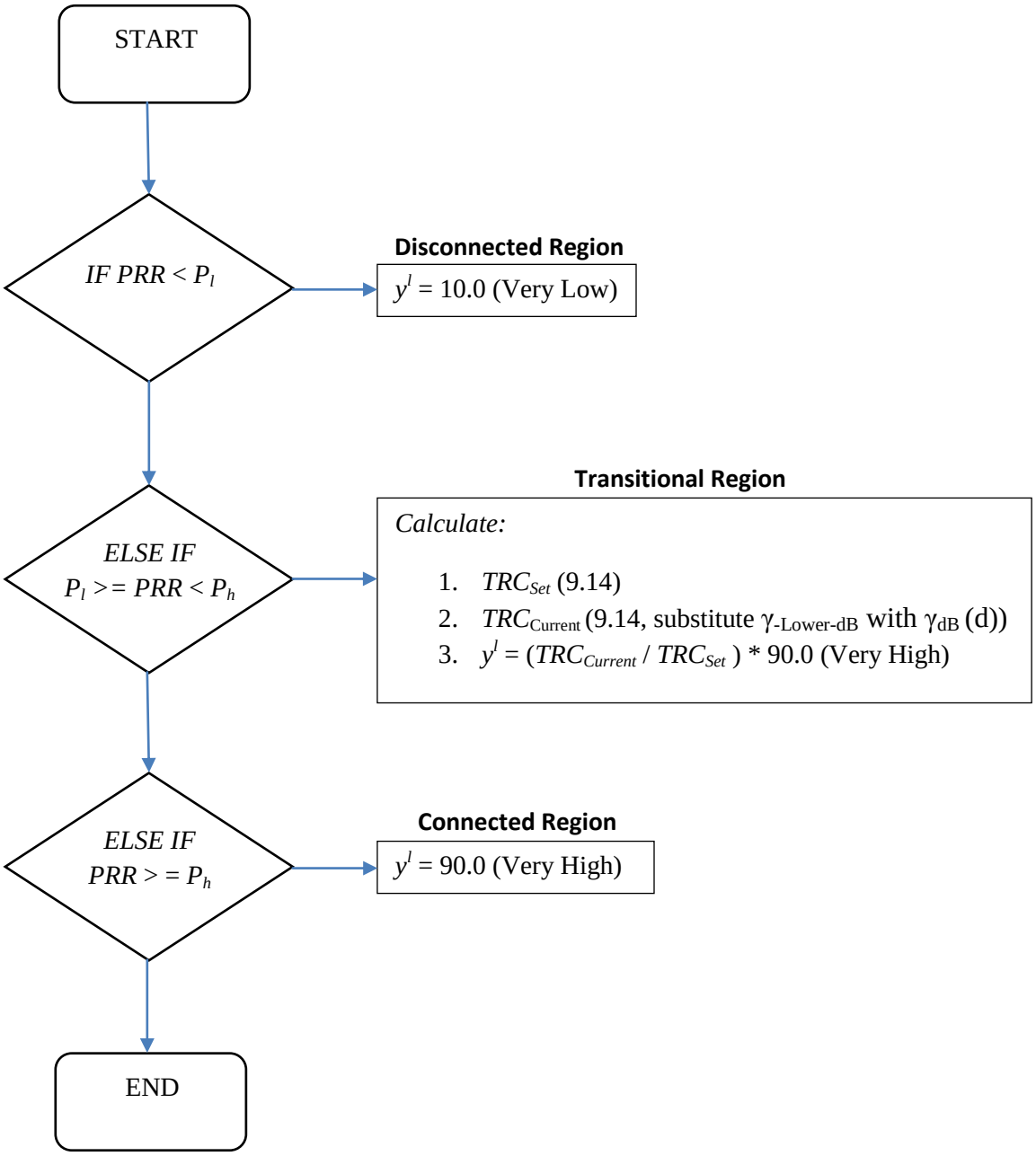

***Part 3**: Calculating the Desired System Output (y^l) for GA Fitness Function Evaluation*

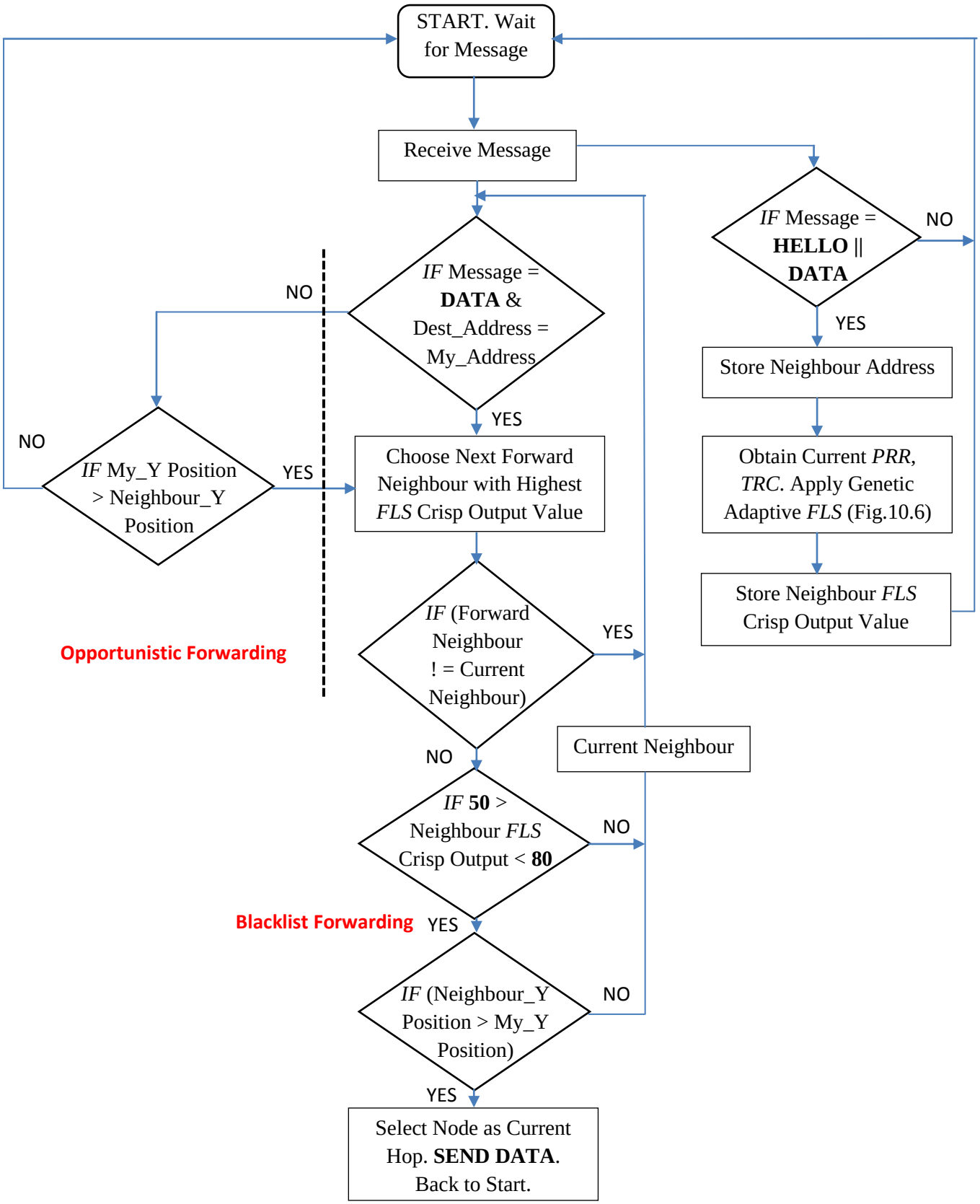

***Part 4**: Overall Algorithm Mechanism for Packet Forwarding using Genetic Adaptive FLS Based Strategy*

References

[1] J.Zheng and A.Jamalipour, "Wireless Sensor Networks: A Networking Perspective", Chapter 1: "Introduction to Wireless Sensor Networks", *Wiley-IEEE Press*, 1st Edition, pp.1-18, 2009.

[2] J.Gehrke and Liu.Ling, "Introduction: Sensor Network Applications", *IEEE Internet Computing*, vol.10, no.2, pp.16-17, March-April 2006.

[3] T. Becker, M.Kulge, J.Schalk, K.Tiplady and C.Paget, "Autonomous Sensor Nodes for Aircraft Structural Health Monitoring", IEEE Sensors Journal, vol.9, no.11, pp.1589-1595, November 2009.

[4] K.Gill, S.H.Yang, F.Yao, X.Lu, "A ZigBee-Based Home Automation System", *IEEE Transactions on Consumer Electronics*, vol.55, no.2, pp.422-430, May 2009.

[5] R.V.Kulkarni, A.Forster and G.K.Venayagamoorthy, "Computational Intelligence in Wireless Sensor Networks: A Survey", *IEEE Communications Surveys and Tutorials*, vol.13, no.1, pp.68-96, January-March 2011.

[6] D.L.Hall, J.Llinas, "An Introduction to Multi-Sensor Data Fusion", *Proceedings of the IEEE*, vol.85, no.1, pp.6-23, January 1997.

[7] J.Clare and D.S.Ryl, "Energy Efficient Area Monitoring for Sensor Networks", *IEEE Computer*, vol.37, no.2, pp.40-46, February 2004.

[8] D.S.Alberts, J.J.Garstka and F.P.Stein, "Network Centric Warfare: Developing and Leveraging Information Superiority", CCRP Publication Series, 2nd Edition, Chapter 5, pp.87-108, February 2000.

[9] D.S.Alberts, J.J.Garstka and F.P.Stein, "Network Centric Warfare: Developing and Leveraging Information Superiority", CCRP Publication Series, 2nd Edition, Chapter 8, pp.140-148, February 2000.

[10] J.L.Burbank, P.F.Chimento, B.K.Haberman and K.T.Kasch, "Key Challenges of Military Tactical Networking and the Elusive Promise of MANET Technology", *IEEE Communications Magazine*, vol.44, no.11, pp.39-45, November 2006.

[11] H.Leung, S.Chandana and S.Wei, "Distributed Sensing Based on Intelligent Sensor Networks", *IEEE Circuits and Systems Magazine*, vol.8, no.2, pp.38-52, May 2008.

[12] I.Akyildiz, W.Su, E.Cayirci, "A Survey on Sensor Networks", *IEEE Communications Magazine*, vol.40, no.8, pp.102-114, 2002.

[13] C.Kreucher, A.Hero, K.Kastella and M.Morelande, "An Information-Based Approach to Sensor Management in Large Dynamic Networks", *Proceedings of the IEEE*, vol.95, no.5, pp.978-998, May 2007.

[14] D.Puccinelli and M.Haenggi, "Wireless Sensor Networks: Applications and Challenges of Ubiquitous Sensing", *IEEE Circuits and Systems Magazine*, vol.5, no.3, pp.19-31, 2005.

[15] R.R Hoffman and J.F. Yates, "Decision Making", *IEEE Intelligent Systems Magazine*, vol.20, no.4, pp.76-83, July/August 2005.

[16] P.K Biswas and S.Phoha, "Self-Organising Sensor Networks for Integrated Target Surveillance", *IEEE Transactions on Computers*, vol.55, no.8, pp.1033-1047, August 2006.

[17] J.E.Bevington, "Distributed Sensor Management and Target Tracking for Unattended Ground Sensor Networks", *Proceedings of SPIE Security and Defence*, Battle-space Digitisation and Network Centric Systems IV, vol.5441, pp.25-35, 2004.

[18] K.Romer, O.Kasten and F.Mattern, "Middleware Challenges for Wireless Sensor Networks", *ACM Mobile Communication and Communications Review*, vol.6, no.2, pp.59-61, October 2002.

[19] Y.Tian and E.Ekici, "Cross-Layer Collaborative In-Network Processing in Multi-hop Wireless Sensor Networks", *IEEE Transactions on Mobile Computing*, vol.6, no.3, pp.297-310, March 2007.

[20] S. Eswaran, M. Johnson, A. Misra, and T. La Porta, "Adaptive In-Network Processing for Bandwidth and Energy Constrained Mission-Oriented Multi-hop Wireless Networks. In Distributed Computing in Sensor Systems", *Proceedings of the 5th IEEE International Conference on Distributed Computing in Sensor Systems (DCOSS)*, Marina Del Rey, CA, USA, pp.87-102, June 2009.

[21] D. Marsh, R. Tynan, D. O'Kane, G. O'Hare, "Autonomic Wireless Sensor Networks", *ELSEVIER Journal of Engineering Applications of Artificial Intelligence*, vol.17, no.7, pp.741-748, October 2004.

[22] S. Dobson, E. Gelenbe, D. Gaiti, A. Fernandez, S. Denazis, F. Massacci, P. Nixon, F. Saffre, N. Schmidt, F . Zambonelli, "A Survey of Autonomic Communications", *ACM Transactions on Autonomous and Adaptive Systems*, vol.1, no.2, pp.223-259, December 2006.

[23] A. Forster, R.V Kulkarni, G.K Venayagamoorthy, "Computational Intelligence in Wireless Sensor Networks: A Survey", *IEEE Communications Survey and Tutorials*, vol.13, no.1, pp.68-96, February 2011.

[24] T.Onel, C.Esroy, "Information Content-Based Sensor Selection and Transmission Power Adjustment for Collaborative Target Tracking", *IEEE Transactions on Mobile Computing*, vol.8, no.8, pp.1103-1116, August 2009.

[25] D.Gracanin, K.P Adams, M.Eltoweissy, "Data Replication in Collaborative Sensor Network Systems", *Proceedings of the 25th International Conference on Performance, Computation and Communications (IPCCC)*, pp. 390-396, Phoenix, Arizona, USA, April 2006.

[26] S.K Singh, "Routing Protocols in Wireless Sensor Networks- A Survey", *International Journal of Computer Science and Engineering Survey (IJCSES)*, vol.1, no.2, pp.63-83, November 2010.

[27] W.Heinzelman, "An Application Specific Protocol Architecture for Wireless Micro Sensor Networks", *IEEE Transactions on Wireless Communications*, vol.1, no.4, pp.660-670, October 2002.

[28] O. Younis and S.Fahmy, "Distributed Clustering in Ad-Hoc Sensor Networks: A Hybrid and Energy Efficient Approach", *Proceedings of the 23rd Conference of the IEEE Communication Society- IEEE INFOCOM*, Hong Kong, 7th-11th March 2004.

[29] W.P Chen, J.C Hou and L.Sha, "Dynamic clustering for acoustic target tracking in wireless sensor networks", *IEEE Transactions on Mobile Computing*, vol.3, no.3, pp.258-271, July-September 2004.

[30] D. Roelant, K. Yen and Z. Hao, " Self Organisation of Unattended Wireless Acoustic Sensor Networks for Ground Target Tracking", *ELSEVIER Journal of Pervasive and Mobile Computing*, vol.5 , no.2, pp.148 -164, April 2009.

[31] J.Lee, K.Cho, S.Lee, T.Kwon and Y.Choi, "Distributed and Energy-Efficient Target Localisation and Tracking in Wireless Sensor Networks", *ELSEVIER Journal of Computer Communications*, vol.29, no.13-14, pp.2494-2505, August 2006.

[32] R.Brooks, C.Griffin and D.S. Friedlander, "Self-Organised Distributed Sensor Network Entity Tracking", *International Journal of High Performance Computer Applications*, vol.16, no.3, pp.207-219, August 2002.

[33] D.Li, K.Wong Y.Hu and A.Sayeed, "Detection, Classification, Tracking of Targets in Micro-Sensor Networks", *IEEE Signal Processing Magazine*, vol.19, no.2, pp.17-29, March 2002.

[34] F.Zhao, J.Shin and J.Reich, "Information-Driven Dynamic Sensor Collaboration", *IEEE Signal Processing Magazine*, vol.19, no.2, pp. 61-72, March 2002.

[35] F.Zhao, J.Liu, L.Guibas, J.Reich, "Collaborative Signal and Information Processing: An Information-Directed Approach", *Proceedings of the IEEE*, vol.91, no.8, pp. 1199-1209, August 2003.

[36] L.Guibas, "Sensing, Tracking, and Reasoning with Relations", *IEEE Signal Processing Magazine*, vol.19, no.1, pp.73-85, March 2002.

[37] R.Roman, J.Lopez, S.Gritzalis, "Situation Awareness Mechanisms for Wireless Sensor Networks", *IEEE Communications Magazine*, vol.46, no.4, pp.102-107, April 2008.

[38] M.R.Endsley, "Toward a Theory of Situation Awareness in Dynamic Systems", Journal of Human Factors, vol.37, no.1, pp.32-64, March 1995.

[39] C.Bisdikian, "On Sensor Sampling and Quality of Information: A Starting Point", *Proceedings of the 5th Annual IEEE Conference on Pervasive Computing and Communication (PERCOM)*, White Plains, New York, USA, pp.279-284, March 2007.

[40] M.Walchli, T.Braun, M.Meer, P.Skoczylas, "Distributed Event Localization and Tracking with Wireless Sensors", *5th International Conference on Wired/Wireless Internet Communications (WWIC)*, Coimbra, Portugal, pp.247-258, May 2007.

[41] K.Romer, "Discovery of Frequent Distributed Event Patterns in Sensor Networks", *Proceedings of the 5th European conference on Wireless sensor networks (EWSN)*, Bologna, Italy, pp.106-124, January 2008.

[42] E.Onur, C.Ersoy, H.Delic and L.Akarun, "Surveillance Wireless Sensor Networks: Deployment Quality Analysis", *IEEE Network*, vol.21, no.6, pp.48-53, November/December 2007.

[43] E.Onur, C.Ersoy and H.Delic, "Quality of Deployment in Surveillance Wireless Sensor Networks", *International Journal of Wireless Information Networks*, vol.12, no.1, pp.61-67, January 2005.

[44] X.Y.Li, P.J.Wan and O.Frieder, "Coverage in Wireless Ad Hoc Sensor Networks", *IEEE Transactions on Computers*, vol.52, no.6, pp.753-763, June 2003.

[45] J.A.R Marshall, "On optimal decision making in brains and social insects", *Journal of the Royal Society*, pp.1-10, January 2009.

[46] P.C Trimmer, "Mammalian Choices", *Proceedings of the Royal Society*, pp. 2353-2361, July 2008.

[47] E.Onur, C.Ersoy and H.Delic, "How Many Sensors for An Acceptable Breach Probability Level?", *Journal of Computer Communications*, vol.29, no.2, pp.172-82, January 2006.

[48] J.P.Egan, "Signal Detection Theory and ROC Analysis", New York, Academic Press pp.16-18,

[49] D.Kazakos, P.P.Kazakos, "Detection and Estimation", Computer Science Press, Rockville, MD, 1990.

[50] K.F.Wong, "A Recurrent Network Mechanism of Time Integration in Perceptual Decisions", *Journal of Neuroscience*, vol.26, no.4, pp.1314-1328, January 2006.

[51] S.Zahedi and C.Bisdikian. "A Framework for QoI-Inspired Analysis for Sensor Network Deployment Planning", *2nd International Workshop on Performance Control in Wireless Sensor Networks (PWSN)*, Austin, Texas, USA, October 2007.

[52] C.Bisdikian, R.Damarala, T.Pham, V.Thomas, "Quality of Information in Sensor Networks", *2nd Annual Conference of the International Technology Alliance (ACITA)*, London, U.K, September 2008.

[53] G. Jakobson, J. Buford, L. Lewis, "A framework of cognitive situation modelling and recognition", *Proceedings of the 25th IEEE Military Communications Conference (MILCOM)*, Washington, USA, pp. 1-7, October 2006.

[54] P.Smart, A.Bahrami, D.Braines, D.M.Spencer, J.Yuan and N.R.Shadbolt, "Semantic Technologies and Enhanced Situation Awareness", *1st Annual Conference of the International Technology Alliance (ACITA)*, East Adelphi, Maryland, USA, September 2007.

[55] J.Salerno, M.Hinman, D.Boulware, "Building a Framework for Situation Awareness", *Proceedings of the 7th International Conference on Information Fusion*, Stockholm, Sweden, pp.219-226, June 2004.

[56] F.V.Jensen, "Bayesian Networks and Decision Graphs", *Springer*, New York, 2nd Edition, 2007.

[57] X.Ye, G.Kamath and L.A.Osadciw, "Using Bayesian Inference for Sensor Management of Air Traffic Control Systems", *IEEE Symposium on Computational Intelligence in Multi-Criteria Decision Making*, Nashville, Tennessee, USA, pp.23-29, March 2009.

[58] S.Das, D.Lawless, "Trustworthy Situation Assessment via Belief Networks", *Proceedings of the 5th International Conference on Information Fusion*, Annapolis, Maryland, USA, pp.543-549, July 2002.

[59] A.Ranganathan, J.Al-Muhtadi, R.Campbell, "Reasoning about Uncertain Contexts in Pervasive Computing Environments", *IEEE Pervasive Computing*, vol.3, no.2, pp.62-70, July 2004.

[60] P.Krause, "Representing Uncertain Knowledge", *Intellect Books*, 1st Edition, pp.52-56, 1993.

[61] R.M.Perianu, C.Lombriser, P.Havinga, H.Scholten and G.Troster, "Tandem: A Context-Aware Method for Spontaneous Clustering of Dynamic Wireless Sensor Nodes", *Proceedings of the 1st International Conference on The Internet of Things, Appears in Lecture Notes in Computer Science*, vol.4952, pp.341-359, March 2008.

[62] C.Lombriser, M.M.Perianu, R.M.Perianu, D.Rogen, P.Havinga, G.Troster, "Organizing Context Information Processing in Dynamic Wireless Sensor Networks", *Proceedings of the 3rd International Conference on Intelligent Sensors, Sensor Networks and Information Processing (ISSNIP)*, pp.67-72, Melbourne, Australia, December 2007.

[63] A.Varga, "Using the OMNeT++ Discrete Event Simulation System in Education, *IEEE Transactions on Education*, vol.42, no.4, November 1999.

[64] E.Souto and J.Kelner, "Mires: A Publish/Subscribe Middleware for Sensor Networks", *Journal of Personal Ubiquitous Computing*, vol.10, no.1, pp.37-44, December 2005.

[65] K.Henricksen and R.Robinson, "A Survey of Middleware for Sensor Networks: State-of-the-Art and Future Directions", *Proceedings of the International Workshop on Middleware for Sensor Networks (MidSens)*, pp.60-65, Melbourne, Australia, November/December 2006.

[66] O.H Lerma, "Adaptive Markov Control Processes", Applied Mathematical Sciences, *Springer-Verlag*, New York, 2001.

[67] L.P.Kaelbling, M.L.Litman, A.R.Cassandra, "Planning and Acting in Partially Observable Stochastic Domains", *Journal of Artificial Intelligence*, vol.101, no.1-2, pp.99-134, May 1998.

[68] E.K.P.Chong, C.M.Kreucher, A.O.Hero, "Partially Observable Markov Decision Process Approximations for Adaptive Sensing", *Journal of Discrete Event Dynamic Systems*, vol.19, no.3, pp.377-422, May 2009.

[69] E.K.P.Chong, L.W.Krakow, K.N.Groom, J.Harrington, Y.Li, B.Rigdon, "Control of Perimeter Surveillance Wireless Sensor Networks via Partially Observable Markov Decision Process", *Proceedings of the 40th Annual IEEE International Carnahan Conference on Security Technology (ICCST)*, Lexington, USA, pp.261-268, October 2006.

[70] I.Kadar, "Optimum Geometry Selection for Sensor Fusion", *SPIE: Defence, Security and Sensing, Proceedings of the Conference on Signal Processing, Sensor Fusion and Target Recognition VII*, vol. 3374, Orlando, Florida, USA, pp. 96-107, April 1998.

[71] A.G.Dempster, "Dilution of Precision in Angle-of-Arrival Positioning Systems, *IET Electronics Letters*, vol.42, no.6, 2nd March 2006.

[72] R.A.Burne, I.Kadar, A.Buczak, "A Self-Organising Cooperative Sensor Network for Remote Surveillance: Target Tracking while Optimising the Geometry between Bearing-Reporting Sensors and the Target", *SPIE: Security and Defence, Proceedings of the Conference on Unattended Ground Sensor Technologies and Applications III*, vol.4393, pp.173-182, September 2001.

[73] H.B.Lee, "A Novel Procedure for Assessing the Accuracy of Hyperbolic Multi-lateration Systems", *IEEE Transactions on Aerospace and Electronic Systems*, vol.AES-11, no.1, pp.2-15, January 1975.

[74] D.J.Torrieri, "Statistical Theory of Passive Location Systems", *IEEE Transactions on Aerospace and Electronic Systems*, vol.AES-20, no.2, pp.183-198, March 1984.

[75] J.M.Augenbaugh, B.R.L.Cour, "Metric Selection for Information Theoretic Sensor Management", *Proceedings of the 11th International Conference on Information Fusion*, Cologne, Germany, pp. 1-8, July 2008.

[76] K. Kastella, "Discrimination Gain to Optimize Classification", *IEEE Transactions on Systems, Man & Cybernetics-Part A: Systems and Humans*, Vol.27, no. 1, pp.112-116, January 1997.

[77] M.P.Kolba and L.M.Collins, "Information-Theoretic Sensor Management for Multimodal Sensing," *Proceedings of the IEEE International Geoscience and Remote Sensing Symposium (IGARSS)*, Denver, Colorado, USA, pp. 3935-3938, August 2006.

[78] Y.Dong, W.K.Hon and D.K.Y Yau, "On Area of Interest Area of Coverage in Surveillance Mobile Sensor Networks", *Proceedings of the 15th IEEE International Workshop on Quality of Service*, Evanston, Illinois, USA, pp.87-90, June 2007.

[79] H.Kim, E.Kim and K.Han, "An Energy Efficient Tracking Method in Wireless Sensor Networks", *SpringerLink Lecture Notes in Computer Science*, 6th International Conference on Next Generation Teletraffic and Wired/Wireless Advanced Networking, Volume 4003, pp.278-286, June 2006.

[80] A.T Erman, L.V.Hoesel and P.Havinga, "Enabling Mobility in Heterogeneous Wireless Sensor Networks Cooperating with UAVs for Mission Critical Management", *IEEE Wireless Communications*, vol.15, no.6, pp.38-46, December 2008.

[81] E.P de Freitas, T.Heimfarth, C.E.Pereira, T.Larsson, F.R Wagner and F.M Ferreira, "Evaluation of Coordination Strategies for Heterogeneous Sensor Networks Aiming at Surveillance Applications", *Proceedings of the IEEE Conference on Sensors*, pp.591-596, Christchurch, New Zealand, October 2009.

[82] E.P de Freitas, T.Heimfarth, C.E.Pereira, T.Larsson, F.R Wagner and F.M Ferreira, "Decentralized Task Distribution Among Cooperative UAVs in Surveillance Systems Applications", *Proceedings of the 7th international conference on Wireless on-demand network systems and services (WONS)*, pp.121-128, Obergurgl, Austria, January 2010.

[83] L.Tong, Q.Zhao, S.Adireddy, "Sensor Networks with Mobile Agents", *Proceedings of the IEEE Conference on Military Communications (MILCOM)*, pp.688-693, Boston, U.S.A, October 2003.

[84] I.Stojmenovic, "Position-Based Routing in Ad Hoc Networks", *IEEE Communications Magazine*, vol.40, no.7, pp. 128-134, July 2002.

[85] J.Li, J.Jannotti, D.S.J De Couto, D.R Karger and R.Morris, "A Scalable Location Service for Geographic Ad Hoc Routing", *Proceedings of the 6th ACM international Conference on Mobile Computing and Networking*, pp.120-130, Boston, U.S.A, August 2000.

[86] E.Kranakis, H.Singh and J.Urrutia, "Compass Routing on Geometric Networks", *Proceedings of the 11th Canadian Conference on Computational Geometry*, pp.51-54, Vancouver, August 1999.

[87] G.G.Finn, "Routing and Addressing Problems in Large Metropolitan – Scale Internet Works", *Information Sciences Institute Technical Report ISI/RR-87-180*, March 1987.

[88] D.De.Couto and R.Morris, "Location Proxies and Intermediate Node Forwarding for Practical Geographic Forwarding", *MIT Laboratory for Computer Science Technical Report MIT-LCS-TR-824*, June 2001.

[89] C.Maihofer, "A Survey of Geocast Routing Protocols", *IEEE Communications Surveys & Tutorials*, vol.6, no.2, pp.32-42, Second Quarter 2004.

[90] J.Navas, T.Imielinski, "GeoCast-Geographic Addressing and Routing", Proceedings of the 3rd annual ACM/IEEE International Conference on Mobile Computing and Networking (MobiCom), pp.66-76, Budapest, Hungary, 1997.

[91] Y.B.Ko, N.H.Vaidya, "Flooding Based Geo-casting Protocols for Mobile Ad Hoc Networks", *Journal of Mobile Networks and Applications*, vol.7, no.6, pp.471-480, 2002.

[92] D.B.Johnson, D.A.Maltz, "Dynamic Source Routing in Ad Hoc Wireless Networks", Mobile Computing, *Kluwer Academic Publishers*, 1996.

[93] B.Nath and D.Niculescu, "Routing on a Curve", *ACM SIGCOMM Computer Communications Review*, vol.33, no.1, pp.155-160, January 2003.

[94] B.Warneke, M.Last, B.Leibowitz and K.Pister, "Smart Dust: Communicating with a Cubic-Millimetre Computer", *IEEE Computer*, vol.34, no.1, pp.45-51, January 2001.

[95] A.Boukerche, M.Ahmad, B.Turgut and D.Turgut, "A Taxonomy of Routing Protocols in Sensor Networks", *Algorithms and Protocols for Wireless Sensor Networks*, Wiley, 1st Edition, Chapter 6, pp.129-160, 2008.

[96] K. Chakrabarty and S. S. Iyengar, "Scalable Infrastructure for Distributed Sensor Networks", *New York: Spinger-Verlag*, 1st Edition, 2005.

[97] J.Kephart and D.Chess, "The Vision of Autonomic Computing", *IEEE Computer Magazine*, vol.36, no.1, pp.41-50, 2003.

[98] F.Dressler and O.B.Akan, "A Survey on Bio-Inspired Networking", *ELSEVIER Journal of Computer Networks*, vol.54, no.6, pp.881-900, April 2010.

[99] F.Dressler and O.B.Akan, "Bio-Inspired Networking: From Theory to Practise", *IEEE Communications Magazine*, vol.48, no.11, pp.176-183, November 2010.

[100] E.Bonabeau, M.Dorigo, G.Theraulaz, "Swarm Intelligence: From Natural to Artificial Systems", *Oxford University Press*, New York, USA, 1999.

[101] S.S.Iyengar, H.C.Wu, N.Balakrishnan and S.Y.Chang, "Biologically Inspired Cooperative Routing for Wireless Mobile Sensor Networks", *IEEE Systems Journal*, vol.1, no.1, pp.29-37, 2007.

[102] A.Gosh, A.Halder, M.Kothari, and S.Gosh, "Aggregation Pheromone Density Based Data Clustering", *ELSEVIER Journal of Information Science*, vol.178, no.13, pp.2816-2831, July 2008.

[103] A.T.Hayes, A.Martinoli and R.M.Goodman, "Distributed Odour Source Localization", *IEEE Sensors Journal*, vol.2, no.3, pp.260-271, June 2002.

[104] J.Murlis, J.S.Elkinton, R.T.Carde, "Odour Plumes and How Insects Use Them", *annual review of entomology*, vol.37, pp.505-532, 1992.

[105] D.B.Turner, "Workbook of Atmospheric Dispersion Estimates: An Introduction to Dispersion Modelling", *Lewis Publication*, 2nd Edition, 1994.

[106] X.Li, Y.Mao, Y.Liang, "A Survey on Topology Control in Wireless Sensor Networks", *Proceedings of the 10th International Conference on Control, Automation, Robotics and Vision (ICARCV)*, Singapore, pp.251-255, December 2008.

[107] P.Santi, D.M.Blough, "The Critical Transmitting Range for Connectivity in Sparse Wireless Ad Hoc Networks", *IEEE Transactions on Mobile Computing*, vol.2, no.1, pp.25-39, January-March 2003.

[108] B.Bollobas, "Modern Graph Theory", *Springer*, Chapter 7, 1st Edition, 1998.

[109] J.Diaz, M.D.Penrose, J.Petit and M.Serna, "Convergence Theorems for Some Layout Measures on Random Lattice and Random Geometric Graphs", *Journal of Combinatorics, Probability and Computing*, vol.9, no.6, pp.489-511, 2000.

[110] C.Bettstetter, "On the Minimum Node Degree and Connectivity of a Wireless Multi-hop Network", *Proceedings of the 3rd ACM International Symposium on Mobile Ad Hoc Networking and Computing (MobiHoc)*, pp. 80-91, Lausanne, Switzerland, June 2002.

[111] B.Liu, D.Towsley, "A Study of the Coverage of Large-Scale Sensor Networks", *Proceedings of the IEEE International Conference on Mobile Ad-Hoc and Sensor Systems (MASS)*, pp.475-483, October 2004.

[112] S.Karlin and H.M.Taylor, "A First Course in Stochastic Processes", *Academic Press*, San Diego, CA, section 1.3, 2nd Edition, 1975.

[113] S.Karlin and H.M.Taylor, "A Second Course in Stochastic Processes", *Academic Press*, San Diego, CA, Chapter 16, 1981.

[114] G.Bianchi, "Performance Analysis of the IEEE 802.11 Distributed Coordination Function", *IEEE Journal on Selected Areas In Communications*, vol.18, no.3, pp.535-547, March 2000.

[115] K.C.Huang and K.C.Chen, "Interference Analysis of Non-persistent CSMA with hidden terminals in multi-cell wireless data networks", *Proceedings of the IEEE Conference on Personal, Indoor and Mobile Radio Communications* (*PIMRC*), Toronto, Canada, pp. 907-911, September 1995.

[116] R.Khalaf and I.Rubin, "Throughput and Delay Analysis in Single Hop and Multihop IEEE 802.11 Networks", *Proceedings of the 3rd International Conference on Broadband, Communications and Network systems (BROADNETS)* ,San Jose, U.S.A, October 2006.

[117] C.Intanagonwiwat, D.Estrin, R.Govindan, J.Heidman, and F.Silva, "Directed Diffusion for Wireless Sensor Networks", *IEEE/ACM Transactions on Networking*, vol.11, no.1, pp.2-16, February 2003.

[118] N.Magharei and R.Rejaie. "PRIME: Peer-to-peer receiver-driven mesh-based streaming", *IEEE/ACM Transactions on Networking*, vol.17, no.4, pp.1052–1065, August 2009.

[119] S. Sanghavi, B. Hajek, and L. Massoulie, "Gossiping with multiple messages", *IEEE Transactions on Information Theory*, vol.53, no.12, pp.4640-4654, December 2007.

[120] J.N. Al-Karaki and A.E. Kamal, "Routing Techniques in Wireless Sensor Networks: A Survey", *IEEE Wireless Communications*, vol.11, no.6, pp.6-28, December 2004.

[121] M.Zorzi and R.Rao, "Geographic Random Forwarding for Ad Hoc and Sensor Networks: Multi-hop Performance", *IEEE Transactions on Mobile Computing*, vol.2, no.4, pp.337-347, October-December 2003.

[122] M.Zorzi and R.Rao, "Geographic Random Forwarding for Ad Hoc and Sensor Networks: Energy and Latency Performance", *IEEE Transactions on Mobile Computing*, vol.2, no.4, pp.349-365, October-December 2003.

[123] Z.Zhang, "Routing in Intermittently Connected Mobile Ad Hoc Networks and Delay Tolerant Networks: Overview and Challenges", *IEEE Communications Surveys and Tutorials*, vol.8, no.1, pp.24-37, 1st Quarter 2006.

[124] R.Vidhyapriya and P.T.Vanath, "Energy Aware Routing for Wireless Sensor Networks", *Proceedings of the IEEE International Conference on Signal Processing, Communications and Networking (ICSCN)*, pp.554-550, February 2007.

[125] Z.Ren, G.Wang, Q.Chen, H.Li, "Modelling and Simulation of Rayleigh Fading, Path Loss and Shadowing Fading for Wireless Mobile Networks", *ELSEVIER Journal of Simulation Modelling Practise and Theory*, vol.19, no.2, pp.626-637, February 2011.

[126] A.Goldsmith, "Wireless Communications", *Cambridge University Press*, 1st Edition, pp. 31-34, 2005.

[127] B.Sklar, "Rayleigh Fading Channels in Mobile Digital Communication Systems Part 1: Characterization", *IEEE Communications Magazine*, vol.35, no.7, pp.90-100, July 1997.

[128] S.Y.Seidel, "Path Loss, Scattering and Multipath Delay Statistics in Four European Cities for Digital Cellular and Microcellular Radiotelephone", *IEEE Transactions on Vehicular Technology*, vol.40, no.4, pp.721-30, November 1991.

[129] J.B.Andersen, T.S.Rappaport and S.Yoshida, "Propagation Measurements and Models for Wireless Communications Channels", *IEEE Communications Magazine*, vol.33, no.1, pp.42-49, January 1995.

[130] F.Hansen, "Mobile Fading-Rayleigh and Lognormal Superimposed", *IEEE Transactions on Vehicular Technology*, vol.26, no.4, pp.332-335, November 1977.

[131] R.L.Bogusch, F.W.Guigliano, D.L.Knepp, A.H.Michelet, "Frequency Selective Propagation Effects on Spread-Spectrum Receiver Tracking", *Proceedings of the IEEE*, vol.69, no.7, pp.787-96, July 1981.

[132] A.Woo, T.Tong and D.Culler, "Taming the Underlying Issues of Reliable Multi-hop Routing in Sensor Networks", *Proceedings of the 1st International Conference on*

Embedded Networked Sensor Systems (SenSys), Los Angeles, U.S.A, pp.14-27, November 2003.

[133] J.Zhao and R.Govindan, "Understanding Packet Delivery Performance in Dense Wireless Sensor Networks", *Proceedings of the 1st International Conference on Embedded Networked Sensor Systems (SenSys)*, Los Angeles, U.S.A, pp.1-13, November 2003.

[134] M.Zuniga and B.Krishnamachari, "Analyzing the Transitional Region in Low Power Wireless Links", *Proceedings of the 1st IEEE Conference on Sensor, Ad-Hoc and Communication Networks (SECON)*, Santa Clara, U.S.A, pp.517-526, October 2004.

[135] M.Zuniga and B.Krishnamachari, "An Analysis of Unreliability and Asymmetry in Low-Power Wireless Links", *ACM Transactions on Sensor Networks*, vol.3, no.2, Article Number 7, June 2007.

[136] R.Draves, J.Padhye, B.Zill, "Routing in Multi-Radio, Multi-Hop Wireless Mesh Networks", *Proceedings of the 10th Annual International Conference on Computing and Networking (MobiCom)*, Philadelphia, Pennsylvania, U.S.A, pp.114-128, October 2004.

[137] E.N.Gilbert, "Capacity of a Burst-Noise Channel", *Bell Systems Technical Journal*, vol.39, pp.1253-1265, 1960.

[138] E.O.Elliot, "Estimates of Error Rates for Codes on Burst-Noise Channels, *Bell Systems Technical Journal*, vol.42, pp.1977-1997, 1963.

[139] D.S.J. De Couto, D.Aguayo, J.Bicket, R.Morris, "A High-Throughput Path Metric for Multi-Hop Wireless Routing", *Proceedings of the 9th Annual International Conference on Computing and Networking (MobiCom)*, San Diego, California, U.S.A, pp.134-146, September 2003.

[140] M.Conti, S.Giordano, M.May, A.Passarella, "From Opportunistic Networks to Opportunistic Computing", *IEEE Communications Magazine*, vol.48, no.9, pp.126-138, September 2010.

[141] M.Conti, L.Pelusi, A.Passarella, "Opportunistic Networking: Data Forwarding in Disconnected Mobile Ad Hoc Networks", *IEEE Communications Magazine*, vol.44, no.11, pp.134-141, November 2006.

[142] H.Liu, Z.Baoxian, H.Mouftah, M.Jian, S.Xiaojun, "Opportunistic Routing for Wireless Ad Hoc and Sensor Networks: Present and Future Directions", *IEEE Communications Magazine*, vol.47, no.12, pp.103-109, December 2009.

[143] M.Xufei, T. Shaojei, X.Xu, "Energy-Efficient Opportunistic Routing in Wireless Sensor Networks", *IEEE Transactions on Parallel and Distributed Systems*, vol.22, no.11, pp.1934-1942, November 2011.

[144] Z.Zhong and S.Nelakuditi, "On the Efficacy of Opportunistic Routing", *Proceedings of the 4th Annual IEEE Conference on Sensor, Ad-Hoc and Communication Networks (SECON)*, San Diego, U.S.A, pp.441-450, June 2007.

[145] Z.Zhong and S.Nelakuditi, "On Selection of Candidates for Opportunistic Any-Path Forwarding", *ACM SIGMOBILE Mobile Computing and Communications Review*, Vol.10, no. 4, pp.1-2, October 2006.

[146] S.Gosh, "A Survey of Recent Advances in Fuzzy Logic in Telecommunications Networks and New Challenges", *IEEE Transactions on Fuzzy Systems*, Vol. 6, No.3, pp.443-447, August 1998.

[147] J.N. Al-Karaki and A.E.Kamal, "Routing Techniques in Wireless Sensor Networks: A Survey", IEEE Wireless Communications, vol.11, no.6, pp. 6-28, December 2004.

[148] S. Lindsey, C. Raghavendra and K.M.Sivalingam "Data Gathering Algorithms in Sensor Networks Using Energy Metrics", *IEEE Transactions on Parallel and Distributed Systems*, vol.13, no.9, pp.924-935, 2002.

[149] E.H.Mamdani, "Applications of Fuzzy Logic to Approximate Reasoning Using Linguistic Systems", *IEEE Transactions on Systems, Man and Cybernetics*, Vol.26, no.12, pp.1182 -1191, 1977.

[150] Q.Liang, "Fault-Tolerant and Energy Efficient Wireless Sensor Networks: A Cross-Layer Approach", *Proceedings of the 24th IEEE Conference on Military Communications (MILCOM)*, Atlantic City, New Jersey, U.S.A, pp.1862-1868, October 2005.

[151] J.M.Mendel, "Fuzzy Logic Systems for Engineering: A Tutorial", *Proceedings of the IEEE*, vol.83, no.3, pp.345-377, March 1995.

[152] L.A.Zadeh, "Fuzzy Sets", Journal of Information and Control, vol.8, pp.338-353, 1965.

[153] L.A.Zadeh, "Outline of a New Approach to the Analysis of Complex Systems and Decision Processes", *IEEE Transactions on Systems, Man and Cybernetics*, Vol.3, no.1, pp.28-44, 1973.

[154] J.Yen, R.Langari and L.Zadeh, "Industrial Applications of Fuzzy Logic and Intelligent Systems", *IEEE Press*, 1st Edition, New York, 1995.

[155] O.Gnawali, M.Yarvis, J.Heidemann, and R.Govindan "Interaction of Retransmission, Blacklisting, and Routing Metrics for Reliability in Sensor Network Routing", *Proceedings of the 1st IEEE Conference on Sensor, Ad-Hoc and Communication Networks (SECON)*, Santa Clara, U.S.A, pp.34-43, October 2004.

[156] H.Takagi, L.Kleinrock, "Optimal Transmission Ranges for Randomly Distributed Packet Radio Terminals", *IEEE Transactions on Communications*, vol.32, no.3, pp.246-257, March 1984.

[157] T.C.Hou, V.O.K.Li, "Transmission Range Control in Multi-Hop Packet Radio Networks", *IEEE Transactions on Communications*, vol.34, no.1, pp.38-44, January 1986.

[158] B.D.Liu, "Design of Adaptive Fuzzy Logic Controller Based on Linguistic-Hedge Concepts and Genetic Algortitms", *IEEE Transactions on Systems, Man and Cybernetics*, Vol.31, no.1, pp.32-52, February 2001.

[159] F.Herera, "Tuning Fuzzy Logic Controllers by Genetic Algorithms", *International Journal of Approximate Reasoning*, Vol.12, pp.299 -315, April-May 1995.

[160] J.Casillas, O.Cordon, F.Herrera, "Genetic Tuning of Fuzzy Rule Deep Structures for Linguistic Modelling", *IEEE Transactions on Fuzzy Systems*, Vol.13, no.1, pp.13-29, 2005.

[161] A.S.Fabio, M.Vinicius and L. Barrosso, "An Application of Genetic Fuzzy Systems for Wireless Sensor Networks", *Proceedings of the IEEE International Conference on Fuzzy Systems (FUZZ)*, Taipei, Taiwan, pp.2473-2480, June 2011.

[162] F.Herera, L.Magdalena, "Genetic Fuzzy Systems: A Tutorial", *Tatra Mountains Mathematical Publications*, Vol.13, pp.93 -121, 1997.

[163] S.Phoha, "Guest Editorial: Special Section on Mission-Oriented Sensor Networks", *IEEE Transactions on Mobile Computing*, vol. 3, no.3, p.209, July-August 2004.

[164] S.Phoha and T.LaPorta, "Overview of Mission-Oriented Sensor Networks", *In Sensor Network Operations (eds S. Phoha, T. LaPorta and C. Griffin)*, John Wiley & Sons, Inc., Hoboken, NJ, USA, 2005.

[165] E.Eswaran, S.Misra and T.La Porta, "Utility-Based Adaptation in Mission-Oriented Wireless Sensor Networks", *5th Annual IEEE Conference on Sensor, Mesh and Ad-Hoc Communications and Networks (SECON)*, San Francisco, California, USA, pp.278-286, June 2008.

[166] X.Chang, R.Tan, G.Xing, Z.Yuan, C.Lu, Y.Chen and Y.Yang, "Sensor Placement Algorithms for Fusion-Based Surveillance Networks", *IEEE Transactions on Parallel and Distributed Systems*, vol.28, no.8, August 2011.

[167] S.G.Pierce, Y.B.Haim, K.Worden, G.Manson, "Evaluation of Neural Network Robust Reliability Using Information-Gap Theory", *IEEE Transactions on Neural Networks*, vol.17, no.6, pp. 1349-1361, November 2006.